FUNCTIONALIZED OLIGOTHIOPHENES FOR APPLICATION IN ORGANIC SOLAR CELLS

Dissertation

zur Erlangung des akademischen Grades

„Doktor der Naturwissenschaften“ (Dr. rer. nat.)

der Fakultät der Naturwissenschaften

der Universität Ulm

vorgelegt von

Roland Fitzner

geboren in Ludwigshafen am Rhein

Ulm, 2015

Amtierender Dekan:	Prof. Dr. Joachim Ankerhold
Erstgutachter:	Prof. Dr. Peter Bäuerle
Zweitgutachter:	Prof. Dr. Mika Lindén
Drittgutachterin:	Prof. Dr. Sabine Ludwigs
Tag der Promotionsprüfung:	15. Juli 2015

This work has been elaborated between April 2009 and September 2013 at the Institute of Organic Chemistry II and Advanced Materials, University of Ulm, Germany.

DANKSAGUNG / ACKNOWLEGEMENT

Zunächst möchte ich mich bei Prof. Dr. Peter Bäuerle für die interessante Themenstellung im aufregenden Forschungsbereich der Organischen Elektronik, die hervorragende Betreuung und die Möglichkeit an internationalen Konferenzen teilzunehmen bedanken.
Prof. Dr. Mika Lindén und Prof. Dr. Sabine Ludwigs danke ich für die freundliche Übernahme der Gutachten, sowie Prof. Dr. Tanja Weil, Prof. Dr. Sven Rau und Prof. Dr. Gerhard Taubmann für ihre Teilnahme am Dissertationskolloquium.
Mein besonderer Dank gilt außerdem Dr. Elena Mena-Osteritz für die Hilfestellung bei spektroskopischen, quantenchemischen und röntgenstrukturanalytischen Fragen, Astrid Vogt für die unzähligen praktischen Tipps, Dr. Gisela Schulz für die Hilfe bei der Herstellung löslichkeitsprozessierter Solarzellen, Dr. Egon Reinold für die fachliche Betreuung besonders in der Anfangszeit, Dr. Amaresh Mishra für die Unterstützung beim Schreiben der ersten Publikation, Dr. Günther Götz für die Einführung in Cyclovoltammetrie und Vakuumsublimation, Dr. Markus Wunderlin für die Messung der MALDIs und Prof. Dr. Fan Zhang für die Hilfe bei der Suche nach Einkristallen.
Bei allen Mitarbeitern der OCII und besonders bei meinen Laborkolleginnen Astrid, Gisela und Hanne möchte ich mich für die angenehme und freundschaftliche Arbeitsatmosphäre bedanken.
Herzlich bedanken möchte ich mich bei meinen Kooperationspartnern Prof. Dr. Karl Leo, Dr. Moritz Riede, Dr. Christian Körner, Dr. Hannah Ziehlke, Dr. Chris Elschner vom Institut für Angewandte Photophysik an der TU Dresden; bei Dr. Martin Pfeiffer, Dr. Christian Uhrich und Dr. Karsten Walzer von der Heliatek GmbH; bei Dr. Denis Andrienko und Dr. Manuel Schrader vom Max Planck Institut für Polymerforschung in Mainz; bei Prof. Dr. Andrew Holmes, Dr. Wallace W. H. Wong und Dr. Jegadesan Subbiah von der University of Melbourne und bei Prof. Dr. José I. Pascual von der Freien Universität Berlin.
Nicolas Trinks, Matthias Arzt, Philipp Kratzer, Patrick Nagl, Janina Belka und Vitali Weißbecker danke ich für den Einsatz während ihrer Praktika bzw. Bachelorarbeiten.
Dr. Maria Heuschmid und Ingrid Bopp danke ich für die hervorragende organisatorisch-administrative Betreuung.
Zu guter Letzt möchte ich mich ganz herzlich bei meinen Freunden und meiner Familie für ihre Geduld und ihre unverzichtbare moralische Unterstützung bedanken.

TABLE OF CONTENTS

TABLE OF CONTENTS ..... **i**

ABBREVEATIONS ..... **v**

PREFACE ..... **ix**

I. INTRODUCTION **1**

1. Solar Energy **1**

2. Basic Materials and Working Principle of Organic Solar Cells **2**

3. Device Architecture and Fabrication **5**

3.1 Photoactive Layer 5

3.2 Device Stack 7

4. Solar Cell Performance Characteristics **8**

3.1 Open Circuit Voltage 9

3.2 Short Circuit Current 10

4.3 Fill Factor 10

4.4 Power Conversion Efficiency 10

4.5 External Quantum Efficiency 11

5. Material Requirements **11**

6. Applied Materials **13**

6.1 Polymeric Donor Materials 13

6.2 Molecular Donor Materials for Solution-Processing 15

6.3 Molecular Donor Materials for Vacuum-Processing 19

References **23**

II. OVERVIEW OFT THE THESIS **29**

Chapter III **29**

Chapter IV **32**

Chapter V **34**

Chapter VI **37**

Chapter VII **40**

Personal Contributions to the Joined Publications **42**

References **44**

III. DICYANOVINYL-SUBSTITUTED OLIGOTHIOPHENES: STRUCTURE-PROPERTY RELATIONSHIPS AND APPLICATION IN VACUUM-PROCESSED SMALL MOLECULE ORGANIC SOLAR CELLS 47

Abstract 48

1. Introduction 49

2. Synthesis of Dicyanovinyl-Functionalized Oligothiophenes DCVnT 50
2.1 Linear Syntheses 50
2.2 Convergent Syntheses 51

3. Thermal Properties 51

4. Structure Analysis 53

5. Optical and Redox Properties 58
5.1 Steady-State Spectroscopy 58
5.2 Electrochemical Characterization 61
5.3 Quantum Chemical Calculations 63

6. Fabrication and Characterization of DCV*n*Ts in Organic Solar Cells 64
6.1 Planar Heterojunction Solar Cells 64
6.2 Bulk Heterojunction Solar Cells 67

7. Conclusion 70

8. Experimental 71
Instruments and Spectroscopic Measurements 71
Thin Film and Device Fabrication 72
Photovoltaic Characterization 73
Reagents and Chemicals 73
Synthesis and Characterization 74

Acknowledgements 76

References 77

IV. INTERRELATION BETWEEN CRYSTAL PACKING AND SMALL MOLECULE ORGANIC SOLAR CELL PERFORMANCE 81

Abstract 82

Acknowledgements 93

References 94

Supporting Information 95
Instruments, Spectroscopic Measurements, and Methods 95
Synthesis and Characterization 96
X-Ray Diffraction Analysis 98
Differential Scanning Calorimetry (DSC) 101
Thermogravimetric Analysis (TGA) 102
Cyclic Voltammetry (CV) 102
References 103

V. CORRELATION OF II-CONJUGATED OLIGOMER STRUCTURE WITH FILM MORPHOLOGY AND ORGANIC SOLAR CELL PERFORMANCE 105

Abstract 106

Acknowledgements 115

References 116

Supporting Information 117

Materials and Methods 117
Synthesis and Characterization 117
Optical and Electrochemical Measurements 123
X-ray Single Crystal Analysis 123
Thin Film and Device Fabrication 124
Thermal Analysis 126
Cyclic Voltammetry (CV) 127
Solar Cell Device Stacks 127
Photovoltaic Characteristics of optimized Solar Cells (Stack B) 128
Comparison of EQE of initial (A) and optimized stack (B) 128
Thin Film X-ray Diffraction Measurement 129
Statistics for Several Stack 3(B) Solar Cell Parameters 130
X-ray Reflection (XRR) 131
References 132

VI. A-D-A-TYPE OLIGOTHIOPHENES FOR SMALL MOLECULE ORGANIC SOLAR CELLS: EXTENDING THE II-SYSTEM BY INTRODUCTION OF RING-LOCKED DOUBLE BONDS 133

Abstract 134

1. Introduction 135

2. Results and Discussion 136

2.1 Synthesis 136
2.2 Thermal Properties and Solubility 137
2.3 X-ray Structure Analysis 140
2.4 Optoelectronic Properties 143
2.5 Photovoltaic Properties 150

3. Conclusion 153

4. Experimental Section 153

Instruments and Measurements 153
Quantum Chemical Calculations 155
Thin Film and Device Fabrication 155
Photovoltaic Characterization 155
Reagents and Chemicals 155
Synthesis and Characterization 156

Acknowledgements 159

References **160**

Supporting Information **162**
Single Crystal X-ray Analysis 164
Theoretical Calculations 164

VII. STRUCTURAL MODIFICATION OF THE TERMINAL GROUPS IN A-D-A OLIGOTHIOPHENES FOR SOLUTION-PROCESSED SOLAR CELLS **165**

Abstract **166**

1. Introduction **167**

2. Results and Discussion **168**

3. Conclusion **178**

4. Experimental **179**
Materials and Methods 179
Device Fabrication 180
Synthesis and Characterization 180

Acknowledgements **183**

References **184**

SUMMARY **187**

ZUSAMMENFASSUNG **191**

PUBLICATIONS AND PRESENTATIONS **195**

CURRICULUM VITAE **200**

ABBREVEATIONS

A	Acceptor
abs	Absorption
AM1.5	Air Mass 1.5 global
BHJ	Bulk heterojunction
BPAPF	9,9-Bis[4-(N,N-bis-biphenyl-4-yl-amino)phenyl]-9H-fluorene
Bu	Butyl
calc.	Calculated
CI	Chemical ionization
CN	Chloronaphthalene
CT	Charge transfer
CV	Cyclic voltammetry
D	Donor
d	Doublet
DCC	Dicyanocyclohexenone
DCM	Dichloromethane
DCV	Dicyanovinyl
DIO	1,8-Diiodooctane
DMF	N,N-Dimethylformamide
DMSO	Dimethyl sulfoxide
DPV	Differential pulse voltammetry
DSC	Differential scanning calorimetry
E_g	Band gap
EI	Electron impact
em	Emission
eq.	Equivalent
EQE	External quantum efficiency
Et	Ethyl
Fc/Fc^+	Ferrocene/ferrocenium couple
FF	Fill factor

FHJ	Flat heterojunction
HOMO	Highest occupied molecular orbital
HTL	Hole transporting layer
I_{SC}	Short-circuit current
ITO	Indium tin oxide
J	Coupling constant
JSC	Short-circuit current density
LUMO	Lowest unoccupied molecular orbital
m	Multiplet
M.p.	Melting point
MALDI	Matrix assisted laser desorption/ionization
Me	Methyl
NBS	N-Bromo succinimide
n-BuLi	*n*-Butyllithium
NIR	Near infrared
NMR	Nuclear magnetic resonance
OFET	Organic field effect transistor
opt	Optical
OSC	Organic solar cell
Ox	Oxidation
P3HT	Poly(3-hexylthiophene)
PCBM	Phenyl fullerene butyric acid methyl ester
PCE	Power conversion efficiency
PEDOT	Poly(3,4-ethylenedioxythiophene)
PHJ	Planar heterojunction
ppm	Parts per million
r.t.	Room temperature
Red	Reduction
s	Singlet
t	Triplet
$TBAPF_6$	tetrabutylammonium hexafluorophosphate
TCE	1,1,2,2-Tetrachloroethane
T_D	Decomposition temperature
TGA	thermogravimetric analysis

Th	Thiophene
THF	Tetrahydrofurane
TOF	Time of flight
UV	Ultra-violet
V	Voltage
vis	Visible
V_{OC}	Open-circuit voltage
w/w	Weight-to-weight
XRD	X-Ray diffraction

PREFACE

The central goal of this work was to elucidate relationships between the molecular structure of acceptor-substituted oligothiophenes and their unique material properties, with special regard to the application in organic solar cells (OSC, *Chapter I*). To this end, various series of acceptor-donor-acceptor (A-D-A)-type oligothiophene compounds (Chart 1) with systematic variation of specific structural parameters were designed. Chapters III thru VII deal with one of these oligomer series, respectively, describing synthesis, thermal and optoelectronic properties as well as crystal packing behavior or thin film morphology. These characteristics are used to rationalize the photovoltaic properties of the compounds in organic solar cells, emphasizing a different aspect in each contribution.

This thesis comprises five publications which are presented in the chronological order of their completion. The first four reports are published, and the last one is intended for submission. The central findings of the individual publications are summarized and correlated to each other in *Chapter II*. A more detailed description of synthesis and material characteristics is found in the respective Chapters III thru VII.

The first three publications describe dicyanovinyl (DCV)-substituted oligothiophenes. In *Chapter III*, alkyl-free terminally DCV-capped oligothiophenes (**DCVnTs**, Chart 1a) up to the sexithiophene (n = 6) are presented. Optical, electrochemical, and thermal properties of all compounds are discussed in detail, identifying the longer homologues **DCV4T** to **DCV6T** as suitable candidates for use as donor materials in organic solar cells in combination with C_{60} fullerene as the acceptor material. The optoelectronic properties of these three compounds are then related to their photovoltaic properties in vacuum-processed planar heterojunction devices. **DCV5T** is additionally tested in bulk heterojunction solar cells. In the following two Chapters, the influence of alkyl substituents in DCV-capped quarter- and quinquethiophenes is investigated with a focus on crystal structures and morphological properties. In *Chapter IV*, thermal, optoelectronic, and photovoltaic properties of methyl- and ethyl-substituted tetramers **DCV4T-Me** and **DCV4T-Et** (Chart 1b) are compared to alkyl-free parent derivative **DCV4T** introduced in the previous chapter. Differences in single crystal packing are analyzed extensively and correlated to the photovoltaic performance of the three compounds in bulk heterojunction solar cells made by vacuum-processing. In *Chapter V*, a series of three methylated DCV-substituted quinquethiophenes with varied alkyl-substitution patterns

(**DCV5T-Me 1-3**, Chart 1c) is described. The photovoltaic properties of the **DCV5T-Me** derivatives in vacuum-processed bulk heterojunction solar cells are discussed in comparison to the respective alkyl-free derivative **DCV5T** (Chapter III). Grazing incidence X-ray spectroscopy measurements are employed to characterize thin film morphologies, rationalizing the differing solar cell performances.

In the last two Chapters, oligothiophenes bearing dicyanomethylenecyclohexene (DCC) units at both α-termini are reported. A series of alkyl-free or methylated oligomers up to the tetramer is presented in *Chapter VI* (**DCCnTs**, Chart 1d). Trends in thermal and optoelectronic properties as a function of the number of thiophene units are identified and contrasted to the characteristics of the **DCVnT** oligomers (Chapters III to V). Single crystal packing and intermolecular interactions of **DCC3T-Me** are examined and compared to the very similar **DCV5T-Me** crystal structure. The trimers **DCC3T** and **DCC3T-Me** are applied in vacuum-processed OSCs. In *Chapter VII*, a series of butyl-substituted quinquethiophene molecules, functionalized with DCV-, DCC- or methylated DCC (MeDCC) acceptor units, is introduced (Chart 1e). The opto-electronic properties are characterized and all compounds are applied as donor materials in solution-processed bulk heterojunction devices. Solvent additives are used to optimize the photoactive layer morphology, which is investigated by atomic force microscopy (AFM).

Chart 1. *Molecular structures of (a)* ***DCVnT****, (b)* ***DCV4T****, (c)* ***DCV5T-Me****, (d)* ***DCCnT****, (e)* ***DCV5T-Bu****,* ***DCC5T-Bu****, and* ***MeDCC5T-Bu*** *oligomers presented in chapters III thru VII.*

a) DCVnT series, Chapter III

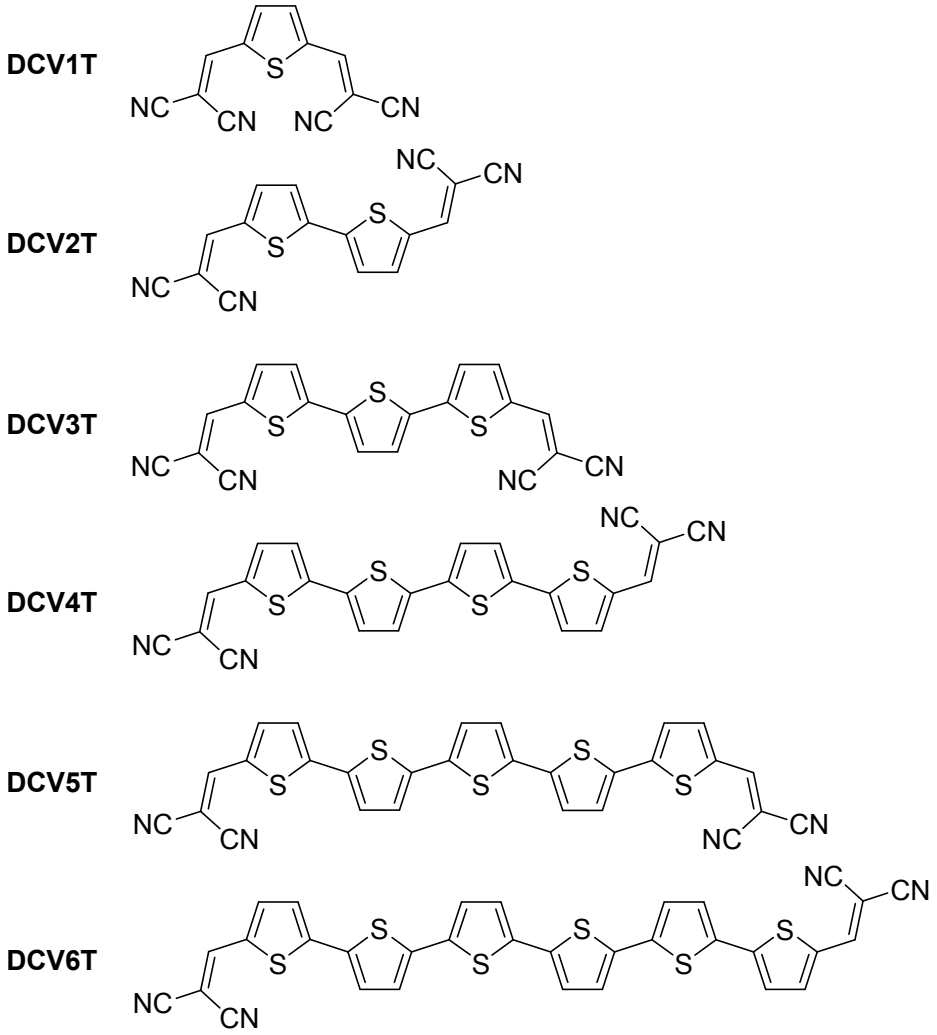

b) DCV4T series, Chapter IV

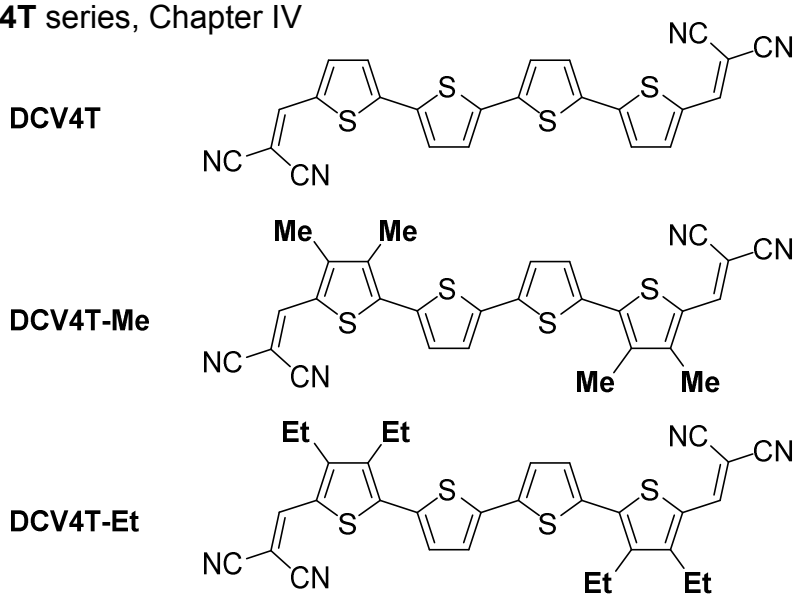

Chart 1 (continued).

c) DCV5T-Me series, Chapter V

DCV5T-Me 1

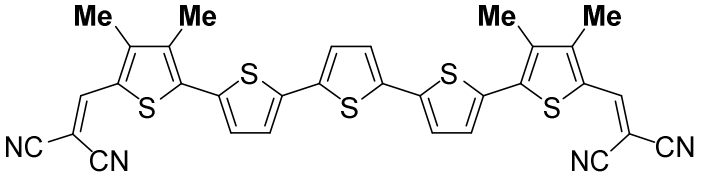

DCV5T-Me 2

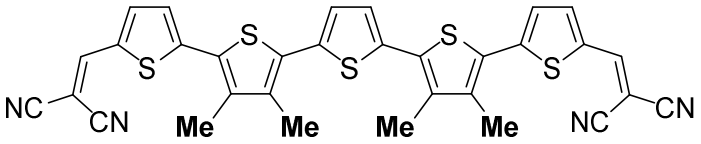

DCV5T-Me 3

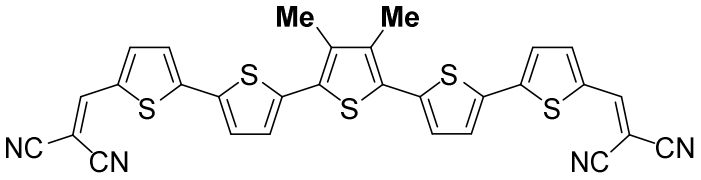

d) DCCnT series, Chapter VI

DCC1T

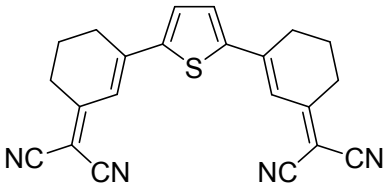

DCC2T

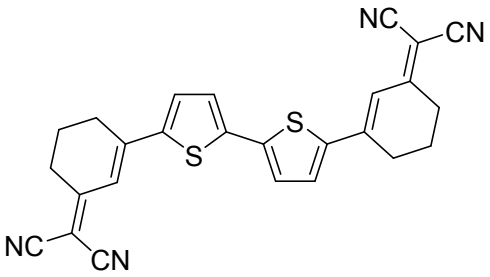

DCC3T (R = H)
DCC3T-Me (R = Me)

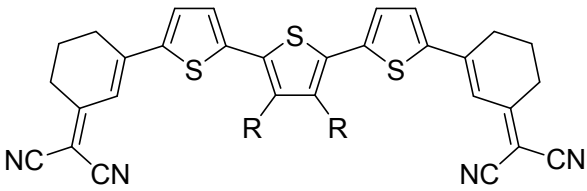

DCC4T

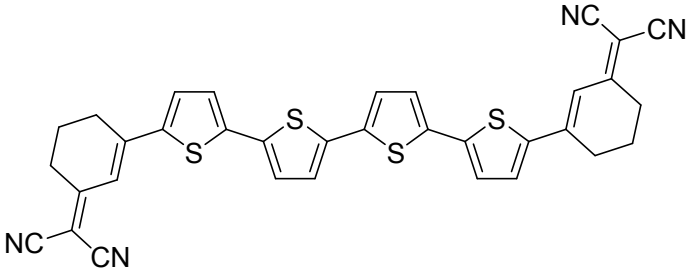

Chart 1 (continued).

e) Chapter VII

DCV5T-Bu

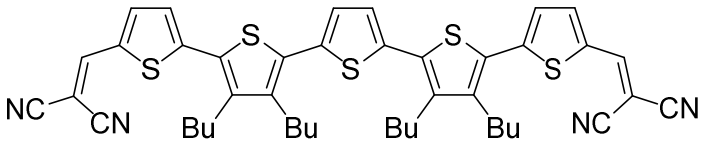

DCC5T-Bu

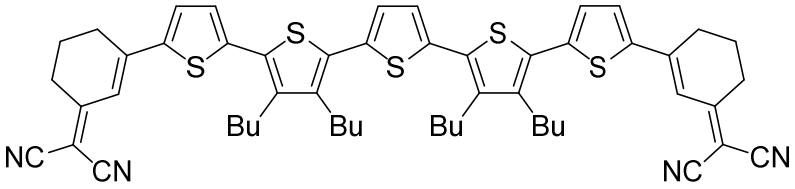

MeDCC5T-Bu

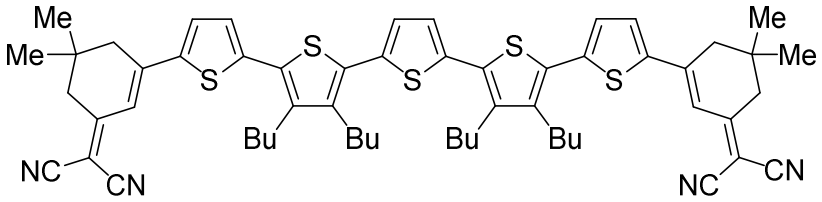

CHAPTER I

INTRODUCTION

1. SOLAR ENERGY

Solar radiation represents by far the largest source of renewable energy exceeding the global energy demand by several thousand times.[1] Direct conversion of the radiative energy of sunlight into electricity may be accomplished using photovoltaic devices also referred to as solar cells. The photovoltaic effect was first observed by A. E. Becquerel in 1839, when he detected a current flow between illuminated and dark platinum electrodes placed in an electrolyte bath.[2] The first solid state solar cell device, demonstrated by Fritts in 1883, consisted of a thin layer of selenium sandwiched between different work-function metal electrodes and showed a power conversion efficiency (PCE) of about 1%.[3] In 1905, Einstein published a comprehensive theoretical description of the photoelectric effect, for which he received the Noble price in physics in 1921.[4]

The great variety of modern photovoltaic technologies is usually categorized into three groups corresponding to three generations of solar cells. In 1953, Chapin, Fuller and Pearson at Bell laboratories reported the first photocell incorporating a silicon p-n junction with an efficiency of 6%.[5] Based on this finding, first generation silicon wafer-based solar cells have been continuously enhanced over the last decades reaching PCE values of 25% for laboratory devices and 16-21% in commercial panels.[6,7] Despite the energy intensive production process of highly pure electronic grade crystalline silicon, first generation photovoltaic solar cells are dominating today's commercial market. Second-generation thin film technologies incorporate very thin layers of semiconductor materials like amorphous silicon, cadmium telluride (CdTe), or copper indium gallium diselenide (CIGS). Lower material consumption and less costly manufacturing processes lead to reduced production costs for thin-film devices compared to first generation crystalline silicon technology. CIGS and CdTe solar cells reach record laboratory efficiencies of about 20% and up to 15% in commercial products.[7] The greatest challenges for second generation concepts are the still relatively high energy costs in the production and the usage of limited and toxic elements. Third generation photovoltaics covers more recent developments including organic-inorganic hybrid technologies like dye-sensitized solar cells or methyl-

ammonium lead halide-based perovskite devices as well as organic donor/acceptor (D/A) heterojunction solar cells. These approaches offer the potential for a clean and inexpensive large-scale production using continuous roll-to-roll coating processes onto flexible substrates. Special features such as transparency, light weight, and flexibility may be implemented into commercial products opening new application areas such as the integration into building façades, cars, or low weight structures. Third generation photovoltaic technologies are on the verge of commercialization, reaching laboratory performance levels of approximately 12% for dye-sensitized and organic solar cells.[8,9] Maximum PCE values of perovskite-based devices have increased at an unprecedented rate over the recent years to a current record value of about 20%.[6]

2. Basic Materials and Working Principle of Organic Solar Cells

The first organic solar cell devices were based on a single layer of one molecular p-type material sandwiched between metal or conducting glass electrodes of different work functions.[10-12] Early examples of these single layer devices published in the 1970s contained chlorophyll a,[13-15] magnesium phthalocyanine (**MgPc**),[16] or a hydroxy squarylium dye (**OHSq**)[17] as the absorber materials (Figure 1) and displayed very poor power conversion efficiencies below 0.1%. In 1978 Morel *et al.* reported a single layer organic solar cell made by thermal vacuum deposition employing merocyanine dye **1** (Figure 1) sandwiched between thin layers of aluminium and silver (Figure 2a), which exhibited an improved efficiency of 0.7% under AM1 illumination.[18]

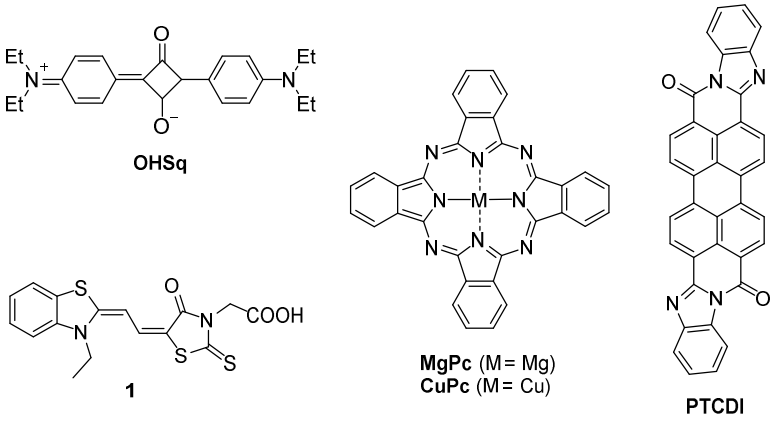

Figure 1. *Molecular structures of photoactive materials employed in early single layer and planar heterojunction organic solar cells.*

In 1986, Tang reported a novel type of organic photovoltaic cell based on a bilayer planar heterojunction (PHJ) between thin films of two different of organic materials exhibiting an at that time outstanding power conversion efficiency of about 0.95% under simulated AM2 illumination.[19] The cell was fabricated by subsequent thermal vacuum deposition of thin layers of copper phthalocyanine (**CuPc**) and a perylenetetracarboxylic acid diimide derivative (**PTCDI)** onto indium tin oxide coated glass as transparent conductive substrate, followed by the evaporation of an opaque silver layer as top electrode (Figure 2b).

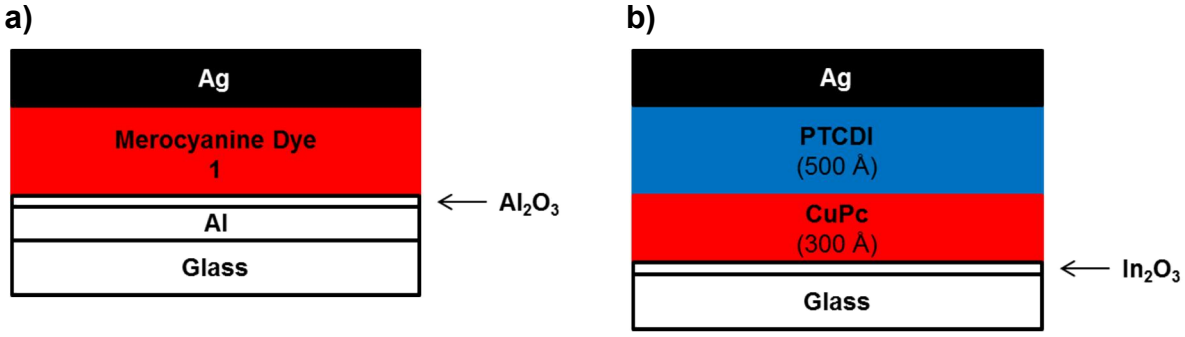

Figure 2. *Device configurations single layer and planar heterojunction devices reported by (a) Morel et al*[18] *and (b) Tang,*[19] *respectively.*

By combining a low ionization potential p-type donor (D) material (**CuPc**) with a high electron affinity n-type acceptor (A) material (**PTCDI**) a strong electric field was created at the D/A interface facilitating effective separation of the strongly bound electron-hole-pairs formed upon photo-excitation. Today's highest OSC device performances have been achieved based on the D/A hetreojunction concept by optimization of the applied material combination, photoactive layer morphology and device architecture, *vide infra*.

Figure 3 depicts the cascade of elementary processes that occur in an illuminated D/A heterojunction solar cell leading to the conversion of light energy into electric energy. For the introduction of the basic OSC working principle, a simple bilayer device setup of donor and acceptor materials sandwiched between electrodes of different work functions (compare Figure 2b) has been chosen as model system.

In the first step (Figure 3a), upon absorption of an incoming photon, an electron is promoted from the highest occupied molecular orbital (HOMO) to the lowest unoccupied molecular orbital (LUMO) of a donor molecule. The resulting electronically excited molecular state can be regarded as an electron (e^-)-hole (h^+) pair with both charges located on the same molecule. The electron-hole pair is strongly bound by electrostatic Coulomb forces due to the small dielectric constant in organic solids and can be regarded as an electrically neutral quasiparticle, the so-called Frenkel exciton.

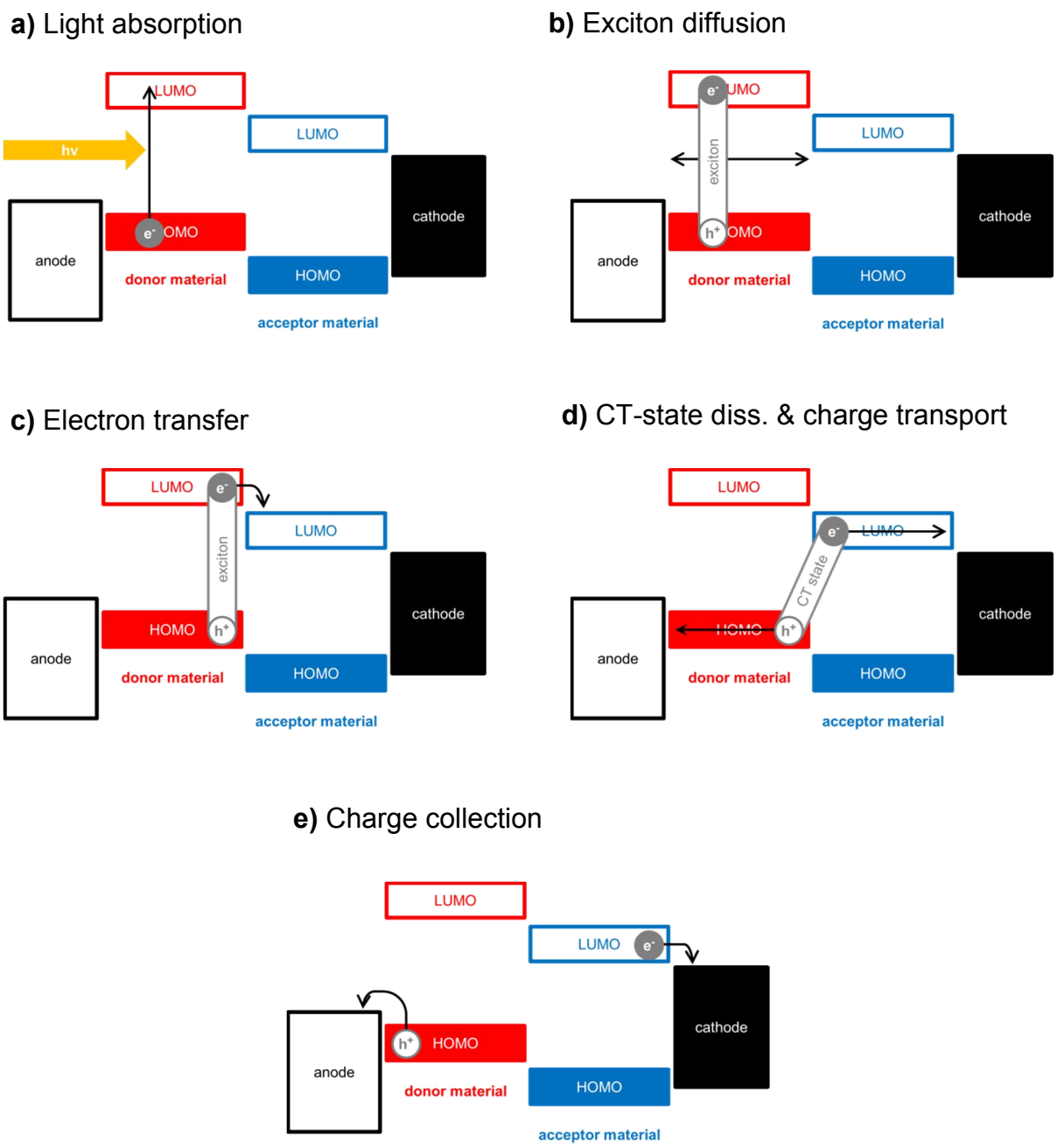

Figure 3. *Fundamental processes in donor/acceptor heterojunction OSCs.*

The photo-generated exciton diffuses within the donor phase hopping from one molecule to another until it reaches the interface with the acceptor material (Figure 3b).[20] Due to the offset in LUMO energy between donor and acceptor an electron is transferred from the LUMO of the excited donor molecule to the LUMO of a neighboring acceptor molecule (Figure 3c). Excitons formed upon absorption of light in the acceptor material can also be dissociated at the donor/acceptor-interface via hole-transfer from the HOMO of the acceptor to the energetically higher HOMO of the donor material. The resulting interfacial pair of an electron and a hole on either side of the bulk heterojunction is called charge transfer (CT) state. The CT state possesses

only a small Coulomb binding energy due to the spatial separation of the charges on two different molecules. The CT-state dissociates into free charge carriers in the next step (Figure 3d). The nature of the driving force for this process is still not completely clear. The discussed explanations are ionization by the internal electric field,[21] thermal,[22] or assisted thermal ionization.[23] The free charge carriers are subsequently transported away from the D/A interface along the in-build potential of the solar cell to the electrodes. In the last step, the positive and negative charge carriers are finally collected at the respective electrodes (Figure 3e).

3. Device Architecture and Fabrication

3.1 Photoactive Layer

As the formation of free charge carriers occurs at the interface between donor and acceptor, the way how both material phases are arranged in the photoactive zone of the device is of crucial importance for the functioning and the performance of an organic solar cell.

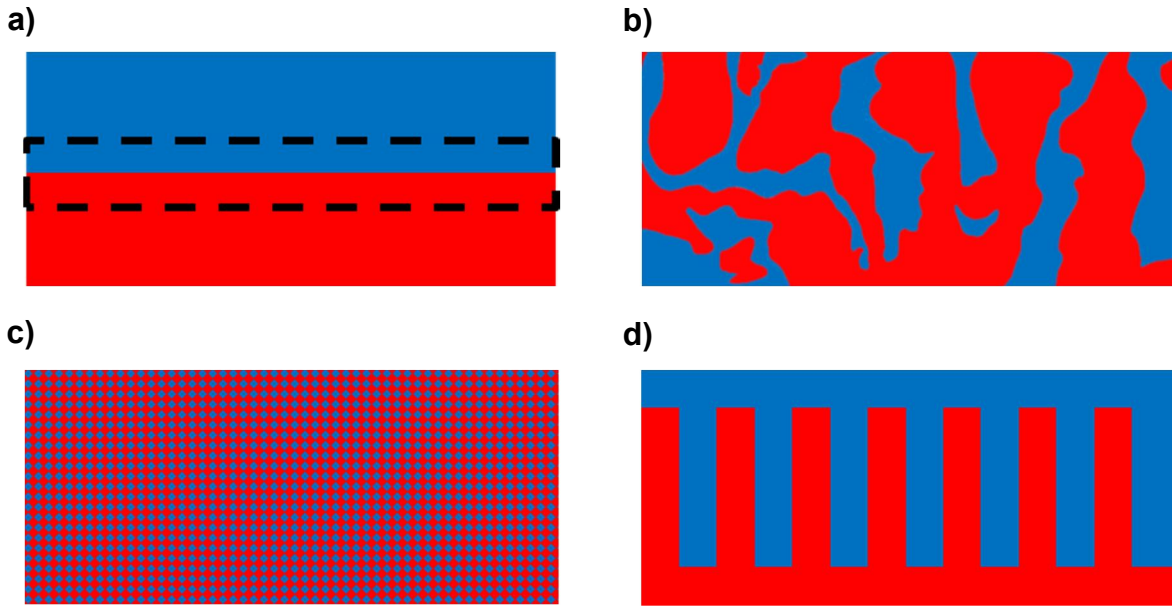

Figure 4. *Schematic cross-sections of nanomorphologies of the photoactive layers of donor/acceptor heterojunction OSCs.*[24] *a) Flat/planar heterojunction (FHJ/PHJ), b) bulk heterojunction (BHJ), c) finely mixed donor and acceptor materials, d) ideal morphology* of a BHJ active layer.

The flat/planar heterojunction (FHJ/PHJ) setup employed in Tang's first bilayer solar cell represents the most basic active layer morphology. It consists of neat layers of donor and

acceptor material stacked on top of each other forming a planar interface (Figure 4a). Using vacuum-processing, the PHJ layout is efficiently realized by subsequent vacuum-deposition of both photoactive compounds in separate thin layers. The fabrication of PHJ morphologies by solution-processing is limited to orthogonally soluble material combinations to avoid the destruction of the first neat layer during the coating of the second layer.[24]

Whereas the PHJ setup guarantees efficient charge carrier transport, its performance is usually limited by incomplete charge generation caused by the typically short exciton diffusion length L_D in organic materials of about 5-10 nm.[25] Excitons created upon photo-excitation in the bulk material further away from the D/A interface than L_D are not separated into free charge carriers and decay without contributing to the photo-current. Thus, the effective photoactive area where the absorption of incident photons contributes to the photocurrent is limited to a thin zone close to the D/A interface (dashed box in Figure 4a). Although organic absorber materials show very high extinction coefficients, a donor layer thickness in the range of the exciton diffusion length is usually not enough to absorb all incoming photons.

To circumvent the drawbacks of the PHJ setup with respect to insufficient charge carrier generation, the bulk heterojunction (BHJ) active layer architecture has been introduced (Figure 4b).[26] The highest power conversion efficiencies reported today for organic solar cells are achieved using this active layer design. In the BHJ setup, the planar bilayer junction is replaced by a phase-separated blend layer of donor and acceptor materials significantly enlarging the donor/acceptor interface compared to the PHJ design. The theoretically ideal bulk heterojunction morphology depicted in Figure 4d is a bi-continuous interpenetrating network of donor- and acceptor-phases, which are twice the exciton diffusion length in diameter.[27] This arrangement is a compromise between a maximized interfacial area, corresponding to a finely mixed D/A blend (Figure 4c) and the bilayer PHJ design, which offers optimal perculation pathways for the transport of the generated charge carriers. The ideal BHJ morphology is very hard to prepare and in general not achieved. Figure 4b shows a sketch of the cross-section of a typical BHJ layer in a real device.

Using solution-processing, D/A blend films are usually fabricated by spin-coating of solutions containing both, donor, and acceptor materials. The resulting blend morphology may be beneficially influenced by the proper selection of the solvent, the use of solvent additives or post-deposition thermal treatment as well as solvent vapor annealing.[25] The preparation of BHJ layers is also possible for vacuum-processed molecular materials by simultaneous co-evaporation of both photoactive components. Here, the choice of substrate temperature during the deposition is crucial for the morphology and crystallinity of the bulk heterojunction layer.

3.2 Device Stack

Organic solar cells are usually prepared by subsequent deposition of the different layers onto substrates pre-coated with a transparent conductive electrode material. Owing to its outstanding properties with respect to transparency and conductivity, indium tin oxide (ITO) sputtered on glass substrates is commonly used as bottom electrode. Materials like silver nano wires,[28] carbon nano tubes,[29] or graphene[30] are investigated as possible alternatives, as the high price and low abundance of indium might become a limiting factor for the large scale production of ITO-based organic solar cells.

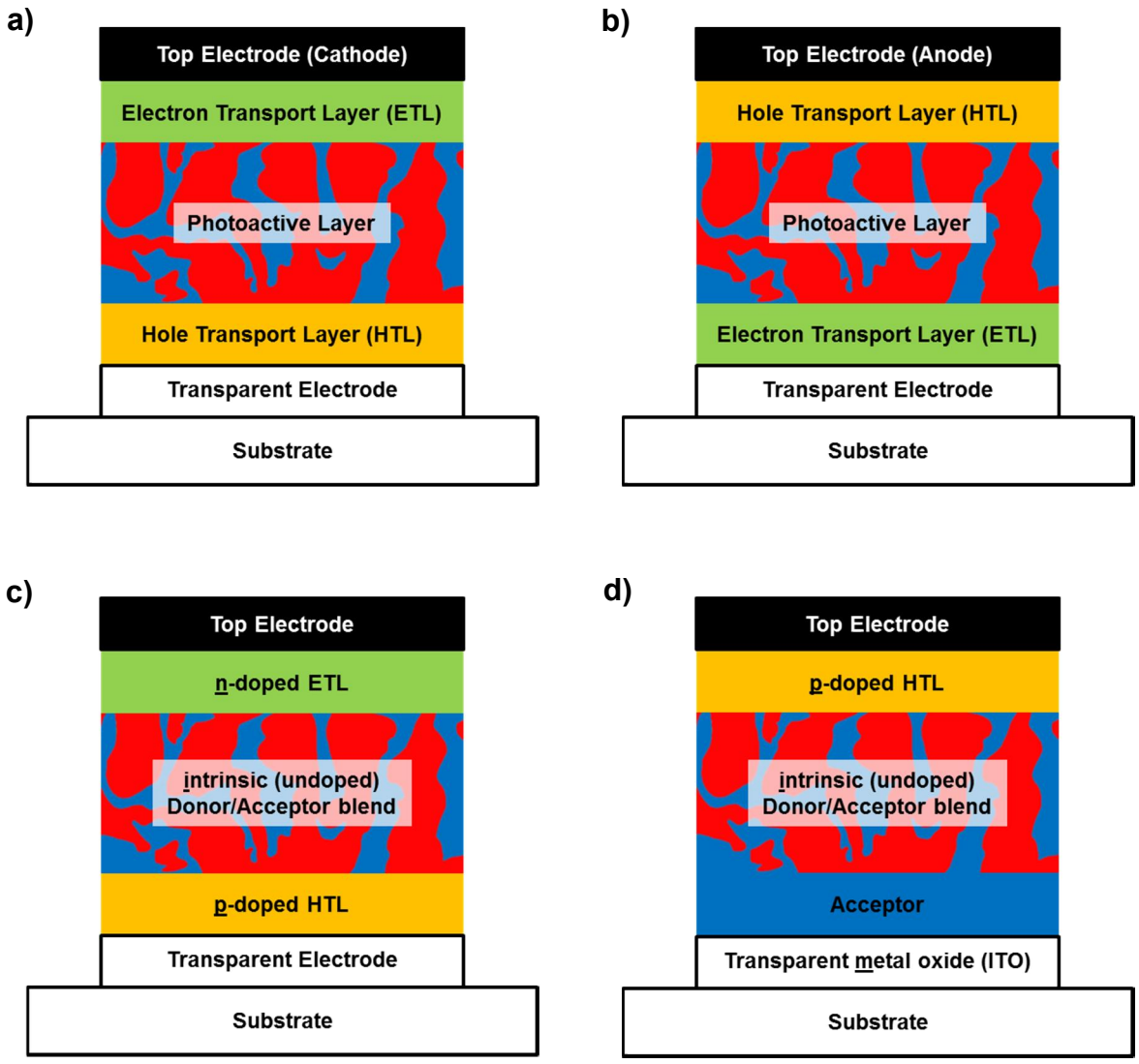

Figure 5. *Schematic representation of the layer structure of bulk heterojunction solar cells with (a) standard and (b) inverted device design;[24] (c) p-i-n and (d) m-i-p configuration.*

Figures 5a and b depict the layer structure of the typical device architecture used for organic solar cells with the photoactive layer sandwiched between a hole transport layer (HTL) and an

electron transport layer (ETL). In the standard configuration (Figure 5a), the HTL is deposited onto the transparent electrode and the electrons are injected from the ETL into the low work function metal top electrode, which acts as the cathode. In the inverted design (Figure 5b), the HTL is deposited on top of the active layer and a high work function metal is used for the top electrode (anode). This improves the device stability under ambient conditions. Using solution-processing, the transport layers are typically fabricated by spin-coating of aqueous dispersions. For the HTLs, poly(3,4-ethylenedioxythiophene) (PEDOT) blended with poly(styrenesulfonate) (PSS) (Chapter VII) as p-dopant or transition metal oxides like MoO_3 or V_2O_5 are frequently used.[31] The optional electron transport layers are usually made from aqueous solutions of ZnO or TiO_2 nanoparticles.[32] For the coating of the photoactive blend layers organic solvent systems are employed. Using vacuum-processing, doped transport layers may be fabricated by co-evaporation of hole or electron transport materials together with molecular dopants.[33] Solar cells incorporating an undoped intrinsic photoactive layer sandwiched between p- and n-doped transport layers (p-i-n configuration, Figure 5c) may be prepared by this technique. Due to the high conductivity of the doped transport layers their thicknesses may be varied over a large range in order to put the photoactive layer into the interference maximum of the incoming light optimizing the device performance (Chapter V).[34,35] In a simplified design, the p-doped ETL is omitted and the intrinsic layer is directly deposited onto the conductive metal (m) oxide (m-i-p configuration, Figure 5d). This is possible due to the already good conductivity of the fullerene acceptor material.

4. Photovoltaic Performance Characteristics

The precise characterization of the photovoltaic device performance is of fundamental importance as it provides the basis for the evaluation of the employed donor/acceptor material combination. Standard test conditions have been established to guarantee the comparability of the results obtained for different device setups in different laboratories.[36,37] For the determination of current-voltage characteristics, the Air Mass 1.5 Global (AM 1.5) light spectrum is used to illuminate the solar cells devices during the measurement. In radiation intensity (100 mW cm^{-2}) and spectral composition, the AM 1.5 spectrum corresponds to sun light at a zenith angle of 48.2°. This is equivalent to the yearly average of solar radiation in temperate climate zones, where most of the world's population is located. The standard measuring temperature is 25 °C.

The central means to analyze the performance of a photovoltaic cell is the determination of the current-voltage (*I-V*) curve. During the measurement a variable external voltage is applied to the illuminated solar cell device and the photocurrent is recorded as a function of the applied bias. To investigate to diode behavior of the device, the measurement is repeated without illumination to obtain the dark curve. Figure 6 depicts a typical example of an *I-V* curve. The important photovoltaic parameters that can be derived from the plot are presented and discussed in the following.

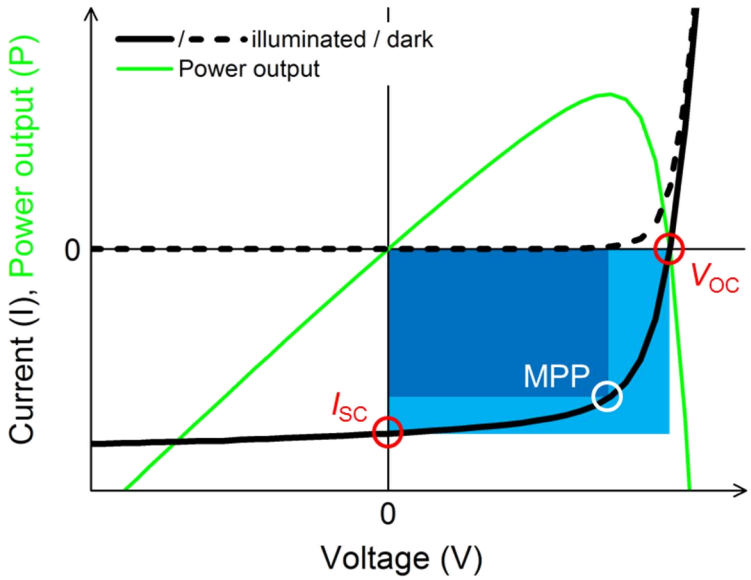

Figure 6. *Typical I-V curve of a solar cell device in the dark and under illumination (fundamental photovoltaic parameters highlighted in circles).*

4.1 Open Circuit Voltage

The open circuit voltage (V_{OC}) corresponds to the intersection of the *I-V*-curve with the current-axis (Figure 6). The V_{OC} value sets the upper limit to the external potential that can be applied to the solar cell without suppressing the conversion of light energy into electric energy. At open circuit conditions all generated charge carriers recombine so that the device produces no current. The open circuit voltage in a donor/acceptor heterojunction solar cell depends on the interfacial band gap, i.e., the energy difference between the HOMO of the donor material and the LUMO of the acceptor. Empirical Equation 1 can be used to estimate the V_{OC} value of a new material combination.[38]

$$V_{OC} \approx \{|E_{HOMO}(donor)| - |E_{LUMO}(acceptor)|\} \cdot e^{-1} - 0.4\ \mathrm{V} \qquad (1)$$

4.2 Short Circuit Current

The short circuit current (I_{SC}) is the intersection of the *I-V*-curve with the voltage-axis (Figure 6). It represents the photocurrent generated by the solar cell at short-circuit conditions with no external voltage applied. The short circuit current density (J_{SC}) is calculated by dividing the short circuit current by the active device area (Equation 2). As it is independent of the size of the solar cell, the J_{SC} value is generally used in literature facilitating the comparison of different devices.

$$J_{SC} = \frac{I_{SC}}{A} \tag{2}$$

4.3 Fill Factor

The fill factor (FF) is defined as the ratio between the maximum power output of a solar cell and the theoretical power output calculated as the product of I_{SC} and V_{OC} (Equation 3). The device generates maximum power at the maximum power point (MPP, Figure 6), where the product of current and voltage reaches its largest value. Graphically, the fill factor corresponds to the area ratio of the blue rectangles depicted in Figure 6. The FF provides a measure for the quality of the solar cell device with respect to charge transport and charge carrier collection. The best devices in literature show FF values in the range of 0.7-0.75.

$$FF = \frac{V_{MPP} \cdot I_{MPP}}{V_{OC} \cdot I_{SC}} \tag{3}$$

4.4 Power Conversion Efficiency

The power conversion efficiency (PCE, η) is defined as the ratio between the electric power output of a solar cell at the maximum power point and the power input of the incident light given by the AM 1.5 spectrum. As the central characteristic of a device, it represents a measure for its ability to convert the energy of solar light into electrical energy. According to Equation 4, the PCE is proportional to the open circuit voltage, short circuit current, and fill factor, which means that all three values need to be maximized at the same time in order to optimize the overall device performance.

$$\eta = \frac{P_{out}}{P_{in}} = \frac{V_{MPP} \cdot I_{MPP}}{P_{in}} = \frac{V_{OC} \cdot I_{SC} \cdot FF}{P_{in}} \tag{4}$$

4.5 External Quantum Efficiency

The external quantum efficiency (EQE), also denoted as incident photon to current efficiency (IPCE), is defined as the ratio between the number of charge carrier pairs generated by the device and the number of incoming photons at a certain wavelength (Equation 5). Usually, the EQE is determined at short circuit conditions and plotted versus the wavelength in the form of a spectrum.

$$\eta_{EQE}(\lambda) = \frac{N_{Collected\ Carrier\ Pairs}(\lambda)}{N_{Inciden\ Photons}(\lambda)} \tag{5}$$

As the injection of charge carriers into the electrodes is the final result of the linear chain of elementary processes, which occur in an illuminated D/A heterojunction solar cell (Chapter I.2), the EQE represents a measure for the combined efficiency of all these steps. According to Equation 6, it can be regarded as the product of the efficiencies of light absorption η_{Abs}, exciton diffusion η_{Diff}, charge carrier dissociation η_{Diss}, charge transport η_{Trans}, and collection η_{CC}.[39]

$$\eta_{EQE}(\lambda) = \eta_{Abs}(\lambda) \cdot \eta_{Diff} \cdot \eta_{Diss} \cdot \eta_{Trans} \cdot \eta_{CC} \tag{6}$$

5. Material Requirements

To ensure the efficient performance of a D/A heterojunction OSC device, the applied donor and acceptor material combination requires a number of optoelectronic properties.[40] Firstly, the photo-active materials have to display strong and broad absorption bands (Figure 7a) in order to absorb as much light energy as possible in the relatively thin photoactive layer of an organic solar cell. Maximizing the amount of generated excitons, efficient absorption is the basis for high J_{SC} values. Secondly, the employed donor/acceptor material combination has to show a LUMO offset of approximately 0.2-0.3 eV to provide a large enough driving force for exciton dissociation without losing more exciton energy than necessary.[41] Finally, the HOMO of the donor should be sufficiently low in energy to ensure a large open circuit voltage according to a large interfacial D/A band gap (Figure 7b). At the same time, the absorption of the donor material should cover a large part of the solar spectrum in the visible and near infra-red (NIR) range. A band gap of 1.5 eV provides the optimum compromise between both competing

requirements.[42] Furthermore, both photoactive materials should show high charge carrier mobilities to allow for efficient charge transport and good fill factors.

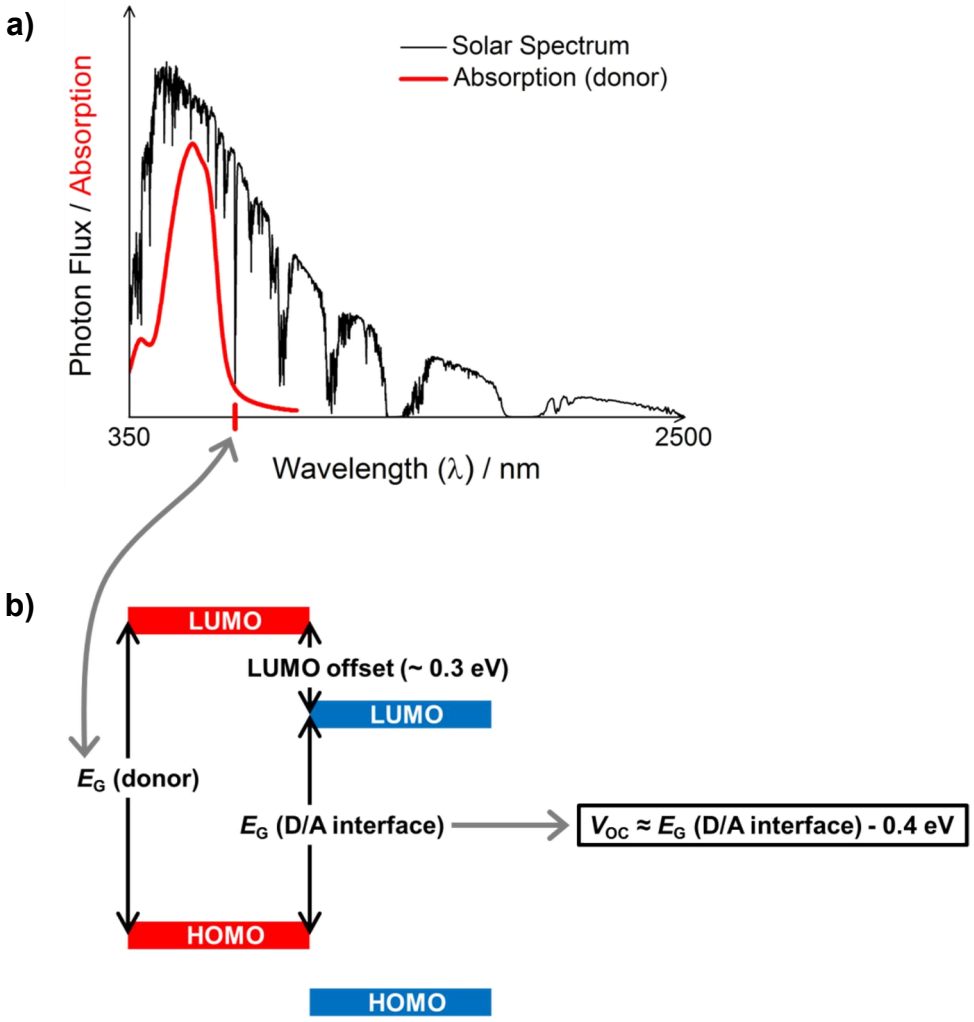

Figure 7. *(a) Solar Spectrum corresponding to AM1.5 conditions compared the absorption spectrum of a typical oligomeric donor material, and (b) relative frontier orbital energies of donor (red) and acceptor (blue) materials.*

In addition to the optoelectronic requirements, the physical properties of the active materials have to allow for the preparation of functional bulk hetrojunction morphologies (Chapter I.3) using one of the two standard fabrication methods. Solution-processing requires good solubility in organic solvents, wheras for vacuum deposition both components have to show high thermal stability and are limited with respect to their molecular weight. The BHJ blend layer morphology formation is influenced by D/D and D/A intermolecular interactions and may be influenced to some extend by the optimization of processing conditions and post deposition annealing procedures.

6. APPLIED MATERIALS

OSC devices may be categorized with respect to the applied material system and fabrication method. Two classes of donor materials are typically applied as photoactive material in organic solar cells: π-conjugated polymers and π-conjugated molecular materials. While polymers can only be processed from solution, the structure of molecularly defined materials may be optimized for solution- or vacuum-processing. Due to their outstanding n-type charge transport properties, fullerenes C_{60} or C_{70} as well as soluble derivatives [6,6]-phenyl-C_{61}-butyric acid methyl ester ($PC_{61}BM$)[26] or [6,6]-phenyl-C_{71}-butyric acid methyl ester ($PC_{71}BM$)[43] are by far the most commonly used electron acceptor materials.

6.1 POLYMERIC DONOR MATERIALS

Among the large variety of π-conjugated polymers applied in organic solar cells, poly(3-alkylthiophenes) (**P3AT**) are a prominent and extensively investigated class of materials. Regioregular poly(3-hexylthiophene) (**P3HT**, Figure 8) is the most commonly used derivative, as it combines the advantages of good solubility induced by the hexyl substituents and a high charge carrier mobility. The material is efficiently synthesized via Grignard metathesis polymerization of 2,5-dibromo-3-hexylthiophene, developed by McCullough *et al*. in 1999.[44] This method provides great side-chain regioregularity and high molecular weight. Both parameters are of crucial importance for the charge transport properties of the material.[45,46] By optimization of the acceptor material and morphological modifications, the highest power conversion efficiencies, reported for **P3HT**-based bulk heterojunction solar cells, have been increased over the last decade from 4-5%[47] to values over 7%.[48,49]

Inspite of these great results, the frontier energy levels of **P3HT** are not optimal. Due to the relatively high HOMO level of **P3HT**, solar cells made from it in combination with the commonly used fullerene acceptors exhibit rather low open circuit voltages. The polymer has a quite large band gap of about 1.9 eV, which results in an absorption onset at about 650 nm in thin films. Thus, a large part of the solar spectrum in the red and NIR region is not absorbed and cannot contribute to the photo-current. To circumvent these problems, research has focused on donor-acceptor π-conjugated polymers over the recent years. Due to inter-chain charge transfer from electron-rich (donor) to electron-poor (acceptor) repeating units in the conjugated chain, these low band gap polymers show strong absorption in the red and NIR region.[50] A selection of successfully applied polymer donor materials containing the most important building blocks is displayed in Figure 8.

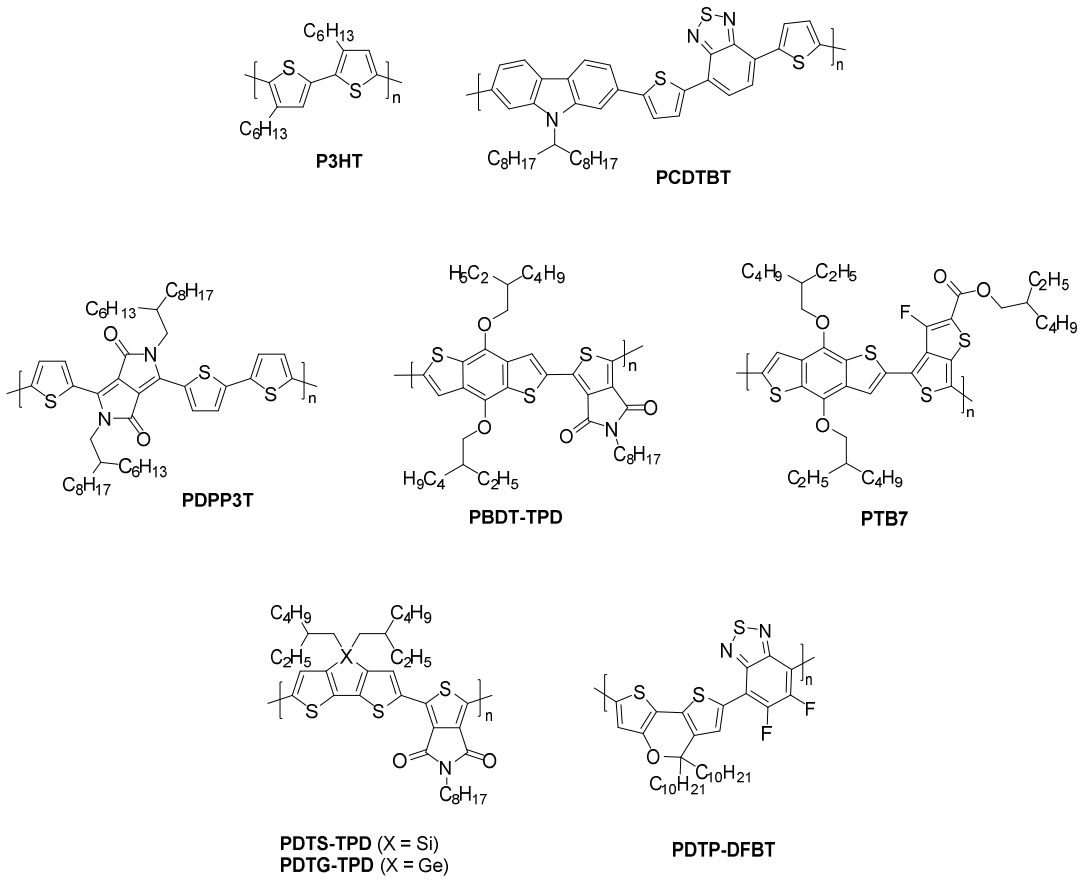

Figure 8. *Molecular structures of high performance polymeric donor materials.*

In 2007, Leclerc *et al.* reported an efficiency of 3.6% for a D-A-co-polymer containig carbazole and benzothiadiazole units (**PCDTBT**)[51] which could be improved to 6.1% by introduction of a solution-processed titanium oxide electron transport layer to the stack of a BHJ device with $PC_{71}BM$ as acceotor.[52] In 2009, Janssen *et al.* presented the low band gap polymer **PDPP3T** combining diketopyrrolopyrrole with terthiophene units which showed photo-response up to 930 nm.[53] By increasing the molecular weight of the polymer and due to optimization of the **PDPP3T**:$PC_{71}BM$ BHJ morphology, the initial PCE value of 4.7% could be improved to 6.7%.[54] In 2010, Frechet *et al.* published a series of N-alkylthieno[3,4-c]pyrrole-4,6-dione (TPD)-based polmers **PBDT-TPD** with variation of the alkyl-substituents on the TPD unit.[55] The octyl-substituted polymer yielded the highest efficiencies of up to 6.8% in BHJ devices with $PC_{61}BM$ due to an enhaced crystallinity of the donor phase determined by grazing inciden X-ray scattering (GIXRD). Recently, power conversion efficiencies over 7% have been realized using highly sophisticated polymeric donor materials using $PC_{71}BM$ as acceptor. In 2010, Yu *et al.* reported a PCE of 7.4% for co-polymer **PTB7**, combining benzo[1,2-b:4,5-b']dithiophene units with fluorinated thieno[3,4-b]thiophene, which stabilizes the quinoid structure, thus reducing the bandgap.[56] In 2012, an impressive efficiency of 9.2% was achieved by Cao *et al.*

applying the **PTB7** donor material in an inverted device structure.[57] Reynolds *et al.* prepared two conjugated polymers by polycondensation of thieno-pyrrolodione with dithienogermole or dithienosilole and obtained an enhanced PCE value of 7.3% for germanium-containing **PDTG-TPD** compared to 6.6% for **PDTS-TPD**.[58] Yang *et. al.* reported an efficiency of 8.0% for regiorandom D-A-polymer **PDTP-DFBT**, prepared by polymerization of electron-rich 5*H*-dithieno[3,2-b:2',3'-d]pyran with the strongly electron-deficient difluorobenzothiadiazole unit.[59] A certified PCE value of 10.6% was obtained, when **PDTP-DFBT** was incorporated with $PC_{61}BM$ in a tandem solar cell setup using **P3HT** and indene-C_{60} bisadduct ICBA in the second subcell.[60]

6.2 Molecular donor Materials for Solution-Processing

Early examples of solution-processed bulk heterojunction devices using so-called small molecules did not exceed performance levels of 3% limited by poor fill factors or low photocurrents.[61] In 2009, a report of Nguyen *et al.* created great attention presenting a power conversion efficiency of 4.4% obtained for a solution-processed BHJ solar cell using D-A-D type benzofuran-substituted thienyl-diketopyrrolopyrrole **DPP(TBFu)$_2$** (Figure 9) as donor in combination with $PC_{71}BM$ as acceptor material.[62] The publication showed, that the morphology of the photoactive blend layer and thus the device performance is highly sensitive to the donor/acceptor ratio and post-deposition thermal treatment. It was found, that the as-cast blend layers were very smooth and showed very little phase separation, which led to poor device performances. Thermal annealing at 110 °C lead to favorable blend layer morphology, boosting the short circuit current density from 1.5 to 10.0 mA/cm^2 and improving the fill factor from 24 to 48% for the optimized D/A blend ratio.

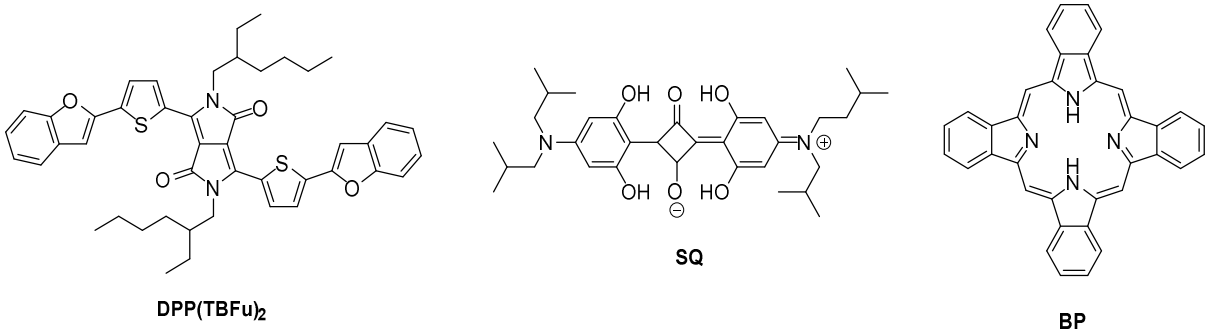

Figure 9. *Molecular structures of oligomeric donor materials for solution-processing.*

In 2011, Forrest *et al.* reported a power conversion efficiency of 5.2% applying squaraine **SQ** (Figure 9) in a BHJ device with $PC_{71}BM$.[63] The squaraine dye was used in a very dilute D:A

mixture of 6:1 to account for the very limited exciton diffusion length and large extinction coefficient of the donor material. Nakamura *et al.* published a PCE value of 5.2% for a BHJ solar cell containing tetrabenzoporphyrin **BP** (Figure 9) as donor and bis(dimethyl-phenylsilylmethyl)[60]fullerenes (SIMEF).[64] The active layer was processed by spin-coating of a solution containing soluble precursor derivative tetraethanotetrabenzoporphyrin and was subsequently converted into the desired insoluble **BP** donor material by thermal treatment.

Bazan and his group systematically developed highly efficient, soluble D^1-A-D^2-A-D^1-type oligomers (Figure 10).[65] In 2011, an efficiency of 6.7% was achieved for the **DTS(PTTh$_2$)$_2$** donor material incorporating electron-rich dithienosilole as central and bithiophene as terminal units in combination with thiadiazolopyridine electron-withdrawing moieties.[66] A small percentage of diiodooctane was used as solvent additive during solution-processing to optimize the domain sizes of the **DTS(PTTh$_2$)$_2$**:$PC_{71}BM$ blend.

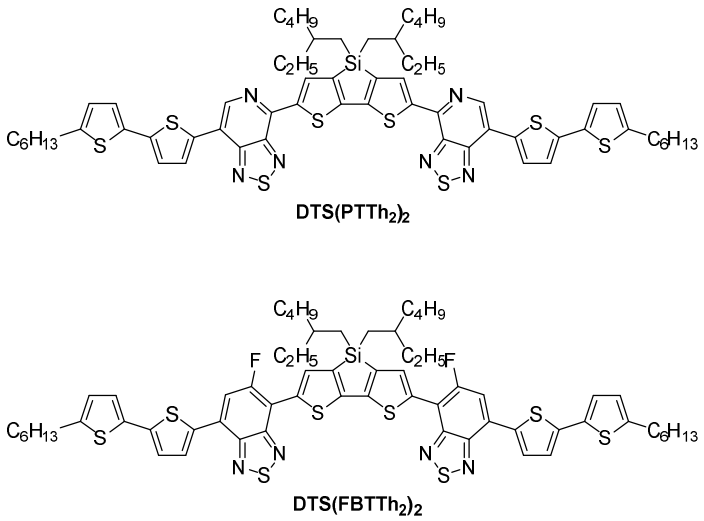

Figure 10. *Molecular structures of D^1-A-D^2-A-D^1-type donor materials developed by Bazan et al.*

A subtle structural modification of the molecular donor material by replacing the thiadiazolopyridine unit by fluorobenzothiadiazole in **DTS(FBTTh$_2$)$_2$** resulted in an increased device performance of 7.0%.[67] By use of a modified ZnO electron transport layer in an inverted device structure an improved efficiency of 7.9% with an impressive J_{SC} value of 15.2 mA/cm^2 was achieved.[68] The introduction of a thin barium interlayer between the aluminium top electrode and the **DTS(FBTTh$_2$)$_2$:**$PC_{71}BM$ layer using the standard device structure resulted in an further enhanced PCE value of 8.6% due to an impressive fill factor of 75%.[69]

Chen and his group systematically investigated high molecular weight oligothiophene-based A-D-A donor materials for application in solution-processed small molecule organic solar cells

(SMOSC) (Figure 11).[70] In 2010, a DCV-capped septithiophene with six solubilizing octyl side-chains (**DCN7T**) was reported. In a solution-processed BHJ device without special treatment, the oligomer showed power conversion efficiencies of up to 2.45% with an impressive J_{SC} value of 10.2 mA/cm^2 and a good V_{OC} of 0.82 V, but a poor fill factor of 29%.[71] By optimization of the device structure, the PCE could be increased to 3.7% due to improvements in FF (0.34) and current density (12.4 mA cm^{-2}).[72] The low fill factors obtained for the **DCN7T**-based devices were ascribed to bad film qualities caused by the poor solubility of the donor material.

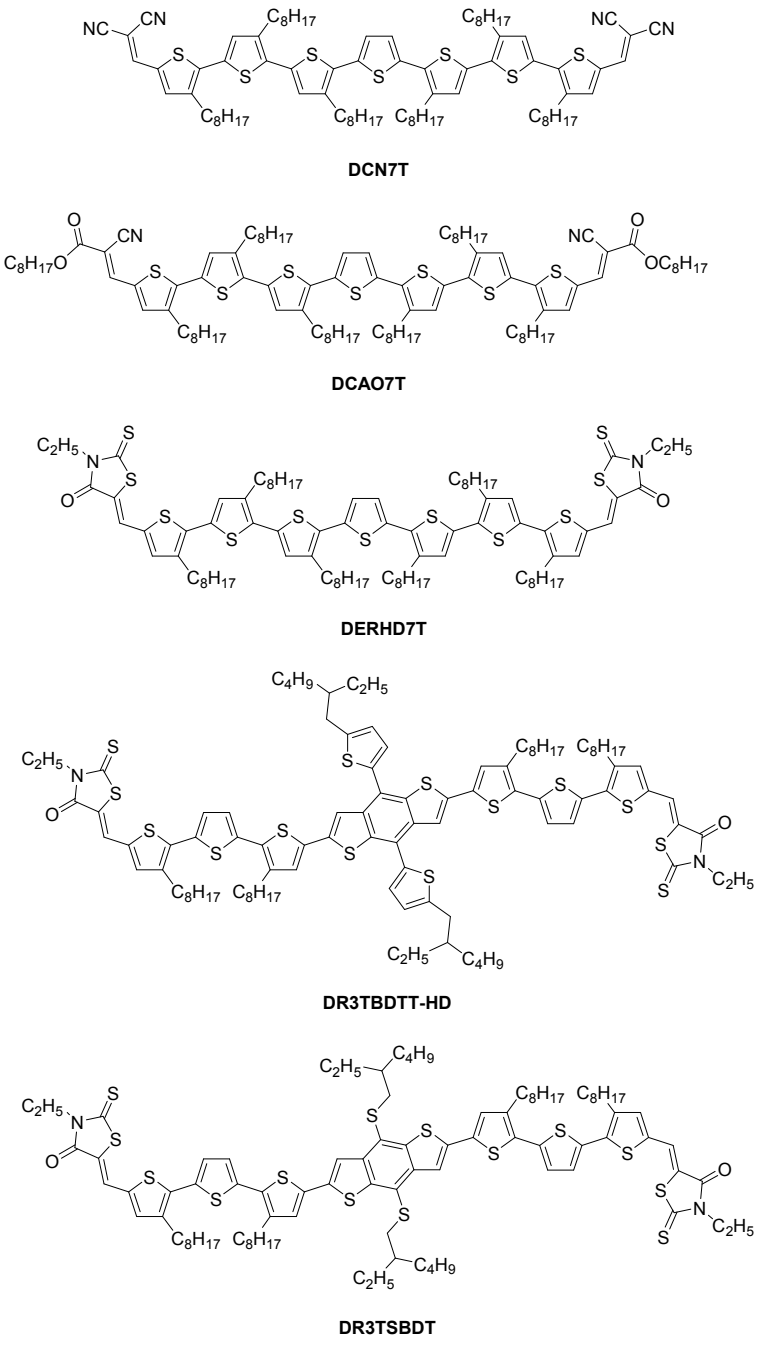

Figure 11. *Molecular structures of A-D-A-type oligothiophene donors developed by Chen et al.*

Replacing the dicyanovinyl units in **DCN7T** by alkyl cyano acetate groups the solubility in chloroform significantly increased to values of up to 204 mg mL^{-1} determined for octyl derivative **DCAO7T**.[73] BHJ solar cells made by spin-coating of **DCAO7T** and $PC_{61}BM$ from chloroform solution exhibited similar J_{SC} and V_{OC} values of up to 10.7 mA cm^{-2} and 0.86 V, respectively, compared to the previously reported **DCN7T**-based devices. Due to a strongly increased fill factor of 55%, a PCE of 5.1% could be obtained.

In 2012, Chen *et al.* attached the ethylrhodanine acceptor unit to the conjugated septithiophene backbone by reaction of the corresponding oligothiophene dialdehyde with 3-ethylrhodanine.[74] The new material (**DERHD7T**) showed a very high molar extinction coefficient of 90'000 L mol^{-1} cm^{-1} exceeding the values determined for **DCN7T** and **DCAO7T**. In the solar cell device, the strong absorption of the new donor material resulted in a remarkable short circuit current density of almost 14 mA cm^{-2} pushing the device performance to 6.1%. In a recent contribution, a series of novel optimized A-D-A-type donor materials based on the **DERHD7T** structure is presented.[75] By replacement of the central thiophene unit of **DERHD7T** with a thienyl-substituted benzodithiophene block, structural planarization and extension of the conjugated π-system is achieved. Under optimized solution-processing conditions using polydimethylsiloxane (PDMS) as solvent additive, an excellent power conversion efficiency of 8.1% has been measured for the best-performing derivative **DR3TBDTT-HD** in combination with $PC_{71}BM$ as the acceptor material. Yang *et al.* reported a PCE of 10.1% for a solution processed homo-tandem device incorporating very similar octyl-rhodanine derivative **SMPV1** in both subcells.[76] In late 2014, a record PCE value of 9.95% was published for a single BHJ device using $PC_{71}BM$ and the further optimized donor material **DR3TSBDT** with dialkylthiol-substituted benzodithiophene as the central building block.[77] A combination of thermal and subsequent solvent vapor annealing was appled to improve the morpology of the photoactive layer, resulting in an outstanding fill factor of 0.74 (V_{OC} = 0.92 V, J_{SC} = 14.6 mA cm^{-2}) for the most efficient solar cell.

6.3 Molecular donor Materials for Vacuum-Processing

Progress in vacuum-processed devices using small molecular donor materials has been enormous since Tang published the first PHJ OSC using copper phthalocyanine (**CuPc**, Figure 12) as donor and perylenetetracarboxylic acid diimide as acceptor.[78] A selection of successful donor materials developed for processing by thermal evaporation is shown in Figure 12. In 2001, Forrest *et al.* achieved an efficiency of 3.6% combining **CuPc** as donor and fullerene C_{60} as acceptor.[79] By optimization of the device structure, the photovoltaic performance of the

CuPc:C_{60}-based solar cells could be improved to 4.2%[80] in 2004 and 5.0%[81] in 2005. Leo and his work group developed efficient OSC device architectures thoroughly investigating the zink phthalocyanine (**ZnPc**):C_{60} donor/acceptor combination. In 2003, p-i-n-type solar cells incurporating a co-evaporated intrinsic BHJ layer sandwiched between p- or n-doped charge transport layers were reported showing efficiencies of up to 1.04% (V_{OC} = 0.50 V, J_{SC} = 6.3 mA cm^{-2}) under AM1.5 illumination.[82] By optimization of the applied charge transport layers an improved PCE value of 1.9% was achieved.[83] In 2004, a power conversion efficiency of 1.44% was published for a m-i-p-type **ZnPc**:C_{60}-based BHJ device using a p-doped hole transport layer below the gold top contact.[84]

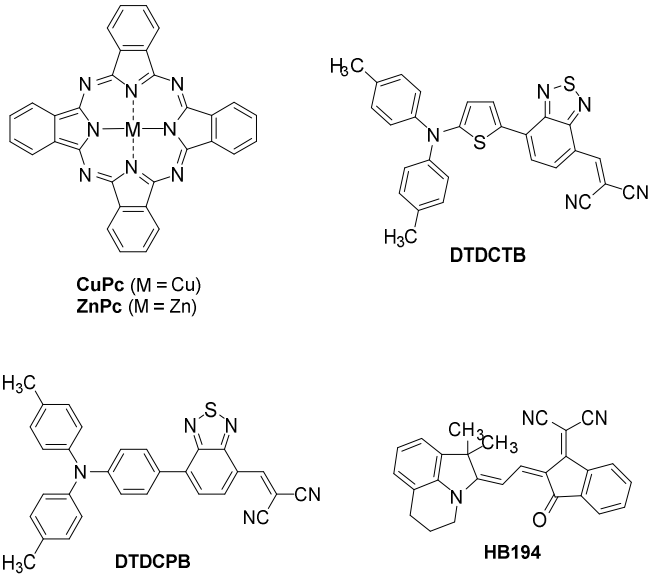

Figure 12. *Molecular structures of selected molecular donor materials designed for vacuum-processing.*

Over the recent years, Wong and co-workers systematically studied very low molecular weight D-A-A-type donor materials bearing dicyanovinyl (DCV) electron-withdrawing groups. In 2011, a PCE value of 5.8% was achieved using fullerene C_{70} as acceptor in combination with **DTDCTB** as donor, in which an electron-donating ditolylaminothienyl moiety and the electron-withdrawing DCV unit are bridged by another electron-accepting benzothiadiazole block.[85] A slight structural variation, replacing the central thiophene moiety by a phenylene unit in **DTDCPB** allowed for an increased device performance of 6.6% for a hybrid planar-mixed heterojunction device with C_{70}.[86] Recently, Holmes et al. achieved a further improved average PCE value of 7.9% for a **DTDCPB**:C_{70}-based solar cell, using a uniform BHJ active layer.[87] In 2011, Würthner *et al.* reported an efficiency of 6.1% for a vacuum-processed BHJ-SMOSC incorporating merocyanine donor **HB194**,[88] which had initially been implemented in solution-processed solar cells.[89]

In 2014, Heremans et al. published a PCE value of 6.0% for a fullerene-free PHJ device incorporating α-sexithiophene (**α-6T**, Figure 13) as donor and boron subnaphthalocyanine chloride (**SubNc**) as acceptor.[90] Combination of **SubNc** with its subphthalocyanine (**SubPc**) homologue as second acceptor material in a three-layer device structure with **α-6T** resulted in an improved efficiency of 8.4% due to an increased photocurrent of 14.6 mA cm^{-2}.

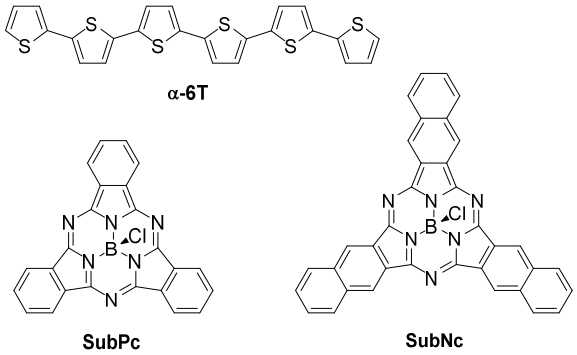

Figure 13. *Molecular structures of photoactive materials used in a three-layer OSC device reported by Heremans et al.*

The Bäuerle group in collaboration with the physics research group of Leo thoroughly investigated alkylated acceptor-substituted oligothiophene donor materials (Figure 14). In 2006, a PCE value of 3.4% under simulated sun light illumination of 118 mW cm^{-2} was published for a vacuum-processed OSC incorporating a PHJ of butyl-substituted DCV-capped quinquethiophene **DCV5T-Bu** and fullerene C_{60} sandwiched between a highly p-doped hole transport layer and a wide-bandgap exciton blocking layer.[91] The device showed a high V_{OC} of 0.98 V as a result of the low lying HOMO energy level corresponding to the large ionization energy of 5.6 eV determined by ultraviolet photoelectron spectroscopy (UPS). In 2007, butylated terthiophene derivative **DCV3T-Bu** was applied as acceptor material in combination with 4,4'-bis-(N,N-diphenylamino)quaterphenyl (4P-TPD) as donor in a m-i-p-type PHJ device structure, reaching a high open circuit voltage of 1.04 V and a moderate power conversion efficiency of 1.6% due to a low J_{SC} value of 3.8 mA cm^{-2}.[92] The admixture of fullerene C_{60} as second acceptor material to the **DCV3T-Bu** layer was shown to lead to an enhanced generation of long-lived triplet excitons on **DCV3T-Bu** caused by an excitonic ping-pong effect with inter-system-crossing on C_{60}. In a study published in 2008, photoinduced absorption (PIA) spectroscopy in combination with quantum-chemical calculations was used to investigate the electron and energy transfer processes at the donor/C_{60} interface for a homologous series of butylated DCV-capped oligothiophene donors from the trimer **DCV3T-Bu** to the hexamer derivative **DCV6T-Bu**.[93] Planar heterojunction solar cells prepared for **DCV4T-Bu**, **DCV5T-Bu** and **DCV6T-Bu** yielded

decreasing V_{OC} values of 1.13, 1.00 and 0.93 V, respectively, from **DCV4T-Bu** to **DCV6T-Bu** which was in accordance with the HOMO energy levels determined by UPS and cyclic voltammetry (CV). At 130 mW cm^{-2} simulated sunlight **DCV5T-Bu** showed the highest efficiency of approximately 4.0% due to larger J_{SC} and FF values compared to **DCV4T-Bu** (η = 1.3%) and for **DCV6T-Bu** (η = 2.3%).

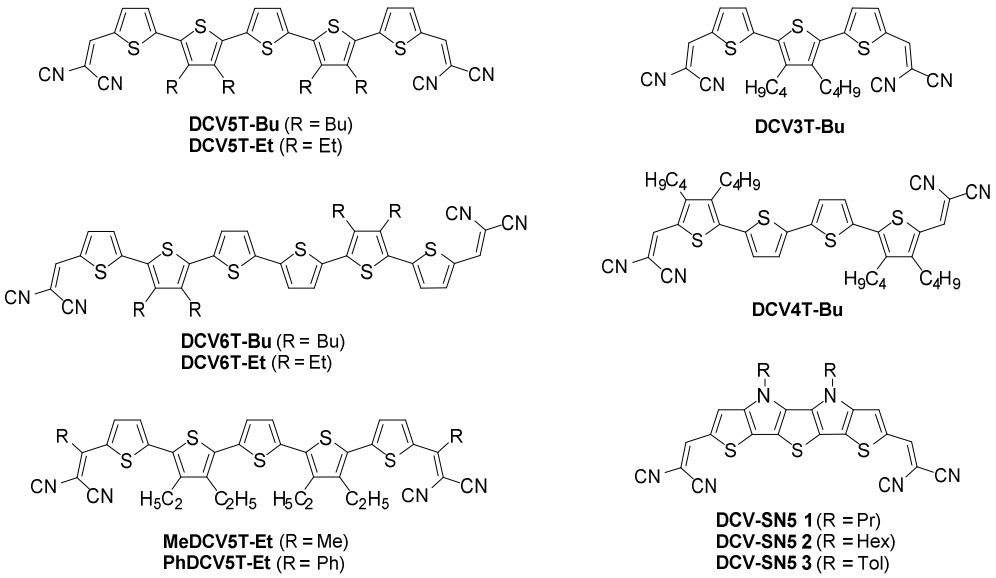

Figure 14. *Molecular structures of selected A-D-A-type oligothiophene donors developed by Bäuerle et al.*

Using the successful **DCV5T-Bu** donor material as a starting point, various structural variations have been realized. Replacement of the butyl substituents by ethyl groups in **DCV5T-Et** repoted in 2008 led to a decreased efficiency of estimated 2.5% in a PHJ device with C_{60} which was due to a lower fill factor in comparison to the **DCV5T-Bu** cell.[94] In 2009, butylated sexithiophene derivative **DCV6T-Bu** was tested in different active layer concepts, showing a PCE value of about 2.1% in the best-performing hybrid planar-mixed heterojunction device architecture.[95] The elongation of the conjugated π-system by one thiophene unit compared to **DCV5T-Bu** resulted in a reduced open circuit voltage of 0.9 V. In 2010, an improved efficiency of 3.8% and a high fill factor of 64% was reported for a BHJ solar cell fabricated by coevaporation of the photoactive layer on a heated substrate combining ethyl-substituted sexithiophene **DCV6T-Et** as donor with C_{60} as acceptor.[96] In a systematic study published in 2011, reduced PCE values of 2.6 and 1.5% in PHJ OSCs using C_{60} as acceptor were reported for the replacement of the vinylic protons of the DCV moiety in **DCV5T-Et** (η = 3.0%) by methyl (**MeDCV5T-Et**) or phenyl (**PhDCV5T-Et**) groups, respectively.[97] Very recently, Bäuerle *et al.* published a series of thiophene-pyrrole-based *S*,*N*-heteroacenes with propyl, hexyl, or tolyl substituents at the ring

nitrogen atoms that provided encouraging efficiencies in m-i-p-type BHJ devices of up to 6.5% determined for propyl derivative **DCV-SN5 1**.[98]

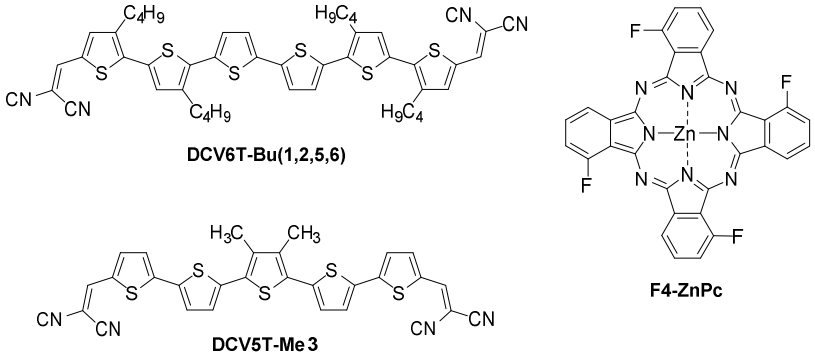

Figure 15. *Molecular structures of selected molecular donor materials designed for vacuum-processing.*

In 2010, Pfeiffer and Leo *et al.* reported a PCE value of 4.9% using regioregularly butyl-substituted sexithiophene **DCV6T-Bu(1,2,5,6)** (Figure 15) in an optimized morphology BHJ solar cell.[99] A tandem device incoporating **DCV6T-Bu(1,2,5,6)** as high energy photon absorbing material in combination with complementary fluorinated zinc phthalocyanine **F4-ZnPc** (Figure 15) in two subcells with fullerene C_{60} yielded an increased efficiency of 6.1%.[100] In 2014, a certified PCE value of 8.3% was published for a single bulk heterojunction solar cell using centrally methylated DCV-substituted quinquethiophene donor **DCV5T-Me** synthesized in this work (Figure 15, Chapter V).[101] When applied in homogeneous double or triple junction devices, consisting of two or three current-matched **DCV5T-Me**:C_{60} subcells even higher record efficiencies of 9.6 or 9.7%, respectively, were realized. The best-perfoming triple junction device showed an impressive fill factor of 72.4%.

REFERENCES

[1] D. Wöhrle, D. Meissner, *Adv. Mater.* **1991**, *3*, 129-138.

[2] A. E. Becquerel, *Comptes Rendus* **1839**, *9*, 145-149.

[3] C. Fritts, *Van Nostrands Engineering Magazine* **1885**, *32*, 388–395.

[4] A. Einstein, *Ann. der Physik* **1905**, *17*, 132-148.

[5] D. M. Chapin, C. S. Fuller, G. L. Pearson, *J. Appl. Phys.* **1954**, *25*, 676-677.

[6] http://www.nrel.gov/ncpv/images/efficiency_chart.jpg; accessed 11/29/2014.

[7] http://www.ise.fraunhofer.de/de/downloads/pdf-files/aktuelles/photovoltaics-report-in-englischer-sprache.pdf; accessed 11/29/2014.

[8] A. Yella, H.-W. Lee, H. N. Tsao, C. Yi, A. K. Chandiran, M. K. Nazeeruddin, E. W.-G. Diau, C.-Y. Yeh, S. M. Zakeeruddin, M. Grätzel, *Science* **2011**, *334*, 629-634.

[9] http://www.heliatek.com/newscenter/latest_news/neuer-weltrekord-fur-organische-solarzellen-heliatek-behauptet-sich-mit-12-zelleffizienz-als-technologiefuhrer/; accessed 11/29/2014.

[10] G. A. Chamberlain, *Solar Cells* **1983**, *8*, 47-83.

[11] G. Horowitz, *Adv. Mater.* **1990**, *2*, 287-292.

[12] D. Wöhrle, D. Meissner, *Adv. Mater.* **1991**, *3*, 129-138.

[13] C. W. Tang, A. C. Albrecht, *Nature* **1975**, *254*, 507-509.

[14] C. W. Tang, A. C. Albrecht, *J. Chem. Phys.* **1975**, *62*, 2139-2149.

[15] C. W. Tang, A. C. Albrecht, *J. Chem. Phys.* **1975**, *63*, 953-961.

[16] A. K. Ghosh, D. L. Morel, T. Feng, R. F. Shaw, J. Charles A. Rowe, *J. Appl. Phys.* **1974**, *45*, 230-236.

[17] V. Y. Merritt, H. J. Hovel, *Appl. Phys. Lett.* **1976**, *29*, 414-415.

[18] D. L. Morel, A. K. Ghosh, T. Feng, E. L. Stogryn, P. E. Purwin, R. F. Shaw, C. Fishman, *Appl. Phys. Lett.* **1978**, *32*, 495-497.

[19] C. W. Tang, *Appl. Phys. Lett.* **1986**, *48*, 183-185.

[20] P. Peumans, A. Yakimov, S. R. Forrest, *J. Appl. Phys.* **2003**, *93*, 3693-3723.

[21] M. Wojcik, M. Tachiya, *J. Chem. Phys.* **2009**, *130*, 104107.

[22] R. A. Street, M. Schoendorf, A. Roy, J. H. Lee, *Phys. Rev. B* **2010**, *81*, 205307.

[23] J. A. Bartelt, Z. M. Beiley, E. T. Hoke, W. R. Mateker, J. D. Douglas, B. A. Collins, J. R. Tumbleston, K. R. Graham, A. Amassian, H. Ade, J. M. J. Fréchet, M. F. Toney, M. D. McGehee, *Adv. Energy Mater.* **2013**, *3*, 364–374.

[24] S. A. Jenekhe, S. Yi, *Appl. Phys. Lett.* **2000**, *77*, 2635-2637.

[25] M. C. Scharber, N. S. Sariciftci, *Prog. Polym. Sci.* **2013**, *38*, 1929-1940.

[26] G. Yu, J. Gao, J. C. Hummelen, F. Wudl, A. J. Heeger, *Science* **1995**, *270*, 1789-1791.

[27] P. K. Watkins, A. B. Walker, G. L. B. Verschoor, *Nano Lett.* **2005**, *5*, 1814-1818.

[28] C. Sachse, L. Müller-Meskamp, L. Bormann, Y. H. Kim, F. Lehnert, A. Philipp, B. Beyer, K. Leo, *Org. Electron.* **2013**, *14*, 143-148.

[29] A. Kaskela, A. G. Nasibulin, M. Y. Timmermans, B. Aitchison, A. Papadimitratos, Y. Tian, Z. Zhu, H. Jiang, D. P. Brown, A. Zakhidov, E. I. Kauppinen, *Nano Lett.* **2010**, *10*, 4349-4355.

[30] S. Bae, H. Kim, Y. Lee, X. Xu, J.-S. Park, Y. Zheng, J. Balakrishnan, T. Lei, H. Ri Kim, Y. I. Song, Y.-J. Kim, K. S. Kim, B. Ozyilmaz, J.-H. Ahn, B. H. Hong, S. Iijima, *Nat. Nanotechnol.* **2010**, *5*, 574-578.

[31] S. Murase, Y. Yang, *Adv. Mater.* **2012**, *24*, 2459–2462.

[32] J. Huang, Z. Yin, Q. Zheng, *Energy Environ. Sci.* **2011**, *4*, 3861–3877.

[33] K. Walzer, B. Männig, M. Pfeiffer, K. Leo, *Chem. Rev.* **2007**, *107*, 1233-1271.

[34] M. Riede, C. Uhrich, J. Widmer, R. Timmreck, D. Wynands, G. Schwartz, W.-M. Gnehr, D. Hildebrandt, A. Weiss, J. Hwang, S. Sudharka, P. Erk, M. Pfeiffer, K. Leo, *Adv. Funct. Mater.* **2011**, *21*, 3019-3028.

[35] C. Falkenberg, K. Leo, M. K. Riede, *J. Appl. Phys.* **2011**, *110*, 124509.

[36] K. A. Emery, C. R. Osterwald, *Solar Cells* **1986**, *17*, 253-274.

[37] V. Shrotriya, G. Li, Y. Yao, T. Moriarty, K. Emery, Y. Yang, *Adv. Funct. Mater.* **2006**, *16*, 2016-2023.

[38] J. C. Bijleveld, M. Shahid, J. Gilot, M. M. Wienk, R. A. J. Janssen, *Adv. Funct. Mater.* **2009**, *19*, 3262-3270.

[39] B. P. Rand, J. Genoe, P. Heremans, J. Poortmans, *Prog. Photovoltaics* **2007**, *15*, 659.

[40] Y. Li, *Acc. Chem. Res.* **2012**, *45*, 723–733.

[41] M. C. Scharber, D. Mühlbacher, M. Koppe, P. Denk, C. Waldauf, A. J. Heeger, C. J. Brabec, *Adv. Mater.* **2006**, *18*, 789-794.

[42] C. Soci, I. W. Hwang, D. Moses, Z. Zhu, D. Waller, R. Gaudiana, C. J. Brabec, A. J. Heeger, *Adv. Funct. Mater.* **2007**, *17*, 632-636.

[43] a) M. M. Wienk, J. M. Kroon, W. J. H. Verhees, J. Knol, J. C. Hummelen, P. A. van Hal, R. A. J. Janssen *Angew. Chem.* **2003**, 115, 3493–3497; b) M. M. Wienk, J. M. Kroon, W. J. H. Verhees, J. Knol, J. C. Hummelen, P. A. van Hal, R. A. J. Janssen, *Angew. Chem. Int. Ed.* **2003**, *42*, 3371-3375.

[44] R. S. Loewe, S. M. Khersonsky, R. D. McCullough, *Adv. Mater.* **1999**, *11*, 250-253.

[45] M. C. Iovu, E. E. Sheina, R. R. Gil, R. D. McCullough, *Macromolecules* **2005**, *38*, 8649-8656.

[46] P. Schilinsky, U. Asawapirom, U. Scherf, M. Biele, C. J. Brabec, *Chem. Mater.* **2005**, *17*, 2175-2180.

[47] W. Ma, C. Yang, X. Gong, K. Lee, A. J. Heeger, *Adv. Funct. Mater.* **2005**, *15*, 1617-1622.

[48] S.-H. Liao, Y.-L. Li, T.-H. Jen, Y.-S. Cheng, S.-A. Chen, *J. Am. Chem. Soc.* **2012**, *134*, 14271–14274.

[49] X. Guo, C. Cui, M. Zhang, L. Huo, Y. Huang, J. Hou, Y. Li, *Energy Environ. Sci.* **2012**, *5*, 7943-7949.

[50] J. Roncali, *Chem. Rev.* **1997**, *97*, 173-206.

[51] N. Blouin, A. Michaud, M. Leclerc, *Adv. Mater.* **2007**, *19*, 2295-2300.

[52] S. H. Park, A. Roy, S. Beaupre, S. Cho, N. Coates, J. S. Moon, D. Moses, M. Leclerc, K. Lee, A. J. Heeger, *Nat. Photon.* **2009**, *3*, 297-302.

[53] J. C. Bijleveld, A. P. Zoombelt, S. G. J. Mathijssen, M. M. Wienk, M. Turbiez, D. M. de Leeuw, R. A. J. Janssen, *J. Am. Chem. Soc.* **2009**, *131*, 16616-16617.

[54] L. Ye, S. Zhang, W. Ma, B. Fan, X. Guo, Y. Huang, H. Ade, J. Hou, *Adv. Mater.* **2012**, *24*, 6335–6341.

[55] C. Piliego, T. W. Holcombe, J. D. Douglas, C. H. Woo, P. M. Beaujuge, J. M. J. Fréchet, *J. Am. Chem. Soc.* **2010**, *132*, 7595-7597.

[56] Y. Liang, Z. Xu, J. Xia, S.-T. Tsai, Y. Wu, G. Li, C. Ray, L. Yu, *Adv. Mater.* **2010**, *22*, E135-E138.

[57] Z. C. He, C. M. Zhong, S. J. Su, M. Xu, H. B. Wu, Y. Cao, *Nat. Photon*. **2012**, *6*, 591-595.

[58] C. M. Amb, S. Chen, K. R. Graham, J. Subbiah, C. E. Small, F. So, J. R. Reynolds, *J. Am. Chem. Soc.* **2011**, *133*, 10062–10065.

[59] L. Dou, C.-C. Chen, K. Yoshimura, K. Ohya, W.-H. Chang, J. Gao, Y. Liu, E. Richard, Y. Yang, *Macromolecules* **2013**, *46*, 3384-3390.

[60] J. You, L. Dou, K. Yoshimura, T. Kato, K. Ohya, T. Moriarty, K. Emery, C.-C. Chen, J. Gao, G. Li, Y. Yang, *Nat. Commun.* **2013**, *4*, 1446.

[61] A. B. Tamayo, X.-D. Dang, B. Walker, J. Seo, T. Kent, T.-Q. Nguyen, *Appl. Phys. Lett.* **2009**, *94*, 103301-103303.

[62] B. Walker, A. B. Tamayo, X.-D. Dang, P. Zalar, J. H. Seo, A. Garcia, M. Tantiwiwat, T.-Q. Nguyen, *Adv. Funct. Mater.* **2009**, *19*, 3063-3069.

[63] G. Wei, S. Wang, K. Sun, M. E. Thompson, S. R. Forrest, *Adv. Energy Mater.* **2011**, *1*, 184-187.

[64] Y. Matsuo, Y. Sato, T. Niinomi, I. Soga, H. Tanaka, E. Nakamura, *J. Am. Chem. Soc.* **2009**, *131*, 16048-16050.

[65] J. E. Coughlin, Z. B. Henson, G. C. Welch, G. C. Bazan, *Acc. Chem. Res.* **2013**, *47*, 257-270.

[66] Y. Sun, G. C. Welch, W. L. Leong, C. J. Takacs, G. C. Bazan, A. J. Heeger, *Nat. Mater.* **2012**, *11*, 44–48.

[67] T. S. van der Poll, J. A. Love, T.-Q. Nguyen, G. C. Bazan, *Adv. Mater.* **2012**, *24*, 3646–3649.

[68] A. K. K. Kyaw, D. H. Wang, V. Gupta, J. Zhang, S. Chand, G. C. Bazan, A. J. Heeger, *Adv. Mater.* **2013**, *25*, 2397–2402.

[69] V. Gupta, A. K. K. Kyaw, D. H. Wang, S. Chand, G. C. Bazan , A. J. Heeger, *Sci. Rep.* **2013**, *3*, 1965.

[70] Y. Chen, X. Wan, G. Long, *Acc. Chem. Res.* **2013**, *46*, 2645-2655.

[71] Y. Liu, X. Wan, B. Yin, J. Zhou, G. Long, S. Yin, Y. Chen, *J. Mater. Chem.* **2010**, *20*, 2464-2468.

[72] B. Yin, L. Yang, Y. Liu, Y. Chen, Q. Qi, F. Zhang, S. Yin, *Appl. Phys. Lett.* **2010**, *97*, 023303.

[73] Y. Liu, X. Wan, F. Wang, J. Zhou, G. Long, J. Tian, J. You, Y. Yang, Y. Chen, *Adv. Energy Mater.* **2011**, *1*, 771-775.

[74] Z. Li, G. He, X. Wan, Y. Liu, J. Zhou, G. Long, Y. Zuo, M. Zhang, Y. Chen, *Adv. Energy Mater.* **2012**, *2*, 74–77.

[75] J. Zhou, Y. Zuo, X. Wan, G. Long, Q. Zhang, W. Ni, Y. Liu, Z. Li, G. He, C. Li, B. Kan, M. Li, Y. Chen, *J. Am. Chem. Soc.* **2013**, *135*, 8484–8487.

[76] Y. Liu, C.-C. Chen, Z. Hong, J. Gao, Y. Yang, H. Zhou, L. Dou, G. Li, Y. Yang, *Sci. Rep.* **2013**, *3*, 3356.

[77] B. Kan, Q. Zhang, M. Li, X. Wan, W. Ni, G. Long, Y. Wang, X. Yang, H. Feng, Y. Chen, *J. Am. Chem. Soc.* **2014**, *136*, 15529.

[78] A. Mishra, P. Bäuerle, *Angew. Chem. Int. Ed.* **2012**, *51*, 2020-2067.

[79] P. Peumans, S. R. Forrest, *Appl. Phys. Lett.* **2001**, *79*, 126-128.

[80] J. Xue, S. Uchida, B. P. Rand, S. R. Forrest, *Appl. Phys. Lett.* **2004**, *84*, 3013-3015.

[81] J. Xue, B. P. Rand, S. Uchida, S. R. Forrest, *Adv. Mater.* **2005**, *17*, 66-71.

[82] D. Gebeyehu, B. Männig, J. Drechsel, K. Leo, M. Pfeiffer, Sol. Energy Mater. Sol. Cells 2003, 79, 81-92.

[83] J. Drechsel, B. Männig, F. Kozlowski, D. Gebeyehu, A. Werner, M. Koch, K. Leo, M. Pfeiffer, *Thin Solid Films* **2004**, 451-452, 515-517.

[84] J. Drechsel, B. Männig, D. Gebeyehu, M. Pfeiffer, K. Leo, H. Hoppe, *Org. Electron.* **2004**, *5*, 175-186.

[85] L.-Y. Lin, Y.-H. Chen, Z.-Y. Huang, H.-W. Lin, S.-H. Chou, F. Lin, C.-W. Chen, Y.-H. Liu, K.-T. Wong, *J. Am. Chem. Soc.* **2011**, *133*, 15822–15825.

[86] Y.-H. Chen, L.-Y. Lin, C.-W. Lu, Z.-Y. Huang, H.-W. Lin, F. Lin, P.-H. Wang, Y.-H. Liu, K.-T. Wong, J. Wen, D. J. Miller, S. B. Darling, *J. Am. Chem. Soc.* **2012**, *134*, 13616–13623.

[87] Y. Zou, J. Holst, Y. Zhang, R. J. Holmes, *J. Mater. Chem. A* **2014**, *2*, 12397-12402.

[88] V. Steinmann, N. M. Kronenberg, M. R. Lenze, S. M. Graf, D. Hertel, K. Meerholz, H. Bürckstümmer, E. V. Tulyakova, F. Würthner, *Adv. Energy Mater.* **2011**, *1*, 888-893.

[89] H. Burckstummer, N. M. Kronenberg, M. Gsanger, M. Stolte, K. Meerholz, F. Wurthner, *J. Mater. Chem.* **2010**, *20*, 240-243.

[90] K. Cnops, B. P. Rand, D. Cheyns, B. Verreet, M. A. Empl, P. Heremans, *Nat. Commun.* **2014**, *5*, 3406.

[91] K. Schulze, C. Uhrich, R. Schüppel, K. Leo, M. Pfeiffer, E. Brier, E. Reinold, P. Bäuerle, *Adv. Mater.* **2006**, *18*, 2872–2875.

[92] C. Uhrich, R. Schueppel, A. Petrich, M. Pfeiffer, K. Leo, E. Brier, P. Kilickiran, P. Bäuerle, *Adv. Funct. Mater.* **2007**, *17*, 2991.

[93] R. Schueppel, K. Schmidt, C. Uhrich, K. Schulze, D. Wynands, J. L. Brédas, E. Brier, E. Reinold, H.-B. Bu, P. Bäuerle, B. Männig, M. Pfeiffer, K. Leo *Phys. Rev. B*, **2008**, *77*, 085311.

[94] K. Schulze, M. Riede, E. Brier, E. Reinold, P. Bäuerle, K. Leo, *J. Appl. Phys.* **2008**, *104*, 074511.

[95] D. Wynands, B. Männig, M. Riede, K. Leo, E. Brier, E. Reinold, P. Bäuerle, *J. Appl. Phys.* **2009**, *106*, 054509.

[96] D. Wynands, M. Levichkova, M. Riede, M. Pfeiffer, P. Bäuerle, R. Rentenberger, P. Denner, K. Leo, *J. Appl. Phys.* **2010**, *107*, 014517.

[97] A. Mishra, C. Uhrich, E. Reinold, M. Pfeiffer, P. Bäuerle, *Adv. Energy Mater.* **2011**, *1*, 265-273.

[98] A. Mishra, D. Popovic, A. Vogt, H. Kast, T. Leitner, K. Walzer, M. Pfeiffer, E. Mena-Osteritz, P. Bäuerle, *Adv. Mater.* **2014**, *26*, 7217-7223.

[99] D. Wynands, M. Levichkova, K. Leo, C. Uhrich, G. Schwartz, D. Hildebrandt, M. Pfeiffer, M. Riede, *Appl. Phys. Lett.* **2010**, *97*, 073503.

[100] M. Riede, C. Uhrich, J. Widmer, R. Timmreck, D. Wynands, G. Schwartz, W.-M. Gnehr, D. Hildebrandt, A. Weiss, J. Hwang, S. Sundarraj, P. Erk, M. Pfeiffer, K. Leo, *Adv. Funct. Mater.* **2011**, *21*, 3019–3028.

[101] R. Meerheim, C. Körner, K. Leo, *Appl. Phys. Lett.* **2014**, *105*, 253508.

CHAPTER II

OVERVIEW OF THE THESIS

CHAPTER III: DICYANOVINYL–SUBSTITUTED OLIGOTHIOPHENES: STRUCTURE-PROPERTY RELATIONSHIPS AND APPLICATION IN VACUUM-PROCESSED SMALL MOLECULE ORGANIC SOLAR CELLS

The initial publication, reproduced in Chapter III, presents a series of alkyl-free terminally dicyanovinyl-substituted oligothiophene molecules (**DCVnT**) comprising one to six thiophene units. Based on the experience with butyl or ethyl-substituted DCV-capped oligothiophenes,[1-8] the series was designed to optimize the molecular structures for vacuum-processing. By omitting solubilizing alkyl sidechains and lowering of the molecular weight improved thermal stabilities and sublimation properties were envisaged.

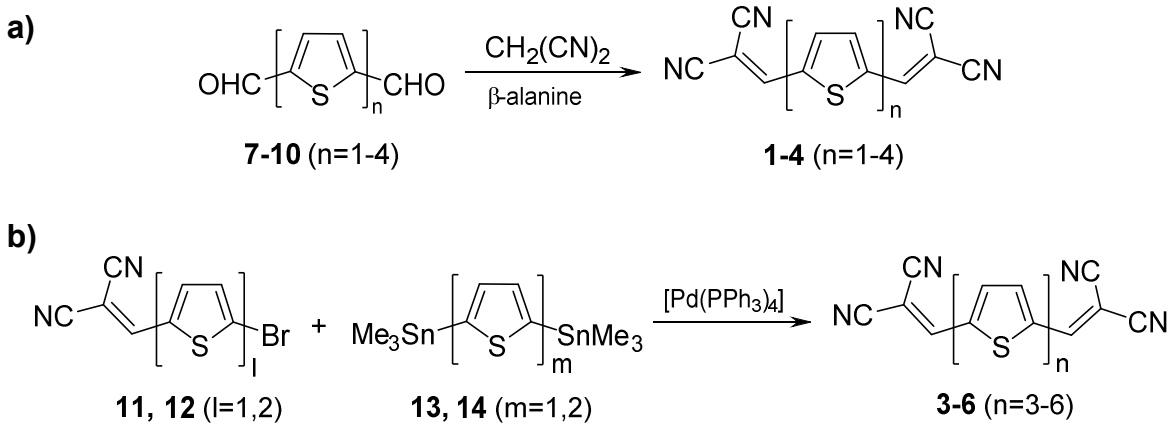

Scheme 1. *Synthesis of* ***DCVnTs*** *via (a) Knoevenagel condensation or (b) Stille-type cross-coupling reactions.*

The shorter oligomers up to the trimer **DCV3T** were prepared by Knoevenagel condensation of the corresponding parent dialdehydes with malononitrile analogous to the synthetic strategy used for the synthesis of the alkylated **DCVnTs** (Scheme 1a).[9] Due to the already very low solubility of the mono-reacted intermediate products, this synthetic approach failed for the longer homologues. For the oligomers **DCV4T** to **DCV6T** a novel efficient synthetic route

using Pd-catalysed Stille-type cross-coupling of brominated DCV-capped terminal building blocks with stannylated central building blocks was developed. Final purification of the very low-soluble target compounds (compare Chapter VI) was achieved by Soxhlet extraction and thermal gradient vacuum sublimation.

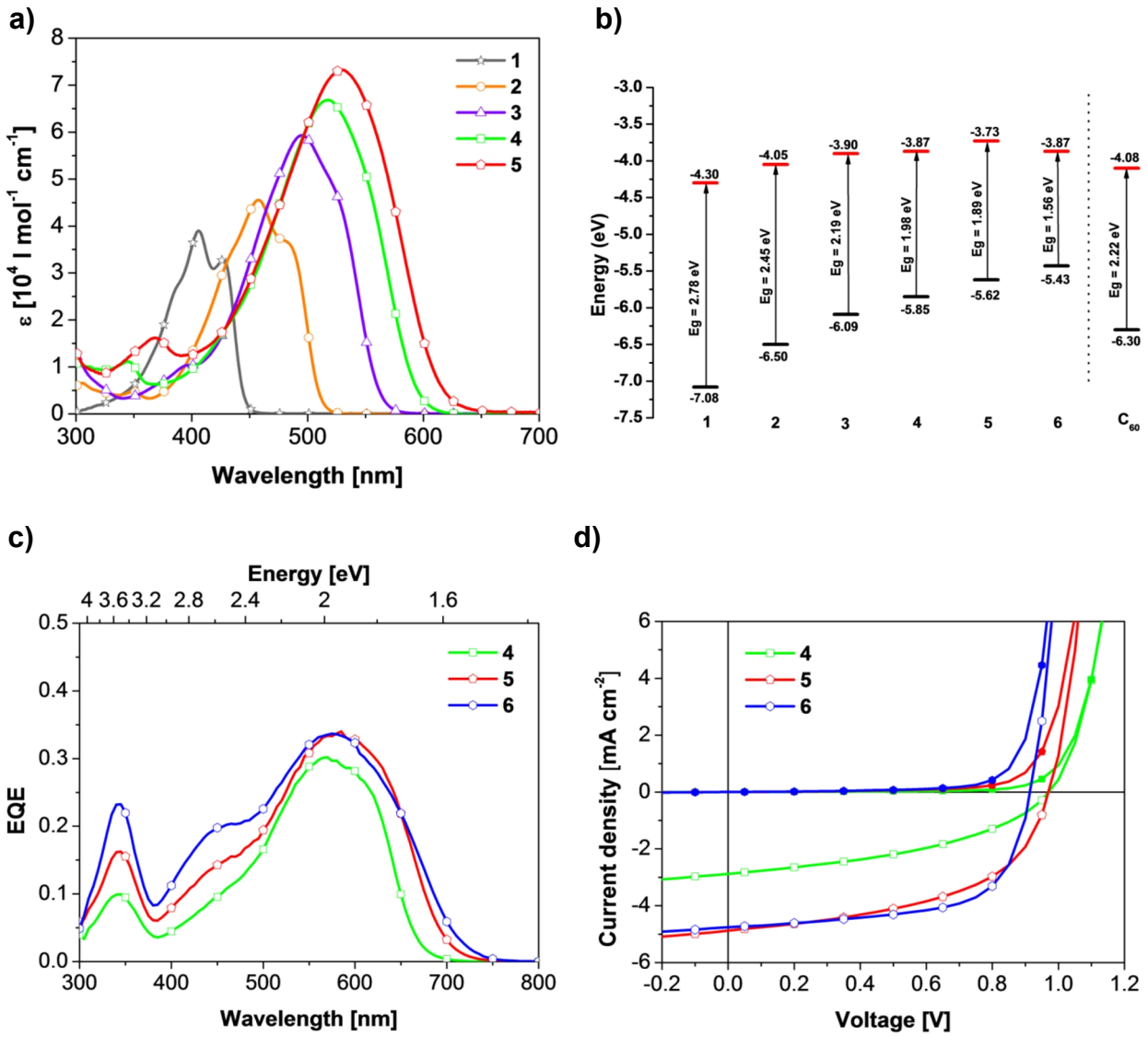

Figure 1. *Optoelectronic and photovoltaic data for alkyl-free* ***DCVnTs 1-6****: (a) UV-vis absorption spactra measured in dichloromethane solution and (b) frontier orbital energy levels derived from electrochemical data. (c) External quantum efficiency spectra and (d) current-voltage characteristics of planar heterojunction solar cells (m-i-p device architecture) using* ***DCVnTs 4-6*** *as donor materials.*

Analysis of the thermal properties by differential scanning calorimetry (DSC) revealed good thermal stabilities and high melting points, which showed an odd-even effect with respect to the number of thiophene units. This was assigned to the different symmetries of odd and even numbered **DCVnTs** obtained from semi-empirical Austin model 1 (AM1) geometry optimi-

zation calculations. X-ray structure analysis of a **DCV4T** single crystal obtained by gradient vacuum sublimation revealed close π-π-stacking and important intermolecular CN···H interactions induced by the DCV acceptor units. The **DCV4T** crystal structure is further discussed in Chapter IV. UV-vis spectroscopy revealed a red-shift of the absorption maximum in solution accompanied by an increase in molar extinction coefficients going from **DCV1T** to **DCV6T** (Figure 1a). Using cyclic voltammetry (CV), the lowering of the band gap with increasing oligothiophene chain-length was assigned to increasing HOMO energies, while the LUMO levels stayed relatively unaffected (Figure 1b). **DCV4T** to **DCV6T** showed adequate frontier orbital energies for the application in D/A heterojunction solar cells with C_{60} as the acceptor. In a comparative study, the three longer oligomers were applied as neat donor layers in vacuum-processed m-i-p-type planar heterojunction solar cells. The **DCV5T** and **DCV6T** devices showed similar PCEs of 2.6 and 2.8%, respectively, compared to 1.2% for **DCV4T** (Figure 1d). The improved performance was mainly due to increased short circuit densities in accordance with the EQE spectra (Figure 1c) which was assigned to the thin film absorption properties of the oligomers. The measured increase in HOMO energies was reflected in the open circuit voltages values of **DCV5T** and **DCV6T**, whereas **DCV4T** showed the same V_{OC} as **DCV5T**.

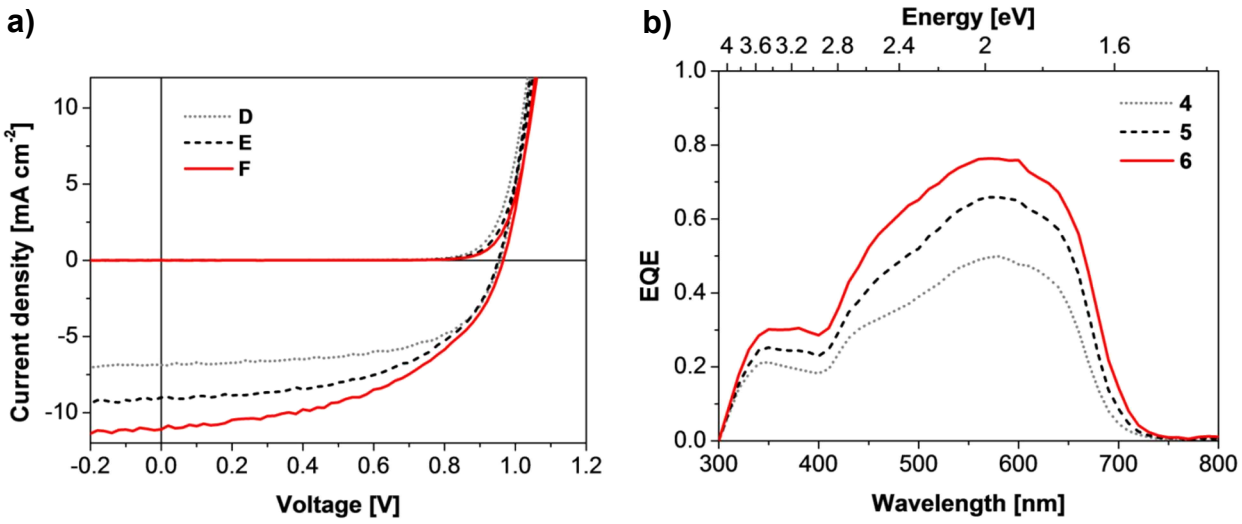

Figure 2. *(a) External quantum efficiencies and (b) current-voltage characteristics of bulk-hetrojunction devices (p-i-n setup) containing* ***DCV5T****:C_{60} active layers in thicknesses of 20, 30 and 40 nm (dotted, dashed and solid lines, respectively).*

The quinquethiophene derivative was additionally investigated in bulk heterojunction solar cells (n-i-p architecture) using co-evaporated **DCV5T**:C_{60} blends of different thicknesses as photoactive layers. With growing thickness of the BHJ layer, J_{SC} significantly increased due to intensified absorption (Figure 2b) over-compensating the decrease in fill factor caused by the

lower charge collection efficiency of the thicker mixed layers. The 40 nm BHJ device showed the best power conversion efficiency of 5.2%, which was one of the highest values reported for vacuum-processed single junction devices at that time.

CHAPTER IV: INTERRELATION BETWEEN CRYSTAL PACKING AND SMALL MOLECULE ORGANIC SOLAR CELL PERFORMANCE

In the second study, the influence of small alkyl substituents attached to the oligothiophene backbone on molecular packing and photovoltaic performance was investigated in a series of DCV-capped quaterthiophenes. Alkyl-free **DCV4T** presented in the previous chapter was compared to methyl- or ethyl-substituted derivatives **DCV4T-Me** and **DCV4T-Et**. The alkylated DCV-capped quaterthiophenes were prepared using the synthetic strategy developed for the synthesis of the longer low soluble alkyl-free **DCVnTs**. Methyl- or ethyl-substituted DCV-capped bromothiophene building blocks were reacted with bisstannylated bithiophene in Stille-type cross-coupling reactions (Figure 3a). Final purification of the low soluble target compounds, which precipitated from the reaction mixture, was achieved by Soxhlet extraction. The investigation of the optoelectronic properties by UV-vis spectroscopy (Figure 3b) and cyclic voltammetry measurements performed on hot tetrachloroethane solutions yielded similar optical band gaps and frontier orbital energy values for all three quaterthiophenes. In thin film, the **DCV4T-Me** absorption band showed the largest red-shift compared to the solution spectrum and exhibited the most intense low-energy shoulder in the oligomer series. This was interpreted as a sign for efficient planarization and aggregation of the **DCV4T-Me** molecules in the bulk. To compare the photovoltaic performances, vacuum-processed m-i-p-type bulk heterojunction solar cells with photoactive quaterthiophene:C_{60} blend layers were prepared for all three **DCV4T** oligomers (Figure 3c). The **DCV4T-Me** device showed the highest power conversion efficiency of 3.8% clearly outperforming the **DCV4T-Et** (2.2%) and **DCV4T** (1.5%) cells due to superior short circuit current density and fill factor values. Differential scanning calorimetry revealed similar melting temperatures for **DCV4T** and **DCV4T-Et** (Figure 3d), whereas **DCV4T-Me** showed no melting before decomposition. This finding indicated the strongest intermolecular interactions in the series for the methylated derivative. Similar to non-alkylated **DCV4T** both alkylated quaterthiophenes showed very good thermal stabilities and gave high sublimation yields.

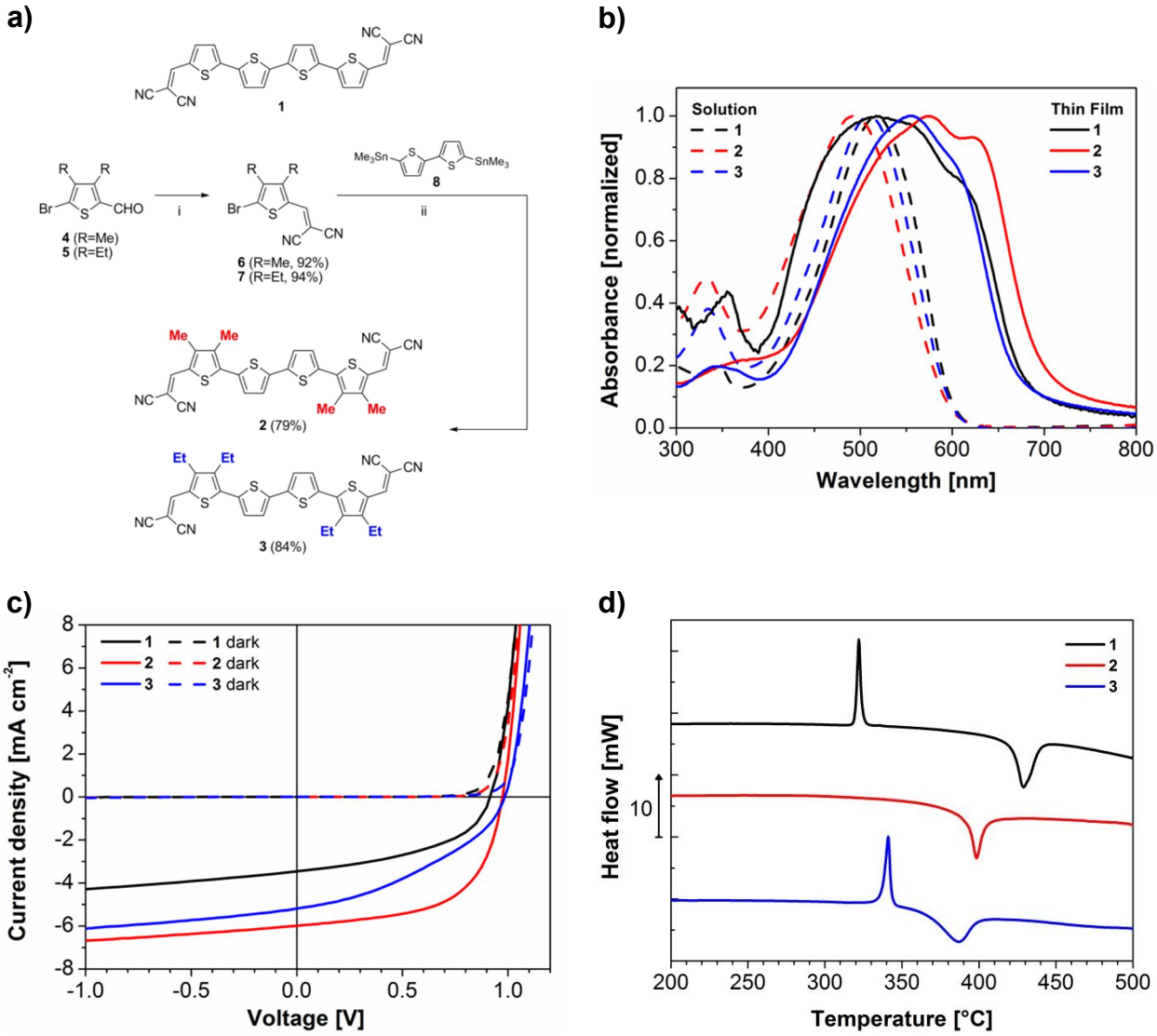

Figure 3. *(a) Synthesis of* ***DCV4T-Me 2*** *and* ***DCV4T-Et 3.*** *Reagents: i) $CH_2(CN)_2$, β-alanine, ethanol/dichloroethane, reflux; ii) $Pd(PPh_3)_4$, DMF, 80 °C. (b) Solution and thin film absorption profiles and (d) differential scanning calorymetry traces of* ***DCV4Ts 1-3****. (c) Current-voltage characteristics of bulk-hetrojunction devices (m-i-p setup) containing* ***DCV4T 1-3****:C_{60} active layers.*

Single crystals of suitable size for structure analysis by XRD could be obtained for all **DCV4Ts** by thermal gradient sublimation. The analysis of intermolecular close contacts shorter than the van-der-Waals distance, corresponding to non-bonding interactions, revealed the highest number of short distances for **DCV4T-Me**, which formed a perfect layer structure and displayed effective π-π-stacking (Figure 4). Grazing incidence X-ray diffraction (GIXRD) measurements on a vacuum-processed mixed layer with C_{60} suggested the formation of crystalline **DCV4T-Me** domains within the blend, which exhibited similar molecular packing as observed in the single crystal structure. The superior device performance of methylated **DCV4T-Me** within the series

of quaterthiophenes was correlated to improved solid state properties, which are decisive for efficient functioning of bulk heterojunction solar cells.

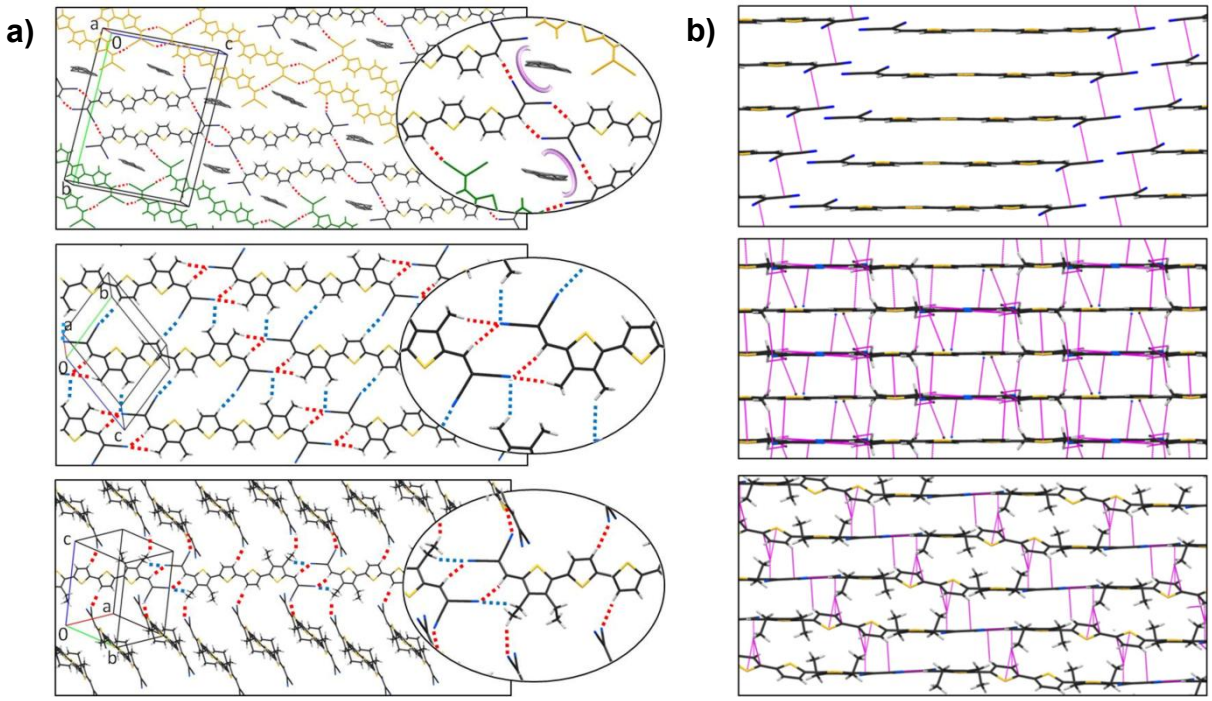

Figure 4. *Single crystal packing (a) in the molecular plane and (b) perpendicular to the molecular plane for* ***DCV4T*** *(top),* ***DCV4T-Me*** *(center) and* ***DCV4T-Et*** *(bottom).*

CHAPTER V:
CORRELATION OF Π-CONJUGATED OLIGOMER STRUCTURE WITH FILM MORPHOLOGY AND ORGANIC SOLAR CELL PERFORMANCE

Encouraged by the excellent solar cell results obtained for methylated **DCV4T-Me**, in the next project a series of methyl-substituted DCV-capped quinquethiophenes **DCV5T-Me 1-3** was investigated. Within this series, going from **DCV5T-Me 1** to **3**, the positioning of the methyl substituents along the conjugated oligomer backbone was systematically varied from the terminal thiophene units to the central ring.

The three **DCV5T-Me** oligomers were prepared by Stille-type cross-coupling reactions of bisstannylated monothiophene central blocks with brominated DCV-capped bithiophenes (Scheme 2). The methylated terminal building blocks were synthesized by Stille- or Suzuki-type coupling of bromothiophene carbaldehydes with stannylated or borylated thiophenes, followed by bromination with n-bromosuccinimide and Knoevenagel condensation with malononitrile.

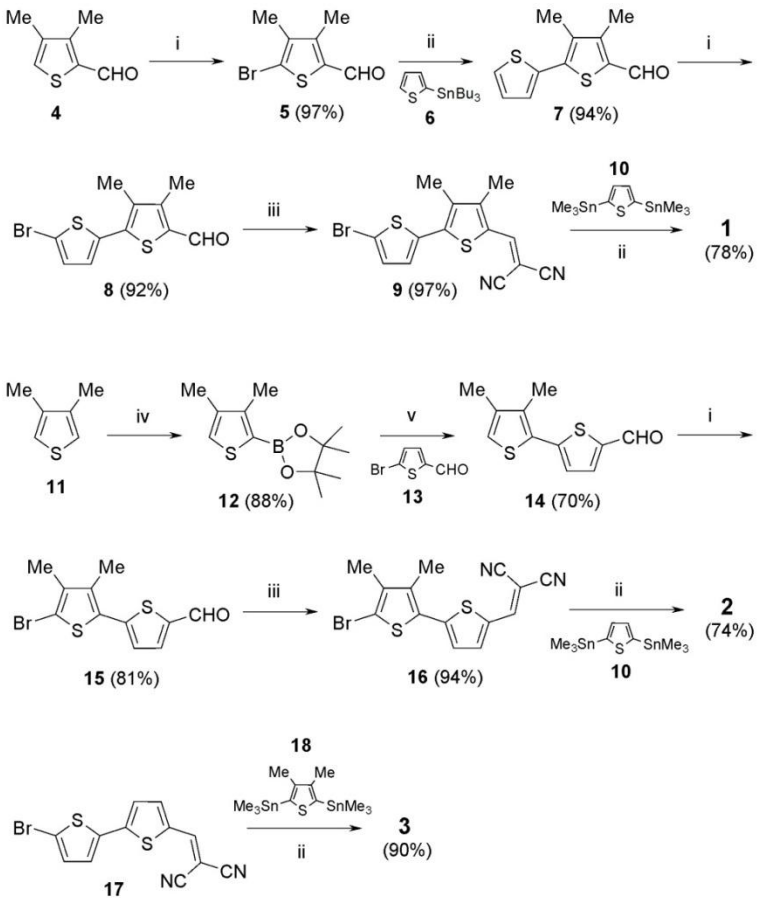

Scheme 2. *Synthesis of DCV-capped quinquethiophenes* ***DCV5T-Me 1-3****. Reagents: (i) NBS, DMF; (ii)* $Pd(PPh_3)_4$*, DMF; (iii)* $CH2(CN)_2$*, β-alanine, EtOH/dichloroethane; (iv) 1. n-BuLi, THF; 2. 2-isopropoxy-4,4,5,5-tetramethyl[1,3,2]dioxoborolane; (v)* K_2CO_3*,* $Pd(PPh_3)_4$*, THF.*

All **DCV5T-Me** derivatives exhibited high thermal stabilities with decomposition temperatures of about 370 °C determined by DSC and thermal gravimetric analysis (TGA). Compared to alkyl-free derivative **DCV5T** (Chapter III), the melting points of the methylated pentamers were significantly increased, with the highest value for terminally substituted **DCV5T-Me 1**, which indicated intensified intermolecular interactions in the bulk. A single crystal of **DCV5T-Me 3** obtained from thermal gradient sublimation was investigated by X-ray structure analysis showing efficient molecular packing and the formation of rows by linear arrangement of the long molecular axes similar to the **DCV4T-Me** crystal structure (Chapter IV). In analogy to the quaterthiophene series (Chapter IV), UV-vis solution spectra (Figure 5a) and electrochemically determined frontier orbital energies were almost identical for all **DCV5T-Me** derivatives, irrespective of the number and positioning of the methyl substituents along the oligothiophene backbone. In thin film absorption spectra, **DCV5T-Me 3** showed the most prominent low-energy shoulder indicating favorable molecular ordering in the bulk. All three derivatives were used as donor material in m-i-p-type bulk heterojunction solar cells with C_{60} as the acceptor

using a very similar layer structure as in the case of the quaterthiophene series (Chapter IV). The **DCV5T-Me 1** and **2** devices showed good photovoltaic performances with similar J_{SC} and FF values and identical power conversion efficiencies of 4.8% (Figure 5b). Oligomer **DCV5T-Me 3**, however, bearing methyl substituents at the central thiophene ring yielded an even higher power conversion efficiency of 6.1% due to an increased short circuit density and an excellent fill factor of 66%.

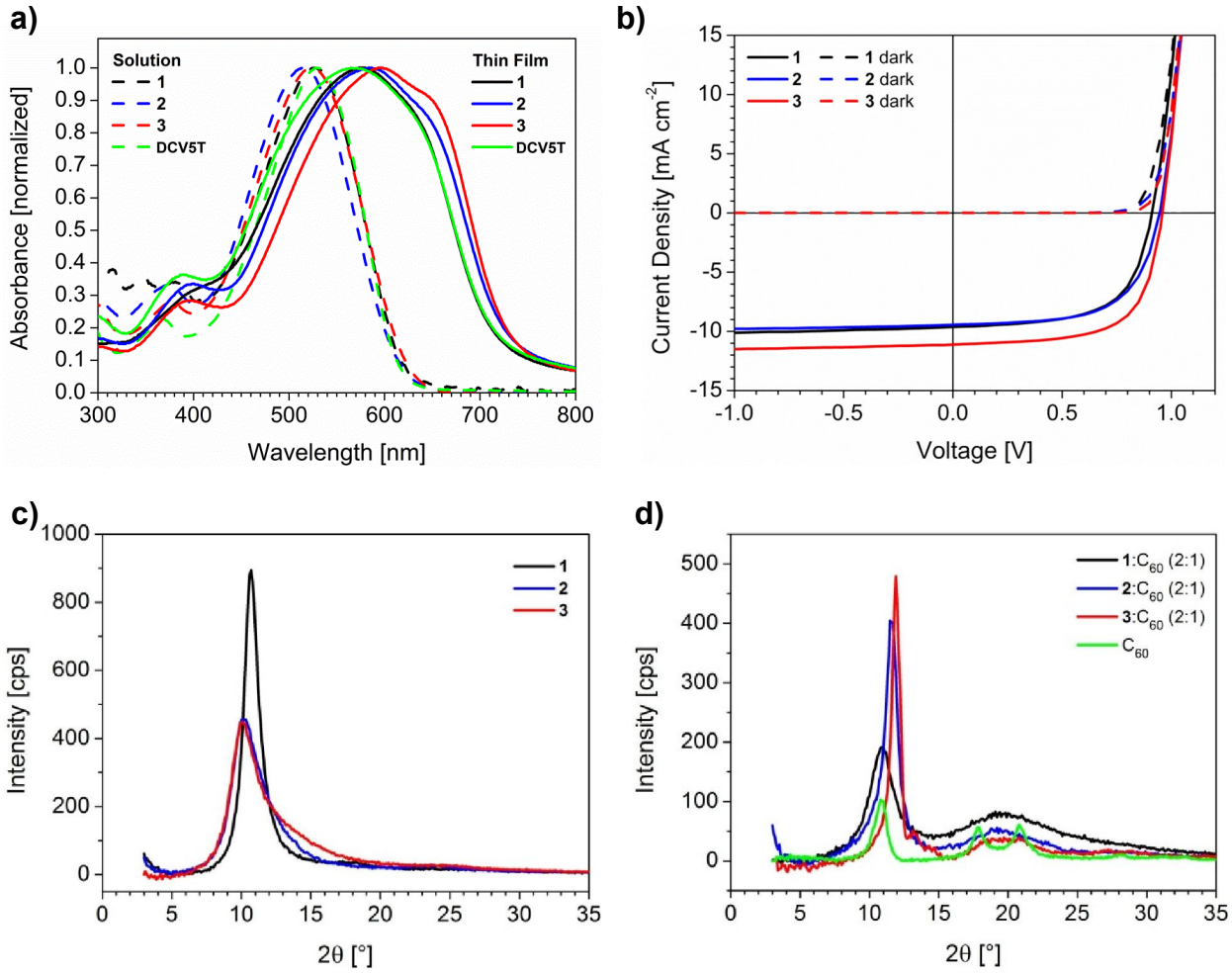

Figure 5. *(a) Solution and thin film absorption spectra of the* ***DCV5T-Me 1-3****. (b) Current-voltage curves of bulk-hetrojunction devices (m-i-p setup) containing* ***DCV5T-Me 1-3****:C_{60} active layers. GIXRD patterns of vacuum-processed (c)* ***DCV5T-Me 1-3*** *neat layers and (d) blend layers with C_{60}.*

In an optimized stack (n-i-p-type) comprising an additional n-doped electron transport layer and modified deposition conditions of the bulk heterojunction layer, the photovoltaic performance was further increased to values up to 6.9% with an average of 6.7% over 32 devices. Thus, methylated **DCV5T-Me 3** yielded a considerably improved PCE compared to the 5.2% efficiency obtained for alkyl-free **DCV5T** (Chapter III) confirming that methyl substituents may

be used to optimize the performance of oligothiophene donors in bulk-heterojunction solar cells. The morphology of vacuum-processed films of neat donor material and D/A mixed layers was investigated by GIXRD and X-ray reflection (XRR) measurements to rationalize the different photovoltaic performances of **DCV5T-Me 1-3**. In contrast to the neat films, in which terminally substituted derivative **1** formed the largest crystallites in the series, the analysis of the blend layers surprisingly showed increasing crystallinity of donor and acceptor material going from **DCV5T-Me 1** to **3**. The superior performance of **DCV5T-Me 3** was correlated to the higher crystallinity of both photoactive components in the blend corresponding to a larger D-A phase separation.

CHAPTER VI: A-D-A-TYPE OLIGOTHIOPHENES FOR SMALL MOLECULE ORGANIC SOLAR CELLS: EXTENDING THE Π-SYSTEM BY INTRODUCTION OF RING-LOCKED DOUBLE BONDS

In the next Chapter, a series of oligothiophenes up to the tetramer terminally substituted with dicyanomethylene-cyclohexene (DCC) units is presented. Optoelectronic, thermal, and photovoltaic behavior as well as single crystal packing are investigated and contrasted to the properties of the DCV-capped oligomers to examine the effect of the introduction of additional C-C double bonds to the conjugated π-system. Inspired by the increase in photovoltaic performance found for methylated **DCV5T-Me 3** (Chapter V) compared to unsubstituted **DCV5T** (Chapter III), methylated terthiophene **DCC3T-Me** was included in the series of alkyl-free oligomers. The cyclohexene ring structure was chosen to lock the double bonds into the *trans* conformation avoiding stereoisomerism.

In order to introduce the DCC terminal unit to the thiophene α-position, cyclohexenone rings were first attached by Stille-type cross-coupling reaction or quenching of lithiated thiophene with methoxycyclohexenone followed by Knoevenagel condensation with malononitrile (Scheme 3). The shorter oligomers **DCC1T** and **DCC2T** were prepared from the diketo precursors **4** and **5**. Twofold Stille-type cross-coupling reactions of DCC-capped bromothiophene **9** with bisstannylated central building blocks were used to synthesize the longer and less soluble terthiophene and quaterthiophene derivatives.

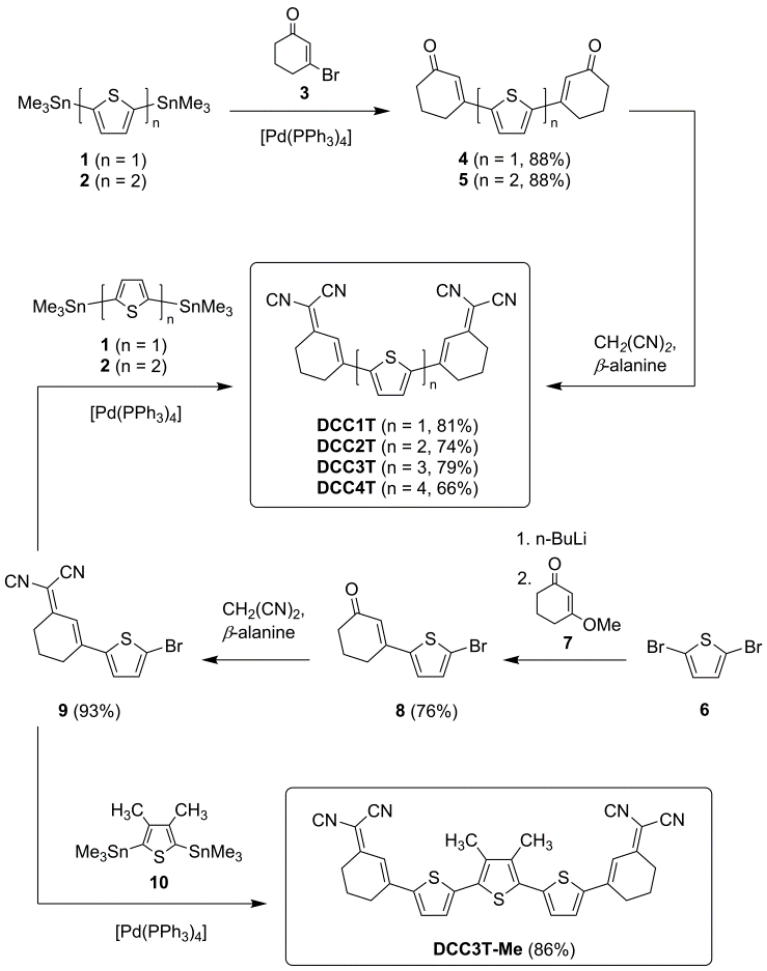

Scheme 3. *Synthesis of the DCC-capped oligothiophenes* ***DCCnT****.*

From the DSC experiments it was found that the **DCCnT** oligomers showed a high, but somewhat reduced thermal stability compared the **DCVnTs**. Gradient sublimation was performed for all oligomers providing crystalline material in almost quantitative yields up to the terthiophene derivatives. Tetramer **DCC4T** showed significant thermal degradation at the elevated temperature required for the sublimation of the relatively high molecular weight material. Trends in melting temperatures and maximum solubilities as a function of the number of thiophene units in the conjugated molecular backbone were analyzed and compared to the properties of the corresponding DCV-substituted oligothiophenes (Figure 6a). While the maximum solubilities in dichloromethane were increased, the **DCCnTs** showed higher melting temperatures compared to the **DCVnTs**, which was assigned to stronger intermolecular interactions. The odd-even effect of the melting points with respect to the number of thiophene units observed for the **DCVnTs** (Chapter V) was retained in the **DCCnT** series. XRD analysis of a **DCC3T-Me** single crystal obtained by vacuum sublimation revealed efficient molecular packing with remarkable similarities to the **DCV5T-Me 3** crystal structure presented in Chapter V.

Optical solution spectroscopy revealed that the bathochromic shift of the absorption band caused by the introduction of the two additional DCC double bonds was equal to the effect of adding one thiophene unit to the conjugated π-system (Figure 6b). Cyclic voltammetry measurements and theoretical investigations showed that despite having the same energy gap, the HOMO/ LUMO energy levels of the **DCCnTs** were raised compared to the corresponding **DCV(n+1)Ts** indicating an improved donor and reduced acceptor strength of the DCC-acceptor unit.

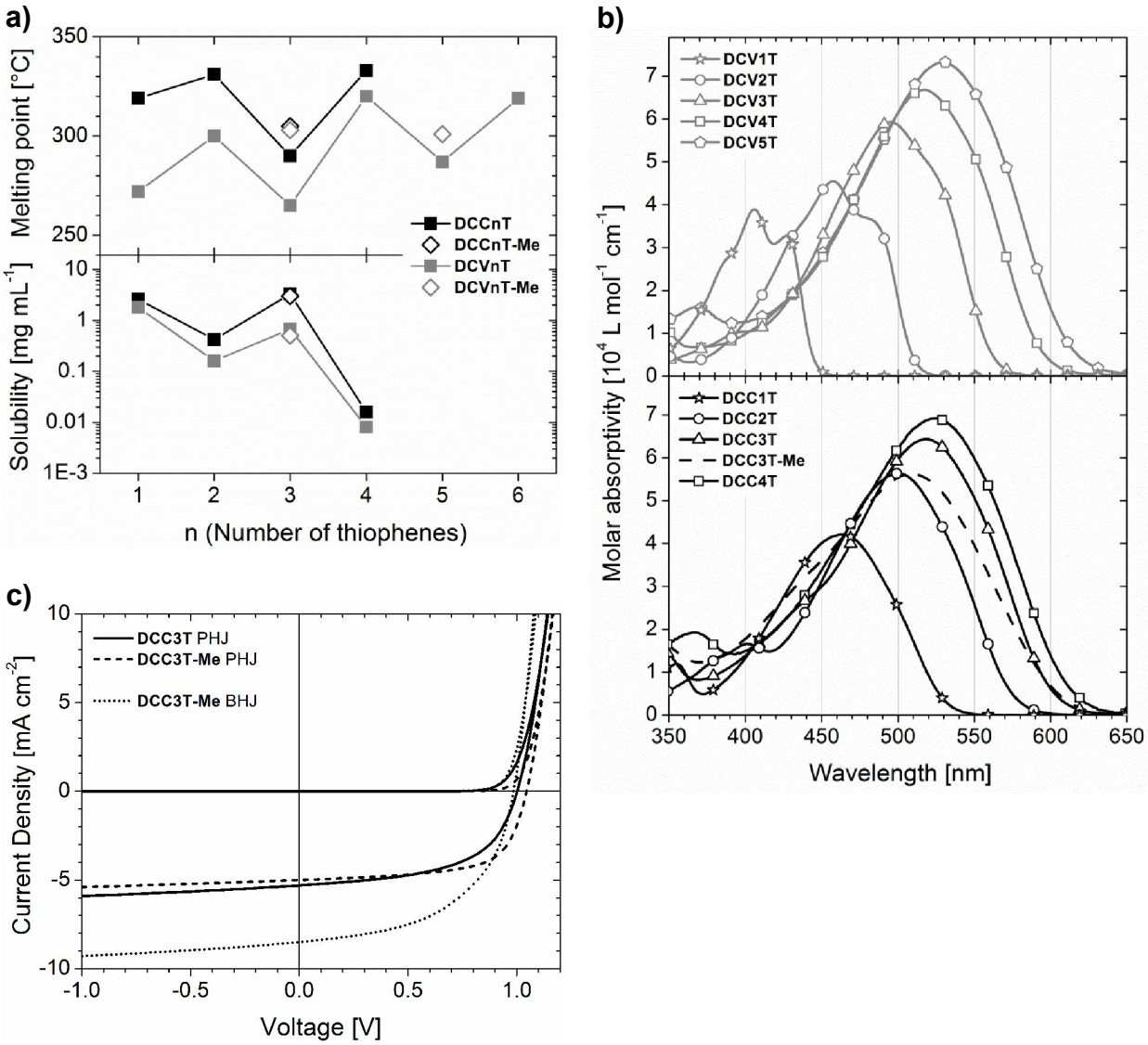

Figure 6. *(a) Melting points (top) and maximum solubilities in D at room temperature (bottom) of* ***DCCnTs*** *and* ***DCVnTs*** *vs the number of thiophene units in the oligothiophene backbone. (b) Absorption spectra of* ***DCCnT*** *(bottom) and* ***DCVnT*** *oligomers (top). (c) J-V characteristics of PHJ and BHJ solar cells containing* ***DCC3T*** *or* ***DCC3T-Me****.*

The assessment of the photovoltaic performances of both terthiophene derivatives in vacuum-processed planar heterojunction OSCs using C_{60} as the acceptor yielded a higher efficiency of

3.4% for methylated **DCC3T-Me**, compared to 3.0% for **DCC3T**. In the BHJ device setup, **DCC3T-Me** showed a further improved PCE value of 4.4% due to a significant increase in short current density, thus surpassing the performance of the energetically similar DCV-capped quaterthiophene donor material **DCV4T-Me** (Chapter IV).

CHAPTER VII:
STRUCTURAL MODIFICATION OF THE TERMINAL GROUPS IN A-D-A OLIGOTHIOPHENES FOR SOLUTION-PROCESSED SOLAR CELLS

In the last Chapter, soluble butylated A-D-A-type quinquethiophenes, end-capped with DCC or methylated MeDCC terminal units are introduced and compared to the well-investigated DCV-substituted derivative **DCV5T-Bu**. To obtain efficient OSCs by solution-processing, this oligomer required the use of hot solutions, which is unpleasant and impairs reproducibility. By replacing the DCV moieties by DCC or MeDCC units, the improvement of solubility and film-forming properties was envisaged using the solubilizing effect of the cyclohexene-containig units discussed in the previous chapter.

For the synthesis of novel oligomers **DCC5T-Bu** and **MeDCC5T-Bu**, acceptor-capped bromothiophenes **6** or **7** were attached to butylated terthiophene **8** by Stille-type cross-coupling reactions (Scheme 4). Final purification of both quinquethiophene derivatives was achieved by column chromatography. MeDCC-substituted terminal building block **7** was prepared using the synthetic strategy applied for the preparation of DCC-capped bromothiophene **6** already presented in Chapter VI.

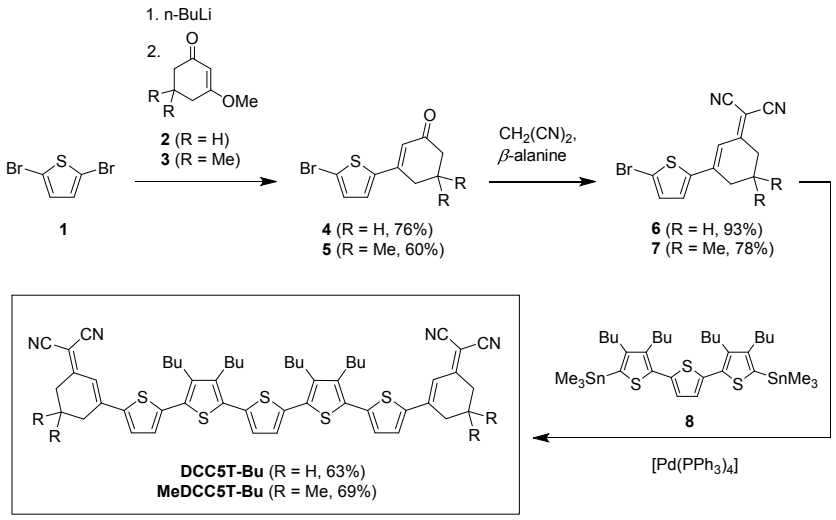

Scheme 4. *Synthesis of* ***DCC5T*** *and* ***MeDCC5T****.*

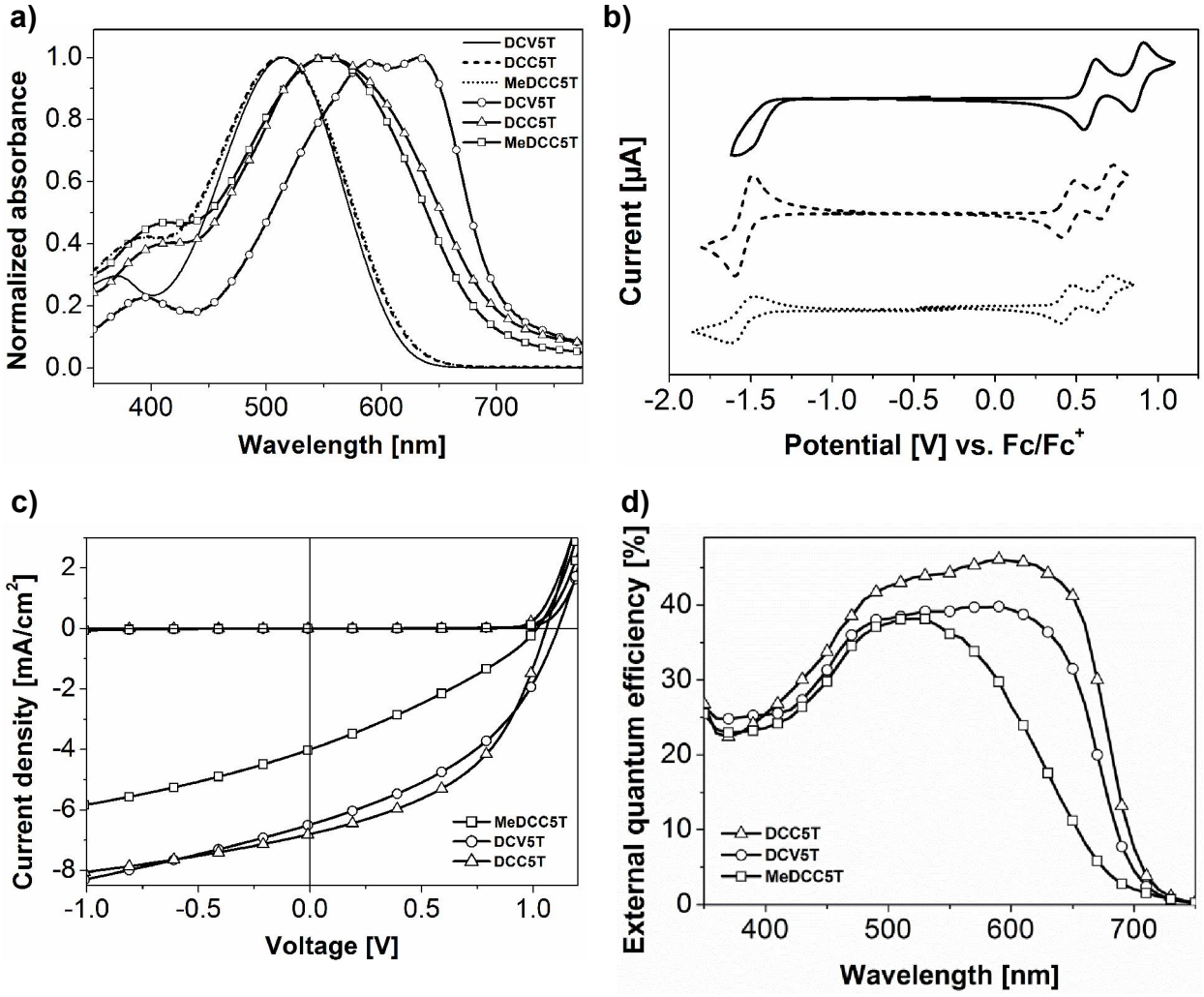

Figure 7. *(a) Absorption spectra of **5T** oligomers measured in chloroform (line without symbol) and of thin films spin-coated from chloroform (line with symbol). (b) Cyclic voltammograms of **5T** oligomers in dichloromethane. **DCV5T** solid line, **DCC5T** dashed line and **MeDCC5T** dotted line. (c) J-V curves of **5T**:$PC_{61}BM$ solution-processed solar cells made from blends spin-coated from best solvent system **DCV5T**:CB/CN, **DCC5T**:$CHCl_3$/DIO and **MeDCC5T**:$CHCl_3$ and (d) the corresponding spectral response.*

In solution, all three pentamers showed practically identical absorption profiles and molar extinction coefficients (Figure 7a). Cyclic voltammetry measurements revealed that the increase in HOMO energy induced by the additional cyclohexene double bonds in **DCC5T-Bu** and **MeDCC5T-Bu** was accompanied by a similar elevation of the LUMO levels, thus leaving the band gap unchanged compared to **DCV5T-Bu** (Figure 7b). UV-vis spectroscopy performed on thin-films spin-casted from chloroform solution revealed smaller red-shifts relative to the solution spectra for the cyclohexene-containing derivatives compared to **DCV5T-Bu** which was assigned to reduced molecular ordering in the bulk. In line with the results obtained for the alkyl-free oligomers (Chapter VI), the maximum solubility in chloroform doubled going from **DCV5T-Bu** to **DCC5T-Bu** with another twofold increase for **MeDCC5T-Bu**. The novel

quinquethiophene derivatives **DCC5T-Bu** and **MeDCC5T-Bu** were incorporated into solution-processed bulk-heterojunction solar cells using phenyl-C_{61}-butyric acid methyl ester ($PC_{61}BM$) as acceptor. Both oligomers yielded high open circuit voltages of about 1 V. Using **DCC5T-Bu** as donor material a maximum PCE value of 3.4% was obtained by adding diiodooctane (DIO) to the chloroform solution of the photoactive materials, compared to 1.4% without solvent additive. This improvement was due to an enhanced short circuit density according to a red-shift and the appearance of a low-energy shoulder in EQE spectra, that could also be tracked in the absorption spectra of solution-processed D:A blend films. **MeDCC5T-Bu** showed a significantly lower BHJ device performance of 1.3% using an optimized D:A blend ratio which may be due the additional methyl groups on the cyclohexene ring hindering efficient molecular packing. Atomic force microscopy (AFM) measurements on **DCC5T-Bu**:$PC_{61}BM$ mixed layers fabricated with solvent additive showed the formation of fibrilar features with finely interdigitated bright and dark regions. **MeDCC5T-Bu** blend layers displayed a finer phase separation. In summary, by replacement of the DCV units in **DCV5T-Bu** with DCC moieties, a small increase in optimized BHJ device performance from 3.0% to 3.4% could be achieved.

Personal Contributions to the Joined Publications

Chapter III

This manuscript is published in *Advanced Functional Materials* (**2011**, *21*, 897-910) under the title:

"Dicyanovinyl–Substituted Oligothiophenes: Structure-Property Relationships and Application in Vacuum-Processed Small Molecule Organic Solar Cells"

by Roland Fitzner, Egon Reinold, Amaresh Mishra, Elena Mena-Osteritz, Hannah Ziehlke, Christian Körner, Karl Leo, Moritz Riede, Matthias Weil, Olga Tsaryova, André Weiß, Christian Uhrich, Martin Pfeiffer and Peter Bäuerle.

I synthesized and characterized all oligomers except **DCV1T** and **DCV2T**, performed thermal gradient sublimation as well as DSC, UV-vis (solution), and CV measurements. Furthermore, I wrote the first draft of the paper in collaboration with Dr. Amaresh Mishra and was involved in the scientific discussion and correction of the manuscript.

CHAPTER IV

This manuscript is published in *Advanced Materials* (**2012**, *24*, 675-680) under the title:

"Interrelation between Crystal Packing and Small Molecule Organic Solar Cell Performance"

by Roland Fitzner, Chris Elschner, Matthias Weil, Christian Uhrich, Christian Körner, Moritz Riede, Karl Leo, Martin Pfeiffer, Egon Reinold, Elena Mena-Osteritz, and Peter Bäuerle.

I synthesized and characterized all oligomers and performed thermal gradient sublimation as well as DSC, UV-vis (solution), and CV measurements. I wrote the first draft of the paper and was involved in the scientific discussion and correction of the manuscript.

CHAPTER V

This manuscript is published in the *Journal of the American Chemical Society (***2012***, 134,* 11064−11067) under the title:

"Correlation of π-Conjugated Oligomer Structure with Film Morphology and Organic Solar Cell Performance"

by Roland Fitzner, Elena Mena-Osteritz, Amaresh Mishra, Gisela Schulz, Egon Reinold, Matthias Weil, Christian Körner, Hannah Ziehlke, Chris Elschner, Karl Leo, Moritz Riede, Martin Pfeiffer, Christian Uhrich, and Peter Bäuerle.

I synthesized and characterized all oligomers and performed thermal gradient sublimation as well as DSC, UV-vis (solution), and CV measurements. Additionally, I wrote the first draft of the paper in collaboration with Dr. Amaresh Mishra and was involved in the scientific discussion and correction of the manuscript.

CHAPTER VI

This manuscript is published in *Advanced Functional Materials* (**2015**, *online*. DOI: 10.1002/ adfm.201404210) under the title:

"A-D-A-Type Oligothiophenes for Small Molecule Organic Solar Cells: Extending the π-System by Introduction of Ring-Locked Double Bonds"

by Roland Fitzner, Elena Mena-Osteritz, Karsten Walzer, Martin Pfeiffer, and Peter Bäuerle.

I synthesized and characterized all oligomers. I performed thermal gradient sublimation as well as DSC, UV-vis (solution), CV and solubility measurements. Further, I wrote the paper and was involved in the scientific discussion and the correction of the manuscript.

CHAPTER VII

This manuscript is intended for submission under the title:

"Structural Modification of the Terminal Groups in A-D-A Oligothiophenes for Solution-Processed Solar Cells"

by Roland Fitzner, Gisela L. Schulz, Florian Henne, Marta Urdanpilleta, Peter Bäuerle.

I synthesized and characterized all oligomers, performed DSC, UV-vis (solution) and CV measurements and prepared the first solar-cell devices under supervision of Dr. Gisela Schulz and Dr. Jegadesan Subbiah. I wrote the paper in collaboration with Dr. Gisela Schulz and was involved in the scientific discussion and the correction of the manuscript.

REFERENCES

[1] K. Schulze, C. Uhrich, R. Schüppel, K. Leo, M. Pfeiffer, E. Brier, E. Reinold, P. Bäuerle, *Proc. SPIE Int. Soc. Opt. Eng.* **2006**, *6192*, 61920C(61921-61926).

[2] K. Schulze, C. Uhrich, R. Schüppel, K. Leo, M. Pfeiffer, E. Brier, E. Reinold, P. Bäuerle, *Adv. Mater.* **2006**, *18*, 2872–2875.

[3] R. Schueppel, K. Schmidt, C. Uhrich, K. Schulze, D. Wynands, J. L. Bredas, B. Männig, M. Pfeiffer, K. Leo, E. Brier, E. Reinold, H.-B. Bu, P. Bäuerle, *Proc. SPIE Int. Soc. Opt. Eng.* **2007**, *6656*, 66560G(66561-66511).

[4] K. Schulze, B. Männig, K. Leo, Y. Tomita, C. May, J. Hupkes, E. Brier, E. Reinold, P. Bäuerle, *Appl. Phys. Lett.* **2007**, *91*, 073521-073523.

[5] M. K. Riede, R. Schueppel, K. Schulze, D. Wynands, R. Timmreck, C. Uhrich, A. Petrich, M. Pfeiffer, E. Brier, E. Reinold, P. Bäuerle, K. Leo, *Proc. SPIE Int. Soc. Opt. Eng.* **2008**, *7002*, 70020G(70021-70028).

[6] R. Schueppel, K. Schmidt, C. Uhrich, K. Schulze, D. Wynands, J. L. Bredas, E. Brier, E. Reinold, H. B. Bu, P. Bäuerle, B. Männig, M. Pfeiffer, K. Leo, *Phys. Rev. B* **2008**, *77*, 085311.

[7] K. Schulze, M. Riede, E. Brier, E. Reinold, P. Bäuerle, K. Leo, *J. Appl. Phys.* **2008**, *104*, 074511.

[8] D. Wynands, B. Männig, M. Riede, K. Leo, E. Brier, E. Reinold, P. Bäuerle, *J. Appl. Phys.* **2009**, *106*, 054509.

[9] G. L. Schulz, M. Urdanpilleta, R. Fitzner, E. Brier, E. Mena-Osteritz, E. Reinold, P. Bäuerle, *Beilstein J. Nanotechnol.* **2013**, *4*, 680-689.

CHAPTER III

DICYANOVINYL–SUBSTITUTED OLIGOTHIOPHENES: STRUCTURE-PROPERTY RELATIONSHIPS AND APPLICATION IN VACUUM-PROCESSED SMALL MOLECULE ORGANIC SOLAR CELLS

Roland Fitzner,[a] Egon Reinold,[a] Amaresh Mishra,[a] Elena Mena-Osteritz,[a] Hannah Ziehlke,[b] Christian Körner,[b] Karl Leo,[b] Moritz Riede,[b] Matthias Weil,[c] Olga Tsaryova,[d] André Weiß,[d] Christian Uhrich,[d] Martin Pfeiffer[d] and Peter Bäuerle[a]*

[a] Institute of Organic Chemistry II and Advanced Materials, University of Ulm, Albert-Einstein-Allee 11, 89081 Ulm, Germany

[b] Institute of Applied Photophysics, TU Dresden, Mommsenstraße 13, 01062 Dresden, Germany

[c] Institut für Chemische Technologien und Analytik, Abteilung Strukturchemie, Technische Universität Wien, Getreidemarkt 9/164-SC, 1060 Vienna, Austria

[d] Heliatek GmbH, Treidlerstr. 3, 01139 Dresden, Germany

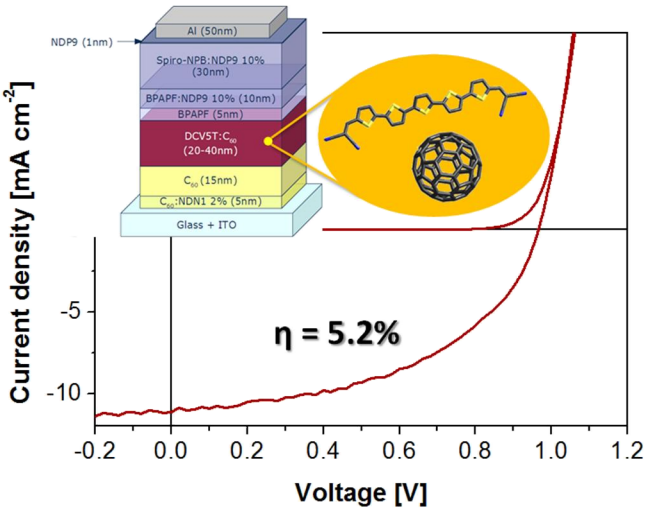

Reproduced and adapted with permission from

R. Fitzner *et al.*, *Advanced Functional Materials* **2011**, *21*, 897-910.

Copyright © 2011 WILEY-VCH Verlag GmbH & Co. KGaA, Weinheim.

ABSTRACT

Efficient synthesis of a series of terminally dicyanovinyl (DCV)-substituted oligothiophenes, **DCV*n*T 1-6**, without solubilizing side chains synthesized via a novel convergent approach and their application as electron donors in vacuum-processed m-i-p-type planar and p-i-n-type bulk heterojunction organic solar cells is described. Purification of the products via gradient sublimation yielded thermally highly stable organic semiconducting materials in single crystalline quality which allowed for X-ray structure analysis. Important insight in the packing features and intermolecular interactions of these promising solar cell materials are provided. Optical absorption spectra and electrochemical properties of the oligomers were investigated and valuable structure-property relationships deduced. Photovoltaic devices incorporating **DCV*n*Ts 4-6** showed power conversion efficiencies up to 2.8% for planar and 5.2% for bulk heterojunction organic solar cells under full sun illumination (mismatch corrected simulated AM 1.5G sunlight). The 5.2% efficiency shown here represents one of the highest values ever reported for organic vacuum-deposited single heterojunction solar cells.

1. INTRODUCTION

Organic solar cells (OSC) have attracted enormous interest in recent years, because of their potential towards low-cost production on flexible substrates.[1-9] The field started by utilization of organic small molecules[2,10-14] and later on by using functional semiconducting polymers,[5,15-20] resulting in remarkable improvement in power conversion efficiencies over the decade from about 1% to over 7%. To date, functionalized oligo- and polythiophenes are among the best materials for application in organic photovoltaics.[16,21]

The most frequently used material for small molecule organic solar cells (SMOSC) prepared by vacuum-evaporation processes are represented by metal phthalocyanines (Pc) as electron donor (D) and fullerene C_{60} as acceptor (A) with reported efficiencies of 5% for a single cell.[22] However, for outdoor applications, the performance of these solar cells should be improved in terms of efficiency along with stability and costs. One aspect of improving efficiency is the use of suitable electron donors and acceptors with optimized energy levels to minimize energetic losses during exciton separation. In this respect, various D-A and A-A substituted oligothiophenes have been prepared and tested in SMOSCs.[23-30]

We have demonstrated that a photovoltage (V_{OC}) of as high as 1.0 V can be obtained by replacing the frequently used metal Pcs by terminally dicyanovinyl (DCV)-substituted oligothiophenes bearing butyl side chains (**DCV5T-Bu**) for solubility reasons as donor when using fullerene C_{60} as acceptor. These solar cells reached power conversion efficiencies of up to 3.4%.[24,25,31-35] The high V_{OC} obtained is due to a high ionization potential (IP) of DCV5T-Bu (IP = -5.6 eV). The effect of the alkyl chain length, attached at the β-position of the conjugated backbone on device performance within the series of DCV-functionalized quinquethiophenes was also established. Solar cells prepared from these derivatives revealed that the butyl-substituted oligomers showed higher efficiencies (η = 3.4%) than the ethyl substituted **DCVnT-Et** (η = 2.5-3.0%).[33] The reduced efficiency was mainly due to the reduced fill factor (*FF*). The difference in performance was explained by the difference in packing, by differences in hole-injection between the hole-transport layer and the oligothiophene as well as a difference in hole mobility of the oligothiophene derivatives.

Photovoltaic properties of **DCVnT-Bu** (n = 4, 5 and 6) with various lengths of the oligothiophene unit were also investigated. The V_{OC} decreased from 1.13V for **DCV4T-Bu** to 1.0V for **DCV5T-Bu** and to 0.93V for **DCV6T-Bu**, which is ascribed to the decrease in their IP, respectively increase in energy of the highest occupied molecular orbital (HOMO). On the other hand, no clear trend was observed for short-circuit current density (J_{SC}) and fill factor (*FF*) values.

The power conversion efficiency of **DCV4T-Bu** was lower compared to **DCV5T-Bu** because of its lower J_{SC} and FF, while the small differences in J_{SC} and *FF* values between **DCV5T-Bu** and **DCV6T-Bu** do not represent a general trend.[34]

One advantage of the vacuum-processable SMOSCs is that tandem cells can easily be fabricated. Very recently, by combining in a tandem device two bulk heterojunctions of C_{60} in blend layers with an optimized **DCVnT**-derivative and a novel pigment with absorption range between 600 and 750 nm developed by BASF, respectively, a certified efficiency of 6.1% on 2 cm^2 active area[36] and shortly after a certified record efficiency of 7.7% on 1.1 cm^2 device have been released.[37]

Herein, we investigate structure-property relationships in a series of **DCVnTs** with conjugated chain lengths of one to six thiophene units (n=1-6) and without solubilizing alkyl side chains, well being aware that synthesis and characterization of longer derivatives might be problematic due to low solubility. However, we expect that these oligomers may show good packing and thermal stability which might influence the solar cell performance.

2. Synthesis of Dicyanovinyl-Functionalized Oligothiophenes DCVnT

2.1. Linear Syntheses

Synthesis of the smaller members of the series, **DCV1T**-**DCV3T 1-3**, were already described in literature and were prepared for non-linear optical properties.[38,39] Based on our experience with alkylated **DCVnTs**, we firstly synthesized **DCV1T**-**DCV4T 1-4** by a linear approach (Scheme 1). Thus, bi-, ter-, and quaterthiophene dialdehydes **8-10**,[40-43] which were prepared by Vilsmeier-Haack formylation of the parent oligothiophenes[44-46] were reacted with malononitrile and ß-alanine as catalyst to form target **DCVnTs 2** and **3** (n=2, 3) in nearly quantitative yield and in high purity. **DCV1T 1** was obtained from commercially available thiophene-2,5-dicarbaldehyde **7** and malononitrile without the use of catalyst. However, due to a dramatic decrease in solubility, reaction of quaterthiophene-dialdehyde **10** resulted in an inseparable mixture of target **DCV4T 4** and the singly reacted intermediate with a DCV-group at one chain end and an unreacted formyl group at the other.

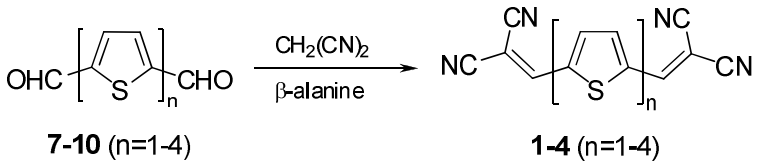

Scheme 1. *Linear synthesis of dicyanovinyl-substituted oligothiophenes* ***DCVnT 1-4****.*

2.2. CONVERGENT SYNTHESES

Due to solubility problems of the longer homologues, only a series up to the trimer could be reliably synthesized by the usual linear synthetic approach. Thus, we developed a convergent route to DCV-capped oligothiophenes **DCV3T 3** to **DCV6T 6** (Scheme 2). Terminal building blocks, DCV-substituted bromothiophene **11**[47] and bithiophene **12**[48] were reacted with central components, distannylated mono- and bithiophene **13** and **14**,[49-51] in a Stille-type coupling under $Pd[PPh_3]_4$-catalysis in DMF as solvent. Thus, in a [1T+1T+1T]-coupling **DCV3T 3** was obtained in 99% yield, **DCV4T 4** in 97% by a [1T+2T+1T]-, DCV5T **5** in 94% by a [2T+1T+2T]-, and finally **DCV6T 6** in 82% by a [2T+2T+2T]-route. THF or toluene as solvent resulted in lower yields and lower purities of the **DCVnT** raw materials. The advantage of this method was that the intermediates coming from the first Stille coupling showed sufficient solubility so that the second coupling worked, whereby the target **DCVnTs** precipitated with already high purity. After washing and extracting with various solvents, the materials were finally purified by gradient vacuum sublimation.

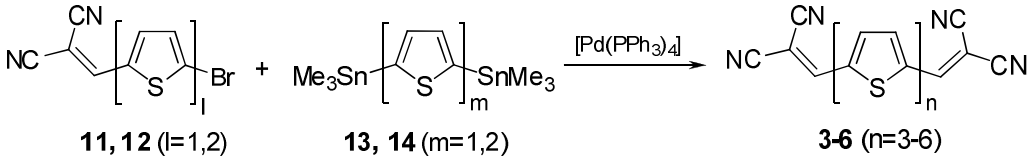

Scheme 2. *Convergent synthesis of dicyanovinyl-substituted oligothiophenes DCVnT* ***3-6****.*

3. THERMAL PROPERTIES

In order to obtain crystalline material of high purity for structure determination by XRD methods, gradient vacuum sublimation ($p < 10^{-5}$ mbar) was performed for **DCVnTs 2-6**. Derivatives **2-4** sublimated almost quantitatively at sublimation temperatures well below their melting points and without significant decomposition. For **DCV5T 5** and **DCV6T 6** sublimation temperatures in the range of the melting points were necessary in order to obtain sublimation

rates allowing for 100 mg scale purification. Due to material degradation, the sublimation yields for compounds **5** and **6** were lower with around 50%.

The melting points were determined using Differential Scanning Calorimetry (DSC) and used to evaluate the purity of target compounds **1**-**6**. Purification was repeated until the melting points remained unchanged for two consecutive purification steps (Soxhlett extraction, gradient vacuum sublimation). As an example, analytical data for **DCV4T 4** measured after each purification step is shown in Table 1. The first sublimation of the raw product, which was filtered off from the reaction mixture and washed with various solvents, did not yield a significant improvement in material purity according to elemental analysis. The second sublimation yielded analytically very pure material, which showed a considerable increase in melting point. A third sublimation did not significantly change the melting point.

Table 1. *Analytical data for* ***DCV4T 4*** *measured after each subsequent purification step.*

	elemental analysis			melting point
	C	H	N	(onset DSC) [°C]
calculated	59.73	2.09	11.61	
washed product	59.11	2.38	11.71	317.6
1. sublimation	59.23	2.11	11.36	318.1
2. sublimation	59.60	2.07	11.46	319.9
3. sublimation	59.67	2.04	11.59	319.6

The melting points of compounds **2**-**6** showed an odd-even-effect with respect to the number of thiophene units present in the oligothiophene backbone (Figure 1). The odd-numbered compounds **DCVnT 3** and **5** melted at significantly lower temperatures than the shorter homologues **2** and **4**. The melting point of compound **5** (287 °C) was about 20 °C higher than that of **3** (265 °C) and the same trend was seen for compounds **4** (320 °C) and **2** (300 °C). However, **DCV6T 6** (319 °C) did not show the expected further increase in melting point with respect to **DCV4T 4**. These results may originate from the difference in symmetry of odd- and even-numbered DCV*n*Ts. Semi-empirical Austin Model 1 (AM1) geometry optimizations under restricted Hartree Fock conditions were carried out for all **DCVnTs** (*vide infra*, section 5). All calculations yielded structures wherein the terminal DCV acceptor units were arranged such that one of the cyano carbon atoms was in close proximity to the sulfur atom of the neighboring thiophene unit (S1…C23 and S2…C20 in Figure 3). The sulfur-carbon interaction locks the DCV-group into one of the two possible planar configurations with respect to the oligothiophene core. This

finding is further confirmed by the single crystal structure analysis of **DCV4T 4** (*vide infra*). Hence, odd-numbered oligomers belong to the C_{2v} symmetry point-group comprising a mirror plane perpendicular to the molecular axis, whereas the even-numbered homologues have a C_{2h} symmetry. Consequently, the latter ones do not include a dipole moment, whereas in the case of the odd-numbered oligomers a strong dipole moment up to 6.5 D was calculated.

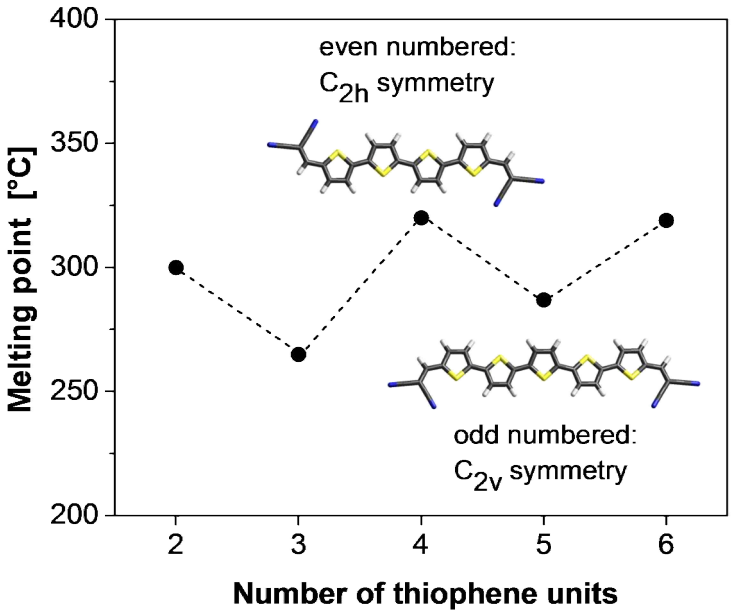

***Figure 1**. Melting points for **DCVnTs 2-6** (determined from the onset of the melting peak in DSC plots).*

4. Structure Analysis

Platelet-like crystals of **DCV4T** were obtained after a gradient sublimation process. The dark-red crystals have a metallic luster and grew larger than 4 mm while the thickness typically remained far under 0.1 mm. Figure 2a shows a cross-section of the sublimation tube containing the compound and Figure 2b an optical micrograph of a crystal. Changes on the crystal orientation induced different behaviors against the absorption of polarized light (Figure 2b, white arrow): the crystal showed a stronger light absorption when the long axis is oriented parallel (shining red-purple) than perpendicular to the polarized light. Because the transition dipole responsible for the light absorption in **DCV4T** is oriented parallel to the long molecular axis, we conclude that the oligothiophene backbone lies, within 30° (see Figure 3), parallel to the longer axis of the crystal.

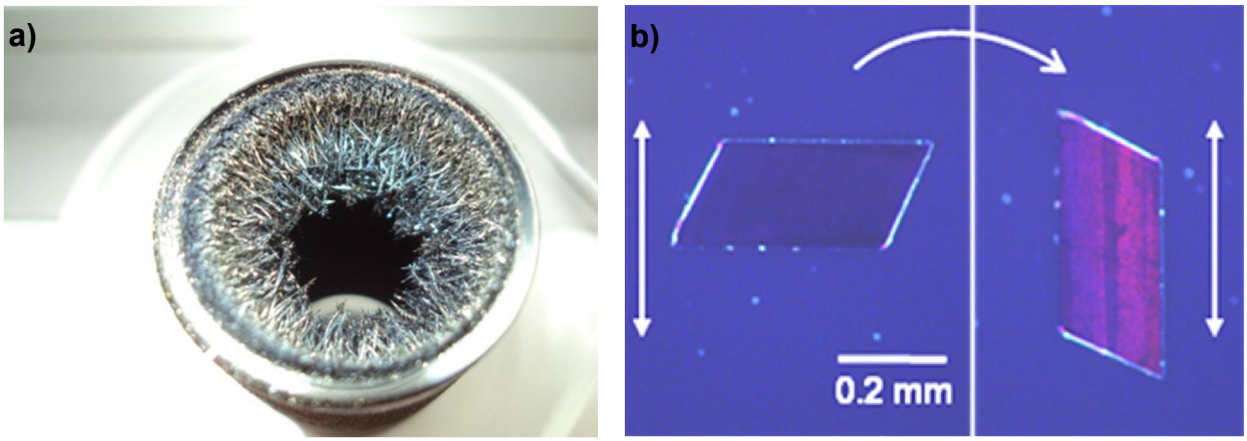

Figure 2. *Picture of a sectioned sublimation tube containing* ***DCV4T*** *crystals (a) and photograph of a single crystal of* ***DCV4T*** *under the polarized light microscope (b).*

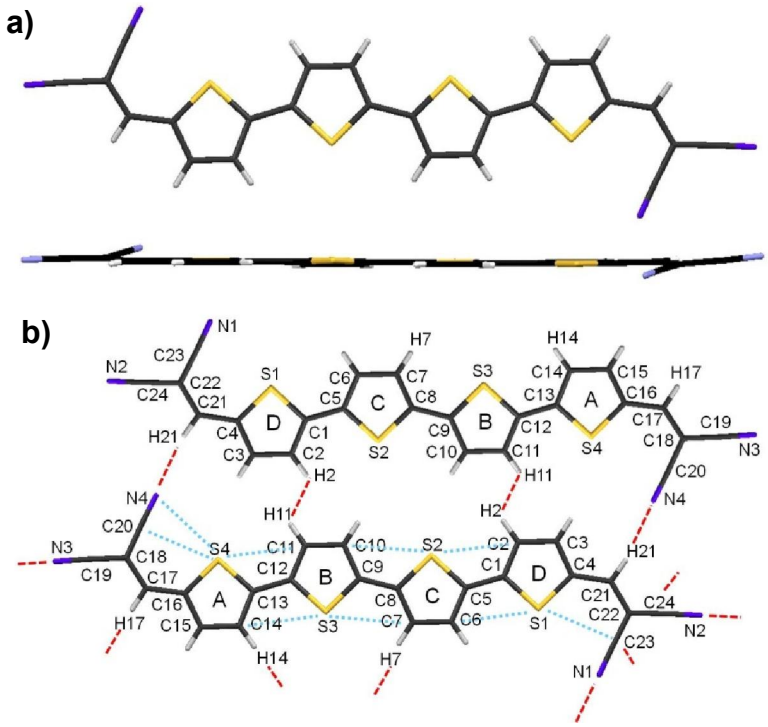

Figure 3. *Molecular structure of* ***DCV4T*** *(front and side view) (a). Atomic numbering scheme and thiophene ring labels (b). Inter- and intramolecular short contact distances are depicted by red and grey lines, respectively. Torsion angles between adjacent thiophene rings: A–B 176.8°, B–C 176.7°, C–D 178.7°, N4–A 6.4°, D-N1 7.8°.*

The crystals belong to the monoclinic space group $P2_1/n$, with 4 molecules in the unit cell, whose parameters are: a = 3.8295(8), b = 27.695(6), c = 22.663(5) Å, β = 91.68(3)°. In Figure 3 the molecular structure of **DCV4T** in the crystal structure is depicted. The thiophene units show *all-trans* conformation while the DCV groups are in an *all-cis* conformation relative to the sulfur atoms of the terminal thiophene units. The molecule evidences an almost planar conformation with dihedral angles between the thiophenes smaller than 4°. Considering all atoms in

the molecule, the RMS deviation from planarity is 0.101 Å, with the N atoms of the DCV groups exhibiting the largest deviation of up to 0.3 Å. Slight differences between the terminal DCV groups and the individual C-S bond lengths (detailed information ESI or CCDC) origin the deviation of **DCV4T** from a centrosymmetric molecule. The bond lengths of the oligothiophene moiety are summarized in Table 2 and the inter- and intramolecular non-bonding atom distances shorter than the sum of the corresponding van der Waals radii are collected in Table 3. The values for the thiophenic C-C double bonds (1.379–1.394 Å), C–C single bonds (1.401–1.412 Å) and the C–C interring bonds (1.445 Å) are comparable with those of other oligothiophenes.[52,53] In contrast to several thiophene compounds, **DCV4T** showed neither *syn*-conformations of adjacent thiophenes nor typical rotational disorder (*syn/anti* conformations).[54,55]

Table 2. *Bond lengths (Å) in the oligothiophene moiety in* ***DCV4T*** *single crystals.*

N1	C23	1.146(3)	C5	S2	1.736(1)	C13	S4	1.732(1)
C23	C22	1.436(2)	C5	C6	1.377(2)	C13	C14	1.387(2)
N2	C24	1.151(3)	C6	C7	1.411(2)	C14	C15	1.400(2)
C24	C22	1.443(2)	C7	C8	1.381(2)	C15	C16	1.389(2)
C22	C21	1.366(2)	C8	S2	1.734(1)	C16	S4	1.745(2)
C21	C4	1.432(2)	C8	C9	1.450(2)	C16	C17	1.426(2)
C4	S1	1.739(1)	C9	S3	1.727(1)	C17	C18	1.361(2)
C4	C3	1.390(2)	C9	C10	1.384(2)	C18	C19	1.440(2)
C3	C2	1.402(2)	C10	C11	1.411(2)	C18	C20	1.435(2)
C2	C1	1.385(2)	C11	C12	1.379(2)	C19	N3	1.151(2)
C1	S1	1.730(1)	C12	S3	1.735(1)	C20	N4	1.149(2)
C1	C5	1.447(2)	C12	C13	1.448(2)			

Table 3. *Short inter- (left) and intra- (middle and right) molecular contacts (Å), below the van der Waals radii, in* ***DCV4T*** *single crystals.*

C23 ··· C24[a]	3.326	C4 ··· C23	3.076	S3 ··· C14	3.198
H2 ··· H11[b]	2.367	S1 ··· C23	3.078	S4 ··· C11	3.227
N1 ··· H14[c]	2.678	S1 ··· C6	3.215	S4 ··· C20	3.110
N2 ··· H7[d]	2.587	S2 ··· C2	3.206	S4 ··· N4	3.347
N3 ··· H17[e]	2.481	S2 ··· C10	3.224	C16 ··· C20	3.072
N4 ··· H2[b]	2.487	S3 ··· C7	3.210		

Symmetry codes: [a] -1+ x, y, z; [b] 1- x, 1- y, 1- z; [c] -1/2 + x, 1/2 - y, 1/2 + z; [d] -1.5 + x, 1/2 - y, 1/2 + z; [e] 4 - x, 1 - y, - z

The unit cell containing four molecules dispose in two centrosymmetric pairs of two antiparallelly arranged molecules (Figure 4). In the crystal, molecules extend in layers parallel to the (9 3 21) plane, leaving space for channels parallel to [100] that represent approximatly 17% of the overall volume. In these channels, disordered molecules are situated (for treatment of the disorder, see experimental section). The analysis of the intermolecular short contacts (atom distances below the van der Waals radii) (Table 3 and Figure 3b) reveals some interesting features: firstly, odd short distances between the hydrogen atoms H2-H11 are observed (Figure 3b). Moreover, relevant weak non-classical C-H…N hydrogen bonding interactions between the hydrogen atoms (H7, H14, H17 and H21) and all nitrogen atoms lead to interatomic distances below the van der Waals radii (Figure 2b and Table 3). The interactions occur with all the neighboring molecules, consolidating in this way the crystal packing.[56]

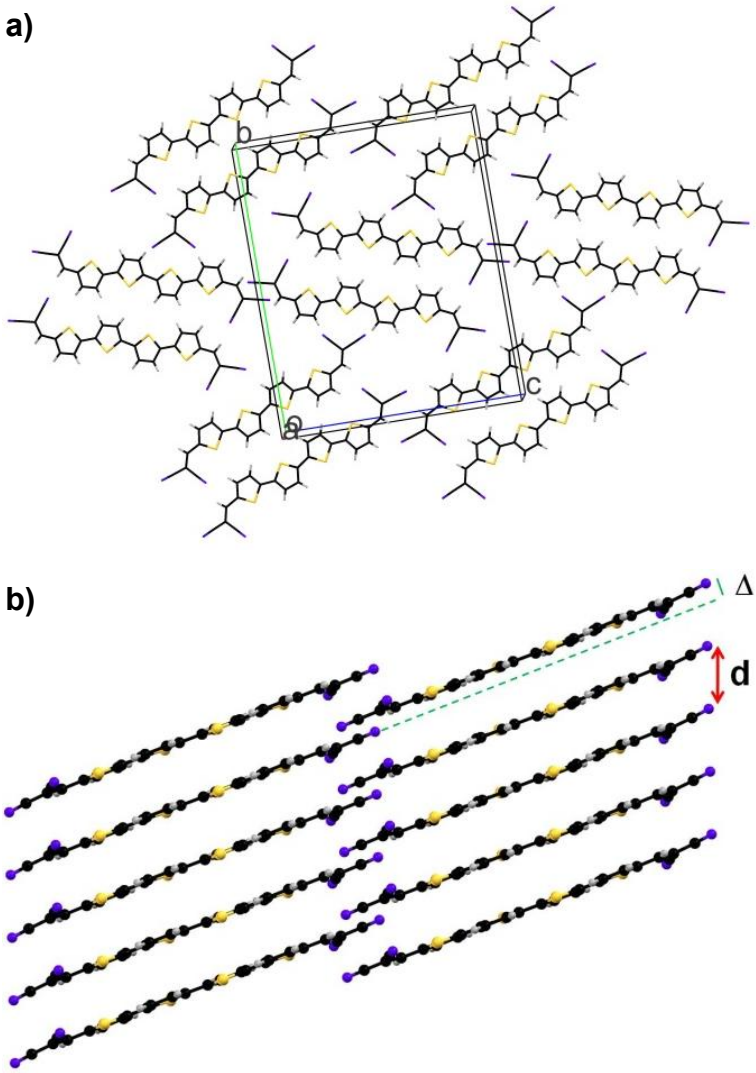

Figure 4. *(a) Molecular packing of* ***DCV4T*** *in the single crystal viewed from the direction normal to the (9 3 21) plane. (b)View from the [101] direction showing the π–π stacking (d) of the molecules.*

DCV4T does not exhibit a herringbone structure in the crystal, like observed for other β-unsubstituted thiophene-based compounds.[52,53,57] The π-conjugated backbone of the molecules in a column are oriented parallel to one another, as it is seen in the view from the [101] direction (Figure 4b). The intermolecular distances, "d", are as close as 3.514 Å, indicating a compact packing and π–π stacking of the thiophene backbones. In the perpendicular direction, the molecules (Figure 4a) are lying in approximate coplanarity with a small offset between neighbouring molecules (Δ = 1.206 Å; Figure 4b). The parallel ordering of the π-conjugated system in DCV4T thus may arise from weak non-classical hydrogen bonding interactions caused by the terminal nitrile residues, which act as supramolecular synthons preventing the herringbone arrangement.[56]

Figure 5 shows the overlap of the molecules viewed from the direction normal to the (9 3 21) plane. The aromatic backbones are almost completely overlapped, showing small slipped offsets of 1.3 Å in both, the long molecular axis and the perpendicular directions. Thus, the coplanarity of the thiophene rings together with a highly efficient overlap between the molecules of **DCV4T** in the crystal, shown by close π–π stacking distances and very small offsets, evidence the conditions for favorable charge carrier transport in **DCV4T**. From X-ray powder diffraction data on intensive pestle samples of the **DCVnTs** can be deduced that all the compounds indeed exhibit a layered structure with a 2θ parameter corresponding with distances between 3.2 and 3.9 Å, which indicates π–π stacking of the molecules in accordance with the X-ray structure data of DCV4T analyzed in this study.

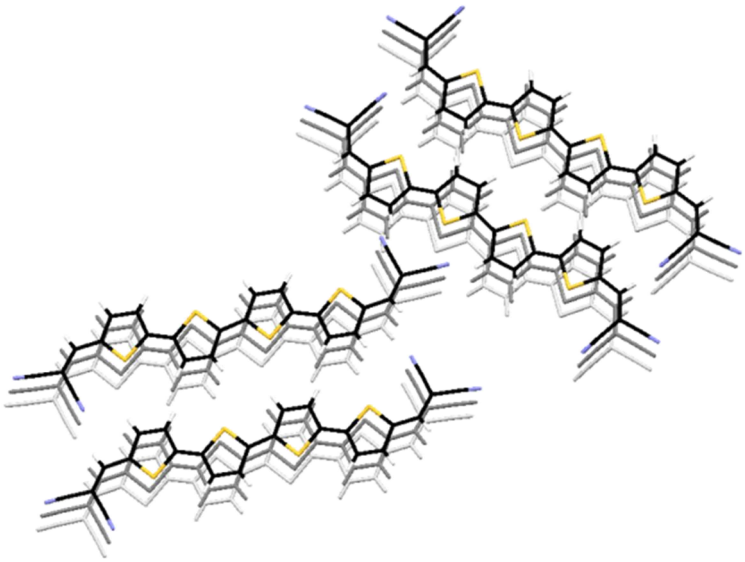

Figure 5. *Overlap of molecules of* ***DCV4T*** *viewed from the direction normal to the (9 3 21) plane. The molecules in adjacent layers are drawn in gray gradation.*

5. Optical and Redox Properties

5.1. Steady-State Spectroscopy

One of our objectives was to investigate optical and redox properties of the **DCVnTs 1-6**, which are important parameters for their application in organic solar cells. Absorption and emission spectra of **1-6** were measured in dichloromethane and are summarized in Table 4. Figure 6 presents the UV-vis and emission spectra of **DCVnTs 1-5**. The molar extinction coefficient of **DCV6T 6** could not be determined due to its limited solubility in dichloromethane.

***Table 4**: Spectroscopic data for **DCVnTs 1-6**. The values in brackets represent shoulders.*

DCVnT	λ_{max}^{abs} [nm] solution	ε_{max} [L mol^{-1} cm^{-1}] solution	λ_{max}^{em} [nm] solution	Stokes shift [cm^{-1}][a]	λ_{max}^{abs} [nm] film	α_{max} [10^5 cm^{-1}] film[b]	λ_{max}^{em} [nm] film	E_g^{opt} [eV] solution[c]	E_g^{opt} [eV] film[d]
1	406 (427)	39000	460 (439)	320				2.78	
2	457 (481)	45500	508 (540)	606				2.42	
3	495 (521)	59300	564 (601)	1047	528 (574)		695	2.20	1.85
4	518	66800	612 (651)	1342	560 (521,620)	1.72	670 (718)	2.09	1.78
5	530	73300	663	1441	570	1.86	767	2.02	1.69
6	532	n.d. [e]	692	1803	579	1.67	795	2.00	1.68

[a] Difference between the 0-0 vibronic transitions of the absorption and emission spectra. The 0-0 vibronic transitions were determined by mathematical Gaussian deconvolution. [b] Thin film absorption coefficients were estimated from reflection corrected absorbance curves using the lambert-beer law. [c] Estimated using the onset of the UV-Vis spectra in DCM. [d] Estimated using the onset of the UV-Vis spectra of films prepared by vacuum sublimation. [e] Due to the low solubility the molar extinction coefficient could not be determined.

Compared to non-functionalized oligothiophenes, lowering of the lowest unoccupied molecular orbital (LUMO) was achieved by introduction of electron-withdrawing DCV end groups. This clearly results in strong absorptions in the visible region. As a general trend, strong bathochromic shifts of the absorption maximum assigned to the π-π* (HOMO→LUMO) transition of the conjugated π-system were observed with increasing number of thiophene units, confirming full conjugation of the π-system. **DCV1T 1** showed a structured absorption band with a maximum at 406 nm and shoulders at 387 and 427 nm. This absorption band shifted to lower energy, became broad and lost structure as the number of thiophene units increases from **2** (457 nm) to **6** (532 nm). Furthermore, the molar extinction coefficients were found to increase with increasing number of thiophene units from **1** (ε = 39000 L mol^{-1} cm^{-1}) to **5** (ε = 73300 L mol^{-1} cm^{-1}).

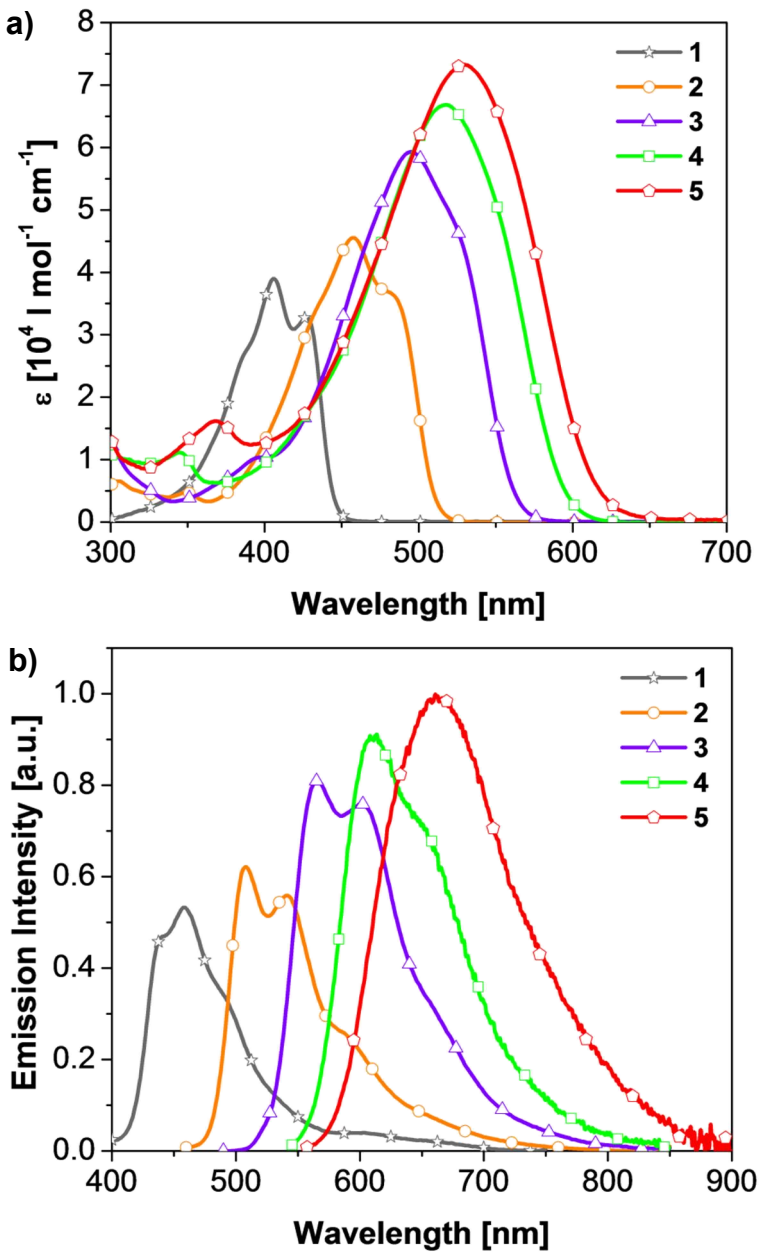

Figure 6. *Electronic absorption (a) and emission spectra (b) of the* ***DCVnT****-series* ***1-5*** *in dichloromethane.*

As shown in Figure 6b the emission maximum undergoes a marked bathochromic shift with increasing number of thiophene units from **1** (λ_{em} = 460 nm) to **6** (λ_{em} = 692 nm). This is further ascribed to the extended conjugation. Similar to the trends seen in the absorption spectra, the vibronic transitions become less prominent with increasing number of thiophene units from **1** to **4**. Structureless emission bands were observed for **DCVnTs 5** and **6**. Moreover, with increasing number of thiophene units from **1** to **6**, a gradual increase in Stokes shift (**1:** 320 cm^{-1}, **6**: 1803 cm^{-1}) was observed. This is an indication of significant structural changes between the ground and the excited state. The lack of vibronic structure in the solution spectra of higher oligomers is a further hint for torsional disorder in the ground state.

Compared to the solution spectra, absorption and emission spectra of **DCVnT** films are significantly broadened and red-shifted (Figure 7). The reason for this red-shift in thin film absorption should be due to coplanarization and ordering of the molecules in the bulk, suggesting better packing in thin films. **DCV4T 4** showed a considerably broad and structured absorption band with a maximum at 560 nm compared to **3** (λ_{abs} = 528 nm), **5** (λ_{abs} = 570 nm) and **6** (λ_{abs} = 579 nm). This may indicate further structural reorganization of **4** in the bulk due to pronounced intermolecular π-π interactions.

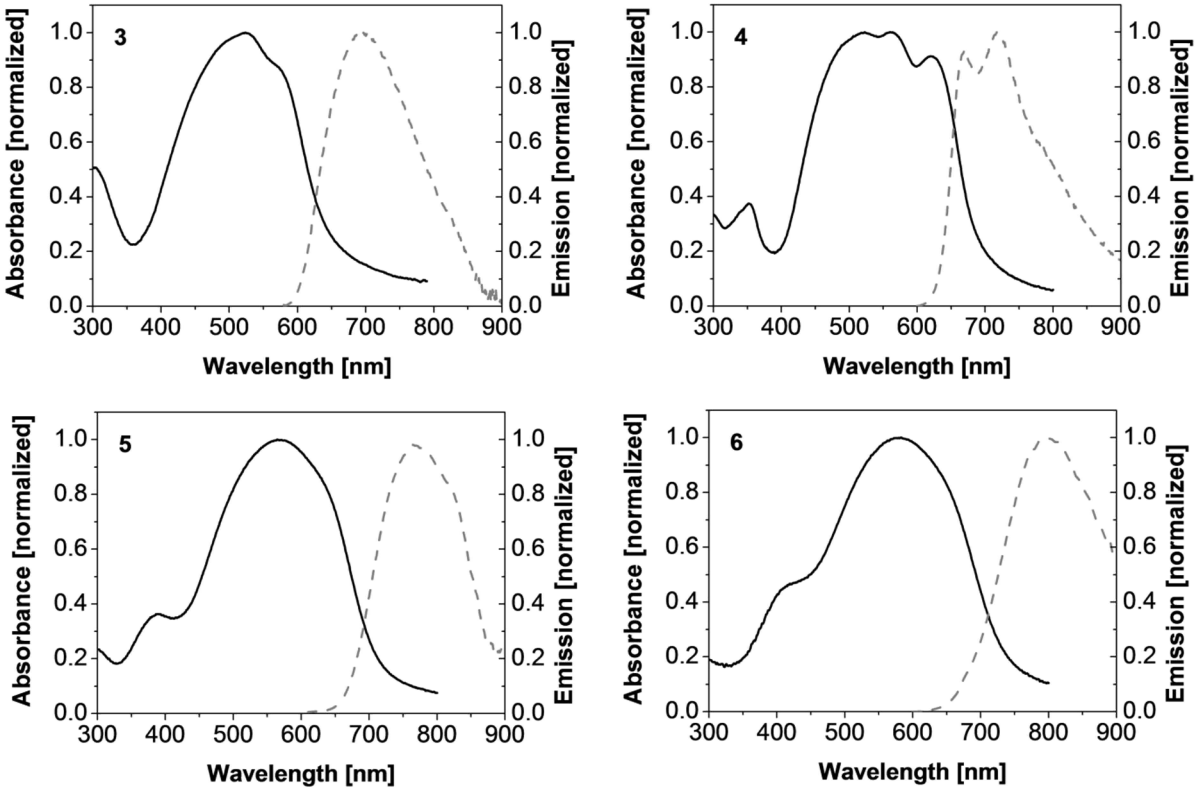

***Figure** 7. Normalized absorption and emission spectra of **DCVnTs 3-6** in thin films (30 nm) prepared by vacuum evaporation onto quartz substrates.*

In solution, the optical band gap (E_g^{opt}) of the **DCVnTs** decreases from 2.78 for **1** to 2.0 eV for **6** with increasing number of the thiophene units and is well in the range of semiconducting oligothiophenes. In thin films, the optical band gaps are lowered by about 0.33-0.35 eV compared to the gaps obtained from solution spectra. We further compared these non-alkylated **DCVnT** compounds **1-6** to some previously reported alkyl-substituted **DCVnTs**.[25,31,34] Due to the planarization of the molecular backbone, the absorption maxima of non-alkylated **DCVnTs** are slightly red-shifted concomitant with a large increase in molar extinction coefficients compared to the alkyl-substituted **DCVnTs**.

5.2. Electrochemical Characterization

The redox properties of **DCVnTs 1-3** measured in 0.1 M CH_2Cl_2/$TBAPF_6$ solutions. Due to the low solubility of longer **DCVnTs 4-6** in dichloromethane the electrochemical characterizations were carried out in tetrachloroethane/$TBAPF_6$ at 80 °C (Figure 8). All data are summarized in Table 5. **DCV1T 1** showed two reversible one-electron reduction processes at -0.87 and -1.21 V, respectively. **DCVnTs 2-6** showed two quasi reversible reduction waves which are positively shifted with increasing number of thiophene units. **DCVnT 2** and **3** showed a single reversible oxidation wave at 1.44 and 1.06 V, respectively, within the measured electrochemical window, indicating the formation of stable radical cations. In contrast, **DCVnTs 4** to **6** showed two reversible oxidation waves corresponding to the formation of stable radical cations and dications, which is typical for oligothiophenes.

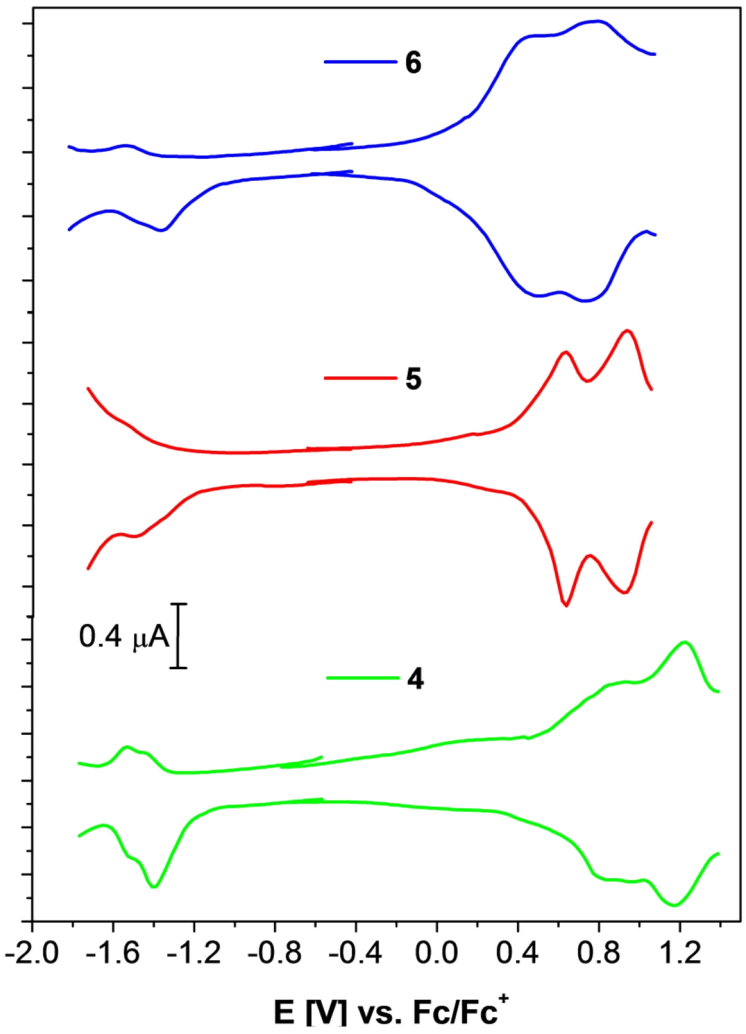

***Figure 8**. Differential pulse voltammograms of **DCVnTs 4-6** (from bottom to top) measured in tetrachloroethane–$TBAPF_6$ (0.1 M), scan rate 100 mV/s, potentials vs. Fc/Fc^+, measured at 80 °C.*

***Table 5**: Electrochemical data and molecular orbital energies of the **DCVnTs 1-6**.*

DCVnT	E^0_{Ox1} [V] [a]	E^0_{Ox2} [V] [a]	E^0_{Red1} [V] [a]	E^0_{Red2} [V] [a]	HOMO [eV] [b]	LUMO [eV] [b]	E_g^{CV} [eV] [c]
1			-0.87	-1.21		-4.30	
2	1.44		-1.12	-1.23	-6.50	-4.05	2.45
3	1.06		-1.25	-1.43	-6.09	-3.90	2.19
4[d]	0.84	1.20	-1.41	-1.52	-5.85	-3.87	1.98
5[d]	0.64	0.93	-1.37	-1.51	-5.62	-3.73	1.89
6[d]	0.46	0.77	-1.39	-1.52	-5.43	-3.87	1.56

[a] Measured in DCM-$TBAPF_6$ (0.1 M), [dye] = 10^{-3} mol·L^{-1}, 25 °C, V= 100 mV·s^{-1}, vs. Fc^+/Fc. [b] set Fc^+/Fc E_{HOMO} = -5.1 eV. [c] Calculated from the difference between the values of E^{onset}_{red1} and E^{onset}_{ox1}. [d] Measured in tetrachloroethane at 80 °C.

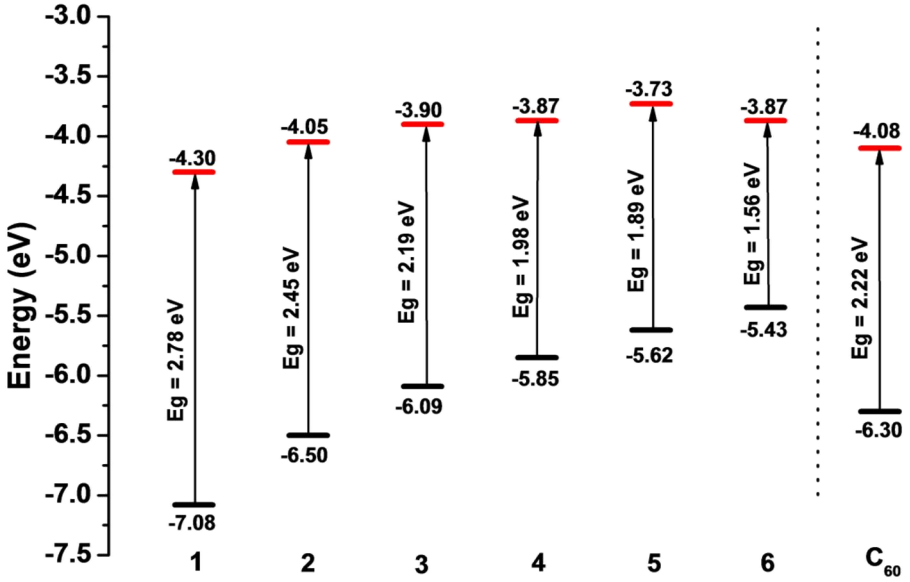

***Figure 9**. Representation of HOMO/LUMO energies of the **DCVnTs 1-6** derived from electrochemical data and compared to C_{60}. The HOMO/LUMO energy levels of C_{60} are taken from ref. [59] and were determined from the onset of the oxidation and reduction waves measured in 0.1 M $TBAPF_6$/tetrachloroethane. The HOMO energy value for **1** was determined from the optical gap using the eq. $E_{HOMO} = E_g^{opt} + E_{LUMO}$.*

The HOMO and LUMO energies of all compounds were calculated from the onset values of the first oxidation and reduction waves using the standard approximation that the Fc/Fc^+ HOMO level is -5.1 eV vs. vacuum.[58] These data are compiled in Table 5 and graphically shown in Figure 9. Due to the low lying HOMO energies **DCVnTs 2** (-6.5 eV) and **3** (-6.09 eV) showed n-type character. On the contrary, the HOMO energies of **DCVnTs 4** to **6** (-5.85 to -5.43 eV) are within the required range for p-type semiconducting materials ensuring high open circuit voltages (V_{OC}) in heterojunction solar cells by using C_{60} as acceptor, because V_{OC} typically depends on the difference between the HOMO level of the donor and the LUMO level of the acceptor.

The HOMO/LUMO energy levels of C_{60} are also presented in Figure 9. With growing number of thiophene units from **DCV2T 2** to **DCV6T 6** the HOMO energy levels significantly increase, whereas the LUMO energy levels remain relatively unaffected. In total, this leads to a lowering of the gap. The calculated electrochemical gaps (E_g^{CV}) for all compounds are in good agreement to the optical gaps (E_g^{opt}).

5.3. Quantum Chemical Calculations

The semi-empirical Austin Model 1 (AM1) method under restricted Hartree Fock conditions was used to analyze the geometry and electron distribution of the frontier orbitals for all DCV compounds. **DCV5T 5** is shown as a representative structure in Figure 10. As illustrated there, the electron density distribution of the HOMO for all molecules is mainly located on the oligothiophene backbone, whereas the electron density of the LUMO is distributed over the whole molecule with higher density on the terminal thiophene and DCV units. With increasing number of thiophene units, it can also be seen that the electron density of the LUMO is reduced at the central thiophene unit(s). This distribution of HOMO-LUMO energies may facilitate charge transfer from the donors to the C_{60} acceptor unit in OSCs.

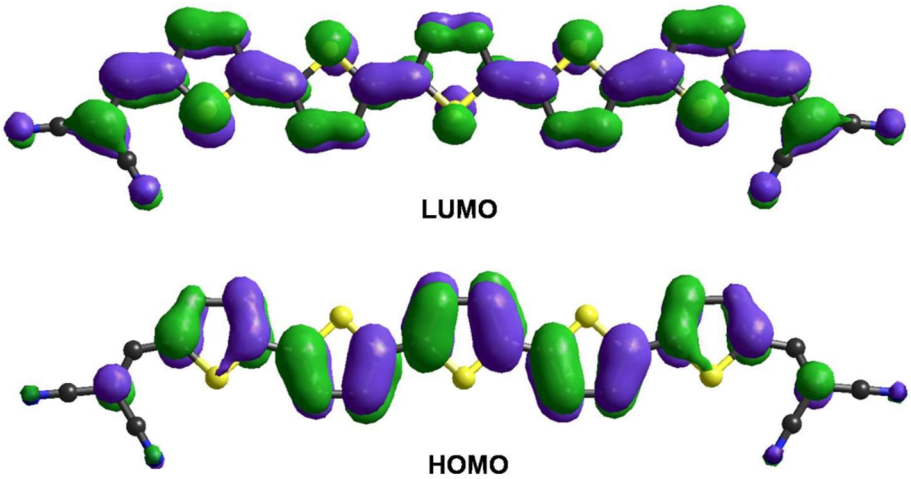

***Figure 10**: Representative frontier orbitals of **DCV5T 5** obtained by semi-empirical AM1-calculation (carbons in black, nitrogens in blue, sulfurs in yellow and hydrogens are omitted for clarity reasons).*

6. Fabrication and Characterization of DCV*n*Ts in Organic Solar Cells

The optical and redox properties of the molecules showed a significant change in absorption (see Figures 6 and 7), as well as in the energy levels along the **DCVnT** series. These changes are expected to significantly affect the properties of solar cells based on DCV*n*Ts. Given the energy levels, compounds **DCVnT 4-6** were selected as donor materials in organic solar cells using C_{60} as electron acceptor. All investigated structures are based on the m-i-p (planar heterojunction) and p-i-n concept (bulk heterojunction) and made by vacuum deposition.[60]

6.1. Planar Heterojunction Solar Cells

For initial characterization, a planar heterojunction structure was chosen. This gives a well-defined interface between donor and acceptor and allows for the investigation of the different electronic properties of the molecules in solar cells without extra effects due to bulk heterojunction morphologies. For all **DCVnTs 4-6**, the layer sequence consisted of 15 nm C_{60} evaporated on ITO coated glass, 6 nm **DCVnT**, 5 nm of undoped and 50nm of p-doped 9,9-bis{4-[di-(p-biphenyl)aminophenyl]}fluorene (BPAPF) as hole transport layer (HTL). The undoped BPAPF layer was introduced to avoid direct contact between the active layer and the doped BPAPF layer that otherwise could lead to quenching of excitons by the dopants.[30] The thickness of the doped BPAPF layer was chosen to have the active layer approximately in the interference maximum. For p-doping, NPD9 was used at 10%wt and another 1 nm thick layer of NDP9 was used between the HTL and the Au top electrode, to facilitate charge extraction. The complete stack is shown in Figure 11.

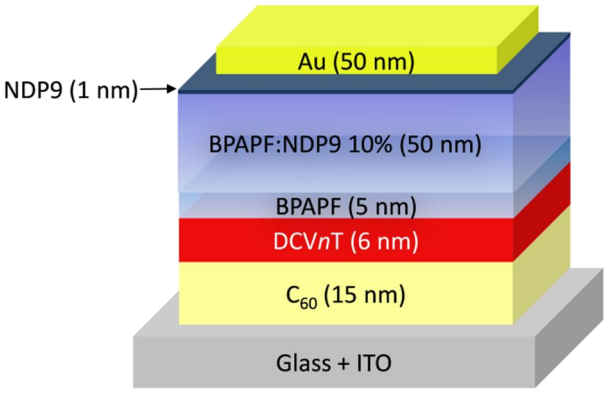

***Figure 11**: Stack structure of the solar cells with a planar heterojunctions of **DCV4T-DCV6T 4-6** and C_{60}.*

In Figure 12 the mismatch corrected current-voltage (*J-V*) characteristics of the flat heterojunction solar cells for **DCV4T 4** (device A), **DCV5T 5** (device B) and **DCV6T 6** (device C) are depicted. The corresponding solar cell parameters derived from these curves are summarized in Table 6.

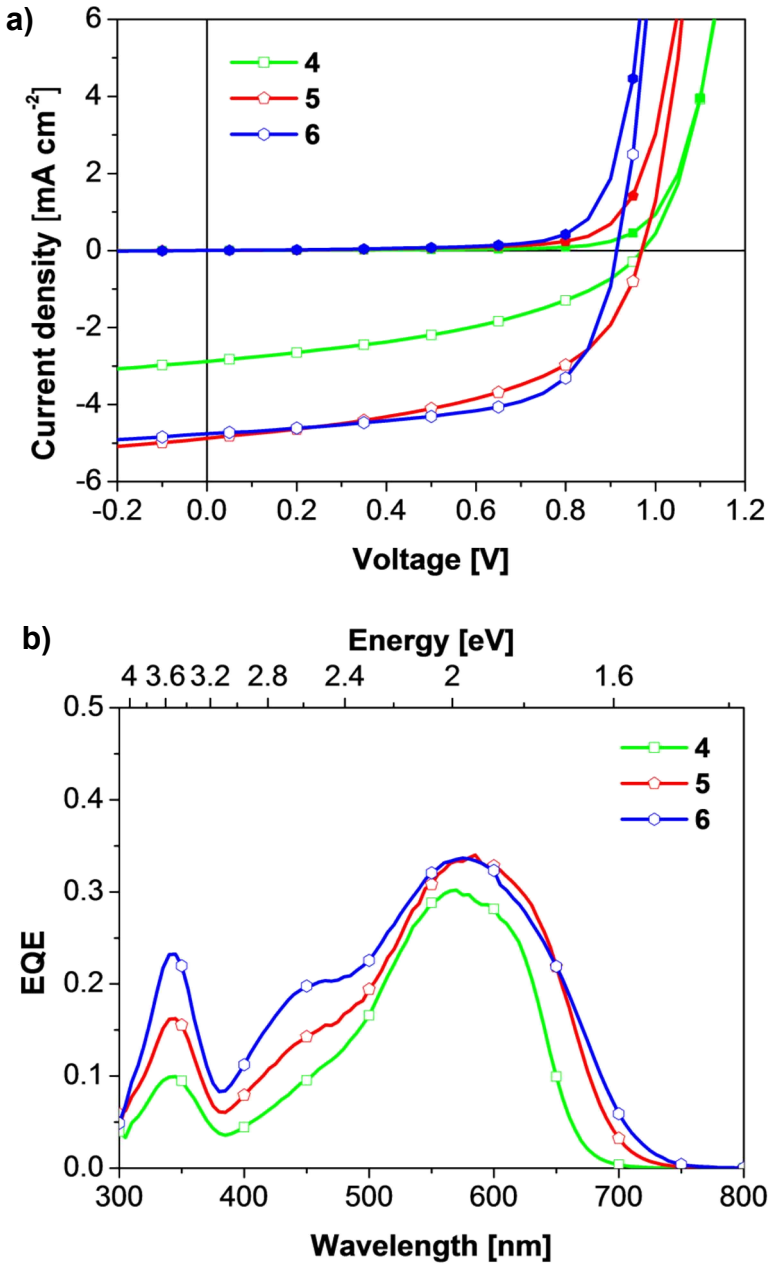

Figure 12. *(a) J-V characteristics of planar heterojunction solar cells containing* ***DCVnTs 4*** *(squares),* ***5*** *(pentagons) and* ***6*** *(hexagons) as donor materials. (b) The corresponding EQE spectra were used to calculate the mismatch factor for the J-V characteristics.*

Table 6. *Photovoltaic parameters of flat heterojunction solar cells containing* ***DCVnTs 4, 5*** *and* ***6****.*

Device	J_{SC} [mA cm²]	V_{OC} [V]	*FF* [%]	η [%]	Intensity [mW cm^{-2}]	Satu-ration	Cell area [mm²]
A (DCV4T **4**)	2.9	0.97	42	1.2	100	1.3	2.96
B (DCV5T **5**)	5.1	0.97	52	2.6	106	1.2	2.83
C (DCV6T **6**)	4.8	0.91	64	2.8	101	1.2	2.96

Device A (**DCV4T 4**) showed a V_{OC} of 0.97 V and the smallest J_{SC} of 2.9 mA/cm^2. The FF was rather low with a value of 42% and the saturation, which is defined as $J_{(-1V)}/ J_{SC}$, had a value of 1.3. The overall efficiency η was determined to 1.2%. Device B (**DCV5T 5**) showed the same V_{OC} as device A, but J_{SC} improved to 5.1 mA/cm^2 and the FF to 52% resulting in an efficiency of 2.6%. In device C (DCV6T **6**) V_{OC} dropped to 0.91 V, but J_{SC} remained with 4.8mA/cm^2 nearly similar to device B. FF reached a maximum of 64% and the resulting efficiency was 2.8%. All devices showed a high V_{OC}, as V_{OC} for flat heterojunction devices is determined by the effective gap, i.e., the energetic distance between the LUMO of the acceptor C_{60} and the HOMO of the donor.[61] However, the shift of HOMO levels with increasing thiophene chain length is only partially reflected in the decrease of V_{OC}. Devices A and B exhibited the same V_{OC} and the difference in V_{OC} for devices B and C (0.06 V) is smaller than what is expected from electrochemical measurements of the energy levels (about 0.2 V, see Table 6) and from TD-DFT calculations of the energy levels (calculated difference: 0.14 V).[34] The main reason for the differences is that both latter values were obtained for single molecules, whereas the values shift due to molecular packing in thin film. Still, the difference between optical gap and eV_{OC} at one sun intensity gives values between 0.7 and 0.8 eV, which is on the lower side in comparison to other organic materials combinations. The smallest observed difference between effective gap and eV_{OC} is about 0.4 eV, close to what is expected from the splitting of the quasi Fermi levels.

The differences in J_{SC} can be explained by the different absorption of the compounds and is reflected in the EQE spectra shown in Figure 12b, in which the contribution of the donor **DCVnT 4-6** (~400 to 800 nm) and of the acceptor C_{60} (~300 to 450 nm) to the photocurrent can be identified. The shift in thin film absorption of the donors with increasing thiophene chain length (see Table 4) is reflected in the behaviour of the EQE. There is a red-shift in EQE peak from 560nm to 580nm for device A to B, whereas there are only small differences with a small blue-shift by less than 10nm between devices B and C, but not as significant as the differences of optical gaps in thin film might suggest. Correspondingly, J_{SC} for devices B and C are

comparable, with A being much lower. In the EQE spectra it can be seen, that for all **DCVnTs 4-6** the majority of the current is coming from the donor materials. However, the EQE peak of C_{60} increases with increasing chain length. This indicates that the separation efficiency of excitons generated on the C_{60} into free charge carriers grows with increasing chain length, as expected from the changes in energy levels. This is also reflected in FF and saturation. FF continuously increases from **DCV4T 4** (42%) to **DCV6T 6** (64%), showing that exciton and charge separation efficiencies become less field-dependent with increasing chain length. Since the charge carrier mobilities in **DCVnTs** are expected to be comparable and given only 6nm of donor material, differences in FF are unlikely to be due to transport limitations. Differences in FF may occur due to injection barriers at the BPAPF interface and this should especially influence device A employing **DCV4T 4** because of its low HOMO level. However, the *J-V* characteristics for device A showed no signs of an S-kink, a feature characteristic for injection barriers.

The behaviour of the saturation is consistent with differences in exciton and charge carrier separation. A saturation value close to unity corresponds to efficient charge separation and extraction while a larger value hints for recombination losses and field dependent dissociation of charge carriers. For **DCV4T 4**, exciton separation appears to be at the limit, but it is becoming sufficient for **DCV5T 5** and **DCV6T 6**, although the peak values for all compounds do not differ much. With values between 1.2 and 1.3, the saturation shows that there is some recombination at J_{SC}-condition and in reverse bias, the increase of current without saturating shows that further charge carriers can be extracted with increasing electric field in the device and it also indicates the presence of a photoshunt.

6.2. Bulk Heterojunction Solar Cells.

In the following, we present three bulk heterojunction (BHJ) solar cells comprising a blend layer of **DCV5T 5** and C_{60} with layer thicknesses of 20, 30 and 40nm. The layer structure and the preparation process of the BHJ solar cells were optimized regarding efficiency and stability. In comparison to the planar heterojunction solar cells described above, an additional layer of n-doped C_{60} was used to stabilize the contact to the ITO and aluminum was used as top contact instead of gold providing better reflection characteristics and less parasitic absorption. Additionally, a p-doped layer of spiro-NPB was introduced in contact to the p-doped BPAPF layer. The blend ratio of **DCV5T 5** and C_{60} is 2:1 in volume, what was found to be optimal for alkylated **DCVnT** compounds.[62] The blend layer was deposited while heating the substrate to

90 °C leading to a more crystalline growth of the blend layer and enhanced fill factors compared to deposition at room temperature.[63,64] The exact layer sequence is depicted in Figure 13.

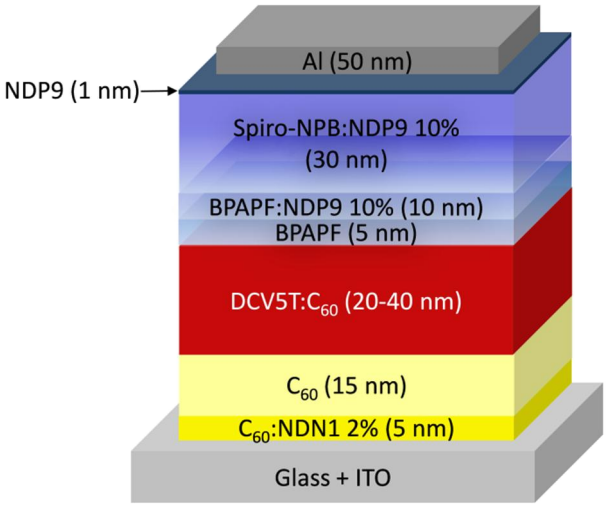

Figure 13: *Layer sequence of BHJ solar cells D, E and F incorporating a blend layer of* ***DCV5T 5*** *and* C_{60}.

Figure 14a shows the *J-V* characteristics of BHJ solar cells D, E, and F with blend layer thicknesses of 20, 30, and 40nm, respectively. The active area of the solar cells was 6.5 mm². In order to exactly determine the solar cell efficiencies, all three cells were measured with an aperture mask of 5.06 mm². The photovoltaic parameters of the three BHJ solar cells are summarized in Table 7. All of the *J-V* characteristics measured in the dark showed good rectifying behavior and similar series resistance at voltages above V_{OC}, while V_{OC} of all cells measured under illumination is almost constant (0.96 V); this is in good agreement with V_{OC} of the planar heterojunction solar cell (device B, 0.97 V) prepared with the same donor material shown above. J_{SC} steadily and significantly increased with increasing blend layer thickness indicating that we were indeed dealing with a BHJ where the complete volume of the blend contributes to the photocurrent. However, with increasing layer thickness a decrease in FF from 61% to 49% was observed. This shows that the charge carrier collection efficiency decreases with increasing layer thickness in the voltage regime around the maximum power point (MPP). The saturation of photocurrent with reverse bias for all cells is almost constant (1.1). This shows that the exciton and charge carrier dynamics at negative voltages are only weakly influenced by the blend layer thickness variations and we already collect most of the geminate carrier pairs at zero bias.

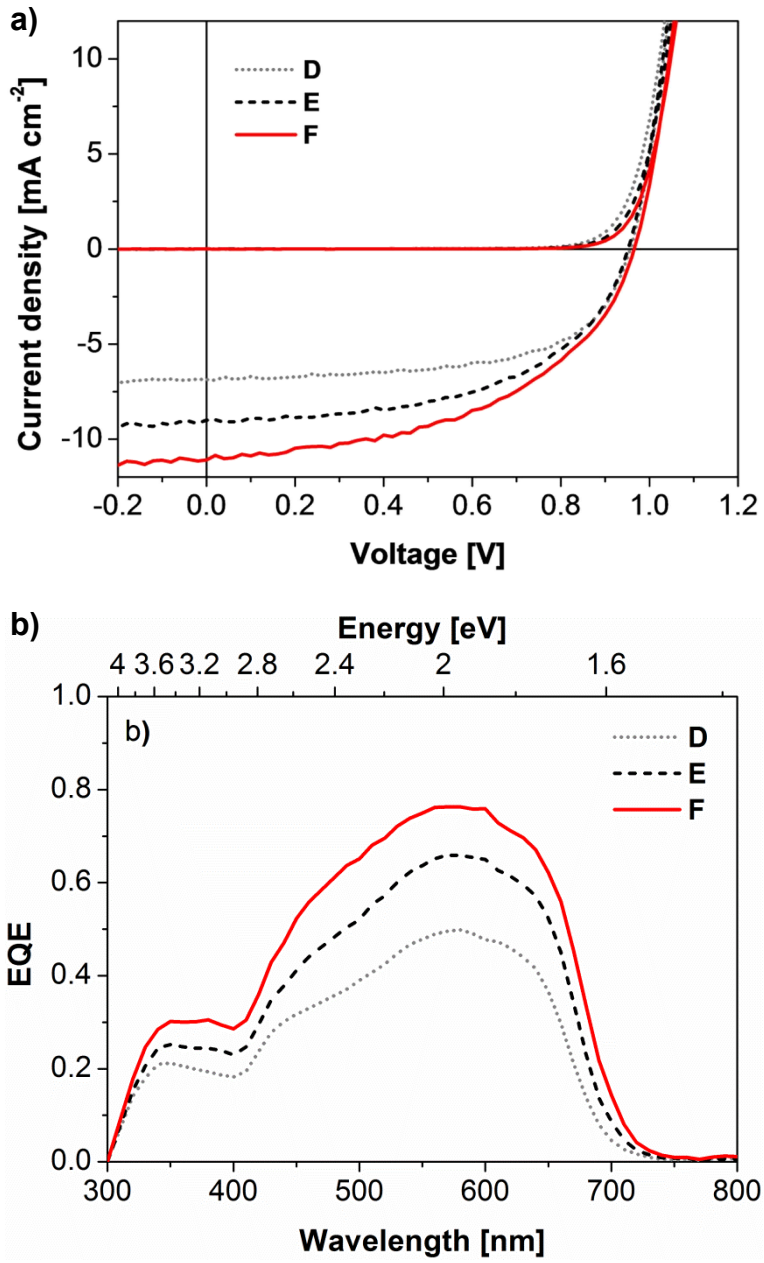

Figure 14. *(a) J-V characteristics of BHJ solar cells D (20 nm), E (30 nm) and F (40 nm) comprising a blend layer of* ***DCV5T 5*** *and* C_{60} *(blend ratio 2:1 in volume) with different thicknesses. (b) EQE spectra of BHJ solar cells D, E and F were used to calculate the mismatch factor and to calculate the corrected short current density* $J_{sc,corr}$ *from the measured J-V characteristics.*

Table 7. *Photovoltaic parameters of bulk-heterojunction solar cells containing* ***DCV5T 5*** *with blend layer thicknesses of 20, 30 and 40 nm.*

Device	Thickness [nm]	J_{SC} [mA cm^{-2}]	V_{OC} [V]	*FF* [%]	η [%]	Intensity [mW cm^{-2}]	Saturation
D	20	6.9	0.96	61	3.9	102.8	1.06
E	30	9.0	0.95	55	4.6	102.5	1.10
F	40	11.1	0.97	49	5.2	102.3	1.10

In Figure 14b, the EQE spectra of the three BHJ solar cells are shown. The spectral shape of the EQEs remained almost unchanged with changing blend layer thickness. The spectra showed a maximum at around 580 nm, a shoulder at about 450nm and a local maximum at 350nm. The maximum at 580 nm is in good agreement with the thin film absorption spectrum of DCV5T **5** (Figure 7) and the EQE spectrum of device B (Figure 13). The shoulder around 450 nm stems from the additional C_{60} in the blend layer. From the EQE spectra, the mismatch factor is calculated to account for the mismatch between sun simulator and the AM1.5 spectrum. The corrected illumination intensities are 103 mW/cm² for device D and E and 102 mW/cm² for device F. The mismatch corrected illumination intensities were used to calculate the conversion efficiencies. The mismatch corrected conversion efficiency (η_{cor}) increased with increasing blend layer thickness from 3.9% at 20nm to 5.2% at 40nm. The efficiency sublinearly increased with the blend layer thickness mostly due to the decrease of FF. This rapid decrease of FF already at moderate blend layer thickness indicates lower mobility values in the blends in spite of the favorable crystal packing for DCV*n*Ts described above. Obviously, the crystalline order seems to be at least partly lost in the blends. Another problem may be a lack of nanoscale phase separation and thus a lack of C_{60} nanocrystallites in the blends. The details of the blend layer morphology require further detailed studies and optimization. Nevertheless, the 5.2% efficiency after mismatch correction shown here already represents one of the highest values ever reported for organic vacuum-deposited single junction solar cells.

7. CONCLUSION

A novel series of terminally acceptor (dicyanovinyl)-substituted oligothiophenes, **DCVnT 1-6**, without solubilising side chains has been synthesized via a convergent approach in high yields. Repeated gradient vacuum sublimation gave thermally highly stable and pure organic semiconducting donor materials. An odd-even effect of the melting points was found and assigned to the symmetry of the molecules. An X-ray structure analysis of tetramer **DCV4T 4** revealed the importance of the DCV groups in the molecular packing in the bulk by providing intermolecular C-N and H-N interactions and a nearly ideal π–π stacking as a prerequisite for good charge transport. Characterization of the optical properties in solution and in thin films brought the expected red-shift, increase in absorptivity, and lowering of the gap with increasing chain length and number of thiophene units in the conjugated backbone. Determination of the redox potentials by cyclic and differential pulse voltammetry resulted in the similar trend, i.e., the

HOMO energies increase with increasing chain length, whereas the LUMO values stay nearly unaffected. The longer oligomers **DCVnT 4-6** were implemented in vacuum-processed planar heterojunction organic solar cells and mismatch-corrected efficiencies of 1.2-2.8% have been achieved under full sun illumination. The optimization of bulk heterojunction solar cells using a 40 nm active layer of **DCV5T 5** and C_{60} in a 2:1-ratio resulted in a mismatch-corrected value of 5.2% for a 5.06 mm^2-sized and masked device. The 5.2% efficiency reported here represents one of the highest values ever reported for organic vacuum-deposited single junction solar cells and clearly shows the advantage of a higher internal interface in bulk heterojunctions compared to planar heterojunctions. Thus, the structural fine-tuning of these A-D-A-type oligothiophenes led to highly efficient materials with sufficiently good electronic and charge transport properties, which are crucial prerequisites in bulk heterojunction devices.

8. EXPERIMENTAL

INSTRUMENTS AND SPECTROSCOPIC MEASUREMENTS

NMR spectra were recorded on a *Bruker* AMX 500 (^{1}H NMR: 500 MHz, ^{13}C NMR: 125 MHz) or an *Avance* 400 spectrometer (^{1}H NMR: 400 MHz), at 25 °C or 100 °C. Chemical shift values (δ) are expressed in parts per million using residual solvent protons (^{1}H NMR, δ_H = 2.50 for DMSO-d_6 and δ_H = 5.93 for tetrachloroethane-d_2; ^{13}C NMR, δ_C = 74.20 tetrachloroethane-d_2) as internal standard. The splitting patterns are designated as follows: s (singlet), d (doublet) and m (multiplet). The assignments are Th*H* (thiophene protons) and DCV*H* (dicyanovinyl protons). Melting points were determined using a *Mettler Toledo* DSC 823^e and were not corrected. Elemental analyses were performed on an *Elementar Vario EL*. CI mass spectra were recorded on a *Finnigan* MAT SSQ-7000.

X-ray diffraction data of **DCV4T** were collected on a *Bruker* APEX-II CCD area detector diffractometer using graphite-monochromated Mo Kα radiation. Correction for absorption (multi-scan method) was applied. The structure was solved by direct methods and refined on F^2 with the SHELXTL program package.[65] All non-H atoms were refined anisotropically. The thiophene H-atoms were placed in calculated positions and refined as riding. The structure contains accessible voids with a volume of *ca.* 400 $Å^3$. These voids represent approximately 17% of the overall volume and are filled with heavily disordered molecules, discernible from the smeared electron density (maximum electron density within the voids 4.2 $e^-Å^{-3}$). This disorder

could not be resolved during refinement; electron density associated with peaks in these voids was eventually omitted by applying the SQUEEZE option in PLATON.[66] **DCV4T**: $C_{24}H_{10}N_4S_4$, M_r = 482.60, dark-red needle with metallic lustre, 0.55x0.12x0.06 mm^3, monoclinic, $P2_1/n$, a = 3.8295(8) Å, b = 27.695(6) Å, c = 22.663(5) Å, β = 91.68(3)°, V = 2402.5(8) $Å^3$, Z = 4, μ = 0.414 mm^{-1}, d_x = 1.334 $g \cdot cm^{-3}$, T = 100 K. 36948 reflections collected (θ_{max} = 35.0°) and merged to 10230 independent data (R_{int} = 0.046); final R indices ($I > 2\sigma(I)$): $R1$ = 0.0488, $wR2$ = 0.1176. Detailed crystallographic data for structure **DCV4T** has been deposited with the Cambridge Crystallographic Data Centre as supplementary publication CCDC 786021.
Optical measurements in solution were carried out in 1 cm cuvettes with *Merck* Uvasol grade solvents. Absorption spectra were recorded on a *Perkin Elmer* Lambda 19 spectrometer and corrected fluorescence spectra were recorded on a *Perkin Elmer* LS 55 fluorescence spectrometer. Cyclic voltammetry experiments were performed with a computer-controlled *Autolab* PGSTAT30 potentiostat in a three-electrode single-compartment cell with a platinum working electrode, a platinum wire counter electrode, and an Ag/AgCl reference electrode. All potentials were internally referenced to the ferrocene/ferrocenium couple.

THIN FILM AND DEVICE FABRICATION

Thin films and heterojunction solar cell devices were prepared by thermal vapor deposition in ultra-high vacuum at a base pressure of 10^{-8} mbar onto the substrate at room temperature. Thin films for absorption and emission measurements were prepared on quartz substrates, solar cells on tin-doped indium oxide (ITO) coated glass (*Thin Film Devices*, USA, sheet resistance of 30 Ω/sq.). Layer thicknesses were determined during evaporation by using quartz crystal monitors calibrated for the respective material. The thin films prepared for absorption and emission measurements are approximately 30 nm thick. . Thin film absorption spectra were recorded on a *Shimadzu* UV-2101/3101 UV-Vis spectrometer. The thin film emission spectra were recorded with a *Edinburgh Instruments* FSP920 fluoresence spectrometer. The flat heterojunction solar cells were prepared layer by layer without breaking the vacuum and were encapsulated after processing using a glass cover under nitrogen atmosphere. The layer structure of the flat heterojunction solar cells is as follows: ITO; 15 nm C_{60} (*Bucky*, USA); 6 nm **DCVnT 4-6**; 5 nm 9,9-bis[4-(N,N-bis-biphenyl-4-yl-amino)phenyl]-9H-fluorene (BPAPF, *Lumtec*, Taiwan; ionization potential (IP) measured -5.6 eV); 50 nm BPAPF doped with p-dopant NDP9 (*Novaled AG*, Germany) with a doping concentration of 10 weight per cent (wt%); 1 nm NDP9; 50 nm Au. BPAPF and C_{60} were purified at least twice by vacuum gradient sublimation prior to

sample preparation; the dopant was used as received. NDP9 is used because of better processability, but doping of materials with low lying HOMO can be achieved in a comparable way using WO_3.

The layer structure of the bulk heterojunction solar cells: ITO; 5nm C_{60} (*Bucky*, USA) n-doped by coevaporation with NDN1 (*Novaled AG*, Germany) (2wt%); 15nm C_{60}; 20 to 40nm blend layer of DCV5T **5** and C_{60} (ratio 2:1 in volume) prepared by coevaporation deposited on heated substrate (90 °C); 5nm BPAPF; 10 nm BPAPF doped with NDP9 (10wt%); 30 nm N,N'-bis-(naphthalen-1-yl)-N,N'-bis(phenyl)-9,9-spirobifluorene (spiro-NPB, *Lumtec*, Taiwan) doped with NDP9 (10wt%); 1 nm NDP9; 100nm aluminium. Instead of acridine orange base (AOB) as n-dopant for C_{60}, NDN1 is used because of better processability, but a comparable doping performance.

PHOTOVOLTAIC CHARACTERIZATION

EQE measurements for the heterojunction solar cell devices were conducted at a custom-made setup utilizing a xenon arc lamp, a monochromator (*Newport Cornerstone*) and a lock-in amplifier (*Signal Recovery* 7265 DSP). A silicon reference diode (*Hamamatsu* S1337) was used to calibrate the setup. *J-V* characteristics were measured using an automated setup consisting of a source-measure unit (*Keithley* SMU 2400) and an AM 1.5G sun simulator (*KHS Technical Lighting* SC1200). The intensity was monitored with a silicon photodiode (*Hamamatsu* S1337) which was calibrated at Fraunhofer ISE. The mismatch between the spectrum of the sun simulator and the AM 1.5G spectrum was determined by taking these spectra as well as the spectral responses of the reference diode and the sample (from EQE measurements) into account. For well-defined active solar cell areas, aperture masks were used.

REAGENTS AND CHEMICALS

Dimethylformamide (Merck) was first refluxed over P_4O_{10} and distilled, then refluxed over BaO and distilled again. All synthetic steps were carried out under argon atmosphere. *n*-butyl lithium (1.6 N in *n*-hexane) and $CuCl_2$ were purchased from *Merck*. Malononitrile, trimethyltin chloride, 2-isopropoxy-4,4,5,5-tetramethyl[1,3,2]dioxaborolane, 2,5-dibromothiophene, 5-bromothiophene-2-carboxaldehyde and thiophene-2,5-dicarbaldehyde **7** were purchased from *Aldrich*.

2,2'-Bithiophene was synthesized from lithiated thiophene by oxidative coupling with $CuCl_2$ in 80% yield.[47] Ter-and quaterthiophene were prepared from 2,5-dibromothiophene and 5,5'-dibromo-2,2'-bithiophene[67] using Suzuki-type coupling with 2-(thien-2-yl)-4,4,5,5-tetramethyl-

[1,3,2]dioxaborolane[68] in yields of 96% and 85%, respectively. The oligothiophenes gave dialdehydes **8-10** by Vilsmeier-Haack formylation.[40-43] Compounds **11** and **12** were synthesized from 5-bromothiophene-2-carboxaldehyde and 5-bromo-5'-formyl-2,2'-bithiophene[43] by reaction with malononitrile in yields of 70% and 93%, respectively.[47,48] Distannylated compounds **13** and **14** were synthesized according to literature.[49-51] and recrystallized before use.

SYNTHESIS AND CHARACTERIZATION

*Synthesis of 2,2'-[thien-2,5-diylbis(methane-1-yl-1-ylidene)]dimalononitrile **1***: A solution of thiophene-2,5-dicarbaldehyde **7** (400 mg, 2.85 mmol) and malononitrile (766 mg, 11.6 mmol) in ethanol (35 mL) was stirred at room temperature for 10 min. The precipitate was filtered off and recrystallized from methanol to give **1** (654 mg, 2.77 mmol, 97%) as yellow needles. M.p. 272 ^{o}C (DSC). ^{1}H NMR (tetrachloroethane-d_2, 100 °C, δ ppm) 7.87 (s, 2H, DCV*H*), 7.79 (s, 2H, Th*H*). ^{13}C NMR (tetrachloroethane-d_2, 100 °C, δ ppm) 148.52, 142.05, 136.49, 112.83, 112.25, 84.58. CI mass 237 [M+H^{+}] (calcd. for $C_{12}H_4N_4S$ 236.02). Elemental analysis for $C_{12}H_4N_4S$: calcd. C, 61.01; H, 1.71; N, 23.71%; found: C, 61.10; H, 1.80; N, 23.58%.

*Synthesis of 2,2'-[2,2'-bithien-5,5'-diylbis(methane-1-yl-1-ylidene)]dimalononitrile **2***: A solution of 2,2'-bithiophene-5,5'-dicarbaldehyde **8** (1.00 g, 4.50 mmol), malononitrile (891 mg, 13.5 mmol) and β-alanine (25 mg, 0.062 mmol) in a mixture of dichloroethane (110 mL) and ethanol (110 mL) was stirred at 60 °C for 22 hours. The reaction mixture was allowed to cool to room temperature, the precipitate filtered off and washed with ethanol. The crude product was washed with hot dichloromethane to provide DCV2T **2** (1.42 g, 4.45 mmol, 99 %) as red solid. The compound was further purified by gradient vacuum sublimation. M.p. 300 ^{o}C (DSC). ^{1}H NMR (DMSO-d_6, δ ppm) 8.71 (s, 2H, DCV*H*), 7.95 (d, 2H, *J* = 4.09 Hz, Th*H*), 7.89 (d, 2H, *J* = 4.07 Hz, Th*H*). CI mass 319 [M+H^{+}] (calcd. for $C_{16}H_6N_4S_2$ 318.00). Elemental analysis for $C_{16}H_6N_4S_2$: calcd. C, 60.36; H, 1.90; N, 17.60%; found: C, 60.46; H, 1.96; N, 17.43%.

*Synthesis of 2,2'-[2,2':5',2''-terthien-5,5''-diylbis(methane-1-yl-1-ylidine)]dimalononitrile **3** by linear synthesis*: A solution of 2,2':5',2''-terthiophene-5,5''-dicarbaldehyde **9** (500 mg, 1.64 mmol), malononitrile (651 mg, 9.9 mmol) and β-alanine (18 mg, 0.2 mmol) in a mixture of dichloroethane (80 mL) and ethanol (80 mL) were stirred under reflux overnight. The reaction mixture was allowed to cool to room temperature, the precipitate filtered off and washed thoroughly with ethanol to provide compound **3** (652 mg, 1.63 mmol, 99 %) as deep red solid.

*Synthesis of 2,2'-[2,2':5',2''-terthien-5,5''-diylbis(methane-1-yl-1-ylidine)]dimalononitrile **3** by convergent synthesis*: A mixture of 2,5-bis(trimethylstannyl)thiophene **13** (25 mg, 0.061 mmol), 2-[(5-bromothiophen-2-yl)methylene]malononitrile **11** (37 mg, 0.13 mmol) and tetrakis-(triphenylphosphine)-palladium(0) (4 mg, 0.003 mmol) was combined in toluene (5 mL) in a screw cap bottle and was agitated at 110 °C for 3 hours. After cooling, the resulting precipitate was filtered off and washed several times with cold toluene, methanol and n-hexane. After drying, the product (24 mg, 0.060 mmol, 99 %) was obtained as deep red solid. The compound was further purified by gradient vacuum sublimation. M.p. 265 °C (DSC). ^{1}H NMR (DMSO-d_6, δ ppm) 8.65 (s, 2H, DCV*H*), 7.91 (d, 2H, *J* = 4.16 Hz, Th*H*), 7.73 (s, 2H, Th*H*), 7.73 (d, 2H, 3.95 Hz, Th*H*). CI mass 401 [M+H$^+$] (calcd. for $C_{20}H_8N_4S_3$ 399.99). Elemental analysis for $C_{20}H_8N_4S_3$: calcd. C, 59.98; H, 2.01; N, 13.99%; found: C, 59.79; H, 2.16; N, 13.96%.

*Synthesis of 2,2'-[2,2':5',2'':5'',2'''-quaterthien-5,5'''-diylbis(methane-1-yl-1-ylidine)]dimalononitrile **4***: A mixture of 5,5'-bis(trimethylstannyl)-2,2'-bithiophene **14** (750 mg, 1.52 mmol), 2-[(5-bromothien-2-yl)methylene]malononitrile **11** (766 mg, 3.20 mmol) and tetrakis-(triphenylphosphine)palladium(0) (88 mg, 0.08 mmol) in degassed DMF (40 mL) was stirred at 80 °C for 4 hours. After cooling, the resulting precipitate was filtered off and washed several times with methanol, *n*-hexane and acetone. After drying, the product (714 mg, 1.48 mmol, 97 %) was obtained as a black solid. The compound was further purified by gradient vacuum sublimation. M.p. 320 °C (DSC). ^{1}H NMR (DMSO-d_6, 100 °C, δ ppm) 8.53 (s, 2H, DCV*H*), 7.93 (d, 2H, *J* = 4.15 Hz, Th*H*), 7.65 (d, 2H, *J* = 3.96 Hz, Th*H*), 7.63 (d, 2H, *J* = 4.12 Hz, Th*H*), 7.52 (d, 2H, *J* = 3.96 Hz, Th*H*). CI mass 483 [M+H$^+$] (calcd. for $C_{24}H_{10}N_4S_4$ 481.98). Elemental analysis for $C_{24}H_{10}N_4S_4$: calcd. C, 59.73; H, 2.09; N, 11.61%; found: C, 59.67; H, 2.04; N, 11.59%.

*Synthesis of 2,2'-[2,2':5',2'':5'',2''':5''',2'''':quinquethien-5,5''''-diylbis(methane-1-yl-1-ylidine)]-dimalononitrile **5***: A mixture of 2,5-bis(trimethylstannyl)thiophene **13** (400 mg, 0.98 mmol), 5-[(5'-bromo-2,2'-bithien-5-yl)methylene]malononitrile **12** (659 mg, 2.05 mmol) and tetrakis(triphenylphosphine)-palladium(0) (56 mg, 0.05 mmol) in degassed DMF (25 mL) was stirred at 80 °C for 8 hours. After cooling, the resulting precipitate was filtered off and washed several times with methanol, *n*-hexane and acetone. After drying, the product (517 mg, 0.92 mmol, 94 %) was obtained as a black solid. The compound was further purified by gradient vacuum sublimation. M.p. 287 °C (DSC). ^{1}H NMR (DMSO-d_6, 100 °C, δ ppm) 8.52 (s, 2H, DCV*H*), 7.92 (dd, 2H, *J* = 0.41 Hz, *J* = 4.15 Hz, Th*H*), 7.63 (d, 2H, *J* = 3.95 Hz, Th*H*), 7.61 (d, 2H, *J* = 4.13 Hz, Th*H*), 7.45 (s, 2H, Th*H*) 7.44 (d, 2H, *J* = 3.95 Hz, Th*H*). CI mass 565 [M+H$^+$] (calcd.

for $C_{28}H_{12}N_4S_5$ 563.97). Elemental analysis for $C_{28}H_{12}N_4S_5$: calcd. C, 59.55; H, 2.14; N, 9.92%; found: C, 59.52; H, 2.24; N, 9.82%.

Synthesis of 2,2'-[2,2':5',2'':5'',2''':5''',2'''':5'''',2''''':5''''',2'''''-sexithien-5,5'''''-diylbis(methane-1-yl-1-yli-dine)]di-malononitrile ***6***: A mixture of 5,5'-bis(trimethylstannyl)-2,2'-bithiophene **14** (1.0 g, 2.03 mmol), 5-[(5'-bromo-2,2'-bithien-5-yl)methylene]malononitrile **12** (1.371 g, 4.27 mmol) and tetrakis(triphenylphosphine)palladium(0) (118 mg, 0.10 mmol) in degassed DMF (50 mL) was stirred at 80 °C for 20 hours. After cooling, the resulting precipitate was filtered off and washed several times with methanol. The crude product was extracted in a Soxhlett extractor with chlorobenzene for 8 days. The extract was cooled to room temperature and the precipitate was filtered off to yield the product (1.078 g, 1.67 mmol, 82%) as a black solid. The compound was further purified by gradient vacuum sublimation. M.p. 319 °C (DSC). ^{1}H NMR (tetrachloro-ethane-d_2, 100 °C, δ ppm) 7.69 (s, 2H, DCV*H*), 7.66 (d, 2H, *J* = 4.01 Hz, Th*H*), 7.34 (d, 2H, *J* = 3.90 Hz, Th*H*), 7.27 (d, 2H, *J* = 4.10 Hz, Th*H*), 7.16-7.18 (m, 4H, Th*H*), 7.14 (d, 2H, *J* = 3.81 Hz, Th*H*). CI mass 647 [M+H$^+$] (calcd. for $C_{32}H_{14}N_4S_6$ 645.95). Elemental analysis for $C_{32}H_{14}N_4S_6$: calcd. C, 59.42; H, 2.18; N, 8.66%; found: C, 59.62; H, 2.37; N, 8.82 %.

Crystallographic data (excluding structure factors) for the structure(s) reported in this paper have been deposited with the Cambridge Crystallographic Data Centre as supplementary publication no. CCDC-786021.

ACKNOWLEDGEMENTS

We would like to thank the German Research Foundation (DFG) for financial support in the framework of special program SPP 1355 and the Ministry for Education and Research (BMBF) in the framework of program OPEG 2010.

Submitted: August 6, 2010
Published online: January 27, 2011

REFERENCES

[1] G. A. Chamberlain, *Solar Cells* **1983**, *8*, 47.

[2] D. Wöhrle, D. Meissner, *Adv. Mater.* **1991**, *3*, 129.

[3] C. J. Brabec, N. S. Sariciftci, J. C. Hummelen, *Adv. Funct. Mater.* **2001**, *11*, 15.

[4] J.-M. Nunzi, *C. R. Physique* **2002**, *3*, 523.

[5] C. Brabec, V. Dyakonov, U. Scherf (Eds.), *Organic Photovoltaics: Materials, Device Physics, and Manufacturing Technologies*, Wiley-VCH verlag, Weinheim, **2008**.

[6] P. Peumans, A. Yakimov, S. R. Forrest, *J. Appl. Phys.* **2003**, *93*, 3693.

[7] B. C. Thompson, J. M. J. Fréchet, *Angew. Chem. Int. Ed.* **2007**, *47*, 58.

[8] M. Pagliaro, G. Palmisano, R. Ciriminna (Eds.), *Flexible Solar Cells*, Wiley-VCH, Weinheim, **2008**.

[9] O. Inganäs, F. Zhang, K. Tvingstedt, L. M. Andersson, S. Hellström, M. R. Andersson, *Adv. Mater.* **2010**, *22*, E100.

[10] C. W. Tang, *Appl. Phys. Lett.* **1986**, *48*, 183.

[11] P. Peumans, S. Uchida, S. R. Forrest, *Nature* **2003**, *425*, 158.

[12] J. Xue, S. Uchida, B. P. Rand, S. R. Forrest, *Appl. Phys. Lett.* **2004**, *85*, 5757.

[13] B. P. Rand, J. Genoe, P. Heremans, J. Poortmans, *Prog. Photovoltaics* **2007**, *15*, 659.

[14] J. Y. Kim, K. Lee, N. E. Coates, D. Moses, T.-Q. Nguyen, M. Dante, A. J. Heeger, *Science* **2007**, *317*, 222.

[15] S. Günes, H. Neugebauer, N. S. Sariciftci, *Chem. Rev.* **2007**, *107*, 1324.

[16] Y.-J. Cheng, S.-H. Yang, C.-S. Hsu, *Chem. Rev.* **2009**, *109*, 5868.

[17] G. Li, V. Shrotriya, J. Huang, Y. Yao, T. Moriarty, K. Emery, Y. Yang, *Nat. Mater.* **2009**, *4*, 864.

[18] H.-Y. Chen, J. Hou, S. Zhang, Y. Liang, G. Yang, Y. Yang, L. Yu, Y. Wu, G. Li, *Nat. Photon.* **2009**, *3*, 649.

[19] L. Huo, J. Hou, S. Zhang, H.-Y. Chen, Y. Yang, *Angew. Chem. Int. Ed.* **2010**, *49*, 1500.

[20] Y. Liang, Z. Xu, J. Xia, S.-T. Tsai, Y. Wu, G. Li, C. Ray, L. Yu, *Adv. Mater.* **2010**, *22*, E135.

[21] A. Mishra, C.-Q. Ma, P. Bäuerle, *Chem. Rev.* **2009**, *109*, 1141.

[22] J. Xue, B. P. Rand, S. Uchida, S. R. Forrest, *Adv. Mater.* **2005**, *17*, 66.

[23] A. Yassar, C. Videlot, A. Jaafari, *Sol. Energy Mater. Sol. Cells* **2006**, *90*, 916.

[24] K. Schulze, C. Uhrich, R. Schüppel, K. Leo, M. Pfeiffer, E. Brier, E. Reinold, P. Bäuerle, *Proc. SPIE Int. Soc. Opt. Eng.* **2006**, *6192*, 61920C.

[25] K. Schulze, C. Uhrich, R. Schüppel, K. Leo, M. Pfeiffer, E. Brier, E. Reinold, P. Bäuerle, *Adv. Mater.* **2006**, *18*, 2872.

[26] K. Schulze, B. Maennig, K. Leo, Y. Tomita, C. May, J. Hupkes, E. Brier, E. Reinold, P. Bäuerle, *Appl. Phys. Lett.* **2007**, *91*, 073521.

[27] P. F. Xia, X. J. Feng, J. Lu, R. Movileanu, Y. Tao, J.-M. Baribeau, M. S. Wong, *J. Phys. Chem. C* **2008**, *112*, 16714.

[28] P. F. Xia, X. J. Feng, J. Lu, S.-W. Tsang, R. Movileanu, Y. Tao, M. S. Wong, *Adv. Mater.* **2008**, *20*, 4810.

[29] D. Wynands, B. Mannig, M. Riede, K. Leo, E. Brier, E. Reinold, P. Bäuerle, *J. Appl. Phys.* **2009**, *106*, 054509.

[30] D. Wynands, M. Levichkova, M. Riede, M. Pfeiffer, P. Bäuerle, R. Rentenberger, P. Denner, K. Leo, *J. Appl. Phys.* **2010**, *107*, 014517.

[31] C. Uhrich, R. Schueppel, A. Petrich, M. Pfeiffer, K. Leo, E. Brier, P. Kilickiran, P. Bäuerle, *Adv. Funct. Mater.* **2007**, *17*, 2991.

[32] R. Schueppel, K. Schmidt, C. Uhrich, K. Schulze, D. Wynands, J. L. Bredas, B. Maennig, M. Pfeiffer, K. Leo, E. Brier, E. Reinold, H.-B. Bu, P. Bäuerle, *Proc. SPIE Int. Soc. Opt. Eng.* **2007**, *6656*, 66560G.

[33] K. Schulze, M. Riede, E. Brier, E. Reinold, P. Bäuerle, K. Leo, *J. Appl. Phys.* **2008**, *104*, 074511.

[34] R. Schueppel, K. Schmidt, C. Uhrich, K. Schulze, D. Wynands, J. L. Bredas, E. Brier, E. Reinold, H. B. Bu, P. Bäuerle, B. Maennig, M. Pfeiffer, K. Leo, *Phys. Rev. B* **2008**, *77*, 085311.

[35] M. K. Riede, R. Schueppel, K. Schulze, D. Wynands, R. Timmreck, C. Uhrich, A. Petrich, M. Pfeiffer, E. Brier, E. Reinold, P. Bäuerle, K. Leo, *Proc. SPIE Int. Soc. Opt. Eng.* **2008**, *7002*, 70020G.

[36] *Heliatek GmbH, press release, 20th August 2009*.

[37] *Heliatek GmbH, press release, 6th April 2010*.

[38] T. Sone, *Bull. Chem. Soc. Jpn.* **1964**, *37*, 1197.

[39] M. V. Joshi, M. P. Cava, M. V. Lakshmikantham, R. M. Metzger, H. Abdeldayem, M. Henry, P. Venkateswarlu, *Synth. Met.* **1993**, *57*, 3974.

[40] Y. Wei, B. Wang, W. Wang, J. Tian, *Tetrahedron Lett.* **1995**, *36*, 665.

[41] Y. Wei, Y. Yang, J.-M. Yeh, *Chem. Mater.* **1996**, *8*, 2659.

[42] R. F. Curtis, G. T. Phillips, *Tetrahedron* **1967**, *23*, 4419.

[43] R. Chen, X. Yang, H. Tian, X. Wang, A. Hagfeldt, L. Sun, *Chem. Mater.* **2007**, *19*, 4007.

[44] K. Tamao, S. Komada, I. Nakajinma, M. Kumada, A. Minato, K. Suzuki, *Tetrahedron* **1982**, *38*, 3347.

[45] C. van Pham, A. Burkhardt, R. Shabana, D. D. Cunningham, H. B. Mark, H. Zimmer, *Phosph. Sulf. Silic. Rel. Elem.* **1989**, *46*, 153

[46] A. Srinivasan, V. M. Reddy, S. J. Narayanan, B. Sridevi, S. K. Pushpan, M. Ravikumar, T. K. Chandrashekar, *Angew. Chem. Int. Ed.* **1997**, *36*, 2598.

[47] T. Qi, Y. Liu, W. Qiu, H. Zhang, X. Gao, Y. Liu, K. Lu, C. Du, G. Yu, D. Zhu, *J. Mater. Chem.* **2008**, *18*, 1131.

[48] M. M. M. Raposo, A. M. C. Fonseca, G. Kirsch, *Tetrahedron* **2004**, *60*, 4071.

[49] C. van Pham, R. S. Macomber, H. B. Mark Jr., H. Zimmer, *J. Org. Chem.* **1984**, *49*, 5250.

[50] S. Kotani, K. Shiina, K. Sonogashira, *J. Organomet. Chem.* **1992**, *429*, 403.

[51] U. Asawapirom, R. Guentner, M. Forster, T. Farrell, U. Scherf, *Synthesis* **2002**, 1136.

[52] D. Fichou, *J. Mater. Chem.* **2000**, *10*, 571.

[53] R. Azumi, M. Goto, K. Honda, M. Matsumoto, *Bull. Chem. Soc. Jpn.* **2003**, *76*, 1561.

[54] T. Kirschbaum, R. Azumi, E. Mena-Osteritz, P. Bäuerle, *New J. Chem.* **1999**, *23*, 241.

[55] R. Azumi, E. Mena-Osteritz, R. Boese, J. Benet-Buchholz, P. Bäuerle, *J. Mater. Chem.* **2006**, *16*, 728.

[56] T. M. Barclay, A. W. Cordes, C. D. MacKinnon, R. T. Oakley, R. W. Reed, *Chem. Mater.* **1997**, *9*, 981.

[57] J. Chisaka, M. Lu, S. Nagamatsu, M. Chikamatsu, Y. Yoshida, M. Goto, R. Azumi, M. Yamashita, K. Yase, *Chem. Mater.* **2007**, *19*, 2694.

[58] T. Johansson, W. Mammo, M. Svensson, M. R. Andersson, O. Inganäs, *J. Mater. Chem.* **2003**, *13*, 1316.

[59] Q. Xie, F. Arias, L. Echegoyen, *J. Am. Chem. Soc.* **1993**, *115*, 9818.

[60] M. Riede, T. Mueller, W. Tress, R. Schueppel, K. Leo, *Nanotechnology* **2008**, *19*, 424001 (12pp).

[61] D. Cheyns, J. Poortmans, P. Heremans, C. Deibel, S. Verlaak, B. P. Rand, J. Genoe, *Phys. Rev. B* **2008**, *77*, 165332.

[62] D. Wynands, M. Levichkova, C. Uhrich, D. Hildebrandt, G. Schwartz, M. Pfeiffer, K. Leo, M. Riede, *Appl. Phys. Lett.* **2010**, in print.

[63] A. Opitz, M. Bronner, W. Brutting, *J. Appl. Phys.* **2007**, *101*, 063709.

[64] M. Y. Chan, S. L. Lai, M. K. Fung, C. S. Lee, S. T. Lee, *Appl. Phys. Lett.* **2007**, *90*, 023504.

[65] G. M. Sheldrick, *Acta Crystallogr*.**2008**, *A64*, 112.

[66] A. L. Spek, *Acta Crystallogr.* **2009**, *D65*, 148.

[67] P. Bäuerle, F. Würthner, G. Goetz, F. Effenberger, *Synthesis* **1993**, 1099.

[68] Y. Dienes, S. Durben, T. Kárpáti, T. Neumann, U. Englert, L. Nyulászi, T. Baumgartner, *Chem. Eur. J.* **2007**, *13*, 7487.

CHAPTER IV

INTERRELATION BETWEEN CRYSTAL PACKING AND SMALL MOLECULE ORGANIC SOLAR CELL PERFORMANCE

Roland Fitzner,[a] Chris Elschner,[b] Matthias Weil,[c] Christian Uhrich,[d] Christian Körner,[b] Moritz Riede,[b] Karl Leo,[b] Martin Pfeiffer,[d] Egon Reinold,[a] Elena Mena-Osteritz,[a,*] and Peter Bäuerle[a,*]

[a] Institute of Organic Chemistry II and Advanced Materials, University of Ulm, Albert-Einstein-Allee 11, 89081 Ulm, Germany

[b] Institute of Applied Photophysics, TU Dresden, Mommsenstraße 13, 01062 Dresden, Germany

[c] Institut für Chemische Technologien und Analytik, Abteilung Strukturchemie, Technische Universität Wien, Getreidemarkt 9/164-SC, 1060 Vienna, Austria

[d] Heliatek GmbH, Treidlerstr. 3, 01139 Dresden, Germany

Dedicated to Prof. Dr. Dr. h.c. Klaus Müllen (Max-Planck-Institut für Polymerforschung, Mainz) one of the outstanding pioneers in molecular and organic electronics, on the occasion of his 65th birthday.

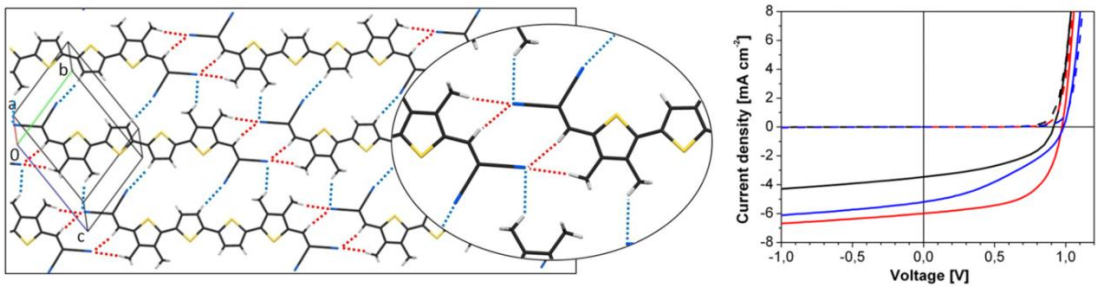

Reproduced and adapted with permission from

R. Fitzner *et al.*, *Advanced Materials* **2012**, *24*, 675-680.

Copyright © 2012 WILEY-VCH Verlag GmbH & Co. KGaA, Weinheim.

ABSTRACT

X-ray investigation on single crystals of a series of terminally DCV-substituted quaterthiophenes and co-evaporated blend layers with C_{60} give insight into molecular packing behavior and morphology, which are crucial parameters in organic electronics. Structural characteristics on various levels and length scales are correlated with the photovoltaic performance of bulk heterojunction small molecule organic solar cells.

The dynamic development in small molecule organic solar cells (SMOSC) has recently led to high power conversion efficiencies (PCE) of >8% approaching those of polymer-based devices.[1] Structurally well-defined oligomeric materials avoid the inherent batch-to-batch variations of physical properties for corresponding polymers and therefore provide higher reproducibility. Various types of donor/acceptor-based π-conjugated oligomeric systems with tailored optoelectronic and transport properties have been straightforwardly synthesized leading to record PCEs of 6.7% for solution-processed bulk-heterojunction (BHJ)[2] and 8.3% for vacuum-processed tandem SMOSCs.[3]

The photovoltaic performance of organic solar cells in general depends on various parameters and besides the optimization of molecular properties, such as optical and redox, the rational improvement of bulk properties responsible for the charge carrier mobility, processability, and thermal stability still remains mostly empirical. The bulk characteristics in turn depend on non-bonding intermolecular interactions, which lead to specific molecular order, packing, and morphology in the solid state.[4-6] A good performance of BHJ SMOSCs is only guaranteed if an interpenetrating network of the oligomeric donor (D) and an electron-acceptor (A), typically a fullerene derivative, is formed at the nanoscale as the photoactive layer.[7-9] Moreover, the size of the D and A homophases is crucially important for the diffusion of excitons to the D-A interface, subsequent charge separation, and effective charge transport to the electrodes.[2,9-11]

Investigation of the morphology of the phase-separated blend layers by transmission electron microscopy (TEM)[12] or X-ray diffraction (XRD)[13] have shed light into this complex puzzle. The use of small molecules in OSCs provides in contrast to polymeric materials another advantage: single crystals suitable for X-ray structure analysis become available providing detailed insight into intermolecular interactions and non-bonding atomic contacts responsible for the observed packing motifs.[14]

In this contribution, synthesis, thermal, and optoelectronic properties of a series of terminally acceptor-substituted quaterthiophenes will be presented. A correlation between X-ray data and photovoltaic performance of corresponding BHJ-SMOSCs will be established.

We have synthesized a series of dicyanovinyl (DCV)-substituted quaterthiophenes **DCV4T 1**,[14] **DCV4T-Me 2**, and **DCV4T-Et 3** by systematical variation of substituents at the terminal thiophene units from hydrogen to methyl and ethyl **(Scheme 1)**. As in the case of parent compound **DCV4T 1**,[14] for the synthesis of quaterthiophenes **DCV4T-Me 2** and **DCV4T-Et 3** a convergent route was chosen. Both compounds were synthesized in good yields by Stille-type cross-coupling reactions of dicyanovinyl (DCV)-substituted bromothiophenes **6** or **7**, bearing methyl or ethyl side groups in the *β*-positions, and bisstannylated bithiophene **8** as central buil-

ding block (Scheme 1). DCV-derivatives **6** and **7** were prepared in good yields from bromothiophene carbaldehydes **4** and **5** by Knoevenagel condensation with malononitrile using *β*-alanine as catalyst.

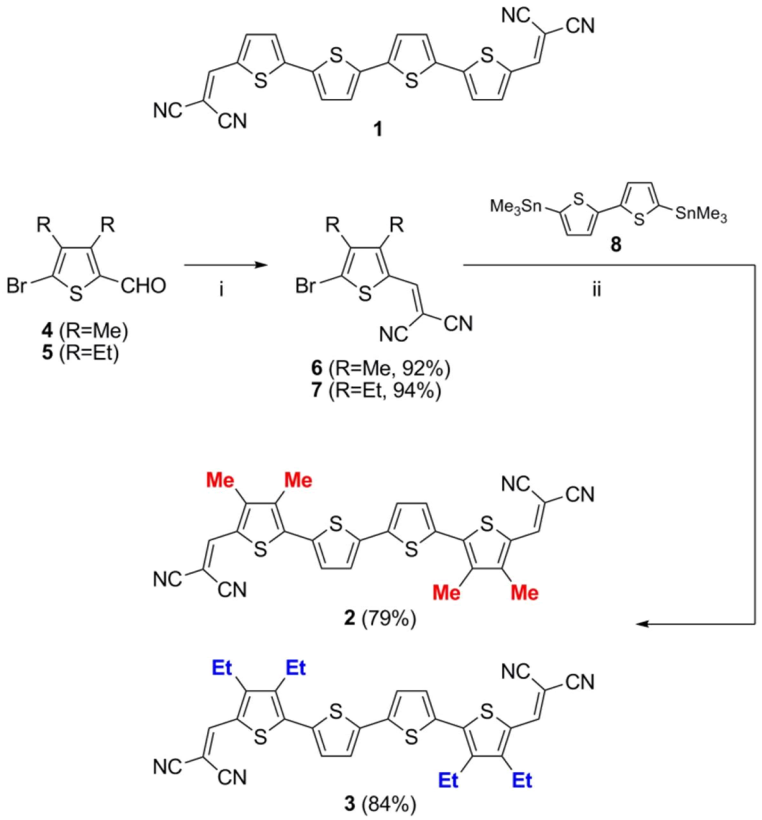

Scheme 1. *Molecular structures of quaterthiophene donors **1-3** and corresponding synthesis of compounds **2** and **3**. Reagents: (i) $CH_2(CN)_2$, β-alanine, ethanol/dichloroethane, reflux; (ii) $Pd(PPh_3)_4$, DMF, 80 °C.*

For the fabrication of organic solar cells by vacuum deposition, good thermal stability of the organic semiconductor materials is an important prerequisite. Thermal properties of tetramers **1-3** were investigated using differential scanning calorimetry (DSC**)** (Figure S1) and thermal gravimetric analysis (TGA) (Figure S2). TGA showed enhanced thermal stability for non-alkylated **DCV4T 1** with an decomposition onset temperature (T_d) of ≈ 400 °C compared to alkylated derivatives **2** and **3** (T_d ≈ 370 °C). DSC revealed melting points in the same temperature region for DCV4T **1** (320 °C) and **DCV4T-Et 3** (337 °C), whereas for methylated **DCV4T-Me 2** melting was not detected before decompositon. This result points to stronger intermolecular interactions in the solid state for **2** compared to derivatives **1** and **3**.

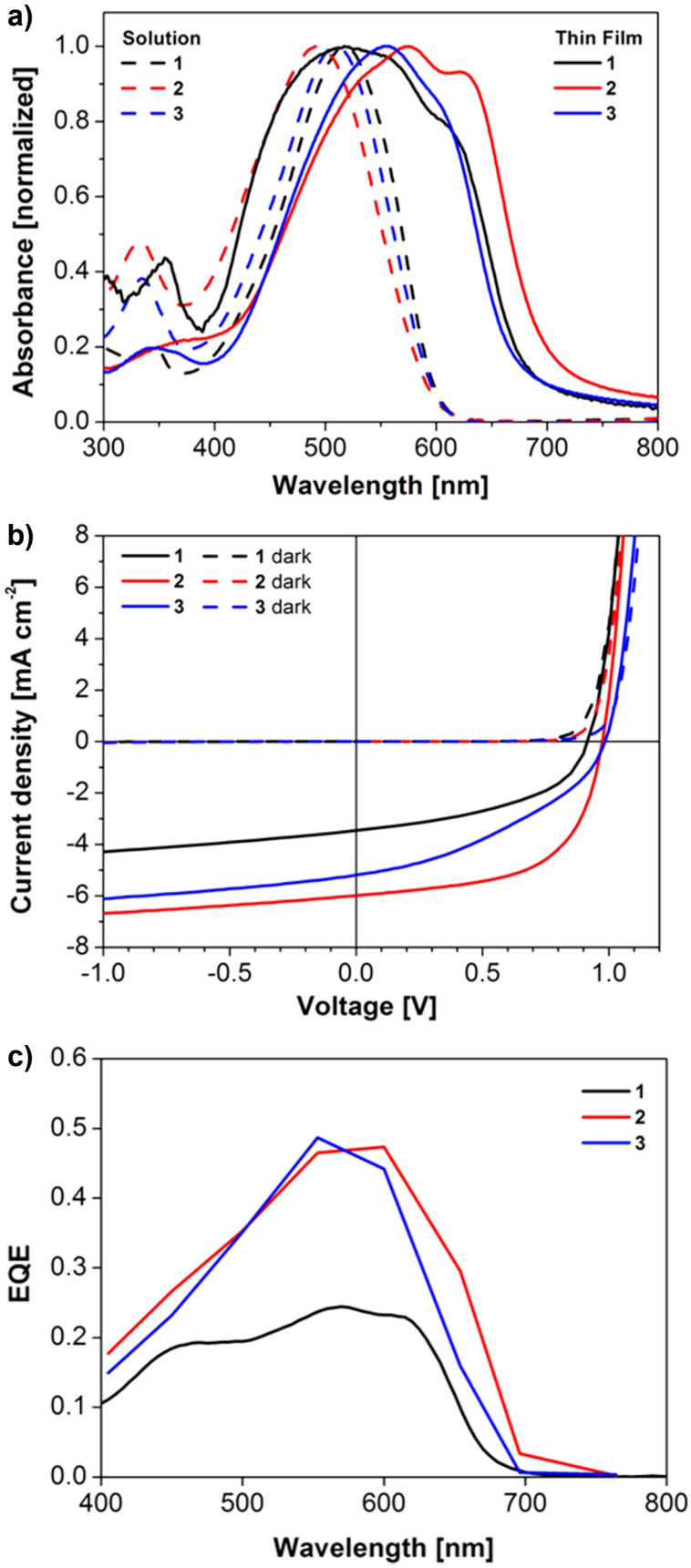

Figure 1. *(a) Absorption spectra of quaterthiophenes* ***1-3*** *measured in tetrachloroethane at 80 °C (dashed lines) and in 30 nm thin films (solid lines). (b) J-V characteristics of bulk heterojunction solar cells containing oligomers* ***1-3*** *as donor materials. c) EQE spectra of BHJ solar cells comprising* ***1-3****.*

Table 1. *Optoelectronic properties of quaterthiophenes* ***1-3****.*

Oligo-mer	λ_{max}^{abs} [nm] sol.[a]	E_g^{opt} [eV] sol. [a],[b]	λ_{max}^{abs} [nm] film	E_g^{opt} [eV] film[b]	$E°_{Ox1}$ [V] sol.[a]	$E°_{Red}$ [V] sol.[a]	HOMO [eV][c]	LUMO [eV][c]	E_g^{CV} [eV] sol.
1[d]	518	2.09	560 (521,620)	1.82	0.84	-1.52, -1.41[e]	-5.85	-3.87	1.98
2	493	2.11	574 (530,634)	1.77	0.76	-1.53	-5.78	-3.73	2.05
3	509	2.09	555 (608)	1.84	0.73	-1.59	-5.73	-3.72	2.01

[a] Measured in tetrachloroethane solution at 80 °C. [b] Optical gaps estimated from onset values in UV-vis spectra. [c] Calculated from the onset of the respective redox waves, Fc/Fc^+ is set to -5.1 eV vs. vacuum. [d] Values taken from ref. 14. [e] Values determined by differential pulse voltammetry (DPV).

Optical data of the quaterthiophene series were obtained from tetrachloroethane solutions at 80 °C and from 30 nm thin films prepared by vacuum deposition on quartz glass (Figure 1a, Table 1). In solution, the unstructured π-π* absorption band reveals reduced conjugation of the oligothiophene backbone in case of the substituted compounds **2** and **3** (λ_{max} = 493 and 509 nm) with respect to **DCV4T 1** (λ_{max} = 518 nm). In thin films, the absorption maxima are red-shifted and exhibit vibronic progression suggesting planarization and aggregation of the molecules in the bulk. Methyl derivative **2** showed the longest red-shift ($\Delta\lambda$ = 81 nm) and the most pronounced low-energy shoulder, which indicates better ordering of the molecules in the bulk. The optical band gaps were determined from the onset of absorption and were in the range of 2.1 eV in solution and 1.8 eV in the solid state.

Redox properties of **DCV4T 1-3** were measured in tetrachloroethane solutions at 80 °C containing tetrabutylammonium hexafluorophosphate (0.1 M) as supporting salt (Figure S3-S4, Table 1). The first oxidation and the first reduction potential, the electrochemical band gap and the calculated energy levels of the frontier orbitals are quite similar for all three compounds. As expected, the HOMO levels of the tetramers lie sufficiently low in energy to guarantee high open circuit voltages (V_{OC}) and the LUMOs sufficiently high to provide efficient electron transfer to the LUMO of the acceptor C_{60} (≈ -4.1 eV).[15]

DCV4T derivatives **1-3** were used as the donor and C_{60} as the electron acceptor in bulk heterojunction SMOSCs made by vacuum deposition with the following layer sequence: 15 nm C_{60} evaporated on ITO-coated glass, followed by the photoactive blend layer of **DCV4T 1-3** and C_{60}, 2:1 by volume through co-evaporation at a substrate temperature of 70 °C, 5 nm of 9,9-bis{4-[di(p-biphenyl)aminophenyl]}fluorene (BPAPF), 50 nm of BPAPF p-doped with 10wt% NDP9, both as hole transport layers. Another 1 nm thick NDP9 layer and the Au top electrode completed the stack (Figure S5).

The photovoltaic data are summarized in Table 2 and *J-V* characteristics of the solar cells are shown in Figure 1b. As expected, high V_{OC}s close to 1 V were found for all three compounds.

The photocurrent density J_{SC} was highest for **DCV4T-Me 2** (6.5 mAcm^{-2}), slightly smaller for **DCV4T-Et 3** (5.7 mAcm^{-2}), and significantly decreased for **DCV4T 1** (3.5 mAcm^{-2}). High saturation (J(-1V)/J_{sc}), i.e., weak voltage bias dependence of the current in reverse direction, was observed in particular for **DCV4T-Me 2** indicating good charge carrier transport through the bulk. These results correlate well with the EQE-spectra (Figure 1c) showing the most effective conversion of incoming photons to charge separated species in the case of **DCV4T-Me 2**. This fits the thin film absorption spectra, which already suggested better ordering of the methylated derivative **2** in comparison to the other **DCV4Ts**. Accordingly, the fill factors varied significantly from 0.59 for **DCV4T-Me 2** to 0.47 for **DCV4T 1** and to 0.39 for **DCV4T-Et 3**. Finally, **DCV4T-Me 2**-based solar cell showed the highest PCE (3.8%) in the series outperforming **DCV4T-Et 3** (2.2%) and **DCV4T 1** (1.5%).

Table 2. *Photovoltaic parameters of bulk heterojunction solar cells containing quaterthiophene donors* ***1-3*** *deposited at a substrate temperature of 70 °C.*

Oligo-mer	V_{OC} [V]	J_{SC} [mA cm^{-2}]	FF [%]	PCE [%]	Intensity [mW cm^{-2}]	Saturation
1	0.92	3.5	47	1.5	102	1.24
2	0.98	6.5	59	3.8	91	1.12
3	0.98	5.7	39	2.2	91	1.18

X-ray methods on homo- and heterophases were applied in order to understand the molecular ordering in the bulk heterojunctions. Thermal gradient sublimation ($p \approx 10^{-6}$ mbar, T = 300-330 °C) was performed for oligomers **2** and **3** providing crystalline material of high purity in almost quantitative yield. Dark red single crystals could be isolated and were investigated by X-ray structure analysis. Both compounds **DCV4T-Me 2** and **DCV4T-Et 3** crystallized in the triclinic space group P-1 with one and two molecules in the unit cell, respectively (see Supporting Information, SI). We include the crystal structure of **DCV4T 1** in the discussion in order to compare and to evaluate the influence of methyl or ethyl groups on the crystal packing.[14]

At the molecular level, only small differences concerning bond lengths, angles and dihedral angles were found for the three derivatives **1-3**: the most relevant ones ($|\Delta| > 0.1$ Å) concern the C-C and C-S single bonds in the terminal thiophene rings which elongate with increasing size of the alkyl groups and the C-CN single bond in the DCV groups (Tables S1, S2). At the outer thiophenes, the S-C-C angle towards the DCV groups slightly decreases (**1**: 126.93°, **2**: 124.86°, **3**: 124.54°) with increasing size and induced steric hindrance of the alkyl substituents.

Derivatives **1** and **2** showed an almost planar conformation whereas ethyl derivative **3** displayed the highest out-of-plane torsional angles of 146.9° and 157.2° for the terminal thiophenes. In the case of **DCV4T-Me 2** the DCV groups are nearly *syn*-coplanar (1.11°), whereas an increasing distorsion was found for **3** (2.17°/4.22°) and **1** (5.13°), respectively.

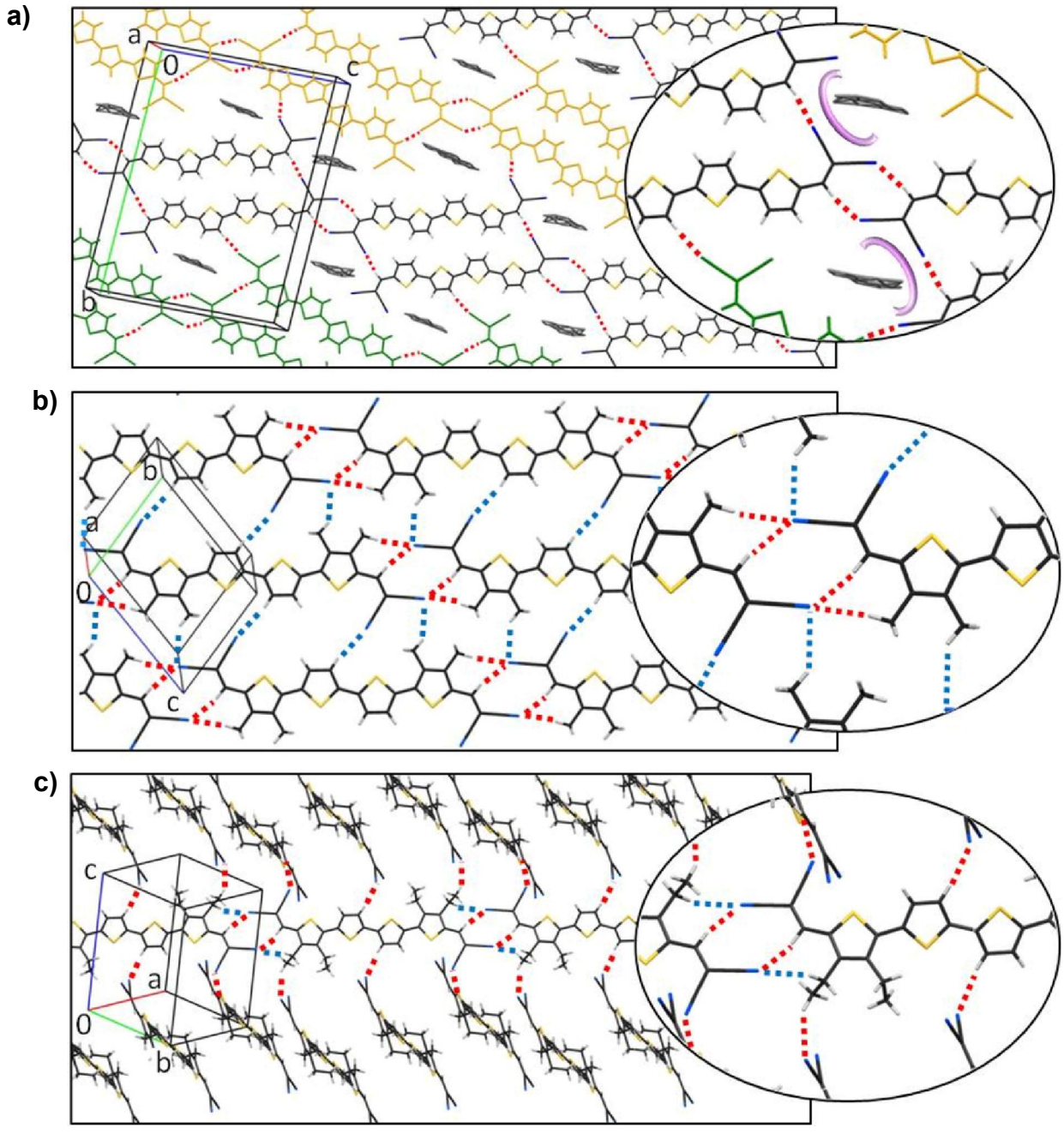

Figure 2. *X-Ray structure analysis of quaterthiophenes a)* ***DCV4T 1****, b)* ***DCV4T-Me 2****, and c)* ***DCV4T-Et 3*** *in the molecular plane of the single crystals and details of the short atomic distances (insets).*

In order to compare the molecular packing of the three compounds, the arrangement close to the *b-c* plane, in which the molecules form an almost layered structure (Figure 2) and in the plane

perpendicular to the molecular layers (Figure 3) are analyzed. **DCV4T-Me 2** exhibits a perfect layer arrangement of the molecules (Figure 2b): In one direction, the molecules form rows interacting via two times four weak C**H**···**N**C hydrogen bonds[16] between vinyl and methyl hydrogens and DCV groups (red lines in Figure 2b). In the perpendicular direction, the rows of molecules are offset by 0.6 nm in plane and the layer formation is greatly stabilized by thiophene-**H**···**N**C interactions (labeled blue in Figure 2b and inset).

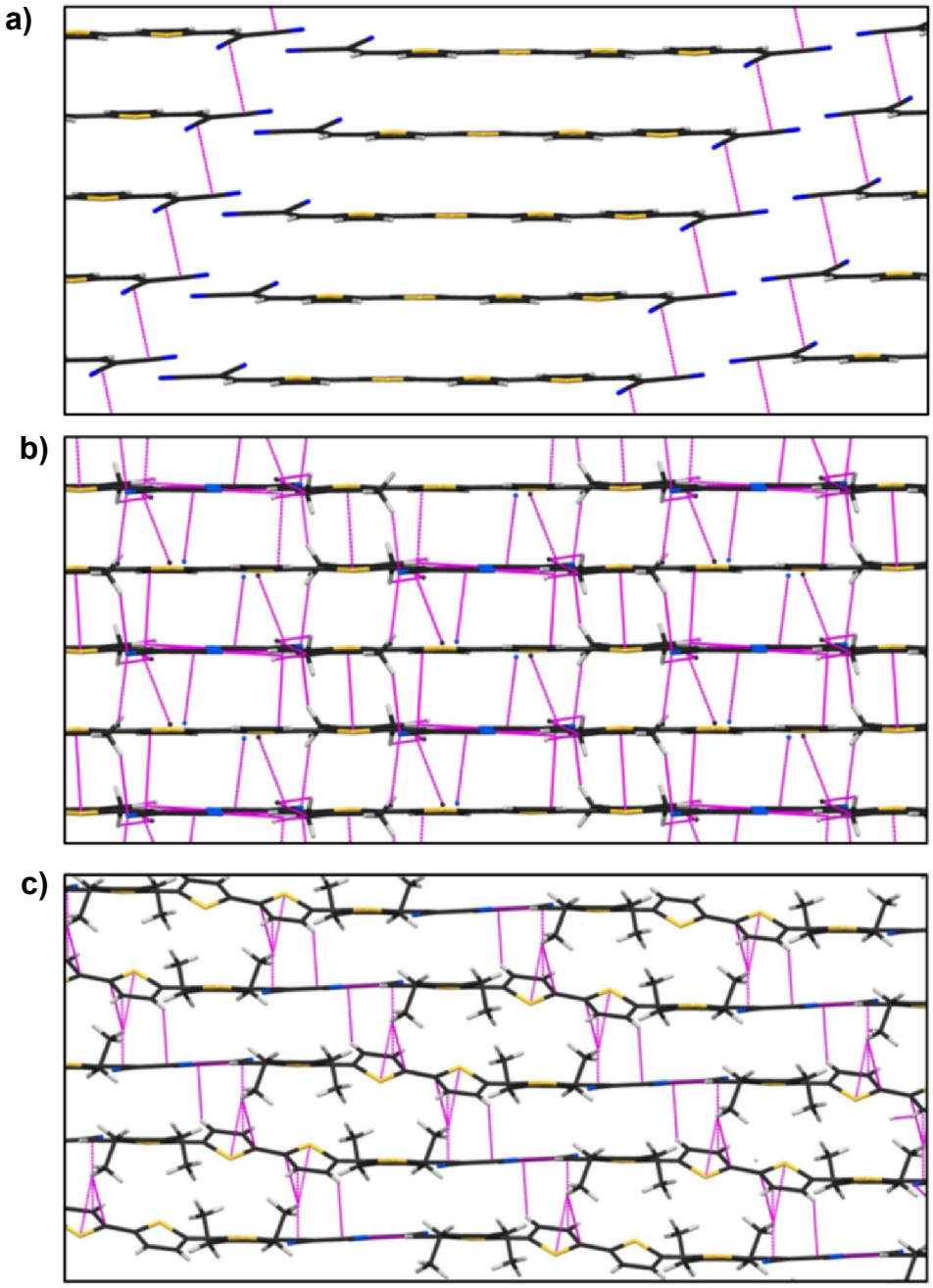

Figure 3. *X-ray structure analysis of the single crystals of compounds a)* ***DCV4T 1****, b)* ***DCV4T-Me 2****, and c)* ***DCV4T-Et 3*** *in the plane perpendicular to the molecular layer (short contacts labeled pink). The perpendicular channels in a) and the escorting molecules in c) are omitted for clarity.*

The crystal structure of DCV4T **1** in the *b-c* plane shows row-forming pairs of molecules interacting via weak vinyl-**H**···**N**C hydrogen-bonds (labeled red in Figure 2a). The rows, which are slightly out of plane (labeled yellow and green in Figure 2a) are interconnected in a network fashion via thiophene-**H**···**N**C hydrogen-bonds. The 2D network presents, however, some vacancies which lead in the 3D crystal to the formation of channels of 1 x 0.6 nm^2 cross section, in which residual high electron density has been found. This corresponds to disordered molecules trapped in columnar voids which interact via multiple contacts with the 2D network (purple crescent lines in Figure 2a inset).

Finally, **DCV4T-Et 3** exhibited a more complex molecular order: As in the former cases, the molecules in a row interact via vinyl-**H**···**N**C hydrogen-bonds and weaker methylene-**H**···**N**C interactions at van der Waals distances (labeled red and blue in Figure 2c). Such a row is escorted by two perpendicular stacks of molecules and interacts via methyl-**H** and thiophene-**H**···**N**C hydrogen-bond motifs. In the escorting rows *π-π* stacking distances as short as 3.332 Å were found (Table 3) despite substantial torsion angles between thiophene units.

The crystal structures of **DCV4T 1-3** in the plane perpendicular to the one described above are depicted in Figure 3. Between two π-π stacked molecules of **DCV4T 1,** only one N**C**···**C**N short distance as close as 3.328 Å is found (Figure 3a). The complex stacks seen in **DCV4T-Et 3** are stabilized by short contacts between the central thiophenes and the DCV part of the adjacent molecules with distances of 3.372 Å to 3.332 Å (Figure 3c, right, Table 3). The closest distances, however, can be found in the π-π stacking direction of the **DCV4T-Me 2** crystal: small values of 3.571 Å, 3.295 Å and 3.176 Å corresponding to **S**···**S**, **C**···**C** and **C**···**N** distances, respectively, were determined (Figure 3b, Table 3). Furthermore, several C**H**···· **π** short contacts strengthen the π-π interaction in the crystal structure of **DCV4T-Me 2**. In contrast to **DCV4T-Et 3** and **DCV4T 1**, crystals of the methyl derivative show a defect-free close packed layered structure.

With respect to the number of molecular interactions in a crystal, **DCV4T 1** showed seven stabilizing short contacts to eight neighboring molecules. In the case of **DCV4T-Et 3**, one molecule showed up to 28 interactions to ten adjacent molecules. One molecule of **DCV4T-Me 2** exhibited 24 interactions to six surrounding molecules. From this analysis we calculated the number of interactions per molecule: 0.9 for **DCV4T 1**, 2.8 for **DCV4T-Et 3**, and 4.0 for **DCV4T-Me 2**. The short contact analysis allows us to postulate a better and persistent bulk order for methylated derivative **2**, whose molecules undergo a significantly more efficient electronic coupling than in **DCV4T 1** and **DCV4T-Et 3**.

Table 3. *Short intermolecular contacts below van der Waals radii in single crystals of* ***DCV4T 1-3****.*

Contacts **DCV4T 1**			Distance [Å]	Contacts **DCV4T 1**			Distance [Å]
C23[a]	····	C24[b]	3.328	H14[a]	····	N1[d]	2.681
H11[a]	····	H2[c]	2.388	H17[a]	····	N3[e]	2.498
H21[a]	····	N4[c]	2.504	H7[a]	····	N2[f]	2.604
Contacts **DCV4T-Me 2**			Distance [Å]	Contacts **DCV4T-Me 2**			Distance [Å]
S1[a]	····	S1[b]	3.571	H19C[a]	····	C17[e]	2.894
N2[a]	····	H22B[b]	2.603	C6[a]	····	C21[b]	3.295
N2[a]	····	C23[c]	3.176	C24[a]	····	C24[c]	3.328
N1[a]	····	H19B[d]	2.666	C17[a]	····	C17[e]	3.376
N1[a]	····	H12[d]	2.483				
Contacts **DCV4T-Et 3**			Distance [Å]	Contacts **DCV4T-Et 3**			Distance [Å]
S1[a]	····	H32A[b]	2.930	C31[a]	····	C28[d]	3.385
C2[a]	····	C12[b]	3.372	C3[a]	····	H31B[b]	2.824
N1[a]	····	H12[c]	2.420	C28[a]	····	H31A[d]	2.832
N2[a]	····	H18[d]	2.660	C26[a]	····	C18[h]	3.332
N3[a]	····	H2[e]	2.696	H3[a]	····	C15[b]	2.840
N4[a]	····	H32B[f]	2.706	C1[a]	····	H32A[b]	2.850
N4[a]	····	H26[g]	2.434				

Symmetry codes (**1**): [a] x,y,z; [b] 1+x,y,z; [c] 1-x,1-y,1-z; [d] 1/2+x,1/2-y,-1/2+z; [e] 4-x,1-y,-z; [f] 1.5+x,1/2-y,-1/2+z. Symmetry codes (**2**): [a] x,y,z; [b] 1-x,1-y,1-z; [c] -x,1-y,-z; [d] -x,-y,-z; [e] -x,-y,1-z. Symmetry codes (**3**): [a] x,y,z; [b] 1+x,y,z; [c] 1-x,1-y,1-z; [d] 1-x,1-y,2-z; [e] 2-x,1-y,2-z; [f] x, -1+y,1+z; [g] 1-x,-y,2-z; [h] -x,1-y,2-z.

In order to gain deeper insight into the morphological behavior of **DCV4T-Me 2** in the device, grazing incidence X-ray diffraction (GIXRD) measurements on 75 nm thick blend layers with C_{60} (2:1 by volume) deposited at a substrate temperature of 70 °C were carried out (Figure 4). For comparison, the GIXRD diagram of pristine C_{60} and the XRD pattern calculated from the single crystal X-ray data of **DCV4T-Me 2** are included. The spectrum of neat C_{60} films (blue line) showed characteristic reflection peaks at 10.8°, 17.78°, and 20.77°. In the blend (black line), however, a broad signal at the fullerene double pattern indicates low crystallinity of the acceptor phase. Thus, the fullerene contribution to the intense reflection at 11.6° (d = 7.63 Å) is practically negligible. Therefore, we can assign the major narrow peak of the blend to the main calculated diffraction at 12° (d = 7.41 Å) of **DCV4T-Me 2** (red line). Furthermore, the small Bragg reflection at 25.95° (d = 3.43 Å) in the blend can be assigned to the calculated X-ray peak of **2** (26.69°, d = 3.34 Å). The shift of the experimentally determined peaks of the blend layer compared to the calculated ones corresponds to a slight relaxation and enlargement of the cell dimensions of about 3%. This exceptional agreement between the packing behavior of **DCV4T-Me 2** in the blend with C_{60} and the single crystal was not found in case of derivatives **1** and **3**.

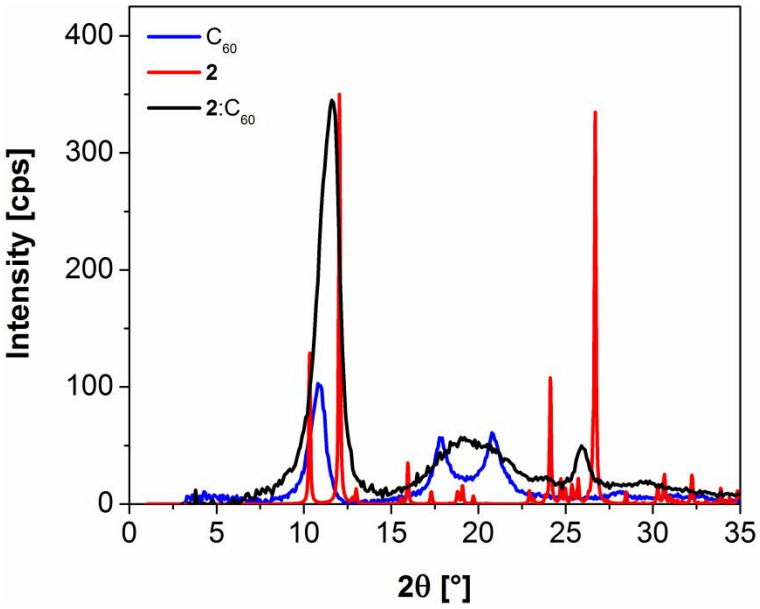

Figure 4. *GIXRD pattern of a 75 nm thick blend layer of* ***DCV4T-Me 2****:C_{60} (2:1 by volume) fabricated by co-evaporation on a glass substrate at 70 °C (black line) compared to pristine C_{60} (blue line) and the powder pattern calculated from the* ***DCV4T-Me 2*** *crystal structure (red line).*

The OFET hole mobilities of the **DCV4T** derivatives **1-3** reinforce the importance of the molecular order and packing in the bulk and correlate with the trend found in the X-ray structure analysis. **DCV4T-Me 2** exhibited the highest value in the series, 2 x 10^{-4} cm^2 V^{-1} s^{-1}, substantially higher than DCV4T **1** and **DCV4T-Et 3** with 9.4 x 10^{-5} $cm^2V^{-1}s^{-1}$ and 2.7 x 10^{-5} cm^2 V^{-1} s^{-1}, respectively.

In summary, a series of terminally DCV-substituted quaterthiophenes **DCV4T 1**,[14] **DCV4T-Me 2**, and **DCV4T-Et 3** in which we systematically varied the substituents at the terminal thiophene units from hydrogen to methyl and ethyl has been synthesized and characterized with respect to thermal, optoelectronic, and photovoltaic properties. Methyl derivative **2** in conjunction with fullerene C_{60} gave the best PCE (3.8%) in the series owing to enhanced photocurrent density (J_{SC}) and fill factor (FF). X-ray investigation on single crystals and co-evaporated blend layers give insight into packing behavior and morphology. In the single crystal, **DCV4T-Me 2** exhibited the highest number of non-bonding short contacts leading to a perfect coplanar layer structure with strong π-π interaction and electronic coupling. GIXRD on the blend layer yielded evidence of a crystalline homophase of **2** with similar molecular packing. The superior solid state properties of **DCV4T-Me 2** are further reflected in the charge carrier mobilities.

We correlate the structural parameters on various levels and length scales with the photovoltaic performance of BHJ-SMOSCs. The small structural variation in the series does not significantly affect the optoelectronic properties as expected, but leads to remarkable differences in solid state

properties that are crucial for exciton diffusion and charge transport and consequently for the photovoltaic performance.

EXPERIMENTAL SECTION

Experimental details, synthesis, and analytical data of the oligomers, device preparation and characterization, plots of DSC, TGA and cyclic voltammetry are available in the Supporting Information. CCDC 816600 and 846475 contain the supplementary crystallographic data for this paper. These data can be obtained free of charge from The Cambridge Crystallographic Data Centre via www.ccdc.cam.ac.uk/data_request/cif.

SUPPORTING INFORMATION

Supporting Information is available from the Wiley Online Library or from the author.

ACKNOWLEDGEMENTS

The work was supported by the German Research Foundation (DFG, priority program SPP 1355) and the Ministry for Education and Research (BMBF, programs OPEG 13N9720 and OPA 13N98872). We thank Dr. L. Wilde (Fraunhofer CNT) for the X-ray measurements, Moritz Hein and Jens Jankowski (IAPP Dresden) for the OFET mobility measurements and Novaled AG for providing NDP9.

Submitted: November 21, 2011
Published online: January 5, 2012

REFERENCES

[1] (a) K. Walzer, B. Männig, M. Pfeiffer, K. Leo, *Chem. Rev.* **2007**, *107*, 1233; b) M. A. Green, K. Emery, Y. Hishikawa, W. Warta, *Prog. Photovolt: Res. Appl.* **2011**, *19*, 84; c) A. Mishra, P. Bäuerle, *Angew. Chem.* in print.

[2] Y. Sun, G. C. Welch, W. L. Leong, C. J. Takacs, G. C. Bazan, A. J. Heeger, *Nat. Mater.* **2011**, *asap*, doi:10.1038/nmat3160.

[3] Heliatek GmbH, press release, October 11, 2010 (http:// www.heliatek.com).

[4] S. Wang, L. Hall, V. V. Diev, R. Haiges, G. Wei, X. Xiao, P. I. Djurovich, S. R. Forrest, M. E. Thompson, *Chem. Mater.* **2011**, *23*, 4789.

[5] H. Bürckstümmer, E. V. Tulyakova, M. Deppisch, M. R. Lenze, N. M. Kronenberg, M. Gsänger, M. Stolte, K. Meerholz, F. Würthner, *Angew. Chem. Int. Ed.* **2011**, doi: 10.1002/anie.201105133.

[6] A. Ojala, A. Petersen, A. Fuchs, R. Lovrincic, C. Pölking, J. Trollmann, J. Hwang, C. Lennartz, H. Reichelt, H. W. Höffken, A. Pucci, P. Erk, T. Kirchartz, F. Würthner, *Adv. Funct. Mater.* **2011**, doi: 10.1002/adfm.201101697.

[7] F. Yang, S. R. Forrest, *ACS Nano* **2008**, *2*, 1022.

[8] B. Walker, A. B. Tamayo, X.-D. Dang, P. Zalar, J. H. Seo, A. Garcia, M. Tantiwiwat, T.-Q. Nguyen, *Adv. Funct. Mater.* **2009**, *19*, 3063.

[9] G. Wei, R. R. Lunt, K. Sun, S. Wang, M. E. Thompson, S. R. Forrest, *Nano Lett.* **2010**, *10*, 3555.

[10] F. Yang, M. Shtein, S. R. Forrest, *Nat. Mater.* **2005**, *4*, 37.

[11] F. Yang, K. Sun, S. Forrest, *Adv. Mater.* **2007**, *19*, 4166.

[12] S. D. Oosterhout, M. M. Wienk, S. S. van Bavel, R. Thiedmann, L. J. A. Koster, J. Gilot, J. Loos, V. Schmidt, R. A. J. Janssen, *Nat. Materials* **2009**, *8*, 818-824.

[13] Z. M. Beiley, E. T. Hoke, R. Noriega, J. Dacuña, G. F. Burkhard, J. A. Bartelt, A. Salleo, M. F. Toney, M. D. McGehee, *Adv. Energy Mater.* **2011**, *1*, 954.

[14] R. Fitzner, E. Reinold, A. Mishra, E. Mena-Osteritz, H. Ziehlke, C. Körner, K. Leo, M. Riede, M. Weil, O. Tsaryova, A. Weiß, C. Uhrich, M. Pfeiffer, P. Bäuerle, *Adv. Funct. Mater.* **2011**, *21*, 897.

[15] Q. Xie, F. Arias, L. Echegoyen, *J. Am. Chem. Soc.* **1993**, *115*, 9818.

[16] a) M. Mazik, D. Bläser, R. Boese *Tetrahedron* **2001**, *57*, 5791-5797; b) M. Mazik, D. Bläser, R. Boese *Tetrahedron Lett.* **2000**, *41*, 5827-5831.

SUPPORTING INFORMATION

INSTRUMENTS, SPECTROSCOPIC MEASUREMENTS, AND METHODS

NMR spectra were recorded on a Bruker AMX 500 (^{1}H NMR: 500 MHz, ^{13}C NMR: 125 MHz) or an Avance 400 spectrometer (^{1}H NMR: 400 MHz, ^{13}C NMR: 100 MHz), at 25 °C or 100 °C. Chemical shift values (δ) are expressed in parts per million using residual solvent protons (^{1}H NMR, δ_H = 7.26 for $CDCl_3$, δ_H = 2.50 for DMSO-d_6 and δ_H = 5.93 for tetrachloroethane-d_2; ^{13}C NMR, δ_C = 77.0 for $CDCl_3$ and δ_C = 39.43 for DMSO-d_6) as internal standard. The splitting patterns are designated as follows: s (singlet), d (doublet), t (triplet) and q (quartet). The assignments are Th*H* (thiophene protons), Me*H* (methyl protons) and DCV*H* (dicyanovinyl protons). GC-MS (EI) mass spectra were recorded on a *Varian* Saturn *2000* and MALDI-TOF mass spectra on a *Bruker* Daltonic Reflex III. Thermogravimetric analysis (TGA) was conducted on a *Mettler Toledo* TGA/SDTA851^e instrument with a heating rate of 10 $^\circ$Cmin^{-1} under nitrogen atmosphere at a flow rate of 50 cm^3 min^{-1}. Differential scanning calorimetric measurements (DSC) were performed on a Mettler Toledo DSC823^e under argon atmosphere at a heating rate of 10 $^\circ$Cmin^{-1}. Melting points were determined using a Büchi B-545 apparatus and were not corrected. Elemental analyses were performed on an Elementar Vario EL.

Optical solution measurements were carried out in 1 cm cuvettes with Merck Uvasol grade solvents, absorption spectra were recorded on a Perkin Elmer Lambda 19 spectrometer. Cyclic voltammetry experiments were performed with a computer-controlled Metrohm Autolab PGSTAT 30 potentiostat in a three-electrode single-compartment cell with a platinum working electrode, a platinum wire counter electrode, and an Ag/AgCl reference electrode. All potentials were internally referenced to the ferrocene/ferrocenium couple.

Thin film samples were prepared by thermal vapor deposition in ultra-high vacuum at a base pressure of lower than 10^{-7} mbar. The layer thicknesses were determined during evaporation using quartz crystal monitors calibrated for the respective material prior to evaporation. The deposition rates for the organic were between 0.2 and 0.4 Ås^{-1}. For UV-vis characterization nominally 30 nm of the pristine material was deposited on quartz glass substrates (Quarzglass QCS). Evaporation rates were around 0.2 Ås^{-1}. The thin film absorbance spectra were recorded on a Perkin Elmer lambda900 spectrometer.

The solar cells were prepared on tin-doped indium oxide (ITO) coated glass (Thin Film Devices, USA, sheet resistance of 30 Ωsq.$^{-1}$) layer by layer without breaking the vacuum. The layer structure of the bulk heterojunction solar cells was as follows: ITO; 15 nm C_{60} (Bucky USA,

used density 1.54 gcm^{-3}); 20nm blend layer of respective DCV4T **1-3** (used density 1.3 gcm^{-3}, confirmed by XRR) and C_{60} (ratio 2:1 in volume) prepared by co-evaporation deposited on heated substrates (70 °C); 5 nm 9,9-bis{4-[di(p-biphenyl)aminophenyl]} fluorene (BPAPF, Lumtec, Taiwan; used density 1.2 gcm^{-3}); 50 nm BPAPF doped with NDP9 (10wt%, purchased from Novaled AG, Germany); 1 nm NDP9; 50 nm Au. The completed solar cells were encapsulated with a transparent encapsulation glass, fixed by UV-hardened epoxy glue, in a nitrogen glovebox. Particular care was taken for the active device area: it was individually determined for each solar cell by comparing the short circuit current without and with an aperture of well-defined size. The average device area was about 6 mm².

The solar cells were characterized by external quantum efficiency (EQE) and current voltage characteristics (*J-V*). The EQE measurements were carried out on a custom-made setup utilizing chopped monochromatic light produced by a xenon arc lamp, a monochromator (Newport Cornerstone) and a chopper wheel. Data acquisition is accomplished with a lock-in amplifier (Signal Recovery 7265 DSP). A silicon reference diode (Hamamatsu S1337) was used to calibrate the setup. From EQE spectra the spectral response of each individual solar cell device was determined and a spectral mismatch factor calculated. The corresponding *J-V* characteristics were recorded on a setup consisting of a source-measure unit (Keithley SMU 2400) and an AM 1.5G sun simulator (KHS Technical Lighting SC1200). The illumination intensity was monitored with a silicon photodiode (Hamamatsu S1337) and the *J-V* measurements were conducted under mismatch corrected intensities.

SYNTHESIS AND CHARACTERIZATION

Dimethylformamide (DMF, Merck) was refluxed over P_4O_{10} (Merck) and distilled. 5-Bromo-3,4-diethylthiophene-2-carboxaldehyde **5**[1] was prepared according to the published literature procedure. Malononitrile and *β*-alanine were purchased from Merck. All synthetic steps were carried out under argon atmosphere.

*Synthesis of 2,2'-[3,4,3''',4'''-tetramethyl-2,2':5',2'':5'',2'''-quaterthien-5,5'''-diylbis(methane-1-yl-1-ylidine)]dimalononitrile **2***: A mixture of 5,5'-bis(trimethylstannyl)-2,2'-bithiophene **8** (800 mg, 1.63 mmol), *2-[(5-bromo-3,4-dimethylthien-2-yl)methylene]malononitrile* **6** (912 mg, 3.42 mmol) and tetrakis(triphenylphosphine)palladium(0) (94 mg, 0.081 mmol) in degassed DMF (50 mL) was stirred at 80 °C for 16 hours. The reaction mixture was allowed to cool to room temperature, the precipitate was filtered off and washed thoroughly with methanol. The crude product was extracted in a *Soxhlet* extractor with 1,2-dichloroethane for 1 day to remove

the most soluble reaction by-products. Subsequently, *Soxhlet* extraction was continued for 10 days using chlorobenzene as solvent. After cooling the resulting extract down to room temperature, the precipitate was filtered off to yield quaterthiophene **2** (692 mg, 1.28 mmol, 79%) as a black solid. ^{1}H NMR (tetrachloroethane-d_2, 100 °C, δ ppm) 7.83 (s, 2H, DCV*H*), 7.32 (d, 2H, *J* = 3.98 Hz, Th*H*), 7.29 (d, 2H, *J* = 3.98 Hz, Th*H*), 2.38 (s, 6H, Me*H*), 2.33 (s, 6H, Me*H*). MS (MALDI, *m*/*z*) 538 [M^+] (calcd. for $C_{28}H_{18}N_4S_4$ 538.04). Elemental analysis for $C_{28}H_{18}N_4S_4$: calcd. C, 62.43; H, 3.37; N, 10.40; S, 23.81%; found: C, 62.55; H, 3.36; N, 10.58; S, 23.67%.

Synthesis of 2,2'-[3,4,3''',4'''-tetraethyl-2,2':5',2'':5'',2'''-quaterthien-5,5'''-diylbis(methane-1-yl-1-ylidine)]dimalononitrile ***3***: A mixture of 5,5'-bis(trimethylstannyl)-2,2'-bithiophene **8** (1.00 mg, 2.03 mmol), *2-[(5-bromo-3,4-diethylthien-2-yl)methylene]malononitrile* **7** (1.26 mg, 4.27 mmol) and tetrakis(triphenylphosphine)palladium(0) (117 mg, 0.102 mmol) in degassed DMF (30 mL) was stirred at 80 °C for 16 hours. The reaction mixture was allowed to cool to room temperature, the precipitate was filtered off and washed thoroughly with methanol. The crude product was extracted in a *Soxhlet* extractor with chlorobenzene for 4 days. After cooling the resulting extract down to room temperature, the precipitate was filtered off to yield quaterthiophene **3** (1.014 mg, 1.70 mmol, 84%) as a black solid. M.p. 337 ^{o}C (DSC). ^{1}H NMR (tetrachloroethane-d_2, 100 °C, δ ppm) 7.81 (s, 2H, DCV*H*), 7.31 (d, 2H, *J* = 3.93 Hz, Th*H*), 7.26 (d, 2H, *J* = 3.91 Hz, Th*H*), 2.84 (q, 4H, *J* = 7.54 Hz), 2.77 (q, 4H, *J* = 7.64 Hz), 1.26-1.22 (m, 12H). MS (MALDI, *m*/*z*) 595 [M^+] (calcd. for $C_{32}H_{26}N_4S_4$ 594.10). Elemental analysis for $C_{32}H_{26}N_4S_4$: calcd. C, 64.61; H, 4.41; N, 9.42; S, 21.56%; found: C, 64.79; H, 4.31; N, 9.55; S, 21.56%.

Synthesis of 2-[(5-bromo-3,4-dimethylthien-2-yl)methylene]malononitrile ***6***: A solution consisting of 5-bromo-3,4-dimethylthiophene-2-carboxaldehyde **4** (6.00 g, 27.4 mmol), malononitrile (5.43 g, 82.2 mmol) and *β*-alanine (146 mg, 1.64 mmol) in a mixture of dichloroethane (150 mL) and ethanol (150 mL) was stirred under reflux for 2 days. The reaction mixture was allowed to cool to room temperature, the precipitate was filtered off and washed thoroughly with ethanol to provide compound **6** (6.73 g, 25.2 mmol, 92 %) as yellow needles. M.p. 204-205 ^{o}C. ^{1}H NMR (DMSO-d_6, 100 °C, δ ppm) 8.50 (s, 1H, DCV*H*), 2.41 (s, 3H, Me*H*), 2.17 (s, 3H, Me*H*). ^{13}C NMR (DMSO-d_6, 100 °C, δ ppm) 151.4, 150.5, 140.3, 130.7, 122.2, 114.9, 114.4, 75.7, 14.7, 14.1. MS (EI, *m*/*z*) 269 [M+H^+] (calcd. for $C_{10}H_7BrN_2S$ 267.95). Elemental analysis for $C_{10}H_7BrN_2S$: calcd. C, 44.96; H, 2.64; N, 10.49%; found: C, 44.82; H, 2.69; N, 10.46%.

Synthesis of 2-[(5-bromo-3,4-diethylthien-2-yl)methylene]malononitrile ***7***: A solution consisting of 5-bromo-3,4-diethylthiophene-2-carboxaldehyde **5** (4.94 g, 20.0 mmol), malononitrile (3.96 g, 60.0 mmol) and *β*-alanine (107 mg, 1.20 mmol) in a mixture of dichloroethane (100 mL) and ethanol (100 mL) was stirred under reflux for 20 hours. The reaction mixture was allowed to cool to room temperature, the precipitate was filtered off and washed thoroughly with ethanol to provide compound **7** (5.57 g, 19.5 mmol, 94 %) as yellow needles. M.p. 163-164 °C. ^{1}H NMR ($CDCl_3$, δ ppm) 7.82 (s, 1H, DCV*H*), 2.74 (q, 2H, J = 7.66 Hz), 2.64 (q, 2H, J = 7.59 Hz), 1.19 (t, 3H, J = 7.63 Hz), 1.15 (t, 3H, J = 7.56 Hz). ^{13}C NMR ($CDCl_3$, δ ppm) 155.1, 149.6, 147.7, 144.48, 130.5, 124.6, 114.5, 113.4, 75.9, 21.5, 21.4, 16.6, 13.8. MS (EI, *m*/*z*) 297 [$M+H^+$] (calcd. for $C_{12}H_{11}BrN_2S$ 295.98). Elemental analysis for $C_{12}H_{11}BrN_2S$: calcd. C, 48.82; H, 3.76; N, 9.49%; found: C, 48.72; H, 3.74; N, 9.46%.

X-Ray Diffraction Analysis

Single crystal X-ray diffraction data of DCV4T-Me **2** and DCV4T-Et **3** were collected at 100(2) K on a Bruker APEX-II CCD area detector diffractometer using graphite-monochromated Mo K_α radiation. Absorption effects were corrected based on a semi-empirical method with the SADABS algorithm.[2] Structure solution by direct methods with SHELXS-97 revealed all atoms of the oligothiophene backbone; additional atoms were assigned from difference Fourier maps during refinement on F^2 with SHELXL-97.[3] For the final model, all non-H atoms were refined anisotropically. H atoms were placed in calculated positions riding the parent C atom with C-H distance constraints of 0.93 Å for aromatic H atoms, 0.96 Å for methyl H atoms and 0.99 Å for methylene H atoms, and with U_{iso}(H) = 1.2U_{eq}(C) for aromatic and 1.5U_{eq}(C) for aliphatic H atoms.

DCV4T-Me **2**: $C_{28}H_{18}N_4S_4$, M_r = 538.74, dark-red rod, 0.50 × 0.40 × 0.20 mm^3, triclinic, *P*-1, a = 7.3460(8) Å, b = 8.8290(10) Å, c = 10.2702(12) Å, α = 103.727(5)°, β = 109.371(5)°, γ = 91.203(6)°, V = 606.82(12) Å^3 , Z = 1, μ = 0.419 mm^{-1} , dx = 1.474 g cm^{-3}, T = 100 K. 11867 reflections collected (θ_{max} = 32.5°) and merged to 4292 independent data (R_{int} = 0.035); final R indices: $R_1(I>2\sigma(I))$ = 0.0396, wR_2 (all) = 0.1092.

DCV4T-Et **3**: $C_{32}H_{26}N_4S_4$, M_r = 594.80, dark-red block, 0.20 × 0.20 × 0.15 mm^3, triclinic, *P*-1, a = 8.1500(10) Å, b = 11.7401(14) Å, c = 15.8219(19) Å, α = 77.658(6)°, β = 86.996(6)°, γ = 73.908(6)°, V = 1420.9(3) Å^3 , Z = 2, μ = 0.365 mm^{-1} , dx = 1.390 g cm^{-3}, T = 100 K. 25541

reflections collected (θ_{max} = 32.0°) and merged to 9711 independent data (R_{int} = 0.029); final *R* indices: $R_1(I>2\sigma(I))$ = 0.0397, wR_2 (all) = 0.1018.

Detailed crystallographic data for structures DCV4T-Me **2** and DCV4T-Et **3** have been deposited with the Cambridge Crystallographic Data Centre as supplementary publication CCDC 816600 and 846475, respectively.

Table S1. *Molecular structure of DCV4T-Me* ***2****, selected bond lengths, dihedral and torsional angles.*

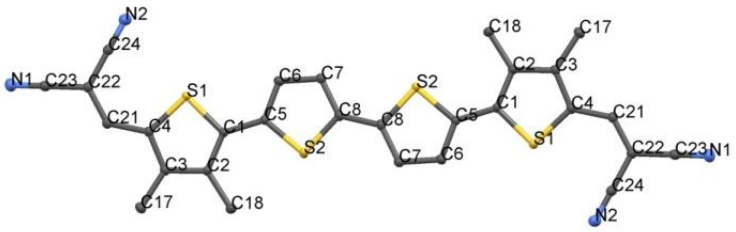

Atom 1	Atom 2	Length [Å]
S1	C1	1.724(2)
S1	C4	1.731(2)
S2	C5	1.726(2)
S2	C8	1.721(2)
N1	C23	1.146(2)
N2	C24	1.155(2)
C1	C2	1.389(2)
C1	C5	1.439(2)
C2	C3	1.414(2)
C2	C18	1.494(2)
C3	C4	1.392(3)
C3	C17	1.494(2)
C4	C21	1.421(2)
C5	C6	1.384(2)
C6	C7	1.407(2)
C7	C8	1.377(3)
C8	C8	1.440(2)
C21	C22	1.359(3)
C22	C23	1.435(2)
C22	C24	1.422(2)

Atom 1	Atom 2	Atom 3	Angle [°]
C24	C22	C21	123.9(2)
C22	C21	C4	129.5(2)
C21	C4	S1	124.9(1)
S1	C1	C5	118.0(1)
C1	C5	S2	122.5(1)
S2	C8	C8	119.6(1)
C8	C8	S2	119.6(1)
S2	C5	C1	122.5(1)
C5	C1	S1	118.0(1)
S1	C4	C21	124.9(1)
C4	C21	C22	129.5(2)
C21	C22	C24	123.9(2)

Table S1 (Continued).

Atom 1	Atom 2	Atom 3	Atom 4	Torsion [°]
C24	C22	C21	C4	0.5(3)
C22	C21	C4	S1	1.1(3)
S1	C1	C5	S2	175.48(9)
S2	C8	C8	S2	-180.00(9)
S2	C5	C1	S1	-175.48(9)
S1	C4	C21	C22	-1.1(3)
C4	C21	C22	C24	-0.5(3)

Table S2. *Molecular structure of DCV4T-Et* ***3****, selected bond lengths, dihedral and torsional angles.*

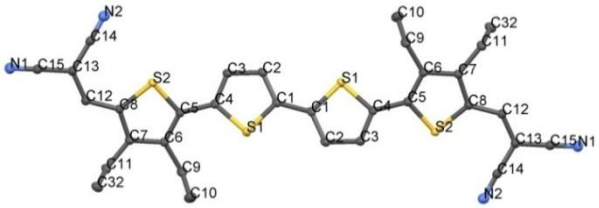

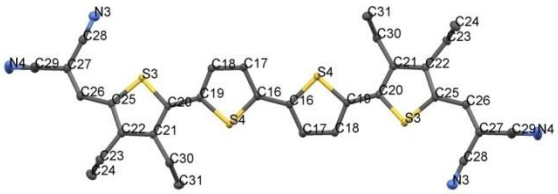

Atom 1	Atom 2	Length [Å]
S1	C1	1.726(1)
S1	C4	1.740(1)
S2	C5	1.723(1)
S2	C8	1.733(1)
C1	C2	1.373(2)
C1	C1	1.451(2)
C4	C5	1.453(2)
C4	C3	1.376(2)
C12	C13	1.367(2)
C12	C8	1.422(2)
C11	C7	1.507(2)
C11	C32	1.530(2)
C2	C3	1.413(2)
C5	C6	1.388(2)
C13	C14	1.433(2)
C13	C15	1.435(2)
C14	H2	1.150(2)
C9	C6	1.507(2)
C9	C10	1.525(2)
C15	H1	1.147(2)
C7	C6	1.421(2)
C7	C8	1.398(2)

Atom 1	Atom 2	Length [Å]
S3	C25	1.729(2)
S3	C20	1.726(1)
S4	C19	1.736(1)
S4	C16	1.725(1)
C19	C18	1.377(2)
C19	C20	1.456(2)
C25	C22	1.401(2)
C25	C26	1.423(2)
C18	C17	1.412(2)
C22	C23	1.507(2)
C22	C21	1.420(2)
C27	C26	1.366(2)
C27	C28	1.432(2)
C27	C29	1.437(2)
C20	C21	1.400(2)
C24	C23	1.531(2)
C28	H3	1.150(2)
C16	C17	1.377(2)
C16	C16	1.449(2)
C21	C30	1.507(2)
C29	H4	1.147(2)
C30	C31	1.528(2)

Table S2 (Continued).

Atom 1	Atom 2	Atom 3	Atom 4	Torsion [°]
C14	C13	C12	C8	-2.4(3)
C13	C12	C8	S2	-4.2(2)
S2	C5	C4	S1	-146.88(9)
S1	C1	C1	S1	180.00(7)
S1	C4	C5	S2	146.88(9)
S2	C8	C12	C13	4.2(2)
C8	C12	C13	C14	2.4(3)

Atom 1	Atom 2	Atom 3	Angle [°]
C14	C13	C12	125.2(1)
C13	C12	C8	130.0(1)
C12	C8	S2	124.5(1)
S2	C5	C4	117.8(1)
C5	C4	S1	123.0(1)
S1	C1	C1	120.1(1)
C1	C1	S1	120.1(1)
S1	C4	C5	123.0(1)
C4	C5	S2	117.8(1)
S2	C8	C12	124.5(1)
C8	C12	C13	130.0(1)
C12	C13	C14	125.2(1)

DIFFERENTIAL SCANNING CALORIMETRY (DSC)

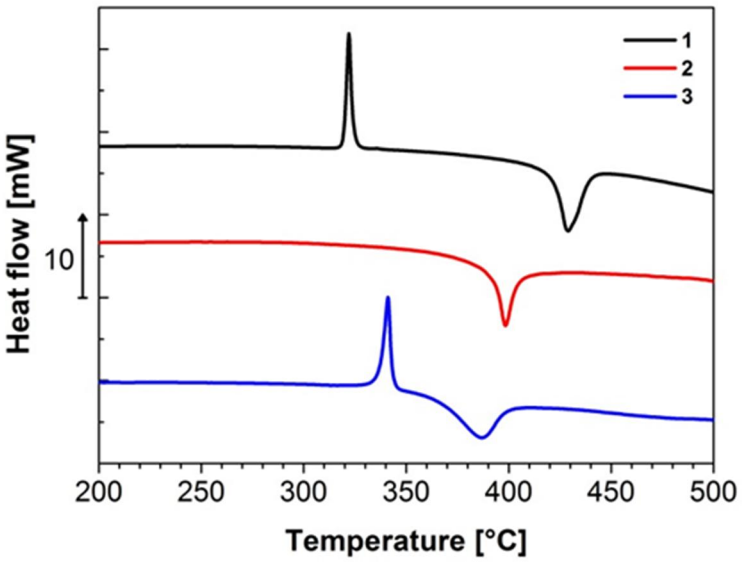

Figure S1. *DSC trace of quaterthiophenes* ***1-3*** *measured under argon flow at a heating rate of 10 °C min^{-1}.*

THERMOGRAVIMETRIC ANALYSIS (TGA)

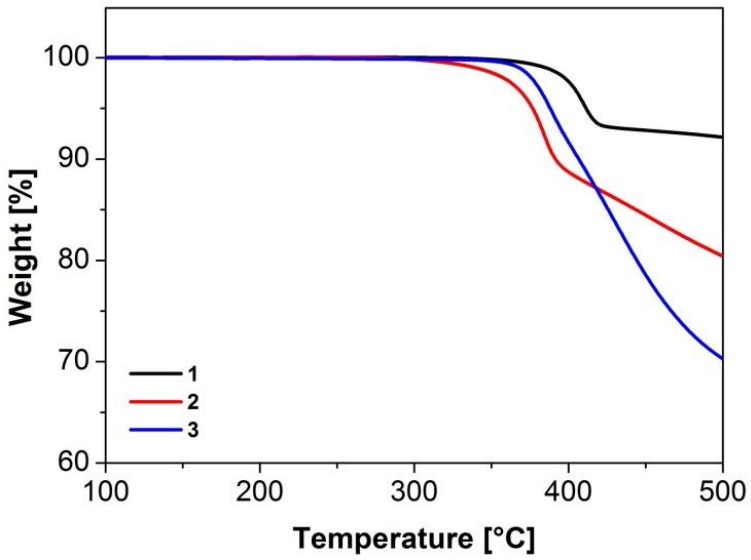

Figure S2. *TGA thermograms of quaterthiophenes* ***1-3*** *measured under nitrogen flow (50 mL min^{-1}) at a heating rate of 10 °C min^{-1}.*

CYCLIC VOLTAMMETRY (CV)

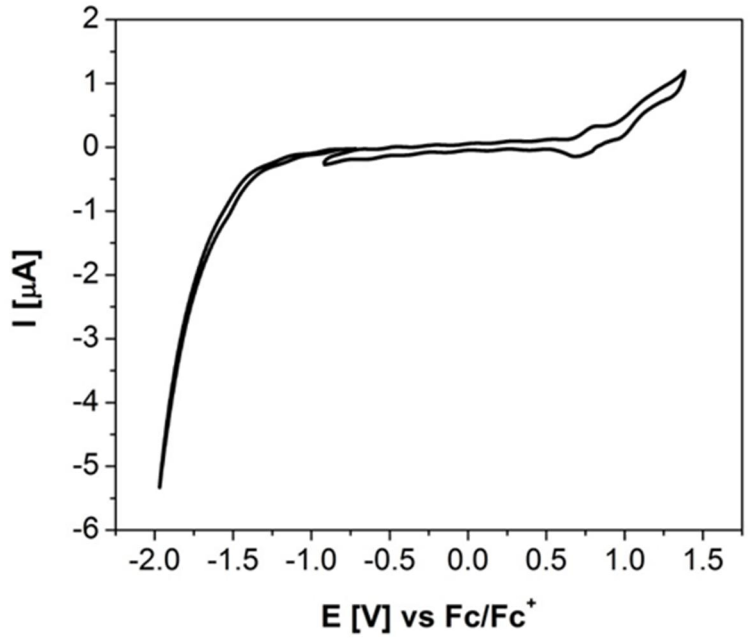

Figure S3. Cyclic voltammogram of quaterthiophene **2** measured in tetrachloroethane-$TBAPF_6$ (0.1 M), scan rate 100 mV s^{-1}, potentials versus Fc/Fc^+, measured at 80 °C.

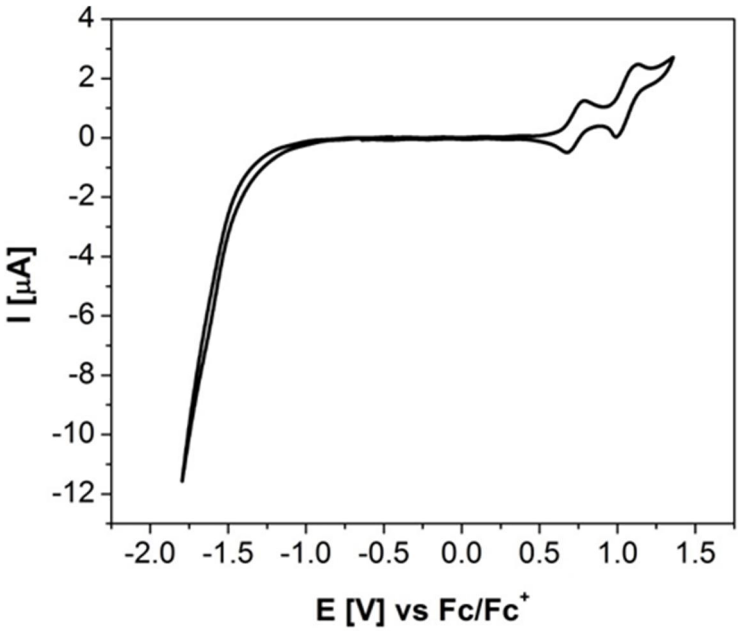

Figure S4. *Cyclic voltammogram of quaterthiophene* ***3*** *measured in tetrachloroethane-TBAPF$_6$ (0.1 M), scan rate 100 mV s^{-1}, potentials versus Fc/Fc$^+$, measured at 80 °C.*

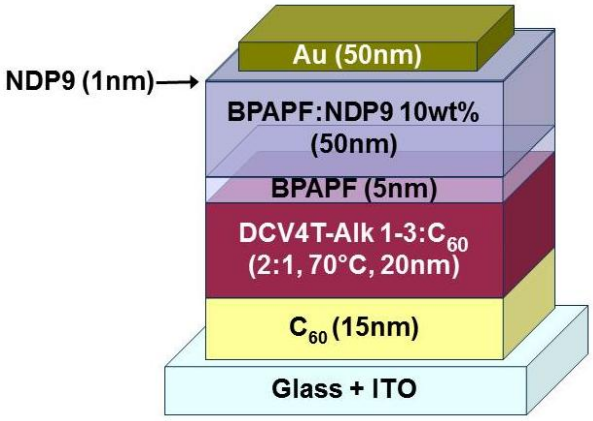

Figure S5. *Layer structure of BHJ solar cells incorporating 20 nm thick blends layer of quaterthiophenes* ***1-3****:C_{60} (2:1 by volume) deposited at a substrate temperature of 70 °C.*

REFERENCES

[1] F. Würthner, S. Yao, T. Debaerdemaeker, R. J. Wortmann, *J. Am. Chem. Soc.* **2002**, *124*, 9431-9447.

[2] G. M. Sheldrick, *Acta Crystallogr*. **2008**, *A64*, 112.

[3] A. L. Spek, *Acta Crystallogr.* **2009**, *D65*, 148.

CHAPTER V

CORRELATION OF π-CONJUGATED OLIGOMER STRUCTURE WITH FILM MORPHOLOGY AND ORGANIC SOLAR CELL PERFORMANCE

Roland Fitzner,[a] Elena Mena-Osteritz,[a] Amaresh Mishra,[a] Gisela Schulz,[a] Egon Reinold,[a] Matthias Weil,[b] Christian Körner,[c] Hannah Ziehlke,[c] Chris Elschner,[c] Karl Leo,[c] Moritz Riede,[c] Martin Pfeiffer,[d] Christian Uhrich,[d] and Peter Bäuerle[a,*]

[a] Institut für Organische Chemie II und Neue Materialien, Universität Ulm, Albert-Einstein-Allee 11, 89081 Ulm, Germany

[b] Institut für Chemische Technologien und Analytik, Abteilung Strukturchemie, Technische Universität Wien, Getreidemarkt 9/164-SC, 1060 Wien, Austria

[c] Institut für Angewandte Photophysik, TU Dresden, George-Bähr-Straße 1, 01062 Dresden, Germany

[d] heliatek GmbH, Treidlerstr. 3, 01139 Dresden, Germany

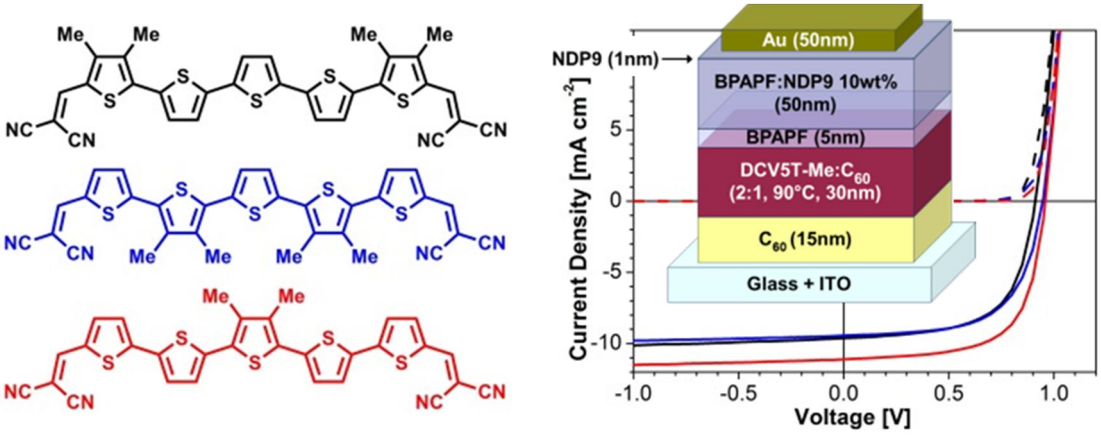

Reproduced and adapted with permission from

R. Fitzner *et al.*, *Journal of the American Chemical Society* **2012**, *134,* 11064−11067.

Copyright © 2012 American Chemical Society.

ABSTRACT

The novel methyl-substituted dicyanovinyl-capped quinquethiophenes **1**−**3** led to highly efficient organic solar cells with power conversion efficiencies of 4.8−6.9%. X-ray analysis of single crystals and evaporated neat and blend films gave insights into the packing and morphological behavior of the novel compounds that rationalized their improved photovoltaic performance.

Organic solar cell (OSC) research is currently undergoing dynamic development due to its great promise for the production of low-cost and flexible large-area modules as renewable energy sources.[1] In OSCs, conversion of sunlight to electrical energy is realized by the use of synthetic molecular materials, organic electron donors (D) and acceptors (A), as active components.[2] Typically, in solution-processed bulk-heterojunction (BHJ) solar cells, a nanophase-separated blend of a semiconducting polymer as the donor and a soluble fullerene derivative as the acceptor is formed, affording power conversion efficiencies (PCEs) exceeding 8%.[3] More recently, small-molecule organic solar cells (SMOSCs) made from conjugated oligomers or dyes have been gaining increasing attention.[4] In this respect, a D-A-D oligomer in combination with a C_{70}-based fullerene acceptor reached a PCE of 6.7% for a solution-processed single-heterojunction (SHJ) device.[5] In vacuum-processed devices, an efficiency of 6.4% was reported for a D−A dye and C_{70}.[6] Stacking of single-junction cells on top of each other allows the construction of tandem cells via vacuum deposition, and this recently led to a certified PCE of 10.7% on an active area of 1.1 cm^2, as disclosed by Heliatek.[7] In comparison to polymeric materials, small molecules and oligomers have the distinct advantages of straightforward synthesis and purification leading to defined molecular structures, which greatly improve the fabrication reproducibility and avoid batch-to-batch variations.

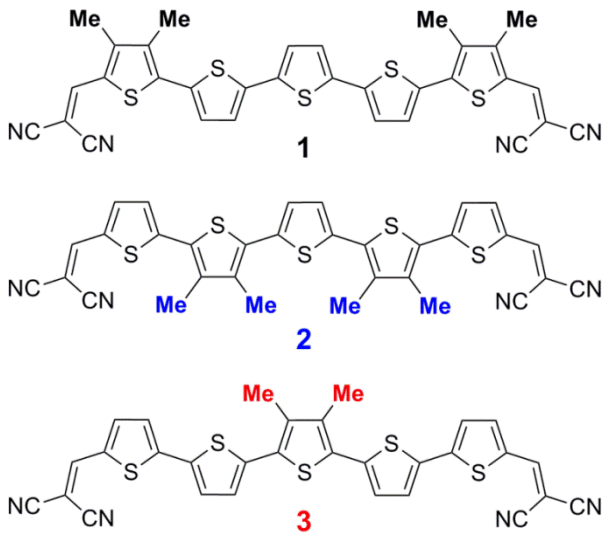

Chart 1. *Molecular Structures of* ***DCV5T-Me*** *Donors* ***1−3****.*

Here we report the synthesis, characterization, and photovoltaic (PV) properties of a novel series of methyl-substituted dicyanovinyl (DCV)-capped A-D-A quinquethiophenes (**DCV5T-Me's**) **1-3** (Chart 1). Within this series, the methyl substitution pattern along the conjugated backbone was systematically varied, leading to improved efficiencies of 4.8-6.1% in SHJ SMOSCs

relative to alkyl-free **DCV5T** (4.6%; see Table 2) and other alkylated derivatives.[8] Further optimization of the processing parameters during device fabrication using **3** afforded a highest PCE of 6.9%. X-ray analysis of single crystals and evaporated neat and blend layers gave further insight into the packing and morphological behavior of the novel oligomers that rationalized the improved PV performance.

DCV5T-Me's 1-3 were prepared according to a method that had previously been successfully applied in the synthesis of a series of alkyl-free **DCVnTs**.[8] In the final synthetic steps leading to the poorly soluble target quinquethiophenes **1-3**, Pd-catalyzed Stille-type cross-coupling reactions were used. Detailed synthetic procedures and characterization of **1-3** can be found in the Supporting Information (SI).

For vacuum-processed SMOSCs, thermal stability of the components is essential. The thermal properties of **1-3** were investigated using differential scanning calorimetry (DSC) (Figure S1 in the SI) and thermogravimetric analysis (TGA) (Figure S2). Relative to the parent **DCV5T** (287 °C),[8] methylation increased the melting point to 301°C for **3** and 302°C for **2**, with a further increase to 368 °C for **1**, indicating additional intermolecular interactions in the solid state. For all three derivatives, thermal degradation started at 370-380°C, as confirmed by DSC and TGA.

Single crystals of **3** were obtained from gradient sublimation, allowing X-ray structure analysis, which provided information about the molecular geometry and the packing behavior. The thiophene units in **3** show an all-trans conformation, with the DCV groups oriented syn to the S atoms of the terminal thiophenes. The unit cell contains four molecules, and the molecular packing is shown in Figure 1. The molecules are arranged in rows interacting via remarkable H-bonds[9] between vinylic or aromatic CH and the N atom of a neighboring cyano group (CH···NC = 2.55 or 2.71 Å; blue lines in Figure 1a). The side view reveals that these rows are offset and interact with one another via additional aromatic-C**H**···**N**C short contacts (2.59 Å; red lines in Figure 1a,b). The molecules in the rows stack via π–π interactions with short contacts as close as 3.28 Å (gray lines in Figure 1b). Important methyl-**H**···**S** dipolar interactions further stabilize the close π-stacking (green lines in Figure 1c). These features, which indicate orbital overlap not only in the stack direction but also perpendicular to the π-stacks, were also found for methylated DCV-capped quaterthiophenes and terthiophenes.[10] In summary, the oligomers are organized in the crystal such that one molecule of **3** interacts with 10 neighboring molecules via 16 well-defined interactions.

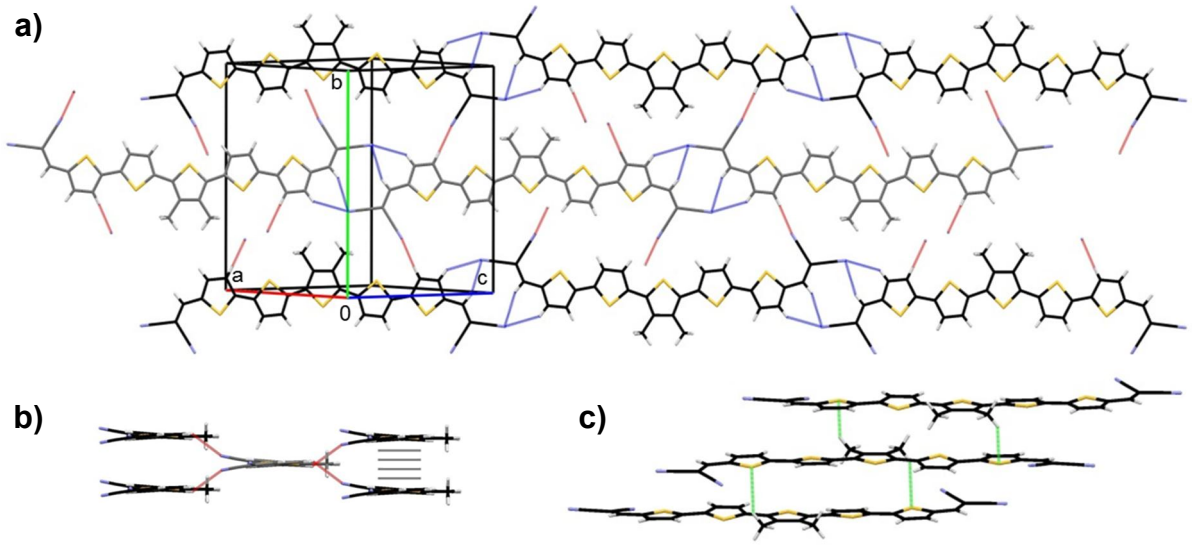

Figure 1. *Packing of **3** in a single crystal viewed perpendicular to the (a) (6 0 4), (b) (6 0 -7), and (c) (1 10 0) planes of the unit cell.*

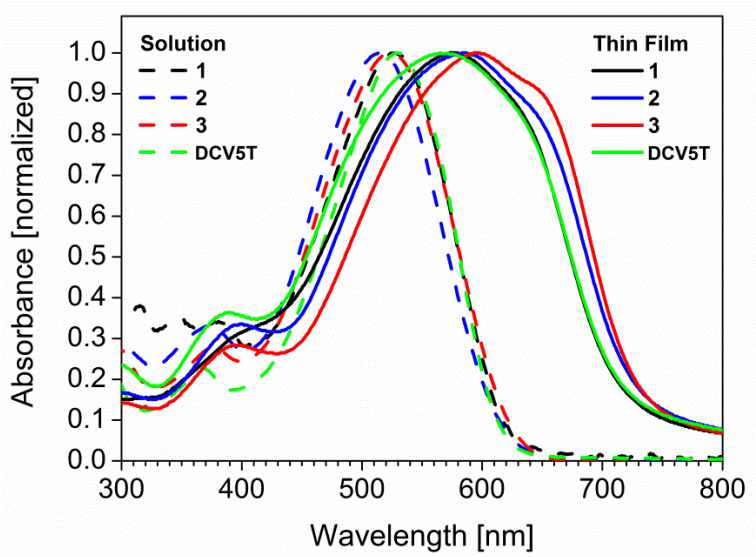

Figure 2. *Absorption spectra of **1−3** and DCV5T in CH_2Cl_2 solution (dashed lines) and 30 nm thick thin films (solid lines).*

Figure 2 shows the absorption spectra of **1-3** in solution and in thin films prepared by vacuum deposition (Table 1). In solution, the location and shape of the bands were quite similar for all three derivatives, and the absorption maximum varied from 514 to 527 nm. In the thin films, **1-3** exhibited red-shifted absorption maxima relative to the solution spectra ($\Delta\lambda$ = 50−72 nm), suggesting planarization of the molecules. Within this series and compared with the previously reported alkyl-free[8] and ethyl- or butyl-substituted **DCV5Ts**,[11] dimethyl derivative **3** showed the most significant red shift of λ_{max} and a more pronounced shoulder at 660 nm, which may indicate better ordering of the molecules in the bulk. The optical gaps for the thin films, as

determined from the absorption onsets, were ~ 1.7 eV, which is ~ 0.3 eV lower than for the solution spectra.

The redox properties of **1-3** were measured in tetrachloroethane/Bu_4NPF_6 solutions at 80 °C (Table 1 and Figure S3). The first oxidation and reduction potentials as well as the band gaps and the calculated HOMO and LUMO energies are very similar for all three pentamers. The relatively low HOMO energies ($E_{HOMO} \approx -5.64$ eV) are expected to result in high open-circuit voltages (V_{OC}) when C_{60} is used as acceptor in OSCs. Also, the LUMO energies ($E_{LUMO} \approx -3.73$ eV) lie in an ideal regime relative to the LUMO of C_{60} (−4.1 eV),[12] which should provide a sufficiently large driving force for charge separation at the D−A interface.

BHJ SMOSCs with a p−i−n-type device architecture[13] were prepared by vacuum deposition of **1−3** as the donor and C_{60} as the acceptor. The layer sequence in the device (stack A) consisted of ITO/C_{60} (15 nm)/donor:C_{60} (30 nm, 2:1 v/v, co-evaporated at 90 °C substrate temperature)[14]/BPAPF (5 nm)/BPAPF:NDP9 (50 nm, 90:10 w/w)/NDP9 (1 nm)/Au (50 nm) (see Figure S4). The triarylamine BPAPF p-doped with 10 wt % NDP9 was used as the hole transport layer, on top of which another 1 nm thick layer of NDP9 was deposited to facilitate charge extraction. The active area of each cell was ~ 6.6 mm^2, as confirmed by comparing short-circuit currents with and without an aperture mask.

***Table 1**. Optoelectronic properties of **DCV5T-Me 1-3** in comparison to parent compound DCV5T.*

Oligo-mer	λ_{max}^{abs} [nm] soln.	ε_{max} [L $mol^{-1}cm^{-1}$] soln.	E_g^{opt} [eV] soln.	λ_{max}^{abs} [nm] film	E_g^{opt} [eV] film	$E°_{Ox1}$ [V] soln.	$E°_{Red}$ [V] soln.	E_g^{CV} [eV] soln.	HOMO [eV][b]	LUMO [eV][b]
1	527	-[a]	2.01	577	1.72	0.63	–1.53	1.91	–5.64	–3.73
2	514	60600	2.03	585	1.69	0.60	–1.56	1.90	–5.61	–3.71
3	524	63300	1.99	596	1.69	0.65	–1.50	1.91	–5.66	–3.75
DCV5T	530	73300	2.02	570	1.69	0.64	–1.51, –1.37[c]	1.89	–5.62	–3.73

[a] Molar absorption coefficient could not be determined due to poor solubility in organic solvents. [b] Calculated from the onset of the respective redox waves, Fc/Fc^+ is set to -5.1 eV vs. vacuum. [c] Values determined by differential pulse voltammetry (DPV).

***Table 2**. Photovoltaic parameters of bulk heterojunction (BHJ) solar cells containing DCV5T-Me **1-3** in comparison to parent DCV5T. GIXRD data of neat films of **1-3** and their blends with C_{60}.*

Oligomer (stack)	V_{OC} [V]	J_{SC} [mA cm^{-2}]	FF [%]	PCE [%]	Intensity [mW cm^{-2}]	Saturation [J(-1V)/J_{sc}]	Crystal size neat [nm]	Crystal size blend [nm]
1 (A)	0.91	9.6	63	4.8	115	1.05	19±5	7±2 nm
2 (A)	0.95	9.4	62	4.8	115	1.04	7±2	26±2 nm
3 (A)	0.96	11.1	66	6.1	115	1.04	6±2	>40 nm
3 (B)	**0.95**	**11.5**	**63**	**6.9**	**100**	**1.06**		
DCV5T[a]	0.95	9.0	55	4.6	103	1.10	n.d.[b]	n.d.[b]

[a] Comparable thickness of the devices (ref. 2i). [b] n.d. = not determined.

The *J*–*V* characteristics of the stack-A solar cells are shown in Figure 3a and Table 2. The corresponding external quantum efficiency (EQE) spectra are depicted in Figure 3b. All of the solar cells showed high V_{OC}'s above 0.9 V. These values are due to the low-lying HOMOs and are similar to those for other DCV5T derivatives.[8],[11a,c] Devices prepared with **1** and **2** turned out to be very similar in terms of short-circuit current density (J_{SC}) (9.6 and 9.4 mA cm^{-2}), fill factor (FF) (63 and 62%), and EQE spectrum (maximum at ~ 600 nm). Consequently, both **1**- and **2**-based solar cells reached similar PCEs of 4.8%. These reasonable values indicate that excitons are efficiently separated at the D–A interface and readily transported through the bulk. The high saturation [defined as $J(-1\ V)/J_{SC}$], indicating a weak voltage bias dependence of the current in the reverse direction, supports this explanation.

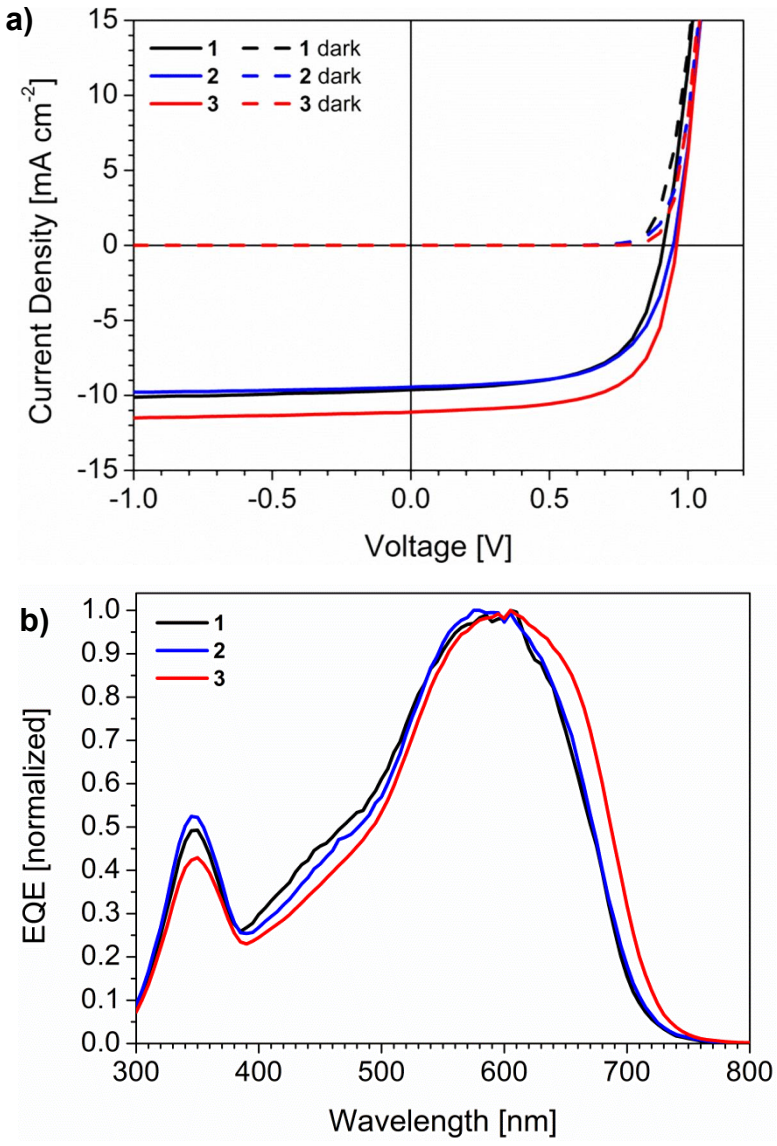

Figure 3. *(a) J–V characteristics and (b) EQE spectra of BHJ solar cells containing oligomers* ***1–3****. The EQE spectra were used to calculate the mismatch factor for determining the illumination intensity for the measured J–V characteristics.*

The PV performance was further enhanced for devices based on **3**:C_{60}, which showed notably larger values of both J_{SC} (11.1 mA cm^{-2}) and FF (66%) due to efficient charge-carrier extraction, leading to an increased PCE of 6.1%. The superior PV performance of **3** is correlated to the EQE spectrum (Figure 3b), which shows a significant red shift and spectral broadening as in the thin-film UV-vis spectrum. Because of the outstanding performance of **3**, we further optimized the device stack and processing parameters, resulting in the following layer sequence (stack B): ITO/C_{60}:W_2(hpp)$_4$ (5 nm, 96:4 w/w)/C_{60} (15 nm)/donor:C_{60} (30 nm, 2:1 v/v, co-evaporated at 75°C substrate temperature)/BPAPF (5 nm)/BPAPF:NDP9 (50 nm, 90:10 w/w)/NDP9 (2 nm)/Al (100 nm) (see Figure S4). Stack B differs from stack A in that the substrate temperature was reduced to 75 °C, a 5 nm C_{60} layer n-doped with 4 wt % W_2(hpp)$_4$ was introduced between the ITO and the intrinsic C_{60} layer, the thickness of the p-dopant layer below the top contact was increased, and Au was replaced by Al as the top electrode material. This led to an observed increase in J_{SC} resulting from a significant reduction of electrode absorption and an increase in the back-contact reflectance. Optical simulations and a comparison of the EQE spectra of stack-A and -B devices containing **3** showed increased absorption between 400 and 550 nm. The calculated ratio of the absorbed photon flux in the active layer matched the J_{SC} ratio for stacks A and B (see the SI).

We prepared 32 identical solar cells on eight different substrates, which were characterized and statistically evaluated. The devices showed a mean J_{SC} of 11.4 ± 0.09 mA cm^{-2}, V_{OC} of 0.95 ± 0.008 V, and FF of 62.6 ± 0.7%, giving an excellent average PCE of 6.78 ± 0.07% (Table S1 in the SI). These very small standard deviations underline the reproducibility and reliability of our results. The best-performing device generated an exceptional PCE of 6.9% with a V_{OC} of 0.95 V, J_{SC} of 11.5 mA cm^{-2}, and FF of 63% (Figure S5).

To gain deeper insight into the morphological behavior of the novel compounds in thin films, grazing-incidence X-ray diffraction (GIXRD) and X-ray reflection (XRR) measurements on evaporated films (50 nm) of neat **1**−**3** and blend layers with C_{60} (75 nm) were carried out (Table 2). The GIXRD patterns of the neat films showed an increasing amount of disorder in going from **1** to **3**: while the diffraction pattern of **1** was symmetric, those of **2** and **3** were asymmetric and strongly broadened, indicating smaller domains of ordered areas (Figure 4a). This finding was further corroborated by XRR, which revealed very smooth film surfaces (Figure S6a). To give a rough estimate of the crystal size, the full width at half maximum (FWHM) was estimated and used in the Scherrer equation with consideration of the instrumental broadening of the GIXRD measurement (this was controlled by a previous Rietveld analysis of test samples). Analysis of the crystal size (lower limit) gave similar values for **2** and **3** (7 ± 2 and 6 ± 2 nm),

whereas **1** formed larger crystallites (19 ± 5 nm), in accordance with the trend in the melting points (see above).

In contrast to the neat films, GIXRD of **1**–**3**:C_{60} blend layers (Figure 4b) surprisingly showed the lowest crystallinity for **1** (7 ± 2 nm), while **2** and **3** exhibited larger crystal sizes of 26 ± 10 and >40 nm, respectively (Table 2). Also, the C_{60} crystal size increased in going from **1**:C_{60} (2.5 ± 0.3 nm) to **2**:C_{60} (2.9 ± 0.4 nm) to **3**:C_{60} (4.1 ± 0.8 nm). These results agree with the XRR data, which showed increasing surface roughness of the films in going from **1** to **3** (Figure S6b). To determine the FWHM of the nanocrystalline C_{60} Bragg reflections, the region 2θ = 15–23° was fitted with two Bragg reflections at identical positions, as for the crystalline neat C_{60} layer.

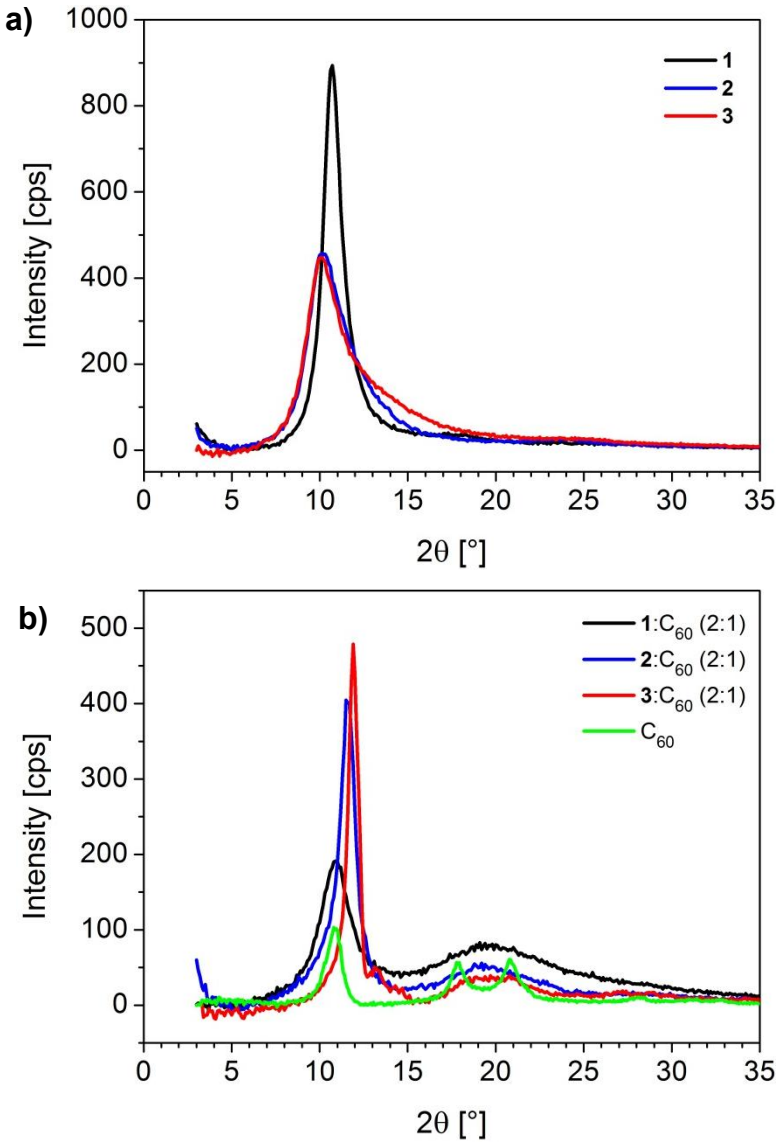

Figure 4. *GIXRD patterns of (a) 50 nm films of neat **1**–**3** deposited on glass substrates at room temperature and (b) 75 nm **1**–**3**:C_{60} (2:1 v/v) blend layers fabricated by co-evaporation on glass substrates at 90°C, with the pattern for pristine C_{60} shown for comparison.*

A comparison of the simulated diffraction pattern of the single-crystal phase and the Bragg reflection of oligomer **3** in the heated blend (Figure 4b) showed a mismatch between the two structures. Nevertheless, we assume that the packing of the molecules in the single crystal should be similar to the packing in blended films. This rationale comes from the similarities of the film growth of DCV-capped quaterthiophenes, which were investigated by X-ray measurements and for which the molecular packing was compared to that in single crystals.[10a] These findings allow us to correlate the morphology of the blend layers (i.e., the size of crystallites) with the solar cell performance. The bigger size of the single-component crystallites for **3**:C_{60} corresponds to a larger D−A phase separation in the blend. This film morphology provides better percolation pathways for the respective charge carriers, which is reflected in the large current density and FF. We attribute the resulting PCE of 6.9% to the high crystallinity of **3** as well as to the relatively high crystallinity of C_{60} compared with the other samples. The C_{60} crystal size marks the significant morphological difference between the blends of **2** and **3**, resulting in large differences in the PCEs of the solar cells.

It still remains an open question why the **1**:C_{60} system showed the smallest phase separation while the small changes in molecular structure in going from **1** to **3** significantly increased the crystallinity and phase separation in **3**:C_{60}. A delicate balance between the homo- and heterointeractions of the two molecular components in the BHJ occurs during the deposition process, which is very sensitive to the substrate temperature. XRD analysis of the D−A blend films showed that the tendency of both components to form larger homophasic crystallites increases in going from **1** to **3**, strongly suggesting reduced π−π D−A interactions. We assume that C_{60} interacts with **1**−**3** at the central thiophene unit, reducing the repulsion between C_{60} and the DCV acceptor groups.

In summary, we have reported on a novel series of acceptor-substituted quinquethiophenes, **DCV5T-Me's 1**−**3**, in which the positioning of methyl substitutents along the conjugated backbone was systematically varied. These oligomers were incorporated into vacuum-processed p−i−n-type BHJ solar cells, which exhibited PCEs of 4.8−6.1%. Through optimization of the processing and fabrication conditions to obtain the best-performing oligomer **3**-based device, the PCE was enhanced to 6.9%, which is the highest reported to date for SMOSCs. XRD measurements of co-evaporated D−A films allowed us to correlate the device performance with the morphology of the photoactive blend layer. Single-crystal X-ray structure analysis of oligomer **3** gave deeper insight into the specific intermolecular interactions and multiple nonbonding short contacts, which are responsible for the layer structure with strong π-π overlap and multidirectional electronic coupling. Finally, our investigations clearly showed that methyl

substitution in oligothiophenes can be used to provide a beneficial influence on the morphology of D−A blends and consequently the device performance. This work emphasizes the advantages of structurally defined oligomers, which provide structure−property relationships (molecular level) as well as information on favorable molecular organization in the bulk (supramolecular level) and pronounced phase separation of the donor and acceptor materials in BHJs (systems level).[15]

SUPPORTING INFORMATION

Experimental procedures, additional results, and a CIF file. This material is available free of charge via the Internet at http://pubs.acs.org. The X-ray data were also deposited with the CCDC (entry 850004).

ACKNOWLEDGEMENTS

This work was supported by the DFG (Priority Program SPP 1355) and BMBF (Programs OPEG 13N9720 and OPA 13N98872). We thank Dr. L. Wilde (Fraunhofer CNT) for the X-ray measurements and Novaled AG for providing NDP9.

REFERENCES

[1] Brabec, C.; Gowrisanker, S.; Halls, J. M. M.; Laird, D.; Jia, S. J.; Williams, S. P. *Adv. Mater.* **2010**, *22*, 3839.

[2] *Organic Photovoltaics: Materials, Device Physics, and Manufacturing Technologies*; Brabec, C., Dyakonov, V., Scherf, U., Eds.; Wiley-VCH: Weinheim, Germany, 2008.

[3] Dou, L.; You, J.; Yang, J.; Chen, C.-C.; He, Y.; Murase, S.; Moriarty, T.; Emery, K.; Li, G.; Yang, Y. *Nat. Photonics* **2012**, *6*, 180.

[4] Mishra, A.; Bäuerle, P. *Angew. Chem., Int. Ed.* **2012**, *51*, 2020.

[5] Sun, Y.; Welch, G. C.; Leong, W. L.; Takacs, C. T.; Bazan, G. C.; Heeger, A. J. *Nat. Mater.* **2012**, *11*, 44.

[6] Chiu, S.-W.; Lin, L.-Y.; Lin, H.-W.; Liu, Y.-H.; Huang, Z.-Y.; Lin, Y.-T.; Lin, F.; Chen, Y.-H.; Wong, K.-T. *Chem. Commun.* **2012**, *48*, 1857.

[7] Heliatek GmbH, press release of April 27, 2012 (http://www.heliatek.com).

[8] Fitzner, R.; Reinold, E.; Mishra, A.; Mena-Osteritz, E.; Ziehlke, H.; Körner, C.; Leo, K.; Riede, M.; Weil, M.; Tsaryova, O.; Weiß, A.; Uhrich, C.; Pfeiffer, M.; Bäuerle, P. *Adv. Funct. Mater.* **2011**, *21*, 897.

[9] Desiraju, G. R.; Steiner, T. *The Weak Hydrogen Bond*; Oxford University Press: New York, 1999.

[10] (a) Fitzner, R.; Elschner, C.; Weil, M.; Uhrich, C.; Körner, C.; Riede, M.; Leo, K.; Pfeiffer, M.; Reinold, E.; Mena-Osteritz, E.; Bäuerle, P. *Adv. Mater.* **2012**, *24*, 675. (b) Schrader, M.; Fitzner, R.; Hein, M.; Elschner, C.; Baumeier, B.; Riede, M.; Leo, K.; Bäuerle, P.; Andrienko, D. *J. Am. Chem. Soc.* **2012**, *134*, 6052−6056.

[11] (a) Schulze, K.; Uhrich, C.; Schüppel, R.; Leo, K.; Pfeiffer, M.; Brier, E.; Reinold, E.; Bäuerle, P. Adv. Mater. 2006, 18, 2872. (b) Schulze, K.; Riede, M.; Brier, E.; Reinold, E.; Bäuerle, P.; Leo, K. *J. Appl. Phys.* **2008**, *104*, No. 074511. (c) Mishra, A.; Uhrich, C.; Reinold, E.; Pfeiffer, M.; Bäuerle, P. *Adv. Energy Mater.* **2011**, *1*, 265.

[12] Xie, Q.; Arias, F.; Echegoyen, L. *J. Am. Chem. Soc.* **1993**, *115*, 9818.

[13] Riede, M.; Mueller, T.; Tress, W.; Schueppel, R.; Leo, K. *Nanotechnology* **2008**, *19*, No. 424001.

[14] Wynands, D.; Levichkova, M.; Leo, K.; Uhrich, C.; Schwartz, G.; Hildebrandt, D.; Pfeiffer, M.; Riede, M. *Appl. Phys. Lett.* **2010**, *97*, No. 073503.

[15] Würthner, F.; Meerholz, K. *Chem. - Eur. J.* **2010**, *16*, 9366.

SUPPORTING INFORMATION

MATERIALS AND METHODS

NMR spectra were recorded on a Bruker AMX 500 (^{1}H NMR: 500 MHz, ^{13}C NMR: 125 MHz) or an Avance 400 spectrometer (^{1}H NMR: 400 MHz, ^{13}C NMR: 100 MHz), at 25 °C or 100 °C. Chemical shift values (δ) are expressed in parts per million using residual solvent protons (^{1}H NMR, δ_H = 7.26 for $CDCl_3$, δ_H = 2.50 for DMSO-d_6 and δ_H = 5.93 for tetrachloroethane-d_2; ^{13}C NMR, δ_C = 77.0 for $CDCl_3$, δ_C = 39.43 for DMSO-d_6 and δ_C = 74.20 tetrachloroethane-d_2) as internal standard. The splitting patterns are designated as follows: s (singlet), d (doublet) and dd (doublet of doublets). The assignments are Th*H* (thiophene protons), Me*H* (methyl protons) C*H*O (aldehyde protons) and DCV*H* (dicyanovinyl protons). GC-MS (EI) mass spectra were recorded on a *Varian* Saturn *2000*, CI mass spectra on a *Finnigan* MAT SSQ-7000 and MALDI-TOF mass spectra on a *Bruker* Daltonic Reflex III. Melting points were determined using a Büchi B-545 apparatus and were not corrected. Elemental analyses were performed on an Elementar Vario EL. Preparative column chromatography was performed on glass columns packed with silica gel (Merck Silica 60, particle size 40-43 μm).

Tetrahydrofurane (THF, Merck) was dried under reflux over sodium/benzophenone (Merck) and distilled. Dimethylformamide (DMF, Merck) was refluxed over P_4O_{10} (Merck) and distilled. The potassium carbonate (Riedel-de Haën) solution was prepared by dissolving in deionised water and was degassed prior to use. 3,4-Dimethylthiophene-2-carboxaldehyde **4**,[1] 2,5-bis(trimethylstannyl)thiophene **10**,[2] 3,4-dimethylthiophene **11**,[3] 2-[(5-bromo-thiophen-2-yl)methylene]-malononitrile **17**[4] and 2,5-bis(trimethylstannyl)-3,4-dimethylthiophen **18**[5] were prepared according to published literature procedures. *n*-Butyl lithium (2.5 M solution in hexanes), 2-isopropoxy-4,4,5,5-tetramethyl[1,3,2]dioxoborolane, 5-bromothiophene-2-carbaldehyde **13**, 2-(tributylstannyl)thiophene **6** and trimethyltinchloride were purchased from Aldrich. *n*-Butyl lithium (1.6 M solution in hexanes) was purchased from Acros. *N*-bromosuccinimide (NBS), malononitrile and *β*-alanine were purchased from Merck. All synthetic steps were carried out under argon atmosphere.

SYNTHESIS AND CHARACTERIZATION

Target compounds **1-3** were obtained in good yields by reacting DCV-capped bromobithiophenes **9**, **16**, **17** and bisstannylated thiophene **10** or 3,4-dimethylthiophene **18** in Pd-catalyzed Stille-type cross-coupling reactions (Scheme S1). Bromobithiophenes **9** and **16** were prepared

from isomeric dimethylated bithiophene carbaldehydes **7** and **14**, respectively, by bromination with NBS, followed by Knoevenagel condensation of the products **8** and **15** with malononitrile and *β*-alanine as catalyst. For the synthesis of bithiophene carbaldehyde **7** 3,4-dimethylthiophene-2-carbaldehyde **4** was brominated with NBS to give corresponding bromide **5** which was subsequently cross-coupled with tributylstannyl thiophene **6** to provide intermediate **7**. For the synthesis of bithiophene carbaldehyde **14** 3,4-dimethylthiophene **11** was converted to pinacol boronic ester **12** and reacted with 5-bromothiophene-2-carbaldehyde **13** in a Suzuki-type cross-coupling reaction to furnish intermediate **14**.

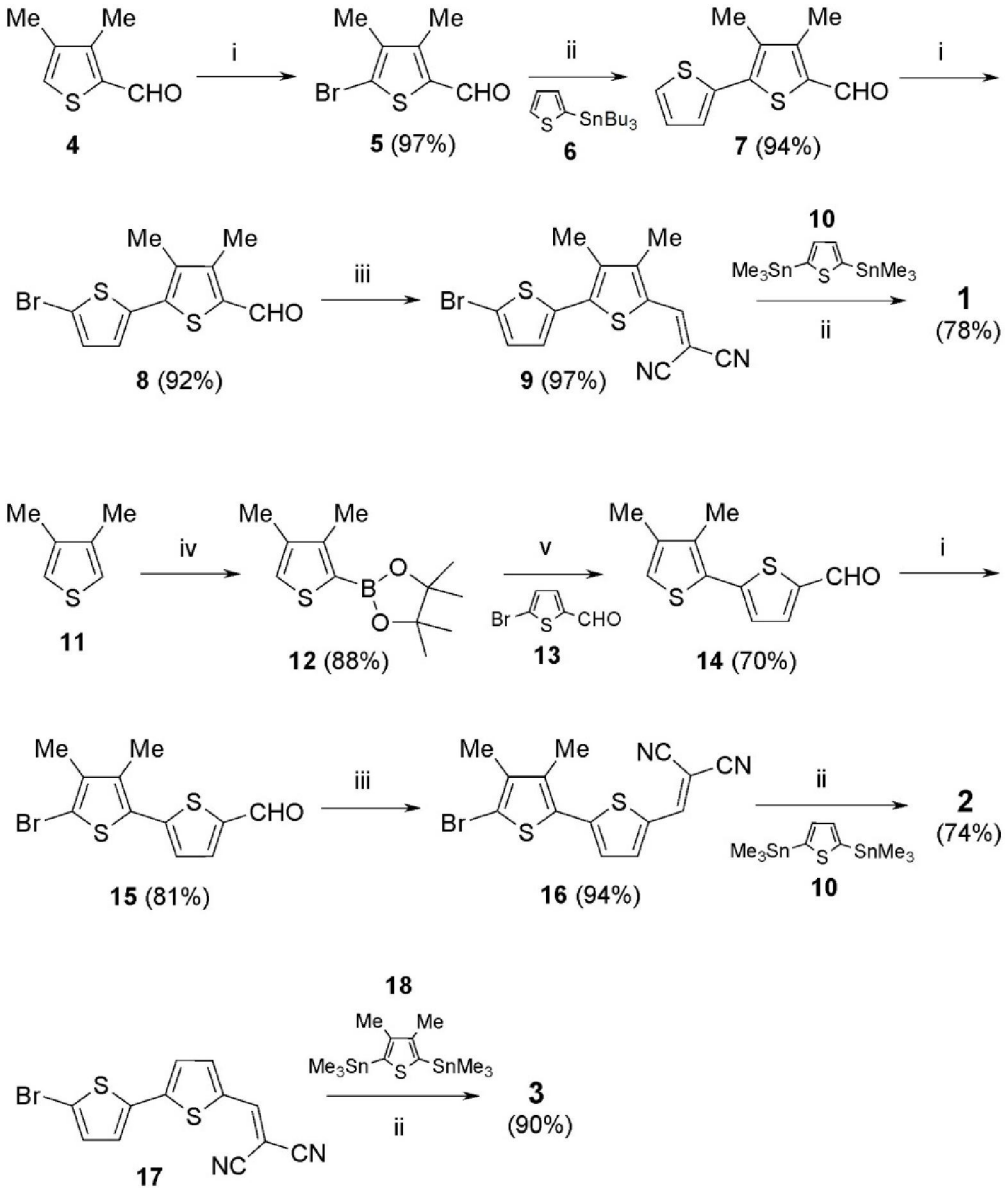

Scheme S1. *Synthesis of quinquethiophenes* ***1-3****. Reagents: (i) NBS, DMF; (ii)* $Pd(PPh_3)_4$*, DMF; (iii)* $CH_2(CN)_2$*, β-alanine, EtOH/dichloroethane; (iv) 1. n-BuLi, THF; 2. 2-isopropoxy-4,4, 5,5-tetramethyl[1,3,2]dioxoborolane; (v)* K_2CO_3*,* $Pd(PPh_3)_4$*, THF.*

*Synthesis of 2,2'-[3,4,3'''',4''''-tetramethyl-2,2':5',2'':5'',2''':5''',2''''-quinquethien-5,5''''-diylbis-(methane-1-yl-1-ylidine)]dimalononitrile **1***: A mixture of 2,5-bis(trimethylstannyl)thiophene **10** (2.50 g, 6.10 mmol), 5-[(5'-bromo-3,4-dimethyl-2,2'-bithien-5-yl)methylene]malononitrile **9** (4.69 g, 13.4 mmol) and tetrakis(triphenylphosphine)palladium(0) (352 mg, 0.31 mmol) in degassed DMF (200 mL) was stirred at 80 °C for 8 hours. The reaction mixture was allowed to cool to room temperature and the precipitate was filtered off. The obtained solid was further refluxed in methanol for 30 min and collected by filtration. The crude product was extracted in a Soxhlet extractor with acetone for 16 hours to remove the most soluble reaction by-products. Subsequently, Soxhlet extraction was continued for 8 days using chlorobenzene. Upon cooling the resulting extract to room temperature, the precipitate was filtered off to yield **1** (2.95 g, 4.76 mmol, 78%) as a black solid. M.p. 368 °C (DSC). ^{1}H NMR (TCE-d_2, 100 °C, δ ppm) 7.83 (s, 2H, DCVH), 7.31 (d, 2H, J = 3.82 Hz, ThH), 7.22 (d, 2H, J = 3.82 Hz, ThH), 7.19 (s, 2H, ThH), 2.38 (s, 6H, MeH), 2.33 (s, 6H, MeH). MALDI-TOF mass 620 [M^+] (calcd. for $C_{32}H_{20}N_4S_5$ 620). Elemental analysis for $C_{32}H_{20}N_4S_5$: calcd. C, 61.91; H, 3.25; N, 9.02; S, 25.82%; found: C, 62.02; H, 3.35; N, 8.83; S, 25.69%.

*Synthesis of 2,2'-[3',4',3''',4'''-tetramethyl-2,2':5',2'':5'',2''':5''',2''''-quinquethien-5,5''''-diylbis-(methane-1-yl-1-ylidine)]dimalononitrile **2***: A mixture of 2,5-bis(trimethylstannyl)thiophene **10** (150 mg, 0.37 mmol), 5-[(5'-bromo-3',4'-dimethyl-2,2'-bithien-5-yl)methylene]malononitrile **16** (269 mg, 0.77 mmol) and tetrakis(triphenylphosphine)palladium(0) (21 mg, 0.012 mmol) was combined in degassed DMF (6.5 mL) in a screw cap vial, and was agitated at 80 °C for 20 hours. After cooling, the resulting precipitate was filtered off and washed several times with methanol and n-hexane. Column chromatography (silica gel, DCM) yielded compound **2** (168 mg, 0.27 mmol, 74%) as a black solid. M.p. 302 °C (DSC). ^{1}H NMR (DMSO-d_6, 100 °C, δ ppm) 8.52 (s, 2H, DCVH), 7.96 (d, 2H, J = 4.17 Hz, ThH), 7.51 (d, 2H, J = 4.13 Hz, ThH), 7.35 (s, 2H, ThH), 2.40 (s, 6H, MeH), 2.37 (s, 6H, MeH). MALDI-TOF mass 621 [M+H^+] (calcd. for $C_{32}H_{20}N_4S_5$ 620). Elemental analysis for $C_{32}H_{20}N_4S_5$: calcd. C, 61.91; H, 3.25; N, 9.02; S, 25.82%; found: C, 62.03; H, 3.30; N, 8.90; S, 25.95%.

*Synthesis of 2,2'-[3'',4''-dimethyl-2,2':5',2'':5'',2''':5''',2''''-quinquethien-5,5''''-diylbis(methane -1-yl-1-ylidine)]dimalononitrile **3***: A mixture of 2,5-bis(trimethylstannyl)-3,4-dimethyl-thiophene **18** (100 mg, 0.23 mmol), 5-[(5'-bromo-3,4-dimethyl-2,2'-bithien-5-yl)methylene]malononitrile **17** (269 mg, 0.77 mmol) and tetrakis(triphenylphosphine)palladium(0) (13 mg, 0.012 mmol) was combined in degassed DMF (4 mL) in a screw cap vial, and was agitated at 80 °C for 8 hours. Upon cooling, the resulting precipitate was filtered off and washed several

times with methanol and n-hexane. After drying, product **3** (122 mg, 0.20 mmol, 90%) was obtained as a black crystalline solid. M.p. 301 °C (DSC). ^{1}H NMR (DMSO-d_6, 100 °C, δ ppm) 8.53 (s, 2H, DCVH), 7.93 (d, 2H, J = 4.22 Hz, ThH), 7.67 (d, 2H, J = 3.95 Hz, ThH), 7.63 (s, 2H, J = 3.95, ThH), 7.35 (s, 2H, J = 3.93, ThH), 2.38 (s, 6H, MeH). MALDI-TOF mass 593 [M+H$^+$] (calcd. for $C_{30}H_{16}N_4S_5$ 592). Elemental analysis for $C_{30}H_{16}N_4S_5$: calcd. C, 60.78; H, 2.72; N, 9.45; S, 27.04%; found: C, 60.62; H, 2.85; N, 9.75; S, 27.32%.

*Synthesis of 5-bromo-3,4-dimethylthiophene-2-carboxaldehyde **5***: Solutions of 3,4-dimethylthiophene-2-carboxaldehyde **4** (20.0 g, 143 mmol) in dimethylformamide (DMF, 150 mL) and NBS (30.5 g, 172 mmol) in DMF (150 mL) were cooled to -18 °C and combined. The reaction mixture was allowed to stand at room temperature for 2 days and then poured onto ice (1 kg). The precipitate was filtered off, washed with water (2 L) and dried under reduced pressure in a desiccator. Recrystallisation of the crude product from n-hexane (70 mL) provided compound **5** (30.2 g, 138 mmol, 97%) as a colourless crystalline solid. M.p. 79-81 °C. ^{1}H NMR (chloroform-d_1, δ ppm) 9.93 (s, 1H, CHO), 2.48 (s, 3H, MeH), 2.14 (s, 3H, MeH). ^{13}C NMR (chloroform-d_1, δ ppm) 181.23, 146.38, 139.57, 138.04, 122.08, 13.70, 13.67. CI mass 219 [M+H$^+$] (calcd. for C_7H_7BrOS 218). Elemental analysis for C_7H_7BrOS: calcd. C, 38.37; H, 3.22; S, 14.63%; found: C, 38.58; H, 3.22; S, 14.53%.

Synthesis of 3,4-dimethyl-2,2'-bithiophene-5-carbaldehyde 7: A degassed solution of 2-tributylstannylthiophene **6** (16.60 g, 44.5 mmol), 5-bromo-3,4-dimethylthiophene-2-carboxaldehyde **5** (8.12 g, 37.1 mmol) and tetrakis(triphenylphosphine)palladium(0) (857 mg, 0.74 mmol) in DMF (200 mL) was stirred at 60 °C for 16 hours. The reaction mixture was poured on ice (500 g), extracted with dichloromethane (3 × 100 mL), filtered over silica gel and concentrated under reduced pressure. Column chromatography (silica gel, DCM) and subsequent recrystallization from n-hexane/dichloromethane afforded compound **7** (7.74 g, 34.8 mmol, 94%) as a yellow crystalline solid. M.p. 100-102.5 °C. ^{1}H NMR (chloroform-d_1, δ ppm) 10.03 (s, 1H, CHO), 7.41 (dd, 1H, J = 5.09 Hz, J = 0.99 Hz, ThH), 7.28 (dd, 1H, J = 3.61 Hz, J = 0.97 Hz, ThH), 7.11 (dd, 1H, J = 5.14 Hz, J = 3.80 Hz, ThH), 2.49 (s, 3H, MeH), 2.31 (s, 3H, MeH). ^{13}C NMR (chloroform-d_1, δ ppm) 182.00, 147.94, 140.81, 135.80, 135.50, 127.76, 127.44, 127.12, 13.41, 13.36. CI mass 222 [M$^+$] (calcd. for $C_{11}H_{10}OS_2$ 222). Elemental analysis for $C_{11}H_{10}OS_2$: calcd. C, 59.43; H, 4.53; S, 28.84%; found: C, 59.58; H, 4.77; S, 28.64%.

*Synthesis of 2'-bromo-3,4-dimethyl-2,2'-bithiophene-5-carbaldehyde **8***: Solutions of 3,4-dimethyl-2,2'-bithiophene-5-carbaldehyde **7** (7.50 g, 33.7 mmol) in DMF (50 mL) and NBS (6.90 g,

38.8 mmol) in DMF (50 mL) were cooled to -18 °C and combined. The reaction mixture was allowed to stand for 2 days at -18 °C, followed by 10 hours at 7 °C and then poured on ice (500 g). The precipitate was filtered off, washed with water and dried under reduced pressure in a desiccator. Recrystallization of the crude product from n-hexane/dichloromethane provided compound **8** (9.31 g, 30.9 mmol, 92%) as yellow needles. M.p. 138-139 °C. ^{1}H NMR (DMSO-d_6, 100 °C, δ ppm) 10.06 (s, 1H, CHO), 7.29 (d, 1H, J = 3.97 Hz, ThH), 7.21 (d, 1H, J = 3.92 Hz, ThH), 2.50 (s, 3H, MeH), 2.27 (s, 3H, MeH). ^{13}C NMR (chloroform-d_1, δ ppm) 182.34, 147.65, 136.96, 135.99, 135.92, 135.46, 130.91, 127.84, 112.48, 12.38, 12.36. EI mass 302 [M+H$^+$] (calcd. for $C_{11}H_9BrOS_2$ 301). Elemental analysis for $C_{11}H_9BrOS_2$: calcd. C, 43.86; H, 3.01; S, 21.29%; found: C, 43.88; H, 3.12; S, 21.18%.

Synthesis of 5-[(5'-bromo-3,4-dimethyl-2,2'-bithien-5-yl)methylene]malononitrile ***9***: A solution consisting of 2'-bromo-3,4-dimethyl-2,2'-bithiophene-5-carbaldehyde **8** (8.50 g, 28.2 mmol), malononitrile (5.59 g, 84.7 mmol) and β-alanine (151 mg, 1.7 mmol) in a mixture of dichloroethane (250 mL) and ethanol (250 mL) was stirred under reflux for 16 hours. The reaction mixture was allowed to cool to room temperature, the precipitate was filtered off and washed thoroughly with water and methanol. Recrystallization of the crude product from dichloromethane/n-hexane provided compound **9** (9.51 g, 27.2 mmol, 97%) as red needles. M.p. 231.5-233 °C. ^{1}H NMR (DMSO-d_6, 100 °C, δ ppm) 8.50 (s, 1H, CHO), 7.33 (d, 1H, J = 3.90 Hz, ThH), 7.28 (d, 1H, J = 4.03 Hz, ThH), 2.40 (s, 3H, MeH), 2.31 (s, 3H, MeH). ^{13}C NMR (DMSO-d_6, 100 °C, δ ppm) 152.15, 149.39, 138.58, 135.56, 135.04, 131.20, 128.72, 127.95, 114.06, 113.73, 113.31, 73.91, 13.25, 12.83. CI mass 350 [M+H$^+$] (calcd. for $C_{14}H_9BrN_2S_2$ 349). Elemental analysis for $C_{14}H_9BrN_2S_2$: calcd. C, 48.14; H, 2.60; N, 8.02; S, 18.36%; found: C, 48.20; H, 2.81; N, 8.29; S, 18.49%.

Synthesis of 2-(3,4-dimethylthien-2-yl)-4,4,5,5-tetramethyl[1,3,2]dioxoborolane ***12***: To a solution of 3,4-dimethylthiophene **11** (10.07 g, 89.9 mmol) in THF (100 mL), stirred at -10 °C, n-butyl lithium (1.6 M solution in hexanes, 56.2 mL, 89.9 mmol) was added dropwise over 45 minutes. The solution was stirred at -10 °C for 30 minutes, allowed to warm to ambient temperature and stirred an additional hour. After cooling to -10 °C again, a solution of 2-isopropoxy-4,4,5,5-tetramethyl[1,3,2]dioxoborolane (16.62 g, 89.9 mmol) in THF (30 mL) was added and stirring was continued for 30 minutes. The reaction was quenched with an aqueous $NaHCO_3$ solution (200 mL) and the product was extracted with diethyl ether (3 × 200 mL). The combined organic extracts were dried over $MgSO_4$, filtered and the solvents were removed in vacuo. Recrystallization from n-hexane yielded boronic ester **12** (18.6 g, 78.1 mmol, 88%) as a

colorless crystalline solid. M.p. 61-62.5 °C. ^{1}H NMR (chloroform-d_1, δ ppm) 7.16 (s, 1H, ThH), 2.37 (s, 3H, ThH), 2.17 (s, 3H, MeH), 1.34 (s, 12 H). ^{13}C NMR (chloroform-d_1, δ ppm) 148.36, 139.26, 127.37, 83.46, 24.79, 14.57, 14.48. EI mass 239 [M+H$^+$] (calcd. for $C_{12}H_{19}BO_2S$ 238). Elemental analysis for $C_{12}H_{19}BO_2S$: calcd. C, 60.52; H, 8.04; S, 13.46%; found: C, 60.27; H, 7.97; S, 13.42%.

*Synthesis of 3',4'-dimethyl-2,2'-bithiophene-5-carbaldehyde **14***: A degassed aqueous potassium carbonate solution (35 mL, 70 mmol) was added to a degassed solution containing boronic ester **12** (4.91 g, 20.6 mmol), 5-bromothiophene-2-carbaldehyde **13** (3.28 g, 17.2 mmol) and tetrakis-(triphenylphosphine)palladium(0) (992 mg, 0.86 mmol) in THF (150 mL). The reaction mixture was stirred under reflux for seven days, whereas after two days another portion of tetrakis(triphenylphosphine)palladium(0) (992 mg, 0.86 mmol) was added. After this, the mixture was poured on water (200 mL), extracted with dichloromethane (3 × 100 mL), washed with water (2 × 100 mL), dried over $MgSO_4$, filtered and concentrated under reduced pressure. Column chromatography (silica gel, DCM) yielded compound **14** (2.67 g, 12.0 mmol, 70%) as yellow needles. M.p. 58-59.5 °C. ^{1}H NMR (chloroform-d_1, δ ppm) 9.87 (s, 1H, CHO), 7.70 (d, 1H, J = 3.97 Hz, ThH), 7.21 (d, 1H, J = 4.00 Hz, ThH), 6.96 (s, 1H, ThH), 2.34 (s, 3H, MeH), 2.20 (s, 3H, MeH). ^{13}C NMR (chloroform-d_1, δ ppm) 182.58, 147.43, 142.07, 139.52, 136.72, 136.26, 130.15, 125.77, 121.54, 15.39, 14.02. EI mass 222 [M$^+$] (calcd. for $C_{11}H_{10}OS_2$ 222). Elemental analysis for $C_{11}H_{10}OS_2$: calcd. C, 59.43; H, 4.53; S, 28.84%; found: C, 59.18; H, 4.31; S, 28.82%.

*Synthesis of 2'-bromo-3',4'-dimethyl-2,2'-bithiophene-5-carbaldehyde **15***: Solutions of 3',4'-dimethyl-2,2'-bithiophene-5-carbaldehyde **14** (1.36 g, 6.12 mmol) in DMF (20 mL) and NBS (1.09 g, 6.12 mmol) in DMF (10 mL) were cooled to -18 °C and combined. The reaction mixture was allowed to stand for 3 days at -18°C and then poured on ice (200 g). The precipitate was filtered off, washed with water and dried under reduced pressure in a desiccator. Recrystallization of the crude product from n-hexane/dichloromethane provided compound **15** (1.49 g, 4.96 mmol, 81%) as yellow needles. M.p. 119-120 °C. ^{1}H NMR (DMSO-d_6, δ ppm) 9.91 (s, 1H, CHO), 8.02 (d, 1H, J = 3.99 Hz, ThH), 7.40 (d, 1H, J = 3.99 Hz, ThH), 2.33 (s, 3H, MeH), 2.12 (s, 3H, MeH). ^{13}C NMR (DMSO-d_6, δ ppm) 183.84, 143.61, 142.14, 139.22, 138.37, 136.30, 129.04, 127.13, 109.47, 14.64, 14.22. EI mass 302 [M+H$^+$] (calcd. for $C_{11}H_9BrOS_2$ 301). Elemental analysis for $C_{11}H_9BrOS_2$: calcd. C, 43.86; H, 3.01; S, 21.29%; found: C, 43.79; H, 2.84; S, 21.37%.

*Synthesis of 5-[(5'-bromo-3',4'-dimethyl-2,2'-bithien-5-yl)methylene]malononitrile **16***: A solution consisting of 2'-bromo-3',4'-dimethyl-2,2'-bithiophene-5-carbaldehyde **15** (1.43 g, 4.73 mmol), malononitrile (938 mg, 14.8 mmol) and β-alanine (26 mg, 0.28 mmol) in a mixture of dichloroethane (150 mL) and ethanol (150 mL) was stirred under reflux for 24 hours. The reaction mixture was allowed to cool to room temperature, the precipitate was filtered off and washed thoroughly with ethanol to provide compound **16** (1.56 g, 4.47 mmol, 94 %) as red needles. M.p. 203-204 °C. ^{1}H NMR (DMSO-d_6, 100 °C, δ ppm) 8.53 (s, 1H, DCVH), 7.94 (d, 1H, J = 4.10 Hz, ThH), 7.44 (d, 1H, J = 4.11 Hz, ThH), 2.37 (s, 3H, MeH), 2.15 (s, 3H, MeH). ^{13}C NMR (DMSO-d_6, 100 °C, δ ppm) 151.47, 145.46, 139.98, 139.07, 136.70, 133.83, 128.41, 126.76, 113.70, 113.09, 110.13, 74.88, 14.20, 13.58. EI mass 350 [M+H$^+$] (calcd. for $C_{14}H_9BrN_2S_2$ 349). Elemental analysis for $C_{14}H_9BrN_2S_2$: calcd. C, 48.14; H, 2.60; N, 8.02; S, 18.36%; found: C, 48.42; H, 2.69; N, 8.21; S, 18.46%.

Optical and Electrochemical Measurements

Optical solution measurements were carried out in 1 cm cuvettes with Merck Uvasol grade solvents, absorption spectra were recorded on a Perkin Elmer Lambda 19 spectrometer. For thin film UV-vis characterization, nominally 30 nm of the pristine material was deposited on quartz glass substrates (Quarzglas QCS). Evaporation rates were around 0.2 Å/s. The thin film absorbance spectra were recorded on a Perkin Elmer lambda 900 spectrometer. Cyclic voltammetry experiments were performed with a computer-controlled Metrohm Autolab PGSTAT30 potentiostat in a three-electrode single-compartment cell with a platinum working electrode, a platinum wire counter electrode, and an Ag/AgCl reference electrode. All potentials were internally referenced to the ferrocene/ferrocenium couple.

X-ray Single Crystal Analysis

X-ray diffraction data of a greenish to black **DCV5T-Me 3** single crystal were collected in a stream of nitrogen at 100(2) K on a Bruker APEX-II CCD area detector diffractometer using graphite-monochromated Mo K_α radiation. Absorption correction based on a semi-empirical method was performed with the SADABS algorithm.[6] The structure was solved by direct methods with SHELXS-97,[7] revealing all atoms of the oligothiophene backbone. Additional atoms were discernible from difference Fourier maps during refinement on F^2 with SHELXL-97.[7] For the final model, all non-H atoms were refined anisotropically. H atoms were placed in calculated positions riding the parent C atom with C-H distance constraints of 0.93 Å for

aromatic H atoms, 0.96 Å for methyl H atoms (allowing for free rotation) and 0.99 Å for methylene H atoms, and with $U_{iso}(H) = 1.2U_{eq}(C)$ for aromatic and $1.5U_{eq}(C)$ for aliphatic H atoms.

DCV5T-Me 3: $C_{30}H_{16}N_4S_5$, M_r = 592.77, greenish to black fragment, 0.18 × 0.18 × 0.07 mm^3, monoclinic, *C*2/*c*, *a* = 13.5670(12) Å, *b* = 15.9004(13) Å, *c* = 12.8460(10) Å, β = 98.956(5)°, *V* = 2737.4(4) $Å^3$, *Z* = 4, μ = 0.452 mm^{-1}, *dx* = 1.438 g cm^{-3}, *T* = 100(2) K. 24684 reflections collected (θ_{max} = 27.0°) and merged to 2983 independent data (R_{int} = 0.079); final *R* indices: $R_1(I > 2\sigma(I))$ = 0.0574, wR_2 (all) = 0.1527. Detailed crystallographic data for the structure of DCV5T-Me **3** have been deposited with the Cambridge Crystallographic Data Centre as supplementary publication CCDC 850004.Details on measurement and refinement are given as below:

Average Bond Precision:	C-C = 0.0051 Å
Wavelength:	0.71073 Å
Measurement temperature:	100(2) K

Cell:	*a* = 13.5670(12) Å	*b* = 15.9004(13) Å	*c* = 12.846(1) Å
	α = 90°	β = 98.956(5)°	γ = 90°
Volume	2737.4(4) $Å^3$	*h,k,l max*	17,20,16
Space group	C2/c	*Nref*	2996
Hall group	-C 2yc	*Tmin, Tmax*	0.922,0.969
Moiety formula	$C_{30}H_{16}N_4S_5$	*Tmin'*	0.922
Sum formula	$C_{30}H_{16}N_4S_5$	*Correction method*	MULTI-SCAN
Mr	592.82	*Data completeness*	0.996
Density	1.439 g/cm^{-3}	*Theta(max)*	27.000
Z	4	*R(reflections)*	0.0574(2281)
Mu	0.452 mm^{-1}	*wR2(reflections)*	0.1527(2983)
F000	1216.0	*S*	1.081
F000'	1218.80	*Npar*	178

THIN FILM AND DEVICE FABRICATION

Thin film samples were prepared by thermal vapor deposition in ultra-high vacuum at a base pressure of lower than 10^{-7} mbar. The layer thicknesses were determined during evaporation using quartz crystal monitors calibrated for the respective material prior to evaporation. The deposition rates for the organic materials were between 0.1 and 0.4 Å s^{-1}. The solar cells were

prepared on tin-doped indium oxide (ITO) coated glass (Thin Film Devices, USA, sheet resistance of 30 Ω sq.$^{-1}$) layer by layer without breaking the vacuum. Two different stacks were used for the solar cells (Figure S4) with the following materials: C_{60} (Bucky USA, used density 1.54 g cm^{-3}); a blend of **DCV5T-Me 1-3** (used density 1.3 g cm^{-3}, confirmed by XRR) and C_{60} (ratio 2:1 by volume) prepared by co-evaporation and deposition on heated substrates (90 or 75 °C); 9,9-bis[4-(N,N-bis-biphenyl-4-yl-amino)phenyl]-9H-fluorene (BPAPF, Lumtec, Taiwan; used density 1.2 g/cm³); For n-doping C_{60}, $W_2(hpp_4)$ (Novaled AG, Germany) is used. For p-doping materials with high ionization potential like BPAPF, NDP9 (Novaled AG, Germany) is used instead of WO_3 because of its better processability.[8] Its doping performance, however, is comparable. The completed solar cells were encapsulated with a transparent encapsulation glass, fixed by UV-hardened epoxy glue, in a nitrogen glovebox. Particular care was taken for the active device area: it was individually determined for each solar cell by comparing the short circuit current without and with an aperture of well-defined size. The average device area was about 6.6 mm².

The external quantum efficiency (EQE) measurements were carried out on a custom-made setup utilizing chopped monochromatic light produced by a xenon arc lamp, a monochromator (Newport Cornerstone) and a chopper wheel. Data acquisition is accomplished with a lock-in amplifier (Signal Recovery 7265 DSP). A silicon reference diode (Hamamatsu S1337) was used to calibrate the setup. From EQE spectra, the spectral response of each individual device was determined and a spectral mismatch factor calculated.[9] The corresponding current density-voltage characteristics (*J-V*) characteristics were recorded on an setup consisting of a source-measure unit (Keithley SMU 2400) and an AM 1.5G sun simulator (KHS Technical Lighting SC1200). The illumination intensity was monitored with a silicon photodiode (Hamamatsu S1337) and the intensities during *J-V* measurements were mismatch corrected.

THERMAL ANALYSIS

Differential scanning calorimetric (DSC) measurements were performed on a Mettler Toledo DSC823^e under argon atmosphere at a heating rate of 10 °C min^{-1}. Thermogravimetric analysis (TGA) was conducted on a Mettler Toledo TGA/SDTA851^e instrument with a heating rate of 10 °C min^{-1} under a nitrogen at a flow rate of 50 cm^3 min^{-1}.

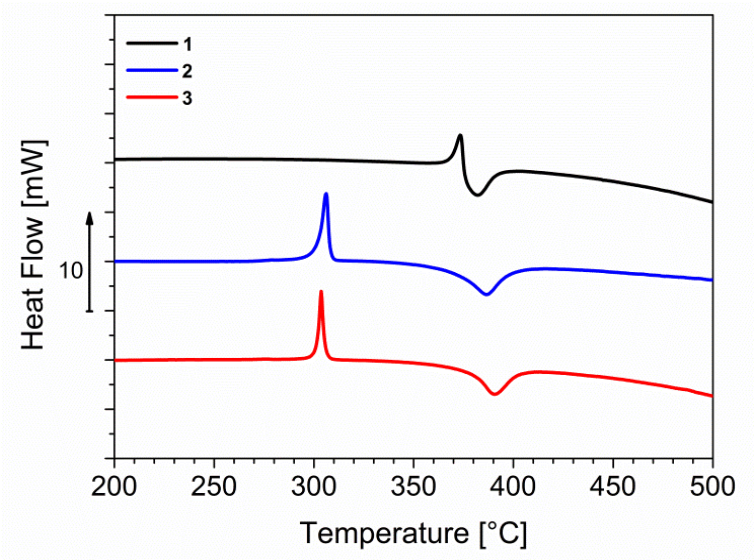

Figure S1. *DSC trace of* ***DCV5T-Me 1-3*** *measured under argon flow at a heating rate of 10 °C/min.*

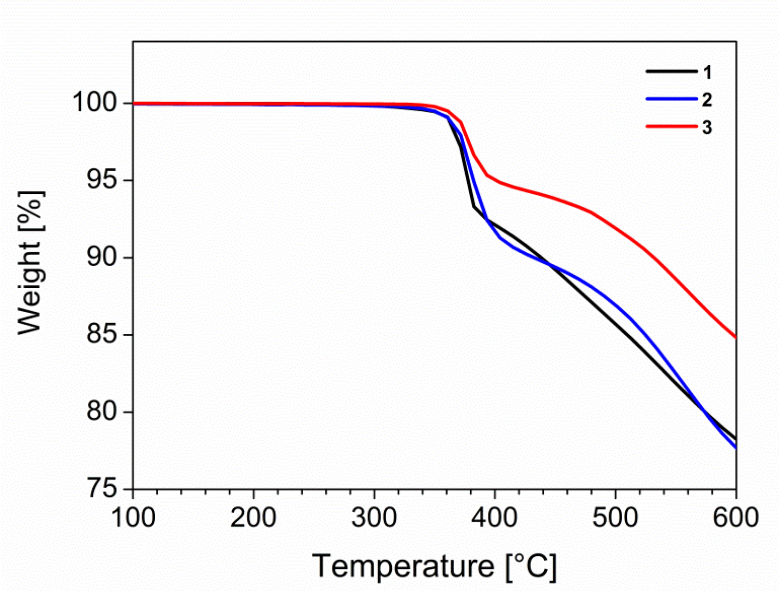

Figure S2. *TGA thermograms of* ***DCV5T-Me 1-3*** *measured under nitrogen flow (50 mL/min) at a heating rate of 10 °C/min.*

CYCLIC VOLTAMMETRY (CV)

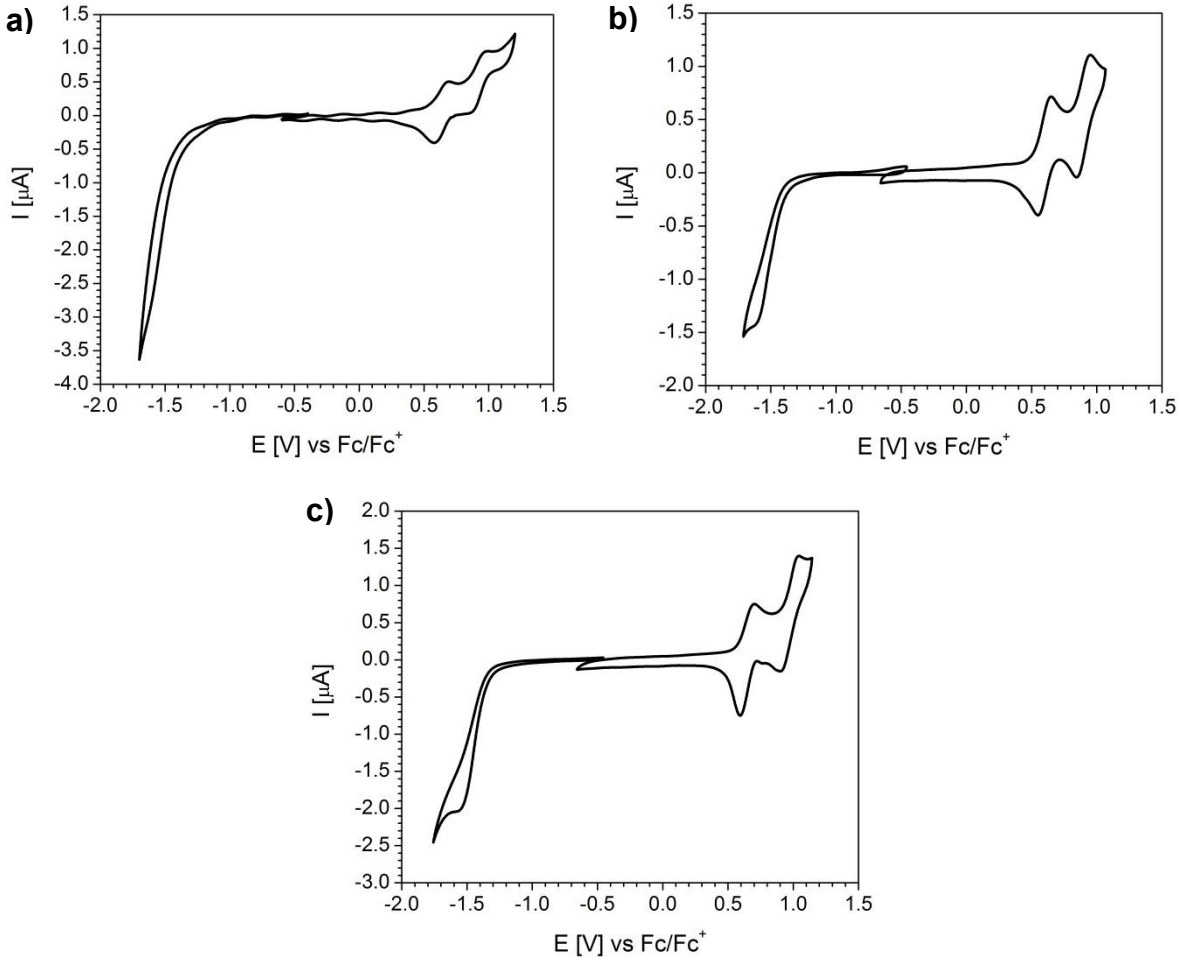

Figure S3. *Cyclic voltammograms of* ***DCV5T-Me 1*** *(a),* ***DCV5T-Me 2*** *(b) and* ***DCV5T-Me 3*** *(c), measured in tetrachloroethane-TBAPF$_6$ (0.1 M), scan rate 100 mV/s, potentials versus Fc/Fc$^+$, measured at 80 °C.*

SOLAR CELL DEVICE STACKS

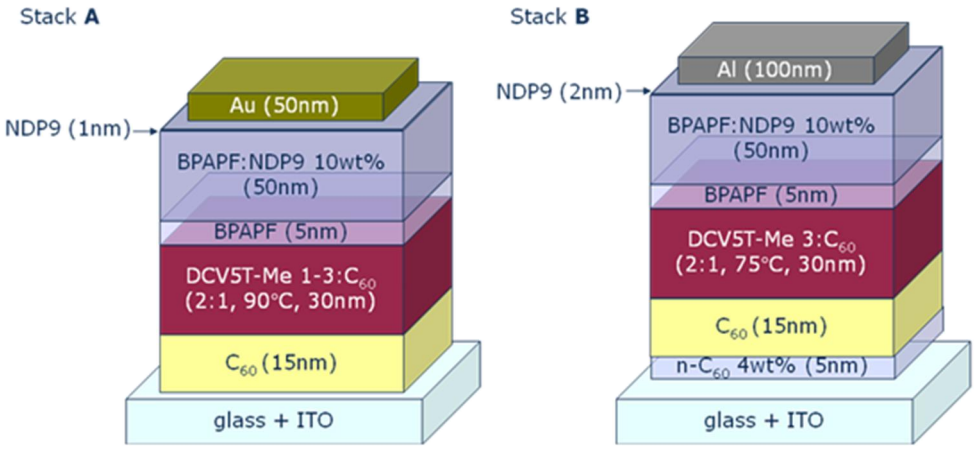

Figure S4. *Layer structure of stack A and B used for the solar cells incorporating a 30 nm blend layer of* ***DCV5T-Me 1-3****:C$_{60}$ (2:1 by volume) deposited at elevated substrate temperature.*

PHOTOVOLTAIC CHARACTERISTICS OF OPTIMIZED SOLAR CELLS (STACK B)

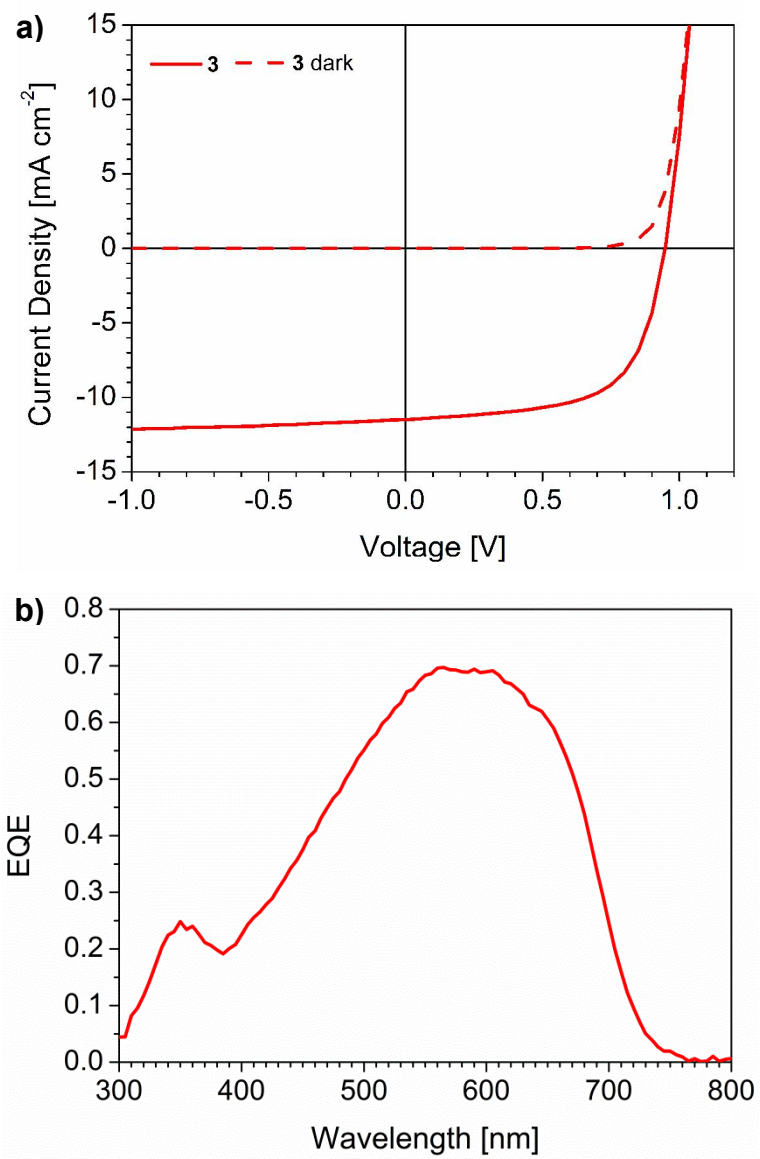

Figure S5. *J-V characteristics (a) and EQE spectra (b) of the highest efficient bulk heterojunction solar cell (Sample 13P4, bold in Table S1) containing oligomer* ***3****:C_{60} (2:1 by volume) employing optimized stack B.*

COMPARISON OF EQE OF INITIAL (A) AND OPTIMIZED STACK (B)

Figure S6a shows a comparison of EQE spectra of solar cells **3**(A) and **3**(B). The increase between 400 and 550nm originates from a decrease in absorption of the back electrode by exchanging Au with Al. This can be inferred from the simulated absorption data in Fig. S6b. The absorption in the **DCV5T-Me 3**-device, the C_{60} and the electrode layer are shown for stack **3**(A) and **3**(B). The simulation also predicts the decrease of absorption in C_{60} which is confirmed by the EQE measurement. Moreover, the calculated absorbed photon flux in the active layer (**DCV5T-**

Me 3 and (i)-C_{60}) are given in the figure. It shows an increase of 18% for stack (B), which correlates with the observed 19% increase in J_{SC}.

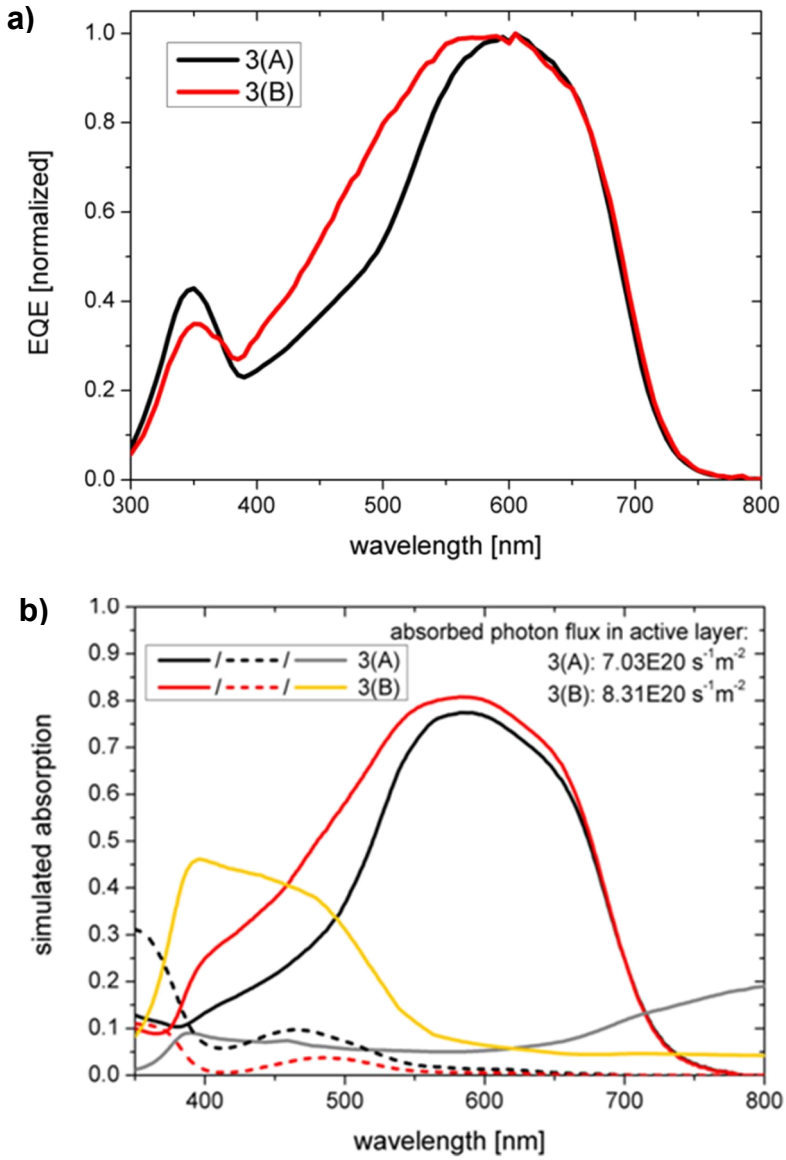

Figure S6. *(a) Comparison of EQE spectra for the initial (A) and optimized (B) solar cell stack using* ***DCV5T-Me 3****. (b) Simulated absorption data for the* ***DCV5T-Me 3*** *(solid lines black/red), the C_{60} (dashed lines black/red) and the electrode layer (yellow/grey) for stack* ***3****(A) and* ***3****(B), respectively.*

THIN FILM X-RAY DIFFRACTION MEASUREMENT

Thin film XRD measurements were carried out on a Bruker AXS D8 Discover. As beam optics, a Göbel mirror and Cu-K_α radiation in combination with a scintillation detector was used. To get highest intensities, a grazing incidence X-ray diffraction scan mode was chosen for the thin film measurements and details are described elsewhere.[10]

STATISTICS FOR SEVERAL STACK 3(B) SOLAR CELL PARAMETERS

Table S1. *Summary of the photovoltaic characteristics of 32 bulk heterojunction solar cells, fabricated on eight different substrates, containing oligomer* ***3*** *and based on the optimized stack B. These data were used to statistically evaluate the reproducibility of the photovoltaic performance. One device (Sample 14P1) was short-circuited.*

Sample	J_{SC} [mA cm^{-2}]	V_{OC} [V]	FF [%]	Saturation	Mismatch Factor	Intensity [mW cm^{-2}]	PCE [%]
11P1	11,3	0,947	63	1,05(9)	0,76(2)	99,9	6,8(1)
11P2	11,4	0,946	63	1,05(5)	0,76(2)	100,0	6,8(0)
11P3	11,4	0,946	63	1,05(9)	0,76(2)	99,9	6,8(1)
11P4	11,4	0,948	63	1,06(1)	0,76(2)	99,9	6,8(5)
12P1	11,4	0,949	63	1,05(8)	0,76(2)	99,9	6,8(0)
12P2	11,4	0,948	62	1,06(0)	0,76(2)	99,9	6,7(6)
12P3	11,4	0,948	62	1,06(0)	0,76(2)	100,0	6,7(1)
12P4	11,5	0,948	62	1,06(0)	0,76(1)	100,0	6,7(3)
13P1	11,5	0,948	63	1,05(9)	0,76(3)	99,8	6,8(6)
13P2	11,5	0,947	63	1,05(9)	0,76(3)	99,8	6,8(6)
13P3	11,4	0,947	63	1,06(0)	0,76(2)	99,9	6,8(3)
13P4	**11,5**	**0,948**	**63**	**1,05(6)**	**0,76(3)**	**99,9**	**6,8(9)**
14P1	-	-	-	-	-	-	-
14P2	11,2	0,946	63	1,05(8)	0,76(2)	99,9	6,6(5)
14P3	11,4	0,946	63	1,05(8)	0,76(2)	99,9	6,7(5)
14P4	11,4	0,947	63	1,05(8)	0,76(2)	99,9	6,8(1)
21P1	11,3	0,948	63	1,06(2)	0,76(3)	99,8	6,7(2)
21P2	11,3	0,947	63	1,06(0)	0,76(3)	99,8	6,7(5)
21P3	11,3	0,947	63	1,05(7)	0,76(3)	99,8	6,7(6)
21P4	11,3	0,947	63	1,05(9)	0,76(2)	99,9	6,7(5)
22P1	11,6	0,949	62	1,06(4)	0,76(3)	99,8	6,8(5)
22P2	11,5	0,948	62	1,06(1)	0,76(3)	99,8	6,7(6)
22P3	11,5	0,948	62	1,06(2)	0,76(3)	99,8	6,7(8)
22P4	11,5	0,948	62	1,06(1)	0,76(3)	99,8	6,7(7)
23P1	11,5	0,949	60	1,06(4)	0,76(3)	99,7	6,5(7)
23P2	11,5	0,948	62	1,05(9)	0,76(3)	99,8	6,7(6)
23P3	11,5	0,947	62	1,06(0)	0,76(3)	99,8	6,8(4)
23P4	11,5	0,948	63	1,06(2)	0,76(3)	99,8	6,8(6)
24P1	11,4	0,948	63	1,05(8)	0,76(2)	99,9	6,7(8)
24P2	11,4	0,947	63	1,05(8)	0,76(3)	99,8	6,7(9)
24P3	11,4	0,947	63	1,05(8)	0,76(3)	99,8	6,7(7)
24P4	11,5	0,948	63	1,05(7)	0,76(3)	99,8	6,8(5)

X-RAY REFLECTION (XRR)

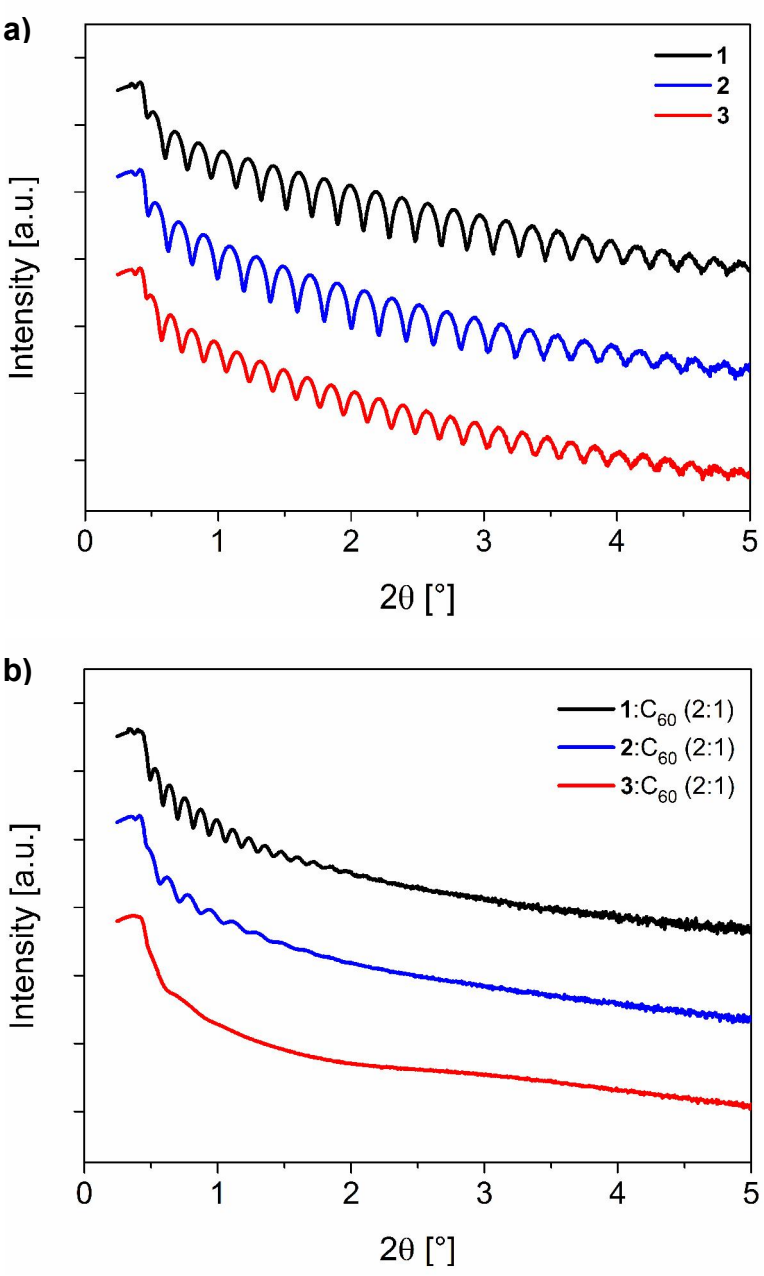

Figure S7. *(a) XRR patterns of neat films of* ***DCV5T-Me 1-3*** *deposited on glass substrates at room temperature. (b) XRR patterns of blend layers of* ***DCV5T-Me 1-3****:C_{60} (2:1 by volume) fabricated by co-evaporation on glass substrates at 90 °C. The strong Kiessig fringes in the XRR pattern of neat films indicate very smooth organic layers, all differences in the reflection curves seem to be originated by the substrate surface and not the organic itself (Figure S4a). The reduced strength of the Kiessig fringes show the increase of surface roughness from compound* ***1*** *to* ***3****, that supports the GIXRD measurements (Figure 3b) of these blend layers, which show an increasing amount of crystallinity, respectively (Figure S6b). The XRR patterns give structural information summarized over the whole sample area (cm^2).*

REFERENCES

[1] (a) Crowe, B. F.; Nord, F. F. *J. Org. Chem.* **1950**, *15*, 1177; (b) King, W. J.; Nord, F. F. *J. Org. Chem.* **1948**, *13*, 635.

[2] Pham, C. V.; Macomber, R. S.; Mark Jr., H. B.; Zimmer, H. *J. Org. Chem.* **1984**, *49*, 5250.

[3] Deng, S.-R.; Wu, T.; Hu, G.-Q.; Li, D.; Zhou, Y.-H.; Li, Z.-Y. *Synth. Commun.* **2007**, *37*, 71.

[4] Fitzner, R.; Reinold, E.; Mishra, A.; Mena-Osteritz, E.; Ziehlke, H.; Körner, C.; Leo, K.; Riede, M.; Weil, M.; Tsaryova, O.; Weiß, A.; Uhrich, C.; Pfeiffer, M.; Bäuerle, P. *Adv. Funct. Mater.* **2011**, *21*, 897.

[5] Ziehlke, H.; Fitzner, R.; Koerner, C.; Gresser, R.; Reinold, E.; Baeuerle, P.; Leo, K.; Riede, M. *J. Phys. Chem. A* **2011**, *30*, 8437.

[6] Sheldrick, G.M. (**2008**). SADABS. University of Göttingen, Germany.

[7] Sheldrick, G. M. *Acta Cryst.* **2008**, *A64*, 112-122.

[8] Meyer, J.; Hamwi, S.; Schmale, S.; Winkler, T.; Johannes, H.-H.; Riedl, T.; Kowalsky, W. *J. Mater. Chem.*. **2009**, *19*, 702.

[9] Shrotriya, V.; Li, G.; Yao, Y.; Moriarty, T.; Emery, K.; Yang, Y. *Adv. Funct. Mater.* **2006**, *16*, 2016.

[10] Elschner, C.; Levin, A.; Wilde, L.; Grenzer, J.; Schroer, C.; Leo, K.; Riede, M. *J. Appl. Cryst.* **2011**, 44, 983.

CHAPTER VI

A-D-A-TYPE OLIGOTHIOPHENES FOR SMALL MOLECULE ORGANIC SOLAR CELLS: EXTENDING THE Π-SYSTEM BY INTRODUCTION OF RING-LOCKED DOUBLE BONDS

Roland Fitzner,[a,c] Elena Mena-Osteritz,[a] Karsten Walzer,[b] Martin Pfeiffer,[b] and Peter Bäuerle[a,*]

[a] Institute of Organic Chemistry II and Advanced Materials, University of Ulm, Albert-Einstein-Allee 11, 89081 Ulm, Germany

[b] Heliatek GmbH, Treidlerstrasse 3, 01139 Dresden, Germany

[c] Heliatek GmbH, Sedanstrasse 14, 89077 Ulm, Germany.

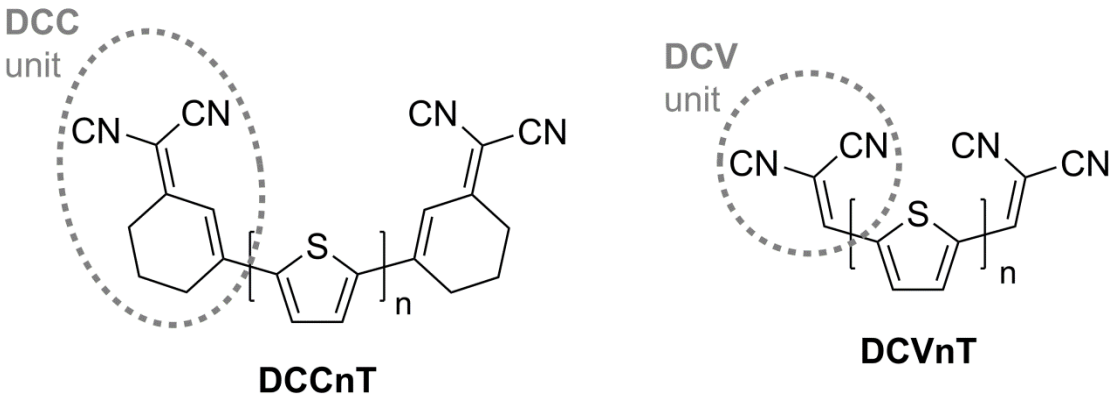

Reproduced and adapted with permission from

R. Fitzner *et al.*, *Advanced Functional Materials* **2015**, 25, 1845-1856.

Copyright © 2015 WILEY-VCH Verlag GmbH & Co. KGaA, Weinheim.

ABSTRACT

A series of novel acceptor-donor-acceptor oligothiophenes terminally substituted with the 1-(1,1-dicyanomethylene)-cyclohex-2-ene (DCC) acceptor has been synthesized. Structural, thermal, optoelectronic, and photovoltaic properties of the π-extended **DCC*n*Ts** (*n* = 1-4) are characterized and contrasted to the trends found for the series of parent dicyanovinyl (DCV)-substituted oligothiophenes **DCV*n*T**. The optoelectronic properties reveal the influence of the additional exocyclic, sterically fixed double bonds in trans-configuration in the novel **DCC*n*T** derivatives. A close correspondence for derivatives with equal number of double bonds, that is, **DCC*n*Ts** and **DCV(*n* + 1)Ts**, is identified. Despite having the same energy gap, the energy levels of the frontier orbitals, HOMO and LUMO, for the DCC - derivatives are raised and more destabilized due to the aromatization energy of a thiophene ring versus two exocyclic double bonds indicating improved donor and reduced acceptor strength. DCC-terthiophenes give good photovoltaic performance as donor materials in vacuum-processed solar cells (power conversion efficiencies ≤ 4.4%) clearly outperforming all comparable **DCV4T** derivatives.

1. INTRODUCTION

Over the recent years, research in organic solar cells (OSC) has attracted great attention fueled by the potential for a future largescale production of clean and inexpensive organic photovoltaic devices onto flexible substrates using continuous roll-to-roll processes. In OSCs, the interface between p- and n-type semiconducting organic materials is used to separate the strongly bound electron-hole pairs, formed upon photoexcitation, into free charge carriers. Besides the use of π-conjugated polymers as photoactive components, π-conjugated oligomers, often denoted as "small molecules," are gaining increasing popularity as they offer small batch-to-batch variations providing high reproducibility.[1-5] In addition to standard solution-processing, molecularly defined materials allow for solvent-free processing by vacuum evaporation techniques. Systematic structural optimization of the oligomer donor materials allowed for an increase in power conversion effi ciencies (PCE) to impressive values of close to 10% for single junction small molecule organic solar cells (SMOSC). Chen and co-workers investigated soluble oligothiophene-based acceptor-donor-acceptor (A-D-A)-type donor materials comprising central benzodithiophene units and could improve PCE to outstanding 9.95%.[1,6] The groups of Bazan and Heeger developed highly efficient D_1-A-D_2-A-D_1-type co-oligomers bearing a central dithienosilole unit leading to PCEs of up to 9% in solution-processed bulk heterojunction (BHJ) solar cells.[2,7] Very recently, Holmes and co-workers reported an efficiency of 7.9% for a vacuum-processed BHJ device using a triarylamine-benzothiadiazole-based D–A donor material,[8] which was introduced before by Wong and co-workers reaching PCEs of 6.8%.[9] Very recently, Cnops et al. published a vacuum-processed three layer device in a cascade architecture combining sexithiophene as donor and two subphthalocyanines as acceptors reaching a remarkable PCE of 8.4%.[10]

Our group explored the family of acceptor-donor-acceptor (A-D-A)-type oligothiophenes representing an efficient and well-investigated family of donor materials for vacuum-processed SMOSC. In particular, 2,2′-dicyanovinyl (DCV) as acceptor proofed to be ideal in order to achieve the optimal optoelectronic properties in the series of DCVnTs (Scheme 1). In the first very promising solar cell application, butyl-substituted quinquethiophene **DCV5T-Bu** was deployed in SMOSC devices yielding a PCE of 3.4%.[11] Meanwhile, this material class has been extensively explored by the synthesis and characterization of several series of **DCV*n*T** oligomers. For example, by variation of the oligothiophene chain length, important structure-property relationships have been derived correlating the number of thiophene units in the conjugated backbone [12] or the length of the alkyl side chains with optoelectronic properties and

photovoltaic performance.[13] A correlation between the packing of molecules in the solid state obtained from X-ray data and photovoltaic performance was established in a series of DCV-capped quaterthiophenes with systematic variation of the alkyl substituents identifying methyl-substituted **DCV4T-Me** as best-performing tetramer (PCE =3.8%).[14] The optimization of the positioning of methyl substituents along the conjugated oligothiophene backbone in a series of quinquethiophenes led to excellent PCE values of 8.3% in single junction and 9.7% in multi junction cells, measured for the centrally methylated derivative.[15] As the next step on the road to optimized A-D-A-type oligothiophene donor materials, we aspired to enlarge the conjugated π-system by introducing additional double bonds between the oligothiophene core and the electron-withdrawing DCV units. We endeavored to avoid structural cis/trans isomerism and to ensure thermal stability by integrating them into a cyclohexene ring.[16] In this contribution, we report on a novel series of A-D-A-type oligothiophenes bearing 1-(1,1-dicyanomethylene)-cyclohex-2-ene (DCC) units at both α-termini (**DCC*n*T**). Structural, thermal, optoelectronic, and photovoltaic properties were characterized and contrasted to the trends found for the series of dicyanovinyl-substituted oligothiophenes **DCV*n*T**, reported earlier (Scheme 1).

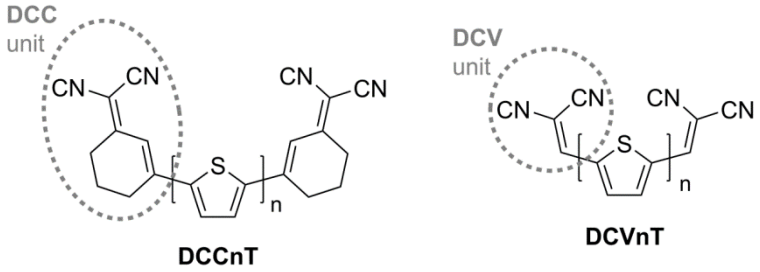

Scheme 1. *Molecular structures of DCC- and DCV-capped oligothiophene series* ***DCCnT*** *and* ***DCVnT****.*

2. Results and Discussion

2.1 Synthesis

For the synthesis of the shorter **DCCnT** derivatives, bromocyclohexenone **3** was reacted with bisstannylated thiophene **1** or bithiopene **2** in Pd-catalyzed Stille-type cross-coupling reactions to afford diketo derivatives **4** and **5**. Subsequent Knoevenagel condensation with malonitrile using *β*-alanine as the catalyst afforded target oligomers **DCC1T** and **DCC2T** in good yields (Scheme 2). The longer less soluble **DCC3T** and **DCC4T** oligomers were synthesized by Stille-

type cross-coupling reactions of DCC-substituted bromothiophene **9** with stannyl derivatives **1**, **2**, or 3,4-dimethylthiophene **10** as central building blocks yielding oligomers **DCC3T**, **DCC4T**, or **DCC3T-Me**, respectively. In order to obtain building block **9,** 2,5-dibromothiophene was monolithiated with *n*-butyl lithium and quenched with methoxycyclohexenone **7** to yield ketone **8**. Knoevenagel condensation with malonitrile provided DCC-substituted bromothiophene **9** as terminal building block.

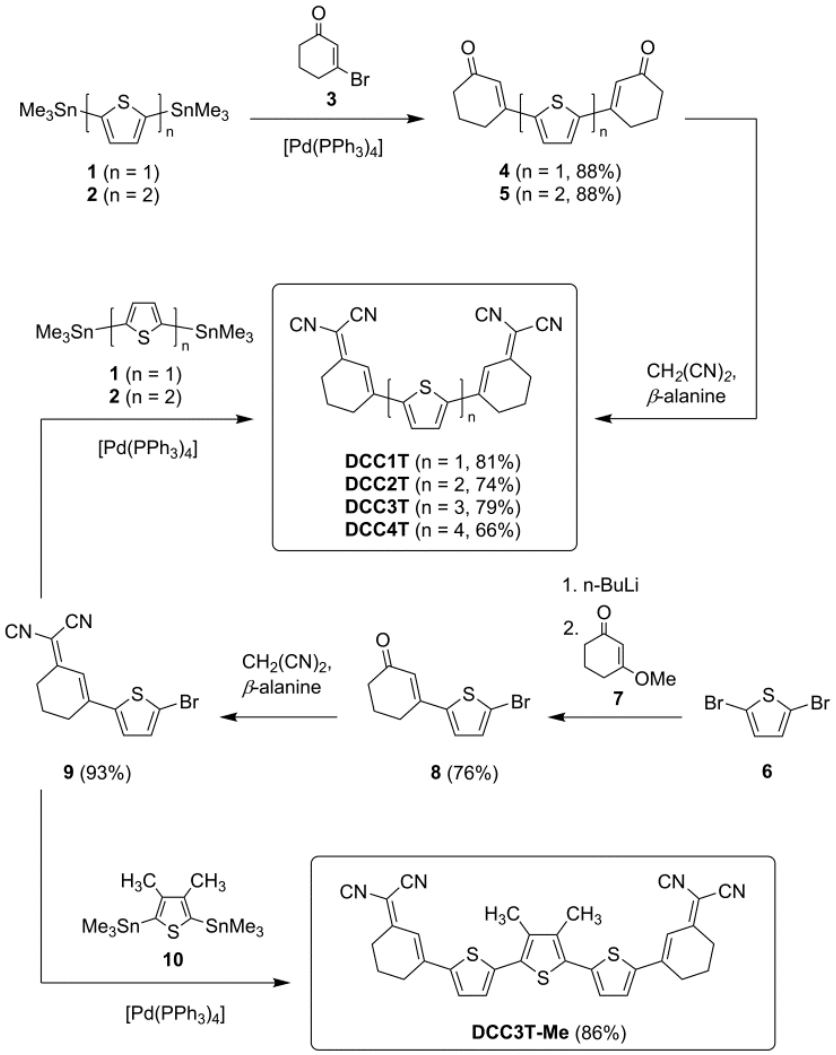

Scheme 2. *Synthesis of* ***DCCnT*** *oligomers.*

2.2 Thermal Properties and Solubility

Differential scanning calorimetry (DSC) was used to investigate the thermal properties of all **DCCnTs**. The decomposition onset temperatures (T_d) estimated from the onset of the exothermic signals in the DSC traces (Figure 1) are compiled in Table 1. Thermal degradation of the **DCCnTs** occured between 344 °C for **DCC1T** and 375 °C for **DCC3T-Me**. This indicates a

high, but somewhat reduced thermal stability in comparison to the alkyl free **DCVnTs**, which exhibited decomposition onset temperatures of about 400 °C.[12c] The **DCCnT** derivatives up to the trimers sublimed at temperatures between 250 and 280 °C ($p \approx 10^{-6}$ mbar) yielding crystalline material of high purity in almost quantitative yield. The sublimation of **DCC4T** occurred at significantly higher temperatures around the melting point and led to poor yields due to material decomposition.

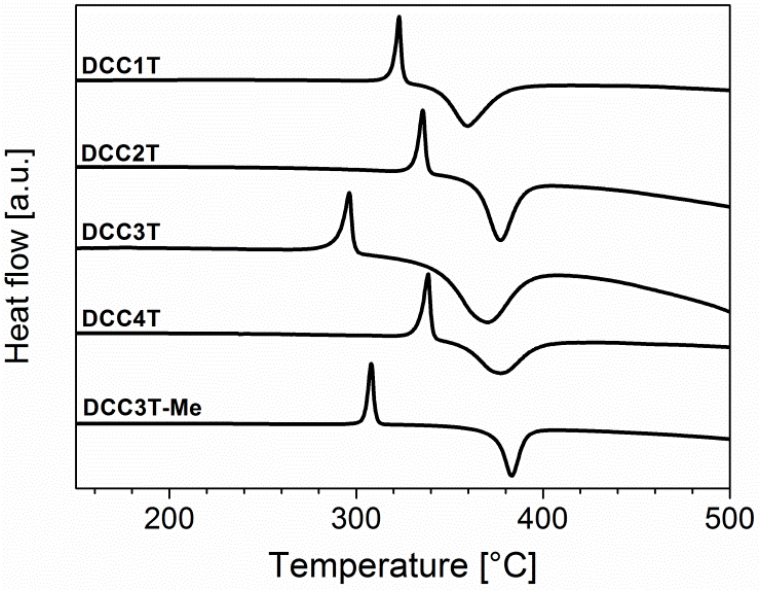

Figure 1. *DSC traces of* ***DCCnTs*** *measured under argon flow at a heating rate of 10 °C/min.*

Melting temperatures (T_m) of the **DCCnT**s (**Table 1**) were determined from the onset of the endothermic signals in the DSC traces. All **DCCnT** derivatives exhibited high melting points between 290 and 333 °C which is an important requirement for efficient sublimation of the materials from the solid phase. In order to compare and to illustrate trends in the melting behavior of both oligothiophene series, in **Figure 2** the melting temperatures of the **DCCnTs** and **DCVnT**s are plotted vs the number of thiophene rings in the respective oligomer.

Comparing oligomers with identical oligothiophene cores, the DCC-substituted derivatives melted at higher temperatures than their DCV-capped analogues. This indicates that the two additional cyclohexene rings in the molecular structure of the **DCCnTs**, which increase the molecular weight by 132 g mol^{-1} compared to the **DCVnTs**, induce additional intermolecular interactions. The differences in melting points between **DCCnT**s and **DCVnTs** (ΔT_m in Table 1) diminished with increasing oligomer length from ΔT_m = 47 °C for the **1T** to 13 °C for the **4T** derivatives. As the number of thiophene units increases, the oligothiophene core dominates the molecular structure and the intermolecular forces. As we have shown previously for the **DCVnT** series, the **DCCnT** oligomers as well exhibited an odd-even effect of the melting points with respect to the

number of thiophene units. Even-numbered **DCVnTs** and **DCCnTs** melt at significantly higher temperatures compared to their odd-numbered homologues. This trend may originate from a variance in molecular dipoles caused by differences in molecular symmetry between odd- and even-numbered oligomers.[10] The methylated oligomers **DCC3T-Me**, **DCV3T-Me**, and **DCV5T-Me** exhibited higher melting temperatures in comparison to the corresponding alkyl free derivatives which indicates additional intermolecular interactions induced by the methyl groups. Compared to their non-alkylated analogues, **DCC3T-Me** and **DCV5T-Me** exhibited similar increases in melting temperature (ΔT_m = 15 °C and 14 °C, respectively), while **DCV3T-Me** showed a larger enhancement in melting point (ΔT_m = 38 °C).

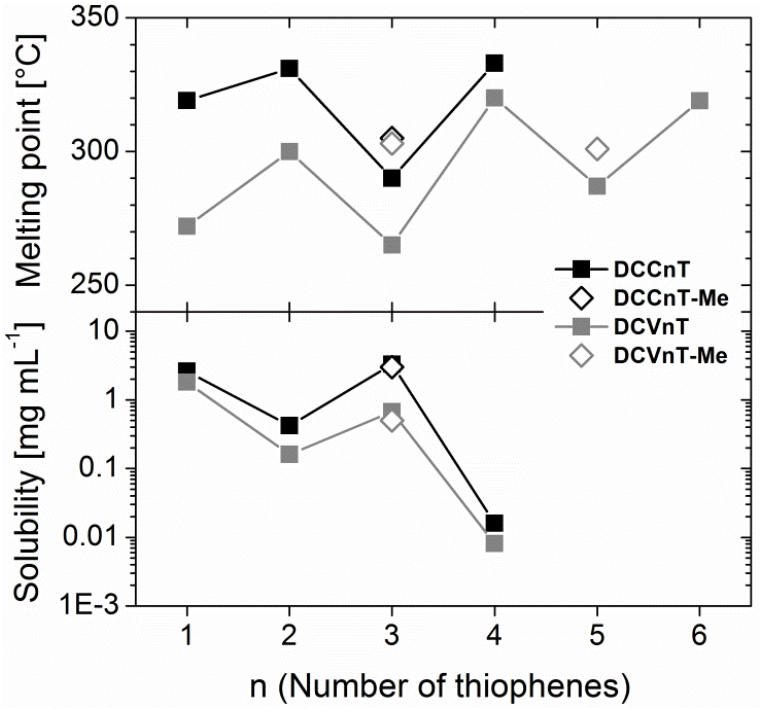

Figure 2. *Melting points (top) and maximum solubilities in dichloromethane at room temperature (bottom) of* ***DCCnTs*** *and* ***DCVnTs*** *versus the number of thiophene units in the oligothiophene backbone.*

Maximum solubilities of **DCCnTs** and **DCVnTs** in dichloromethane were determined up to the tetramers. The corresponding values are compiled in **Table 1** and plotted vs the number of thiophene units in the oligothiophene backbone (**Figure 2**). Despite having higher melting points, the **DCCnTs** displayed enhanced solubility in dichloromethane compared to their DCV-substituted counterparts. Compared to the DCV group, this might be a result of enhanced flexibility and greater rotational freedom of the DCC acceptor moiety around the bond to the oligothiophene core. In both oligomer series, maximum solubilities showed an odd-even effect with respect to the number of thiophene units, where oligomers with an even number of

thiophenes are less soluble than those containing an odd number. This trend is the reverse of that found for the melting point temperatures. Methylated derivatives **DCC3T-Me** and **DCV-3T-Me** were less soluble in dichloromethane compared to the corresponding alkyl free derivatives which is in accordance with the trend observed in melting points. Compared to the extremely insoluble alkyl free or methylated **DCVnTs**, the solubilizing effect of the DCC acceptor moieties might be still not sufficient to enable a reliable fabrication of organic solar cells by solution-processing.

Table 1. *Thermal properties and maximum solubilities of **DCCnT**s and **DCVnT**s in dichloromethane.*

Oligomer	T_m [°C]	T_d (DSC) [°C]	Solubility [mg/mL]	Oligomer	T_m [°C]	Solubility [mg/mL]	ΔT_m [°C]
DCC1T	319	343	2.6	**DCV1T**	272	1.8	47
DCC2T	331	362	0.42	**DCV2T**	300	0.16	31
DCC3T	290	340	3.3	**DCV3T**	265	0.67	25
DCC3T-Me	305	375	3.0	**DCV3T-Me**	303	0.50	2
DCC4T	333	352	$1.6 \cdot 10^{-2}$	**DCV4T**	320	$8.1 \cdot 10^{-3}$	13

2.3 X-RAY STRUCTURE ANALYSIS

Single crystals of **DCC3T-Me** were obtained by vacuum gradient sublimation. X-ray structure analysis provided valuable information about molecular geometry and packing and revealed notable similarities to the crystal structure of centrally methylated DCV-capped quinquethiophene **DCV5T-Me**, reported earlier.[15a] The molecular structures of both oligomers will be compared, followed by an analysis of the crystal packing and intermolecular interactions. The crystals of **DCC3T-Me** and **DCV5T-Me** belong to the monoclinic space group C2/c with two molecules in the unit cell. The molecular structures of both oligomers display C_2 symmetry with the thiophene rings in an all-*anti*-conformation and the DCC or DCV units adopting *syn*-conformations with respect to the sulfur atoms of the terminal thiophene rings (**Figure 3**). The terminal double bonds of the acceptor units take very similar orientations with respect to the long molecular axis forming angles of 118 and 114° for **DCC3T-Me** and **DCV5T-Me**, respectively. Both oligomers displayed almost planar oligothiophene backbones, whereas the inter-ring dihedral angles are particularly small for **DCC3T-Me** (0.7°) compared to **DCV5T-Me** (5°, 7°). The DCC cyclohexene rings in the **DCC3T-Me** structure adopt half-chair conformation, in which the ring double bond is nearly coplanar with the adjacent thiophene ring (2.4°). In both structures, the dicyanomethylene moieties are significantly twisted out of the oligothiophene plane by 24° and

8° for **DCC3T-Me** and **DCV5T-Me**, respectively. This twist appears to be an effect of the particular molecular packing behavior observed for both oligomers, *vide infra*.

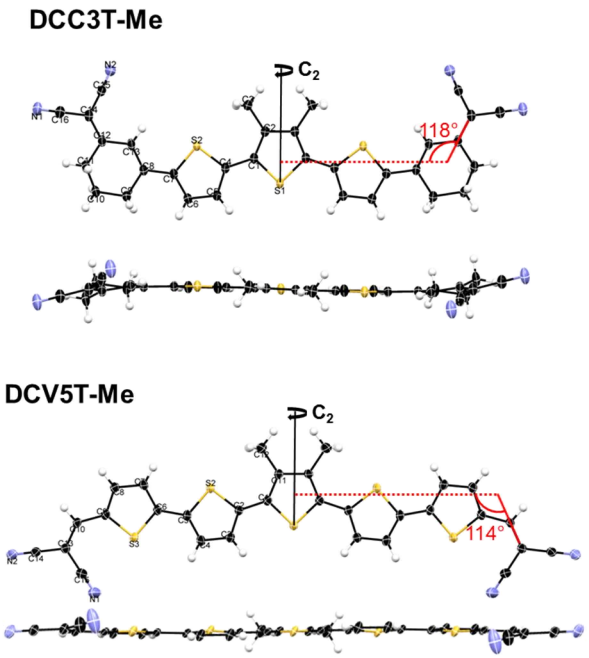

Figure 3. *ORTEP diagrams (50% ellipsoids) of* ***DCC3T-Me*** *(top) and* ***DCV5T-Me*** *(bottom).*

In Figure 4 the crystal packing of **DCC3T-Me** is presented and compared to the very similar molecular arrangement observed for **DCV5T-Me**.[12] A common feature is the antiparallel alignment of the molecules on their long molecular axes, giving rise to the formation of ribbon-like structures (Figure 4a). This arrangement is favored by electrostatic CH···NC interactions between the terminal acceptor units of neighboring molecules (blue lines in Figure 4a and Table 2). In both crystal structures, adjacent molecular ribbons are offset from co-planarity by half the π-π-stacking distance (see side views in Figure 4b). The ribbons stabilize by C*H*···*N*C quasi hydrogen-bonding interactions between vinylic cyclohexenyl hydrogens and cyano nitrogen atoms (red lines in Figure 4a, top). The **DCV5T-Me** crystal structure contains similar interactions between cyano nitrogen atoms and thienyl hydrogen atoms (red lines in Figure 4a, bottom). Figure 4c depicts the molecular packing in the π-π-stacking direction. Both oligomers form slipped π-π-stack assemblies with slip angles of 41° or 57°, for **DCC3T-Me** and **DCV5T-Me**, respectively. The π-π-stacking molecular distances of 3.46 Å in **DCC3T-Me** are identical to the value obtained for **DCV5T-Me** (3.46 Å). Thus, the introduction of the DCC rings in the **DCC3T-Me** structure does not impair efficient π-π-interactions. Besides that, C*H*···π intermolecular interactions involving methyl- or cyclohexene hydrogens appear in both crystal structures (green and orange lines in Figure 4c).

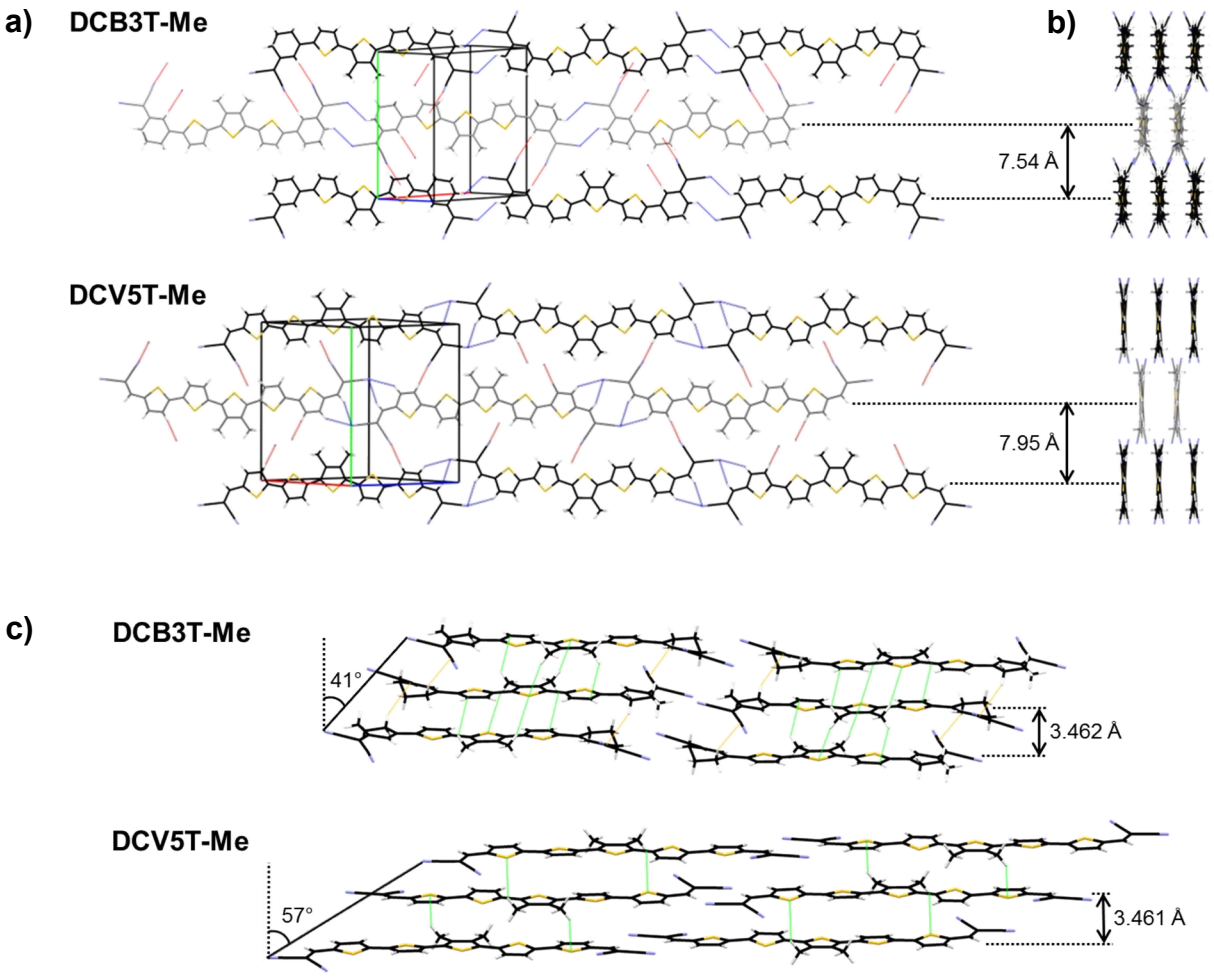

Figure 4. *View of the crystal packing of* ***DCC3T-Me*** *and* ***DCV5T-Me*** *in (a) the molecular plane, (b) end view of the ribbon-like structures, and (c) view perpendicular to the molecular plane showing the π-π-stacking of the molecules.*

Table 2. *Distances corresponding to intermolecular close CH…NC contacts in the crystal structures of* ***DCC3T-Me*** *and* ***DCV5T-Me****.*

Oligomer	Close Contacts (color code in Figure)	d [Å]	d - d_{VDW} [Å]
DCC3T-Me	N1…H11A (blue)	2.673	-0.077
	N2…H13 (red)	2.598	-0.152
DCV5T-Me	N2…H10 (blue)	2.553	-0.197
	N2…H8 (blue)	2.709	-0.041
	N1…H7 (red)	2.589	-0.161

As a measure for the overall packing density, the Kitaigorodskii packing coefficients C_K were determined for both crystal structures by dividing the occupied molecular van-der-Waals volume by the total volume of the unit cell. Comparing **DCC3T-Me** and **DCV5T-Me**, the DCC-substituted oligomer exhibited a somewhat larger coefficient (0.709) than the DCV-capped

derivative (0.674) indicating more efficient 3D packing. In consideration of identical π-π-stacking distances, this finding supports the closer molecular packing observed between the ribbons in the **DCC3T-Me** crystal structure (7.54 Å vs. 7.95 Å for **DCV5T-Me,** Figure 4a).

Figure 5 highlights the alignment of adjacent DCC units in the **DCC3T-Me** crystal structure. Neighboring DCC groups form a linear zipper-like network, which is brought about by the two types of centrosymmetric interaction motifs (blue and red lines) described above. The well polarizable vinyl-hydrogens of the DCC moiety stabilize the arrangement by non-classical hydrogen bond interactions.

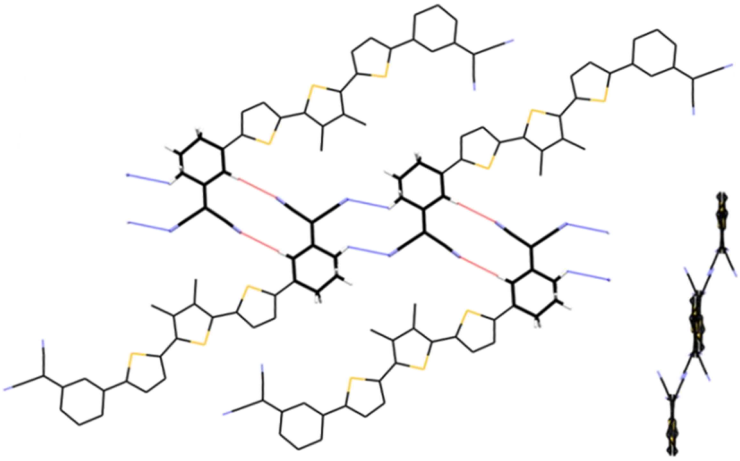

Figure 5. *Intermolecular CN···HC close contacts between adjacent DCC groups in the crystal structure* ***DCC3T-Me*** *(side-view along the molecular axis in inset).*

2.4 Optoelectronic Properties

Optical absorption spectra of the **DCCnT** series determined in dichloromethane solution are presented in comparison to the **DCVnT** spectra in Figure 6. The corresponding values are compiled in Table 3. All **DCCnTs** showed broad absorption profiles in the visible region. The absorption bands exhibited bathochromic shifts and increasing molar absorptivity with growing number of thiophene units indicating efficient conjugation throughout the π-system.

The maximum absorption wavelengths λ_{max}^{abs} and the corresponding extinction coefficients ε_{max} of the **DCCnTs** coincide well with the values determined for the **DCVnT** compounds comprising one additional thiophene unit, respectively. The bathochromic shift caused by the two additional cyclohexene double bonds in the **DCCnTs** is therefore equivalent to adding one extra thiophene unit in the **DCVnT** series. **DCVnT** spectra showed increasing vibronic structure with decreasing number of thiophene units. **DCCnT** π-π* absorption bands, in contrast, are structureless even for the shortest oligomer **DCC1T**. Compared to the DCV group, this may be attributed

to a lower energy barrier of rotation of the DCC unit around the bond to the oligothiophene backbone. The **DCVnTs** exhibit attractive intramolecular interactions between the sulfur atoms of the terminal thiophene rings and a DCV cyano group hindering rotation of the acceptor groups. Owing to the reduced conjugation of the oligothiophene core in solution, methylated **DCC3T-Me** displayed a slightly blue-shifted ($\Delta\lambda_{max}$ = 10 nm) and broadened absorption band with reduced molecular absorptivity compared to non-alkylated **DCC-3T.** This is consistent with the behavior of alkyl substituted **DCVnT** derivatives.

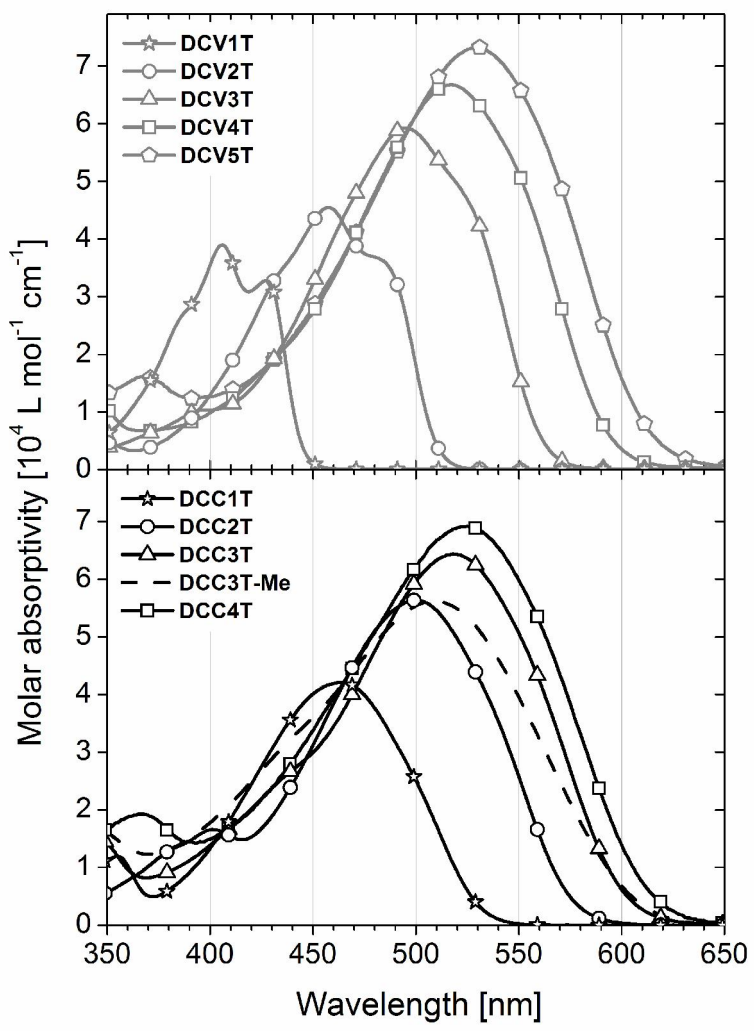

Figure 6. *Absorption spectra of* ***DCCnT*** *(bottom) and* ***DCVnT*** *oligomers (top) measured in dichloromethane at room temperature.*

Emission spectra of the **DCCnTs** and **DCVnTs** measured in dichloromethane solution are depicted in **Figure 7**. The emission maxima shifted bathochromically upon elongation of the π-system (Table 3). Unlike in the absorption spectra, the emission bands of the shorter **DCCnTs** up to **DCC3T** showed vibronic structure which indicates a higher degree of structural rigidity

and planarity of the molecules in the electronically excited state compared to the ground state. Compared to alkyl-free **DCC3T**, the emission band of methyl substituted **DCC3T-Me** is less structured which may be due to increased rotational disorder in the oligothiophene backbone. Within the **DCVnT** series, a gradual increase in Stokes shift with increasing number of thiophene units from 320 cm^{-1} for **DCV1T** to 1803 cm^{-1} **DCV6T** was determined. However, all non-alkylated **DCC-nTs** displayed similar and significant Stokes shifts between 1282 cm^{-1} for **DCC2T** and 1547 cm^{-1} for **DCC4T** suggesting substantial differences in the electron distribution and molecular dipole moment between the ground state and excited state. Alkylated **DCC3T-Me** displayed the largest Stokes shift of 1883 cm^{-1} within the **DCCnT** series.

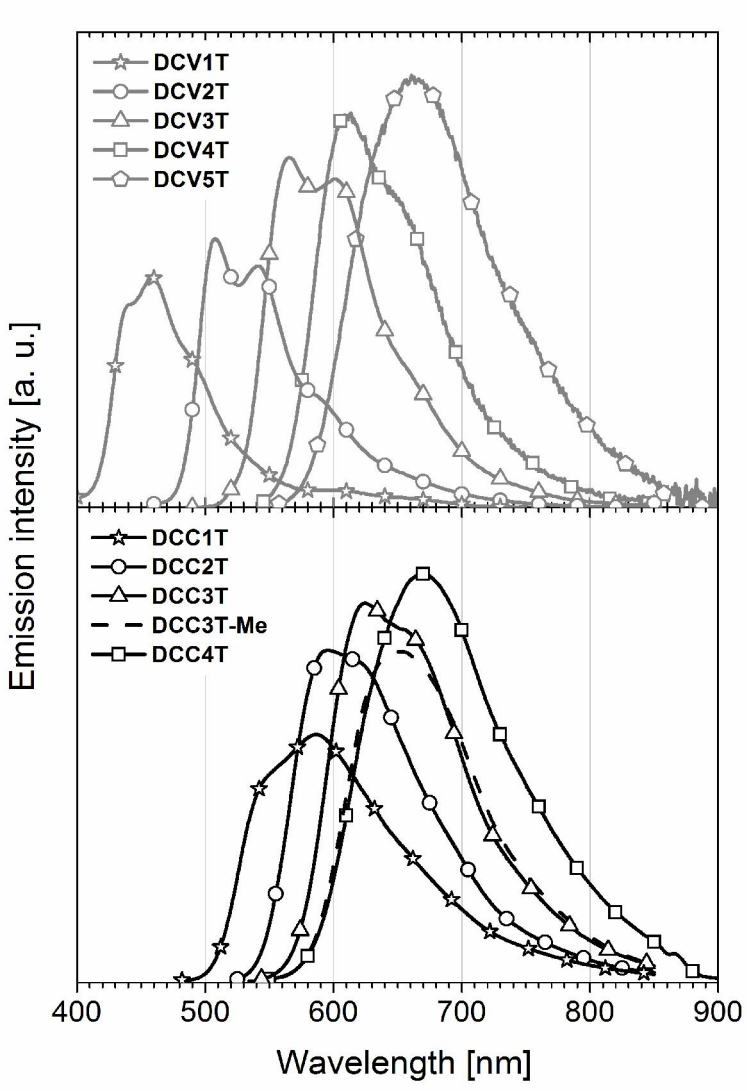

Figure 7. *Emission spectra of* ***DCCnT*** *(bottom) and* ***DCVnT*** *oligomers (top) measured in dichloromethane at room temperature.*

Figure 8 shows absorption and emission spectra of **DCC3T** and **DCC3T-Me** in thin films of equal thickness fabricated by vacuum-deposition. Compared to solution spectra, absorption and

emission bands are red-shifted and significantly broadened in thin films for both oligomers indicating planarization and favorable ordering of the molecules in the bulk. Absorption profiles of the terthiophene derivatives are very similar with maximum optical densities of 0.46 and 0.45 at 544 and 547 nm for **DCC3T** and **DCC3T-Me**, respectively. Compared to **DCC3T** (λ_{max}^{em} = 736 nm), methylated **DCC3T-Me** showed a slightly increased Stokes shift in the thin film with an emission maximum of 766 nm. The optical gaps of the **DCCnT** series determined from the onset of absorption in solution spectra diminished from 2.33 eV for **DCC1T** to 2.03 eV for **DCC4T**. In thin films, the optical gaps of the terthiophene derivatives **DCC3T** and **DCC3T-Me** (E_g^{opt} = 1.79 eV) are reduced compared to the solution by 0.26 and 0.28 eV, respectively, which is comparable to the shifts determined for the **DCVnT** derivatives (ΔE_g = 0.33-0.35 eV).[10]

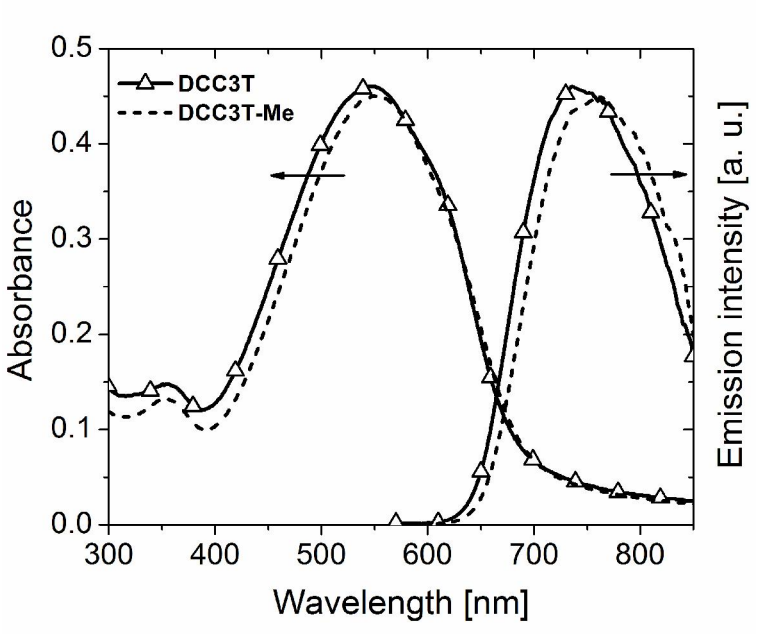

Figure 8. *Absorbance and emission spectra of **DCC3T** and **DCC3T-Me** in 30 nm thick films fabricated by vacuum-deposition onto quartz substrates.*

Cyclic voltammograms of the **DCCnT** oligomers were determined in 0.1 molar solutions of tetrabutyl ammonium hexafluorophosphate ($TBAPF_6$) in dichloromethane and are displayed in Figure 9a. The corresponding data are compiled in Table 3. **DCC1T** and **DCC2T** showed a single reversible oxidation wave within the accessible electrochemical window indicating the formation of stable radical cations. For the longer oligomers **DCC3T**, **DCC3T-Me**, and **DCC4T** two reversible one-electron oxidation processes were detected corresponding to the generation of stable radical cations and dications. The first oxidation potential is gradually shifted to lower values with the extension of the π-conjugated system from **DCC1T** (E_{Ox1} = 1.24 V) to **DCC4T** (E_{Ox1} = 0.63 V) concomitant with the increased delocalization of the radical

cations. All non-alkylated **DCCnTs** displayed reversible reduction signals, which are attributed to the generation of stable radical anions localized on each acceptor group.

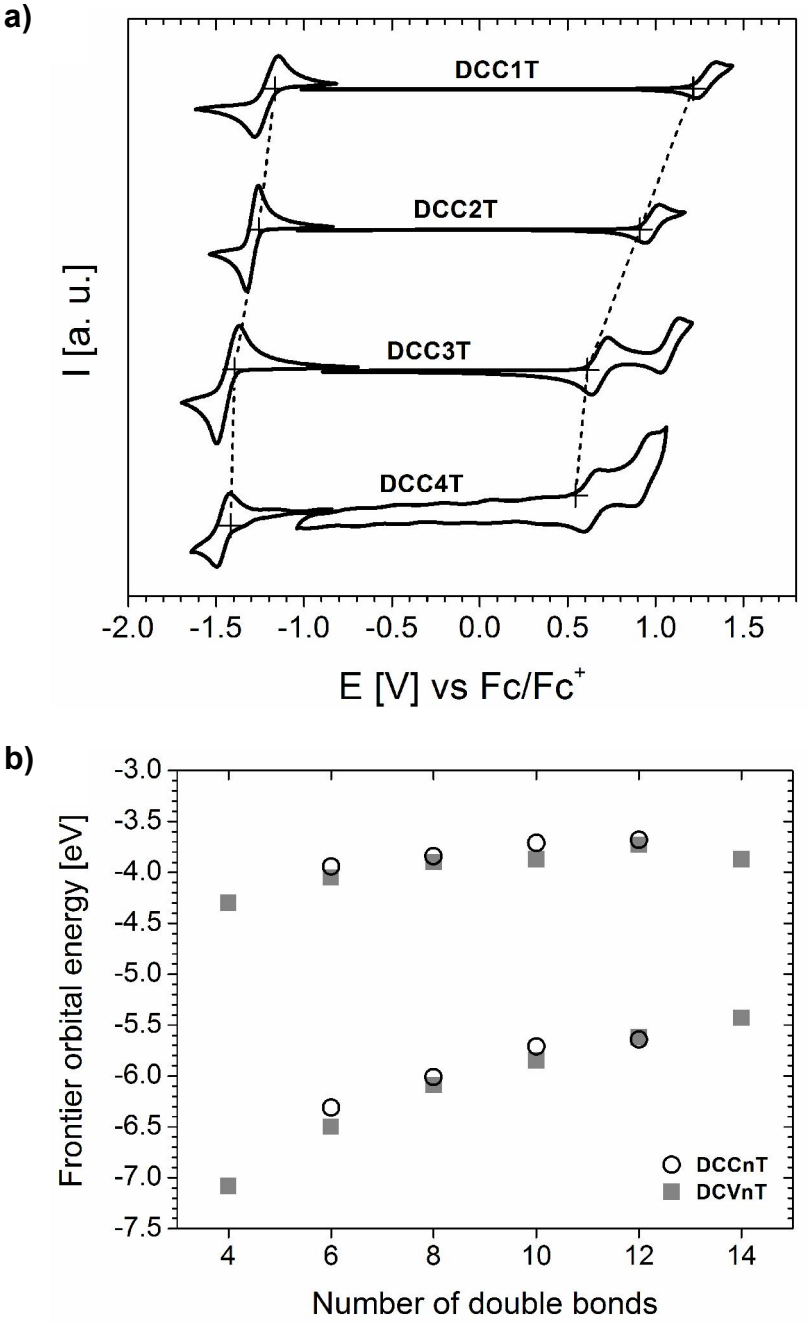

Figure 9. *(a) Cyclic voltammograms of the* ***DCCnT*** *oligomer series measured in dichloromethane and TBAPF$_6$ (0.1 M) as electrolyte, scan rates were 100 mV s^{-1} and potentials are given versus Fc/Fc$^+$. (b) Frontier orbital energies of* ***DCCnTs*** *and* ***DCVnTs*** *derived from electrochemical data versus the number of double bonds in the oligomers.*

In comparison to the **DCVnT** oligomers, which exhibited only quasi-reversible reduction waves, the DCC acceptor moiety further stabilizes radical anionic species. In contrast to the effect seen in the oxidation, the reduction potentials are less affected by the enlargement of the π-system

and $E°_{Red}$ decreased only from -1.21 V for **DCC1T** to -1.46 V for **DCC4T** because the negative charges are rather localized on the electron-withdrawing DCC acceptor moieties. HOMO and LUMO frontier orbital energies were calculated from the onset values of the first oxidation and reduction waves setting the ferrocene HOMO energy to -5.1 eV vs vacuum (Table 3). As a result of the increase in HOMO energies with growing number of thiophene units, the electrochemical gaps decreased from 2.37 eV for **DCC1T** to 1.96 eV for **DCC4T**. In **Figure 9b**, frontier orbital energies of **DCCnTs** and **DCVnTs** are plotted vs the number of double bonds in the oligomers. Comparing both oligomer series, derivatives with equal numbers of double bonds showed very similar HOMO/LUMO energies confirming the trend seen already for the maximum absorption wavelengths λ_{max}^{abs}. Regarding the potential of the oligomers as donor materials in organic solar cells, the LUMO energy levels of **DCC3T** (-3.71 eV), **DCC3T-Me** (-3.64 eV), and **DCC4T** (-3.68 eV) should be sufficiently high to provide a driving force for efficient electron transfer to the LUMO of the acceptor C_{60} (≈ -4.1 eV).

Table 3. *Optoelectronic data of the **DCCnT** oligomers.*

Oligomer	λ_{max}^{abs} [nm]	ε_{max} [L mol^{-1}	E_g^{opt} [eV] [a]	λ_{max}^{em} [nm]	Stokes shift [cm^{-1}]	E^0_{Ox} [V]	E^0_{Red} [V]	E_{Homo} [eV] [c]	E_{LUMO} [eV] [c]	E_g^{CV} [eV]
DCC1T	463	42100	2.33	587 (547)	1517	1.24	-1.21	-6.31	-3.94	2.37
DCC2T	500	56400	2.15	595 (622)	1282	0.98	-1.29	-6.01	-3.84	2.17
DCC3T	519	64400	2.07	624 (660)	1518	0.68, 1.08	-1.43	-5.71	-3.71	2.00
DCC3T-Me	509	56200	2.05	651	1883	0.63, 1.05	-1.47	-5.69	-3.64	2.05
DCC4T	525	69300	2.03	669	1547	0.63, 0.93	-1.46	-5.64	-3.68	1.96

[a] Estimated using the onset of absorption in solution spectra. [b] Calculated as difference between the 0–0 vibronic transitions of absorption and emission spectra, determined by mathematical Gaussian deconvolution. [c] Calculated from onset values of the first oxidation and reduction waves setting the ferrocene HOMO energy to -5.1 eV vs vacuum.

Density functional theory (DFT) calculations [m062x(6-31g+(d))] have been performed on both series of A-D-A oligothiophenes. Figure 10 displays the electronic distribution of the frontier orbitals of **DCC3T** and **DCV4T** as examples, which comprise the same number of double bonds. The HOMO of both derivatives shows a delocalization of the electron density over the donor part up to the vinylic carbon adjacent to the terminal dicyanomethylene groups (labeled by arrows). The delocalization of the LUMO expands over the entire **DCC3T** and **DCV4T** π-conjugated path. The LUMO+1 showed a pronounced shift of the electronic density to the acceptor parts on both derivatives. This virtual energetically high lying orbital can be stabilized

experimentally by the presence of solvent and therefore can be responsible for the charge transfer character of the electronic transition.

The analysis of the calculated molecular orbital energies (Table S5) supports as well the trends found in the electrochemical studies. In Figure 11 the experimentally determined frontier orbital energies are displayed elucidating the effect of the extrinsic double bonds in **DCC3T**: Compared to the DCV-derivatives **DCV3T** and **DCV4T**, the HOMO and the LUMO are lifted up in energy. However, for the derivatives with equal numbers of double bonds (**DCC3T** vs **DCV4T**), the band gap comes out nearly equal (2.0 eV and 1.98 eV), and both are as expected significantly smaller than this of **DCV3T** (2.19 eV), which corresponds to the findings in optical spectroscopy. The destabilization of the HOMO and LUMO energies in **DCC3T** denotes an improved donor and reduced acceptor strength related to the DCV-derivatives. By keeping the acceptor groups unaffected, the lengthening of the π-conjugated system by two double bonds (**DCV3T** ð **DCC3T**) causes a significant raising of the HOMO energy level by 0.38 eV compared to the effect of the lengthening by one thiophene unit (**DCV3T** ð **DCV4T**), which amounts to 0.24 eV. We can explain this difference (0.14 eV) by the more effective aromatic stabilization in a thiophene ring with regard to two exocyclic double bonds. In contrast to the nearly unaffected LUMO energy levels in the DCV-series, the LUMO of **DCC3T** is raised by 0.16–0.19 eV, which can be ascribed as well to the loss of aromatization energy.

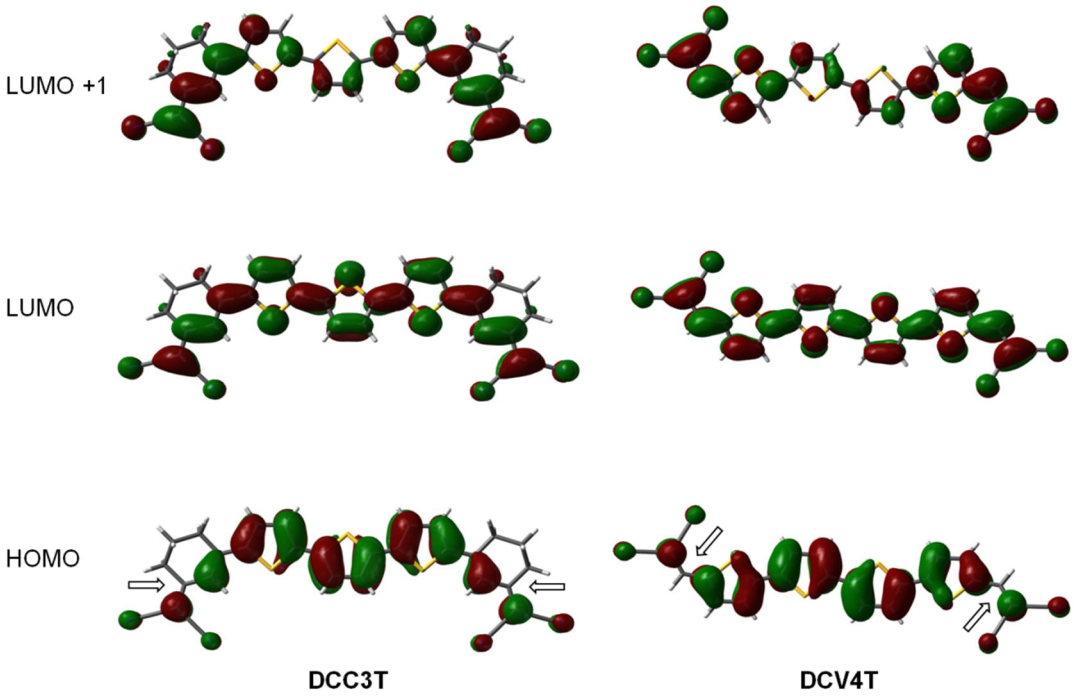

Figure 10. *Representative electron density distribution of the frontier orbitals of* ***DCC3T*** *and* ***DCV4T*** *obtained by DFT-calculation (carbons in black, sulphurs in yellow, and hydrogens in white).*

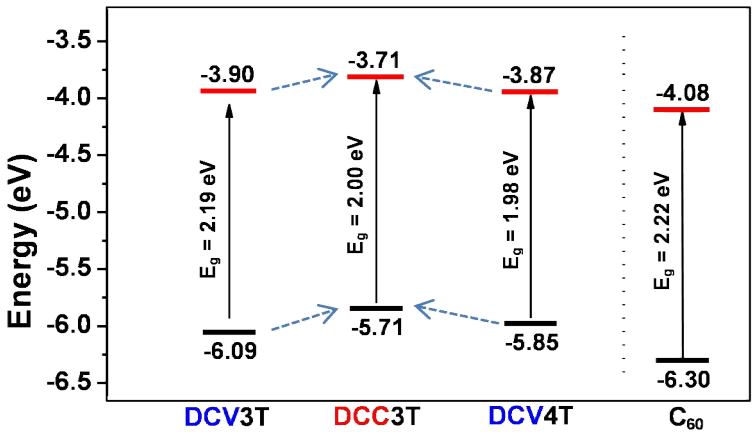

***Figure 11**. Representation of HOMO/LUMO energies of **DCC3T** in comparison to **DCV3T** and **DCV4T** and to C_{60} derived from electrochemical data. The HOMO/LUMO energy levels were determined from the onset of the oxidation and reduction waves (vide supra). The energy values of C_{60} are taken from the literature.*[17]

2.5 Photovoltaic Properties

To evaluate the photovoltaic properties of **DCC3T** and **DCC3T-Me** as donor in combination with C_{60} as acceptor, planar heterojunction (PHJ) organic solar cells have been fabricated by thermal vacuum deposition. For both devices, the following layer sequence was employed: 15 nm C_{60} evaporated on ITO-coated glass, 6 nm donor material, 10 nm of undoped 9,9-bis{4-[di-(p-biphenyl)aminophenyl]}fluorene (BPAPF), followed by 45 nm BPAPF p-doped with NDP9 as hole transport layer (HTL), 1 nm NDP9, and 100 nm aluminum as top electrode. Figure 12 displays the *J-V* characteristics (Figure 12a) and the external quantum efficiency (EQE) spectra (Figure 12b) in comparison to the absorbance spectra of the donors in vacuum-deposited neat films (Figure 12c). The corresponding device parameters are summarized in Table 4. PHJ cells of both, **DCC3T** and **DCC3T-Me**, showed excellent open circuit voltages (V_{OC}) of 1.00 V for **DCC3T** and an increased value of 1.05 V for **DCC3T-Me** which can be attributed to the low lying HOMO energies of the donor oligomers. Similar short circuit current densities (J_{SC}) of 5.3 and 5.0 mA cm^{-2} were determined for the **DCC3T** and **DCC3T-Me** devices, respectively. This is in accordance with very similar EQE spectra measured for both materials, which correlate well with thin film absorption profiles. The **DCC3T-Me** device showed an improved saturation in current density of 1.08, defined as $J(-1V)/J_{SC}$, and a considerably increased fill factor (FF) of 65% compared to values of 1.11 and 56%, respectively, for **DCC3T** devices. In total, the **DCC3T-Me** PHJ device yielded PCE of 3.4% outperforming the **DCC3T** cell with a PCE of 3.0%.

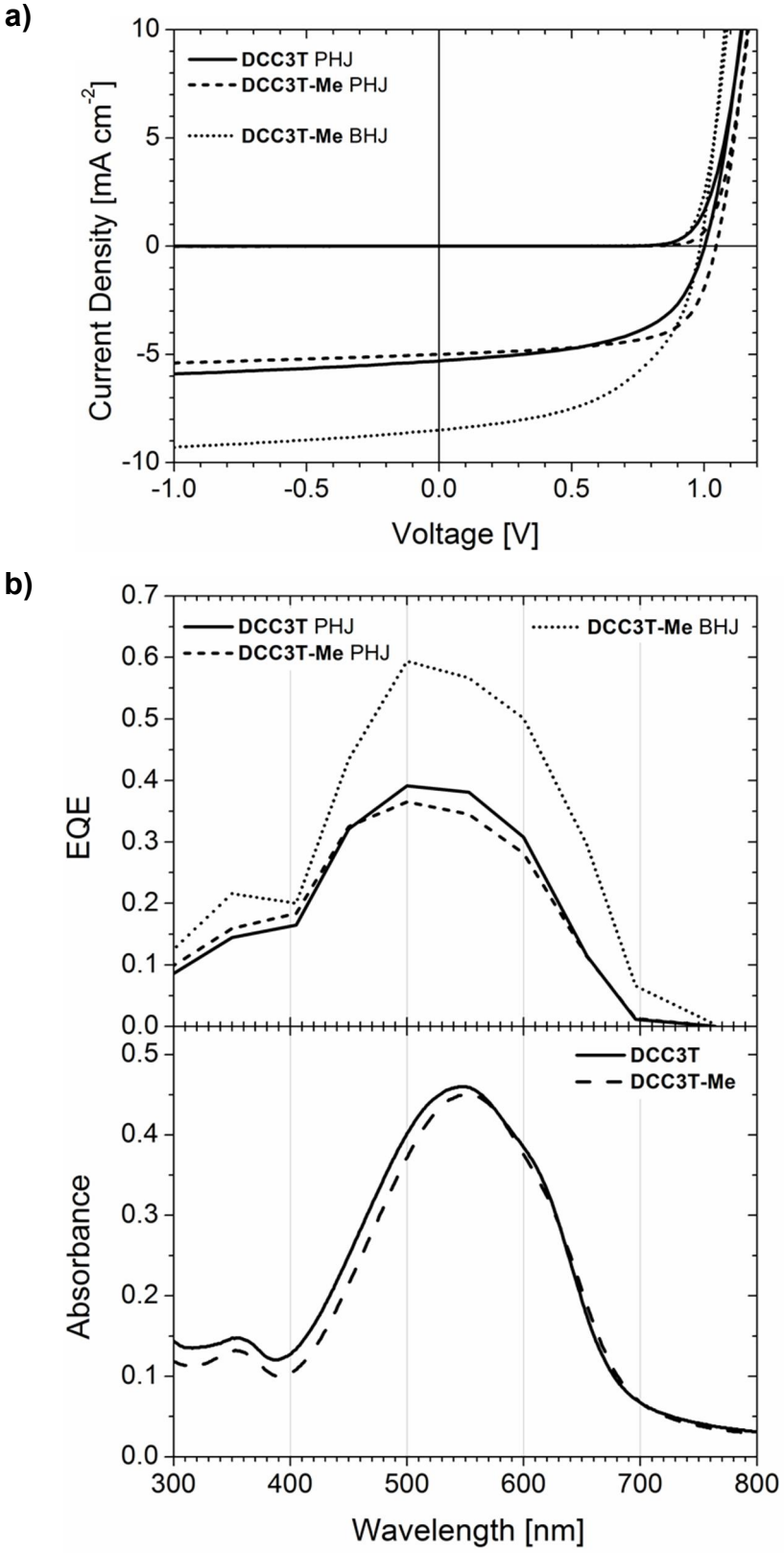

Figure 12. *(a) J-V characteristics of PHJ and BHJ solar cells containing* ***DCC3T***, ***DCC3T-Me***, *or* ***DCV4T-Me*** *as donor material and (b) corresponding external quantum efficiency spectra (top) compared to absorbance spectra (bottom) of thin films (30 nm) fabricated by vacuum-deposition onto quartz substrates.*

We have as well seen this trend for methylated A-D-A quinquethiophenes, which gave an improved performance compared to all other substituted derivatives coming from special intermolecular interactions and thus optimal packing of the oligomers in the solid state.[15a] If we compare these results with PHJ solar cells made from **DCV4T**, which comprises the same number of double bonds and conjugation length as the novel **DCC3T**-derivatives, the DCC-terthiophenes clearly surpass the quaterthiophene **DCV4T** in all photovoltaic parameters, which showed a PCE of only 1.2% under comparable conditions (Table 4). At that point it is noteworthy, that typically terthiophenes such as **DCV3T** and C_{60} did not lead to an efficient exciton separation into charge carrier pairs at the interface, because of the low HOMO offset between the two materials which leads to poor solar cell performance.[12a]

DCC3T-Me as the best performing A-D-A oligomer in PHJs was additionally tested in BHJ solar cells. In the BHJ device stack, the neat donor layer employed in the PHJ setup was replaced by a 20 nm thick blend layer of donor and acceptor fabricated by co-evaporation of **DCC3T-Me** and C_{60} in a ratio of 2:1 by volume. During the deposition of the photoactive layer the substrate was heated to 90 °C. Despite the V_{OC} of the BHJ solar cells was slightly reduced 0.99 V and the fill factor dropped to 53% compared to the PHJ device, a strongly enhanced J_{SC} of 8.5 mA cm^{-2} was found and led to a further improved PCE of 4.4% (Table 4).This is as well represented in the EQE data of **DCC3T-Me**:C_{60}-BHJ devices achieving maximum values of 60% @ 500 nm compared to 35% in the PHJ devices, which can be assigned to the stronger thin film absorption (Figure 12c). Interestingly, this device performance of DCC-substituted terthiophene **DCC3T-Me** excels those of all 4T derivatives even the best one, which is methylated **DCV4T-Me** giving a PCE of 3.8% at a V_{OC} of 0.98 V, a J_{SC} of 6.5 mA cm^{-2}, and a fill factor of 59%.[14]

Table 4. *Photovoltaic characteristics of planar (PHJ) solar cell devices containing* ***DCC3T*** *and* ***DCC3T-Me*** *as donor component and C_{60} as acceptor in comparison to* ***DCV4T*** *and of bulk heterojunction (BHJ) cells with* ***DCC3T-Me****.*

Donor oligomer	Device type	V_{OC} [V]	J_{SC} [mA cm^{-2}]	FF [%]	PCE [%]	Satura-tion [a]	Intensity [mW cm^{-2}]
DCC3T	PHJ	1.00	5.3	56	3.0	1.11	93
DCC3T-Me	PHJ	1.05	5.0	65	3.4	1.08	92
DCV4T[b]	PHJ	0.97	2.9	42	1.2	1.3	100
DCC3T-Me	BHJ	0.99	8.5	53	4.4	1.09	87

[a] Saturation defined as $J(-1V)/J_{SC}$, i.e., voltage bias dependence of the current in reverse direction; [b] Data taken from the literature.[12c]

3. CONCLUSION

In summary, a series of novel A-D-A oligothiophenes, from the mono- to the quarterthiophene, terminally substituted with the DCC acceptor has been synthesized. Structural, thermal, optoelectronic, and photovoltaic properties of the π-extended **DCCnTs** were characterized and contrasted to the trends found for the series of dicyanovinyl (DCV)-substituted oligothiophenes **DCVnT**. We were able to bring out the influence of additional exocyclic, sterically fixed in trans-configuration, located between the acceptor and donor units in such A-D-A oligothiophenes. The direct comparison of the two series showed that (1) the **DCCnTs** had increased melting temperatures and signifi cantly enhanced solubilities including an odd–even effect as a function of the number of thiophene units due to molecular symmetry, whereas the thermal stability is somewhat smaller. (2) Great similarities in crystal packing were observed for **DCC3T-Me** and **DCV5T-Me**, which have the same substitution pattern and the same number of rings including efficient π–π-stacking of the oligothiophene cores. Both acceptor units, DCC and DCV, govern the 2D-arrangement in the molecular plane by multiple nonclassical hydrogen bonding. (3) The comparison of the optical properties of DCC- and DCV-capped oligomers resulted in a close correspondence of the absorption profiles for derivatives with equal number of double bonds, i.e., **DCCnTs** and **DCV(n + 1)Ts**. (4) Electrochemical and theoretical investigations showed that despite having the same energy gap, the HOMO/LUMO energy levels for the DCC-derivatives are raised and more destabilized due to the aromatization energy of a thiophene ring versus two exocyclic double bonds. This result indicates that implementation of DCC-acceptor units lead to improved donor and reduced acceptor strength in the oligomers. (5) The incorporation of the DCC-terthiophenes **DCC3T** and **DCC3T-Me** as donor materials in vacuum-processed planar and bulk heterojunction solar cells resulted in a good photovoltaic performance (PCE $\leq$ 4.4%), which clearly outperformed all comparable **DCV4T** derivatives.

4. EXPERIMENTAL SECTION

INSTRUMENTS AND MEASUREMENTS

NMR spectra were recorded on an Avance 400 spectrometer (^{1}H NMR: 400 MHz, ^{13}C NMR: 100 MHz) or a Bruker AMX 500 (^{1}H NMR: 500 MHz, ^{13}C NMR: 125 MHz), at 25 °C or 100 °C, respectively. Chemical shift values (δ) are expressed in parts per million using residual

solvent protons (^{1}H NMR, δ_H = 7.26 for $CDCl_3$, δ_H = 2.50 for DMSO-d_6 and δ_H = 5.93 for tetrachloroethane-d_2; ^{13}C NMR, δ_C = 77.0 for $CDCl_3$, δ_C = 39.43 for DMSO-d_6 and δ_C = 74.20 tetrachloroethane-d_2) as internal standard. The splitting patterns are designated as follows: s (singlet), d (doublet) and m (multiplet). The assignments are Th*H* (thiophene protons), Me*H* (methyl protons) and V*H* (vinyl protons).

GC-MS (EI) mass spectra were recorded on a Varian Saturn 2000, CI mass spectra on a Finnigan MAT SSQ-7000 and MALDI-TOF mass spectra on a Bruker Daltonic Reflex III. Differential scanning calorimetric measurements (DSC) were performed on a Mettler Toledo DSC823^e under argon atmosphere at a heating rate of 10 °C min^{-1}. Melting points were determined using a Büchi B-545 apparatus and were not corrected. Elemental analyses were performed on an Elementar Vario EL. Preparative column chromatography was performed on glass columns packed with silica gel (Merck Silica 60, particle size 40-43 μm).

Optical solution measurements were carried out in 1 cm cuvettes with Merck Uvasol grade solvents; absorption spectra were recorded on a Perkin Elmer Lambda 19 spectrometer and corrected fluorescence spectra were recorded on a Perkin ElmerLS 55 fluorescence spectrometer. Thin film absorption spectra were recorded on a Shimadzu UV-2101/3101 UV–Vis spectrometer. The thin film emission spectra were recorded with an Edinburgh Instruments FSP920 fluorescence spectrometer. Cyclic voltammetry experiments were performed with a computer-controlled Metrohm Autolab PGSTAT30 potentiostat in a three-electrode single-compartment cell with a platinum working electrode, a platinum wire counter electrode, and an Ag/AgCl reference electrode. All potentials were internally referenced to the ferrocene/ferrocenium couple.

X-ray diffraction data of **DCC3T-Me** were collected on a Agilent SuperNova, Cu at zero, Atlas CCD using graphite-monochromated Cu K_α radiation. Data collection strategy was performed with the APEX2 software, data reduction and cell refinement with SAINT. **DCC3T-Me**: $C_{32}H_{24}N_4S_3$, M_r = 560.73, dark-green platelet, 0.39x0.10x0.06 mm^3, monoclinic, C2/c, a = 21.3166(12) Å, b = 15.0156(7) Å, c = 9.1933(5) Å, β = 118.089(8)°, V = 2596.0(3) Å^3, Z = 4, μ = 2.850 mm^{-1}, d_x = 1.435 g/cm^3, T = 150 K. 4754 reflections collected (θ_{max} = 73.723°) and merged to 2541 independent data (R_{int} = 0.023); final R indices ($I > 2\sigma(I)$): $R1$ = 0.0402, $wR2$ = 0.0457. Detailed crystallographic data for structure **DCC3T-Me** has been deposited with the Cambridge Crystallographic Data Centre as supplementary publication CCDC 1025975. Details on measurement and refinement are given in the Supporting Information.

Quantum Chemical Calculations

Density functional theory was employed with the hybrid functionals B3LYP and the basis set 6-31G* from the NWChem package.[18]

Thin Film and Device Fabrication

Thin films and planar heterojunction solar cell devices were prepared by thermal vapor deposition in ultra-high vacuum at a base pressure of 10^{-7} mbar onto the substrate at room temperature. Thin films for absorption and emission measurements were prepared on quartz substrates; solar cells on tin-doped indium oxide (ITO) coated glass (Thin Film Devices, USA, sheet resistance of 30 Ω/sq.). Layer thicknesses were determined during evaporation by using quartz crystal monitors calibrated for the respective material. The thin films prepared for absorption and emission measurements are approximately 30 nm thick. The bulk-heterojunction solar cell was prepared layer by layer without breaking the vacuum using the following layer structure: ITO; 15 nm C_{60}; 20 nm blend layer of **DCC3T-Me** and C_{60} (ratio 2:1 by volume) prepared by co-evaporation on the heated substrate (90 °C), 10 nm 9,9-bis{4-[di-(p-biphenyl)-aminophenyl]}fluorene (BPAPF), 50 nm BPAPF p-doped with NDP9 (purchased from Novaled AG Germany, 10 wt%); 1 nm NDP9; 100 nm aluminum.

Photovoltaic Characterization

J–V and EQE measurements were carried out in a glove box with nitrogen atmosphere. *J–V* characteristics were measured using a source-measure unit (Keithley SMU 2400) and an AM 1.5G sun simulator (KHS Technical Lighting SC1200). The intensity was monitored with a silicon photodiode (Hamamatsu S1337), which was calibrated at Fraunhofer ISE, Freiburg, Germany. The mismatch between the spectrum of the sun simulator and the solar AM 1.5G spectrum was taken into account for the calculation of current density. For well-defined active solar cell areas, aperture masks (2.76 mm²) were used. Simple EQE measurements were carried out using the sun simulator in combination with color filters for monochromatic illumination. The illumination intensities were measured with a silicon reference diode (Hamamatsu S1337).

Reagents and Chemicals

2,5-Bis(trimethylstannyl)thiophene **1**,[19] 5,5'-bis(trimethylstannyl)-2,2'-bithiophene **2**,[20,21] 3-bromocyclohex-2-enone **3**,[22-24] 3-methoxy-2-cyclohex-2-enon **7**,[25] and 2,5-bis(trimethyl-

stannyl)-3,4-dimethylthiophen **10**[26] were prepared according to published literature procedures. 2,5-Dibromothiophene **6** was purchased from Aldrich. Malonitrile and *β*-alanine were purchased from Merck. *n*-Butyl lithium (1.6 M solution in hexanes) was purchased from Acros. All synthetic steps were carried out under argon atmosphere.

SYNTHESIS AND CHARACTERIZATION

Synthesis of 3,3'-(Thien-2,5-diyl)bis(cyclohex-2-enone) ***4***: A mixture of 2,5-bis(trimethylstannyl)thiophene **1** (200 mg, 488 µmol), 3-bromocyclohex-2-enone **3** (179 mg, 1.03 mmol) and tetrakis(triphenylphosphine)palladium(0) (28 mg, 24 µmol) in degassed DMF (3 mL) was stirred at 80 °C for 3 hours. Upon cooling to -20 °C, the resulting precipitate was filtered off and washed thoroughly with water. The filtrate was poured into dichloromethane (50 mL), washed with water (3 x 50 mL), dried over $MgSO_4$, filtered, and concentrated under reduced pressure. Recrystallization of the combined solids from *n*-hexane/dichloromethane provided compound **4** (117 mg, 430 µmol, 88% yield) as yellow needles. Mp 149 °C (DSC); ^{1}H NMR (DMSO-d_6, δ ppm) 7.69 (s, 2H, Th*H*), 6.34 (s, 2H, V*H*), 2.78 (t, 4H, *J* = 5.7 Hz), 2.38 (t, 4H, *J* = 6.6 Hz), 2.06-2.00 (m, 4H). ^{13}C NMR (DMSO-d_6, δ ppm) 198.12, 151.56, 144.28, 129.56, 122.70, 36.75, 27.02, 21.87. MS (EI) m/z: 272 [M^+]; Elemental analysis for $C_{16}H_{16}O_2S$: calcd. C, 70.56; H, 5.92; S, 11.77%; found: C, 70.41; H, 5.75; S, 11.58%.

Synthesis of 3,3'-[(2,2'-Bithien)-5,5'-diyl]bis(cyclohex-2-enone) ***5***: A mixture of 5,5'-bis(trimethylstannyl)-2,2'-bithiophene **2** (200 mg, 406 µmol), 3-bromocyclohex-2-enone **3** (156 mg, 894 µmol), and tetrakis(triphenylphosphine)palladium(0) (24 mg, 20 µmol) in degassed DMF (5 mL) was stirred at 80 °C for 3 hours. Upon cooling to -20 °C, the resulting precipitate was filtered off and thoroughly washed with methanol. The filtrate was poured into dichloromethane (50 mL), washed with water (3 x 50 mL), dried over $MgSO_4$, filtered, and concentrated under reduced pressure. Recrystallization of the combined solids from *n*-hexane/dichloromethane provided diketone **5** (127 mg, 358 µmol, 88% yield) as orange needles. Mp 214 °C (DSC); ^{1}H NMR (DMSO-d_6, 100 °C, δ ppm) 7.57 (d, 2H, *J* = 4.0 Hz, Th*H*), 7.44 (d, 2H, *J* = 4.0 Hz, Th*H*), 6.27 (s, 2H, V*H*), 2.79 (t, 4H, *J* = 5.5 Hz), 2.39 (t, 4H, *J* = 6.6 Hz), 2.10-2.05 (m, 4H). ^{13}C NMR (DMSO-d_6, 100 °C, δ ppm) 196.91, 150.88, 141,34, 137,87, 128,77, 125.71, 121,66, 36.27, 26.80, 21.43. MS (CI) m/z: 355 [M+H^+]; Elemental analysis for $C_{20}H_{18}O_2S_2$: calcd. C, 67.77; H, 5.12; S, 18.09%; found: C, 67.73; H, 5.28; S, 18.25%.

*Synthesis of 3-(5-Bromothien-2-yl)cyclohex-2-enone **8***: To a solution of 2,5-dibromothiophene **6** (10.07 g, 25.0 mmol) in diethyl ether (75 mL), stirred at -78 °C, *n*-butyl lithium (1.6 M solution in hexanes, 15.6 mL, 25.0 mmol) was added dropwise over 15 minutes. After stirring at -78 °C for 10 minutes, a solution of 3-methoxy-2-cyclohex-2-enon **7** (3.16 g, 25.0 mmol) in diethyl ether (30 mL) was added and stirring was continued for 15 minutes. The solution was warmed to 0 °C, stirred for 3 hours, and subsequently allowed to warm to room temperature and stirred for 16 hours. The reaction was quenched with brine (300 mL) and the product was extracted with diethyl ether (3 × 150 mL). The combined organic extracts were dried over $MgSO_4$, filtered, and the solvents were removed *in vacuo*. Column chromatography (silica gel, DCM) and subsequent recrystallization from *n*-hexane yielded ketone **8** (4.91 g, 19.1 mmol, 76% yield) as a colourless crystalline solid. Mp 90.5-92 °C; ^{1}H NMR ($CDCl_3$, δ ppm) 7.12 (d, 1H, *J* = 4.0 Hz, Th*H*), 7.05 (d, 1H, *J* = 3.9 Hz, Th*H*), 6.29 (s, 1H, V*H*), 2.70 (t, 2H, *J* = 6.0 Hz), 2.45 (t, 2H, *J* = 6.6 Hz), 2.16-2.09 (m, 2H). ^{13}C NMR ($CDCl_3$, δ ppm) 199.08, 151.19, 143.97, 131.20, 127.57, 122.80, 116.38, 37.18, 27.35, 22.29. MS (EI) m/z: 258 [$M+H^+$]; Elemental analysis for $C_{10}H_9BrOS$: calcd. C, 46.71; H, 3.53; S, 12.47%; found: C, 46.97; H, 3.59; S, 12.48%.

*Synthesis of 2-[3-(5-Bromothien-2-yl)cyclohex-2-en-1-ylidene]malonitrile **9***: A solution consisting of 3-(5-bromothien-2-yl)cyclohex-2-enone **8** (4.00 g, 15.6 mmol), malonitrile (3.08 g, 46.7 mmol), and *β*-alanine (83 mg, 0.93 mmol) in a mixture of dichloroethane (100 mL) and ethanol (100 mL) was stirred under reflux for 6 days. The reaction mixture was allowed to cool to room temperature, the precipitate was filtered off and washed thoroughly with water. After concentration of the filtrate *in vacuo* to about half the volume and cooling to room temperature, the resulting precipitate was collected by filtration and washed with water to afford a second crop of **9** (overall: 4.40 g, 14.4 mmol, 93% yield) as an orange crystalline solid. M.p. 195.5-197 °C; ^{1}H NMR ($CDCl_3$, δ ppm) 7.23 (d, 1H, *J* = 3.9 Hz, Th*H*), 7.10 (d, 1H, *J* = 3.9 Hz, Th*H*), 7.01 (s, 1H, V*H*), 2.80 (t, 2H, *J* = 6.4 Hz), 2.74 (t, 1H, *J* = 5.9 Hz), 2.00 (p, 1H, *J* = 6.1 Hz). ^{13}C NMR ($CDCl_3$, δ ppm) 168.85, 149.24, 143.88, 131.71, 128.64, 118.57, 118.25, 113.28, 112.46, 78.34, 29.06, 27.73, 21.11. MS (EI) m/z: 306 [$M+H^+$]; Elemental analysis for $C_{13}H_9BrN_2S$: calcd. C, 51.16; H, 2.97; N, 9.18; S, 10.51%; found: C, 51.38; H, 3.04; N, 9.15; S, 10.54%.

*Synthesis of 2,2'-[(Thien-2,5-diyl)bis(cyclohex-2-en-3-yl-1-ylidene)]dimalonitrile **DCC1T***: A solution consisting of 3,3'-(thien-2,5-diyl)bis(cyclohex-2-enone) **4** (390 mg, 1.43 mmol), malonitrile (570 mg, 8.59 mmol), and *β*-alanine (7 mg, 0.08 mmol) in a mixture of dichloroethane (5 mL) and ethanol (5 mL) was stirred under reflux for 7 days. The reaction mixture cooled to -18 °C, the precipitate was filtered off and recrystallized from dichloromethane to yield **DCC1T**

(427 mg, 1.16 mmol, 81% yield) as an red crystalline solid. M.p. 319 °C (DSC); ^{1}H NMR (tetrachloroethane-d_2, 100 °C, δ ppm) 7.45 (s, 2H, Th*H*), 7.16 (s, 2H, V*H*), 2.80-2.74 (m, 8H), 1.01-1.96 (m, 4H). ^{13}C NMR (tetrachloroethane-d_2, 100 °C, δ ppm) 168.29, 149.26, 146.40, 129.18, 120.56, 113.18, 112.48, 80.02, 29.34, 28.69, 21.51. MS (CI) m/z: 369 [M+H$^+$]; Elemental analysis for $C_{22}H_{16}N_4S$: calcd. C, 71.72; H, 4.38; N, 15.21; S, 8.70%; found: C, 71.98; H, 4.43; N, 15.26; S, 8.83%.

Synthesis of 2,2'-[(2,2'-Bithien-5,5'-diyl)bis(cyclohex-2-en-3-yl-1-ylidene)]dimalononitrile ***DCC2T***: A suspension consisting of 3,3'-(2,2'-bithien-5,5'-diyl)bis(cyclohex-2-enone) **5** (730 mg, 2.06 mmol), malonitrile (680 mg, 10.3 mmol), and *β*-alanine (10 mg, 0.11 mmol) in a mixture of dichloroethane (10 mL) and ethanol (10 mL) was stirred under reflux for 21 days. The reaction mixture was allowed to cool to room temperature, the precipitate was filtered off and recrystallized from dichloroethane to yield **DCC2T** (691 mg, 1.53 mmol, 74% yield) as an dark red solid. M.p. 331 °C (DSC); ^{1}H NMR (tetrachloroethane-d_2, 100 °C, δ ppm) 7.40 (d, 2H, *J* = 4.0 Hz, Th*H*), 7.10 (s, 2H, V*H*), 2.79-2.75 (m, 8H), 2.01-1.96 (m, 4H). ^{13}C NMR was not possible due to low solubility. MS (CI) m/z: 451 [M+H$^+$]; Elemental analysis for $C_{26}H_{18}N_4S_2$: calcd. C, 69.31; H, 4.03; N, 12.43; S, 14.23%; found: C, 69.50; H, 3.96; N, 12.38; S, 14.22%.

Synthesis of 2,2'-[(2,2':5',2''-Terthien-5,5''-diyl)bis(cyclohex-2-en-3-yl-1-ylidene)]dimalonitrile ***DCC3T***: A mixture of 2,5-bis(trimethylstannyl)thiophene **1** (767 mg, 1.87 mmol), 2-[3-(5-bromothien-2-yl)-cyclohex-2-en-1-ylidene]malonitrile **9** (1.20 g, 3.93 mmol), and tetrakis(triphenylphosphine)palladium(0) (108 mg, 94 μmol) in degassed DMF (30 mL) was stirred at 80 °C for 30 hours. Upon cooling, the resulting precipitate was filtered off and washed several times with methanol and *n*-hexane. After drying, **DCC3T** (783 mg, 1.47 mmol, 79% yield) was obtained as a dark purple solid. M.p. 290 °C; ^{1}H NMR (tetrachloroethane-d_2, 100 °C, δ ppm) 7.36 (d, 2H, *J* = 4.0 Hz, Th*H*), 7.20 (s, 2H, Th*H*), 7.16 (d, 2H, *J* = 4.0 Hz, Th*H*), 6.99 (s, 2H, V*H*), 2.74-2.71 (m, 8H), 1.96-1.90 (m, 4H). ^{13}C NMR (tetrachloroethane-d_2, 100 °C, δ ppm) 168.99, 150.23, 141.91, 141.66, 137.17, 130.06, 126.73, 125.75, 118.90, 113.76, 113.04, 77.88, 29.41, 28.33, 21.58. MALDI-TOF MS m/z: 532 [M$^+$]; Elemental analysis for $C_{30}H_{20}N_4S_3$: calcd. C, 67.64; H, 3.78; N, 10.52; S, 18.06%; found: C, 67.70; H, 3.79; N, 10.30; S, 17.89%.

Synthesis of 2,2'-[(2,2':5',2'':5'',2'''-Quaterthien-5,5'''-diyl)bis(cyclohex-2-en-3-yl-1-ylidene)]dimalonitrile ***DCC4T***: A mixture of 5,5'-bis(trimethylstannyl)-2,2'-bithiophene (1.00 mg, 2.03 mmol), 2-[3-(5-bromothien-2-yl)cyclohex-2-en-1-ylidene]malonitrile **9** (1.30 g, 4.27 mmol), and tetrakis(triphenylphosphine)palladium(0) (117 mg, 10 μmol) in degassed DMF (40 mL) was stirred at 80 °C for 16 hours. Upon cooling, the resulting precipitate was filtered off and washed

several times with methanol and *n*-hexane. The crude product was extracted in a *Soxhlet* extractor with chlorobenzene for 6 days. The extract was cooled to room temperature and the precipitate was filtered off to yield **DCC4T** (819 mg, 1.33 mmol, 66% yield) as a black solid. M.p. 333 °C (DSC); ^{1}H NMR (tetrachloroethane-d_2, 100 °C, δ ppm) 7.39 (d, 2H, *J* = 4.0 Hz, Th*H*), 7.21 (d, 2H, *J* = 3.9 Hz, Th*H*), 7.18 (d, 2H, *J* = 4.0 Hz, Th*H*), 7.15 (d, 2H, *J* = 3.9 Hz, Th*H*), 7.07 (s, 2H, V*H*), 2.78-2.75 (m, 8H), 2.00-1.95 (m, 4H). ^{13}C NMR was not possible due to low solubility. MALDI-TOF MS m/z: 614 [M^+]; Elemental analysis for $C_{34}H_{22}N_4S_4$: calcd. C, 66.42; H, 3.61; N, 9.11; S, 20.86%; found: C, 66.59; H, 3.51; N, 8.92; S, 20.60%.

Synthesis of 2,2'-{[3',4'-Dimethyl-(2,2':5',2''-terthien-5,5''-diyl)]bis(cyclohex-2-en-3-yl-1-ylidene)}dimalonitrile ***DCC3T-Me***: A mixture of 2,5-bis(trimethylstannyl)-3,4-dimethylthiophene **10** (400 mg, 913 µmol), 2-[3-(5-bromothien-2-yl)cyclohex-2-en-1-ylidene]malonitrile **9** (586 mg, 1.92 mmol), and tetrakis(triphenylphosphine)palladium(0) (46 mg, 40 µmol) in degassed DMF (15 mL) was stirred at 80 °C for 16 hours. Upon cooling, the resulting precipitate was filtered off and washed several times with methanol and *n*-hexane. After drying, **DCC3T-Me** (443 mg, 787 µmol, 86% yield) was obtained as a dark purple crystalline solid. M.p. 305 °C (DSC); ^{1}H NMR (tetrachloroethane-d_2, 100 °C, δ ppm) 7.42 (d, 2H, *J* = 4.0 Hz, Th*H*), 7.17 (d, 2H, *J* = 4.1 Hz, Th*H*), 7.02 (s, 2H, V*H*), 2.78-2.72 (m, 8H), 2.33 (s, 6H, Me*H*), 1.97-1.91 (m, 4H). ^{13}C NMR (tetrachloroethane-d_2, 100 °C, δ ppm) 169.75, 150.91, 141.96, 141.68, 137.91, 130.67, 130.16, 127.56, 118.38, 114.23, 113.47, 76.95, 29.51, 28.29, 21.56, 15.30. MALDI-TOF MS m/z: 560 [M^+]; Elemental analysis for $C_{32}H_{24}N_4S_3$: calcd. C, 68.54; H, 4.31; N, 9.99; S, 17.15%; found: C, 68.51; H, 4.18; N, 9.98; S, 16.99%.

ACKNOWLEDGEMENTS

The authors would like to thank the German Research Foundation (DFG) for financial support in the framework of special program SPP 1355. The authors thank Novaled GmbH for providing NDP9.

Submitted: November 27, 2014
Revised: January 17, 2015
Published online: February 16, 2015

REFERENCES

[1] Y. Chen, X. Wan, G. Long, *Acc. Chem. Res.* **2013**, *46*, 2645.

[2] J. E. Coughlin, Z. B. Henson, G. C. Welch, G. C. Bazan, *Acc. Chem. Res.* **2013**, *47*, 257.

[3] L. Dou, J. You, Z. Hong, Z. Xu, G. Li, R. A. Street, Y. Yang, *Adv. Mater.* **2013**, *25*, 6642.

[4] a) A. Mishra, P. Bäuerle, *Angew. Chem.* **2012**, *124,* 2060; b) A. Mishra, P. Bäuerle, *Angew. Chem. Int. Ed.* **2012**, *51*, 2020.

[5] M. C. Scharber, N. S. Sariciftci, *Prog. Polym. Sci.* **2013**, *38*, 1929.

[6] a) J. Zhou, Y. Zuo, X. Wan, G. Long, Q. Zhang, W. Ni, Y. Liu, Z. Li, G. He, C. Li, B. Kan, M. Li, Y. Chen, *J. Am. Chem. Soc.* **2013**, *135*, 8484; b) B. Kan, Q. Zhang, M. Li, W. Ni, G. Long, Y. Wang, X. Yang, H. Feng, Y. Chen, *J. Am. Chem. Soc.* **2014**, *136*, 15529.

[7] a) T. S. van der Poll, J. A. Love, T.-Q. Nguyen, G. C. Bazan, *Adv. Mater.* **2012**, *24*, 3646; b) A. K. K. Kyaw, D. H. Wang, V. Gupta, J. Zhang, S. Chand, G. C. Bazan, A. J. Heeger, *Adv. Mater.* **2013**, *25*, 2397; c) V. Gupta, A. K. K. Kyaw, D. H. Wang, S. Chand, G. C. Bazan , A. J. Heeger, *Sci. Rep.* **2013**, *3*, 1965.

[8] Y. Zou, J. Holst, Y. Zhang, R. J. Holmes, *J. Mater. Chem. A* **2014**, *2*, 12397.

[9] Y.-H. Chen, L.-Y. Lin, C.-W. Lu, Z.-Y. Huang, H.-W. Lin, F. Lin, P.-H. Wang, Y.-H. Liu, K.-T. Wong, J. Wen, D. J. Miller, S. B. Darling, *J. Am. Chem. Soc.* **2012**, *134*, 13616.

[10] K. Cnops, B. P. Rand, D. Cheyns, B. Verreet, M. A. Empl, P. Heremans, *Nat. Commun.* **2014**, *5*, 3406.

[11] K. Schulze, C. Uhrich, R. Schüppel, K. Leo, M. Pfeiffer, E. Brier, E. Reinold, P. Bäuerle, *Adv. Mater.* **2006**, *18*, 2872.

[12] a) C. Uhrich, R. Schüppel, A. Petrich, M. Pfeiffer, K. Leo, E. Brier, P. Kilickiran, P. Bäuerle, *Adv. Funct. Mater.* **2007**, *1*, 2991; b) R. Schüppel, K. Schmidt, C. Uhrich, K. Schulze, D. Wynands, J. L. Bredas, E. Brier, E. Reinold, H. B. Bu, P. Bäuerle, B. Maennig, M. Pfeiffer, K. Leo, *Phys. Rev. B* **2008**, *77*, 085311; c) R. Fitzner, E. Reinold, A. Mishra, E. Mena-Osteritz, H. Ziehlke, C. Körner, K. Leo, M. Riede, M. Weil, O. Tsaryova, A. Weiß, C. Uhrich, M. Pfeiffer, P. Bäuerle, *Adv. Funct. Mater.* **2011**, *21*, 897.

[13] K. Schulze, M. Riede, E. Brier, E. Reinold, P. Bäuerle, K. Leo, *J. Appl. Phys.* **2008**, *104*, 074511.

[14] R. Fitzner, C. Elschner, M. Weil, C. Uhrich, C. Körner, M. Riede, K. Leo, M. Pfeiffer, E. Reinold, E. Mena-Osteritz, P. Bäuerle, *Adv. Mater.* **2012**, *24*, 675.

[15] a) R. Fitzner, E. Mena-Osteritz, A. Mishra, G. Schulz, E. Reinold, M. Weil, C. Körner, H. Ziehlke, C. Elschner, K. Leo, M. Riede, M. Pfeiffer, C. Uhrich, P. Bäuerle, *J. Am. Chem. Soc.* **2012**, *134*, 11064; b) R. Meerheim, C. Körner, K. Leo, *Appl. Phys. Lett.* **2014**, *105*,

063306.

[16] K. Staub, G. A. Levina, S. Barlow, T. C. Kowalczyk, H. Lackritz, M. Barzoukas, A. Fort, S. R. Marder, *J. Mater. Chem.* **2003**, *13*, 825.

[17] Q. Xie, F. Arias, L. Echegoyen, *J. Am. Chem. Soc.* **1993**, *115*, 9818.

[18] M. Valiev, E. J. Bylaska, N. Govind, K. Kowalski, T. P. Straatsma, H. J. J. Van Dam, D. Wang, J. Nieplocha, E. Apra, T. L. Windus, W. A. de Jong, *Comput. Phys. Commun.* **2010**, *181*, 1477-1489.

[19] C. van Pham, R. S. Macomber, H. B. Mark Jr., H. Zimmer, *J. Org. Chem.* **1984**, *49*, 5250.

[20] S. Kotani, K. Shiina, K. Sonogashira, *J. Organomet. Chem.* **1992**, *429*, 403.

[21] U. Asawapirom, R. Guentner, M. Forster, T. Farrell, U. Scherf, *Synthesis* **2002**, *9*, 1136.

[22] E. Piers, I. Nagakura, *Synth. Commun.* **1975**, *5*, 193.

[23] C. Shih, J. S. Swenton, *J. Org. Chem.* **1982**, *47*, 2825.

[24] M. E. Jimenez, K. Bush, J. Pawlik, L. Sower, J. W. Peterson, S. R. Gilbertson, *Org. Biomol. Chem.* **2007**, *5*, 3778.

[25] C.-F. Shu, Y.-C. Shu, Z.-H. Gong, *Chem. Mater*. **1998**, *10*, 3284.

[26] H. Ziehlke, R. Fitzner, C. Koerner, R. Gresser, E. Reinold, P. Bäuerle, K. Leo, M. K. Riede *J. Phys. Chem. A* **2011**, *115*, 8437.

SUPPORTING INFORMATION

SINGLE CRYSTAL X-RAY ANALYSIS

Table S1. *Details on measurement and refinement of the* ***DCC3T-Me*** *crystal structure.*

Average Bond Precision:	C-C = 0.0032 Å
Wavelength:	1.54184 Å
Measurement temperature:	150.1(3) K

Cell:	a = 21.3166(12) Å	b = 15.0156(7) Å	c = 9.1933(5) Å
	α = 90°	β = 118.089(8)°	γ = 90°
Volume	2596.0(3) Å^3	*h,k,l max*	26,18,11
Space group	C2/c	*Nref*	2630
Hall group	-C2yc	*Tmin, Tmax*	0.737,0.849
Moiety formula	$C_{32}H_{24}N_4S_3$	*Tmin'*	0.311
Sum formula	$C_{32}H_{24}N_4S_3$	*Correction method*	GAUSSIAN
Mr	560.73	*Data completeness*	0.966
Density	1.435 g/cm^3	*Theta(max)*	73.723
Z	4	*R(reflections)*	0.0402(2243)
Mu	2.850 mm^{-1}	*wR2(reflections)*	0.1147(2541)
F000	1168.0	*S*	1.061
F000'	1174.64	*Npar*	217

Table S2*. Molecular structure of* ***DCC3T-Me****, selected bond lengths, dihedral and torsional angles.*

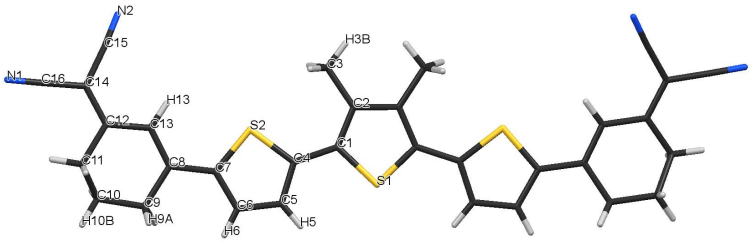

Atom 1	Atom 2	Length [Å]
N2	H13	2.598(2)
N1	H11A	2.673(2)
H11A	N1	2.673(2)
S2	N2	3.272(2)
N1	C16	1.142(2)
C16	C14	1.436(2)
N2	C15	1.147(3)

Atom 1	Atom 2	Atom 3	Angle [°]
N1	C16	C14	179.1(2)
C16	C14	C12	122.1(2)
N2	C15	C14	175.4(2)
C15	C14	C12	124.1(2)
C14	C12	C13	122.9(2)
C12	C13	C8	121.8(2)
C13	C8	C7	123.2(2)

Table S2 (Continued).

Atom 1	Atom 2	Length [Å]
C15	C14	1.430(3)
C14	C12	1.371(3)
C12	C13	1.428(2)
C13	C8	1.361(3)
C12	C11	1.499(3)
C11	C10	1.506(3)
C10	C9	1.517(2)
C9	C8	1.506(3)
C8	C7	1.453(2)
C7	C6	1.376(3)
C6	C5	1.402(2)
C5	C4	1.383(3)
C4	S2	1.730(2)
C7	S2	1.732(2)
C4	C1	1.451(2)
C1	C2	1.380(3)
C2	C2	1.429(2)
C1	S1	1.730(2)
C2	C3	1.504(3)

Atom 1	Atom 2	Atom 3	Angle [°]
C8	C7	S2	122.6(1)
C7	S2	C4	92.53(9)
S2	C4	C5	110.2(1)
C4	C5	C6	113.4(2)
C5	C6	C7	113.6(2)
C6	C7	S2	110.3(1)
C13	C8	C9	121.3(2)
C8	C9	C10	113.3(2)
C9	C10	C11	111.1(2)
C10	C11	C12	110.2(2)
C11	C12	C13	117.5(2)
C9	C8	C7	115.5(2)
C8	C7	C6	127.0(2)
S2	C4	C1	123.9(1)
C5	C4	C1	125.9(2)
C4	C1	S1	117.2(1)
C4	C1	C2	131.4(2)
C1	C2	C3	124.2(2)
S1	C1	C2	111.4(1)

tom 1	Atom 2	Atom 3	Atom 4	Torsion [°]
N1	C16	C14	C12	162(14)
C16	C14	C12	C11	3.3(3)
N2	C15	C14	C12	126(3)
C15	C14	C12	C13	9.0(3)
C12	C13	C8	C7	-169.9(2)
C13	C8	C7	S2	2.4(3)
S2	C4	C1	S1	179.3(1)
C13	C8	C7	C6	179.5(2)
S2	C4	C1	C2	1.5(3)
C4	C1	C2	C3	-3.1(3)

Table S3*. Short contacts from the asymmetric unit in the molecular plane.*

Atom1	Atom2	Symm. M1	Symm. M2	Length [Å]
N1	H11A	x,y,z	1-x,-y,3-z	2.673
H11A	N1	x,y,z	1-x,-y,3-z	2.673
S2	N2	x,y,z	1/2-x,1/2-y,2-z	3.272
H13	N2	x,y,z	1/2-x,1/2-y,2-z	2.598
N2	S2	x,y,z	1/2-x,1/2-y,2-z	3.272
N2	H13	x,y,z	1/2-x,1/2-y,2-z	2.598
N2	N2	x,y,z	1/2-x,1/2-y,2-z	3.014

***Table S4**. Short contacts from the asymmetric unit out of plane (π–π stacking direction).*

Atom 1	Atom 2	Symm. M1	Symm. M2	Length [Å]
S1	H3A	x,y,z	x,-y,-1/2+z	2.987
H3C	C6	x,y,z	x,-y,-1/2+z	2.866
C13	H10A	x,y,z	x,-y,-1/2+z	2.900
H9A	C15	x,y,z	x,-y,-1/2+z	2.831
S1	H3A	x,y,z	-x,-y,1-z	2.987
C6	H3C	x,y,z	x,-y,1/2+z	2.866
H3A	S1	x,y,z	-x,-y,1-z	2.987
C15	H9A	x,y,z	x,-y,1/2+z	2.831
H10A	C13	x,y,z	x,-y,1/2+z	2.900

THEORETICAL CALCULATION

***Table S5.** Calculated energy levels of **DCC3T, DCC4T** in comparison to **DCV3T** and **DCV4T**.*

Oligomer	E_{HOMO} [eV]	E_{LUMO} [eV]	E_{LUMO+1} [eV]	E_{gap} [eV]
DCV3T	-7.47	-3.00	-2.40	4.47
DCV4T	-7.19	-2.85	-2.48	4.34
DCC3T	-7.03	-2.70	-2.32	4.33
DCC4T	-6.87	-2.61	-2.39	4.26

CHAPTER VII

STRUCTURAL MODIFICATION OF THE TERMINAL GROUPS IN A-D-A OLIGOTHIOPHENES FOR SOLUTION-PROCESSED SOLAR CELLS

Roland Fitzner,[a] Gisela L. Schulz,[a] Florian Henne,[a] Marta Urdanpilleta,[b] Peter Bäuerle[a]*

[a] Institute of Organic Chemistry II and Advanced Materials, University of Ulm, Albert-Einstein-Allee 11, 89081 Ulm, Germany

[b] Department of Applied Physics, University of the Basque Country (UPV/EHU), Plaza de Europa, 1, 20018 Donostia - San Sebastián, Spain

Intended for submission.

ABSTRACT

Herein, we present the synthesis of two structurally new electron donor materials for organic solar cells. The first molecule in the series, **DCV5T-Bu**, contains the long-standing dicyanovinyl (DCV) acceptor unit. Solubility and film forming properties of the oligomers could be tuned through insertion of a cyclohexene ring and additional methyl groups. The three target compounds are characterized using optical spectroscopy and cyclic voltammetry. After processing each oligomer in various solvent systems together with $PC_{61}BM$ as electron accepting material, the solar cell parameters of the three oligomers are compared. Structure-property relationships with respect to the modification of the acceptor units and its impact on the photovoltaic performance are discussed. It was found that UV-vis absorption spectroscopy could be used as a predictive tool to determine the optimal amount of solvent additive for the fabrication **DCC5T-Bu**:$PC_{61}BM$ based solar cells. Finally, power conversion efficiencies up to 3.4% were measured.

1. INTRODUCTION

The demand for the development of new materials for applications in solution-processed organic bulk heterojunction solar cells (BHJSC) has been increasing. In the last year alone, dozens of new molecules have been synthesized and tested in photovoltaic devices. Due to their defined structure, reproducible synthesis and verifiable purity, oligomeric structures, also referred to as small molecules, are of particular interest. Most of the research in the small molecule solar cell field focusses on developing new electron donors;[1] however there has been significant progress with respect to new electron acceptor materials as well.[2-4]

To date, several different molecular architectures for electron donors have been investigated, including dendrimers, star shaped molecules, and most frequently, linear oligomers.[1,5] In the following overview, we will focus on linear oligomeric acceptor-donor-acceptor (A-D-A)-type compounds that have been applied in solution-processed BHJSCs. Chen *et al.* have published more than 10 different donor materials containing oligothiophenes,[6-8] dithienosiloles,[9] benzodithiophenes[10-12] as electron rich moieties and dicyanovinyl,[7] alkyl cyanoacetate,[6,11] dimethylpyrimidine-trione[13] and rhodanine[12,14] as terminal electron withdrawing groups. In these reports, power conversion efficiencies (PCE) range between 3.7 and 8.1%. Yang *et al.* have recently described the effect of incorporating selenophene into the oligomer backbone of an A-D-A structure and measured PCEs up to 6.15%.[15] The chemical structure of electron-rich and electron-poor components, incorporated into the molecules, not only influences the absorption and electrochemical behavior of the materials but also its physical properties such as solubility, mixing and film forming abilities. During the fabrication of the solar cell, these physical properties play an important role, influencing the active layer morphology and thus the performance of the devices. In an ideal situation, pathways that will allow for hole and electron transport to the respective electrodes will be formed. They will be approximately the size of the exciton diffusion length in order to minimize recombination losses.

A technique that has developed into a routine method to influence the photoactive layer morphology, is the use of solvent additives. This was initially employed with the conjugated polymer based BHJSCs but more recently has also been shown to be very effective with small molecules systems.[16] The presence of the typically high boiling point additive in the solution used to deposit the BHJ active layer, can strongly influence the D:A morphology by either increasing or decreasing the size of the phase separated domains.[17]

In this paper, we report on a series of quinquethiophene-based A-D-A-type electron donors, describing the effect of the structural variation of the terminal groups on physical,

optoelectronic, and photovoltaic properties of the compounds. The modification to the chemical structure strongly affected the solubility of the molecules, and therefore different solvents and solvent additives were investigated for each electron donor material, in order to tune the active layer morphology.

2. Results and Discussion

The first oligomer in the series, **DCV5T-Bu** (Chart 1), has been extensively investigated in vacuum-processed bulk heterojunction solar cells[18-21] and to a lesser extent recently in solution-processed devices.[22] When processed from solution, this oligomer requires high temperature deposition of the active layer, making reproducibility of results a challenge. The aim of this work was to improve the solubility and film-forming properties of **DCV5T-Bu** by modifying the terminal groups, and to investigate the effect of this structural change on the device properties. As shown in Chart 1, the series of quinquethiophenes (**5T**) presented herein have three different groups at the terminal positions: dicyanovinyl (DCV), 1,1-dicyanomethylene-2-cyclohexene (DCC) as well as the 5,5-dimethyl analogue MeDCC.

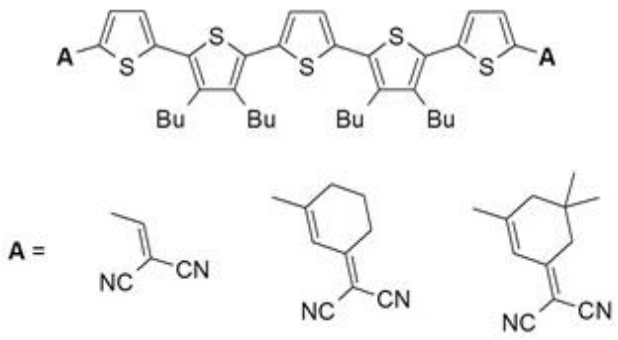

Chart 1. *Chemical structures of* ***DCV5T-Bu****,* ***DCC5T-Bu****, and* ***MeDCC5T-Bu****, shown from left to right.*

The synthesis of the two new oligomers, **DCC5T-Bu** and **MeDCC5T-Bu**, is described in Scheme 1. Both derivatives were obtained by reacting bisstannylated terthiophene **8** as central building block with acceptor-substituted bromothiophenes in Stille-type cross-coupling reactions. To synthesize terminal building blocks **6** and **7**, dibromthiophene was mono-lithiated with *n*-butyllithium and quenched with methoxycyclohexenones **2** or **3**, respectively, to yield keto compounds **4** and **5**. Subsequent Knoevenagel condensation with malononitrile using β-alanine as catalyst provided building blocks **6** and **7**, respectively.

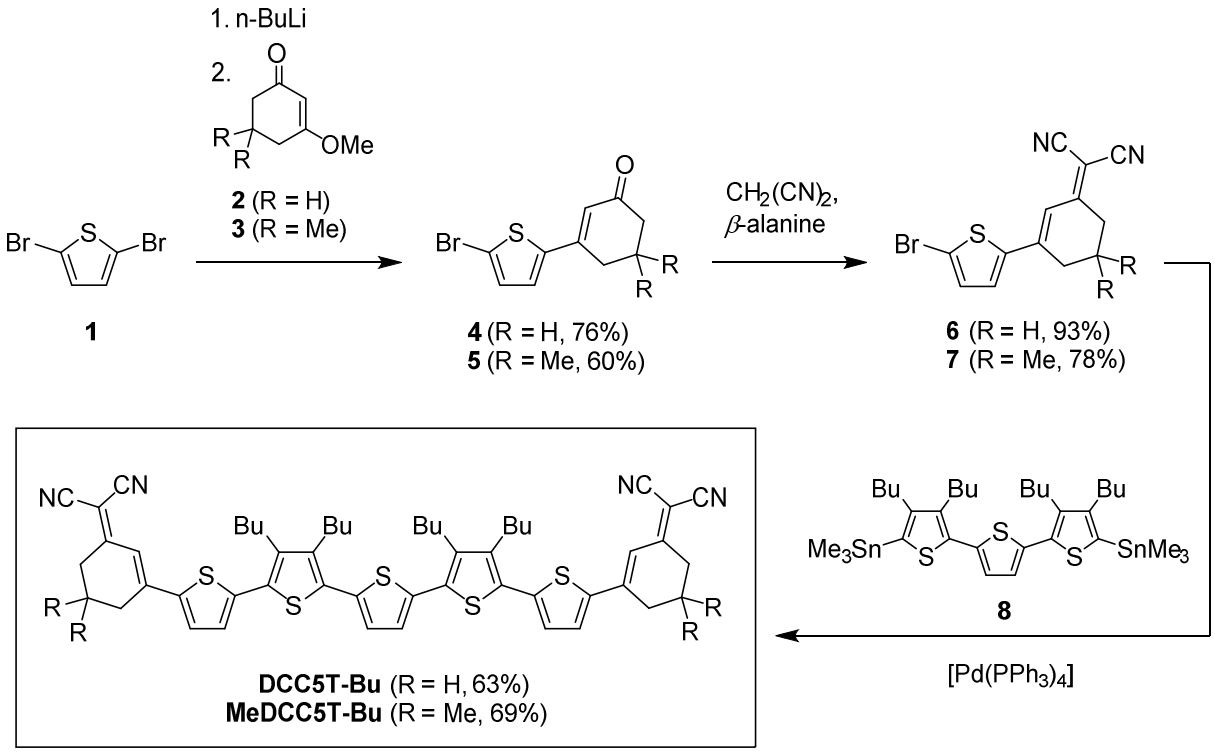

Scheme 1. *Synthetic route used to yield* ***DCC5T-Bu*** *and* ***MeDCC5T-Bu****.*

Figure 1a shows the absorption spectra of the **5T** oligomer series in dilute chloroform solutions and as thin films. The relevant data are also summarized in Table 1. Molar extinction coefficients at λ_{max} were in a similar range between 62 300 and 63 100 L mol^{-1} cm^{-1} for all oligomers. In solution, the spectra are quite similar and display an absorption maximum between 513 and 515 nm. However the neat films show significantly different absorption profiles. The **DCV5T-Bu** thin film displays a large red-shift of 78 nm relative to the spectrum measured in chloroform, as well as a prominent shoulder at 633 nm. In contrast, the **DCC5T-Bu** and **MeDCC5T-Bu** derivatives show a smaller red-shift of 38 and 39 nm, respectively, and structureless absorption profiles. The difference between the DCV and DCC thin film absorption is significant and is attributed to reduced order in the DCC thin films. This will be discussed further in another section later on. The optical bandgap, calculated from the onset of the thin film absorption, was found to increase slightly within the series **DCV5T-Bu**, **DCC5T-Bu** and **MeDCC5T-Bu** from 1.76 to 1.77 to 1.81 eV.

Cyclic voltammetry experiments were performed in dichloromethane solutions containing tetrabutylammonium hexafluorophosphate ($TBAPF_6$) and referenced against the internal ferrocene/ferrocenyl (Fc/Fc^+) redox couple. The electrochemical results are plotted in Figure 1b and summarized in Table 1. **DCV5T-Bu** shows two reversible oxidation waves at 0.58 and 0.87 V, respectively, indicating the formation of stable radical cations on the oligothiophene

backbone. Upon reduction, an irreversible wave was obtained at -1.50 V, which has been attributed to the formation of a radical anion on the terminal electron-poor DCV groups. The onset of the oxidation and reduction waves was used to estimate HOMO and LUMO energy levels of **DCV5T-Bu** to be -5.6 eV and -3.7 eV, respectively.

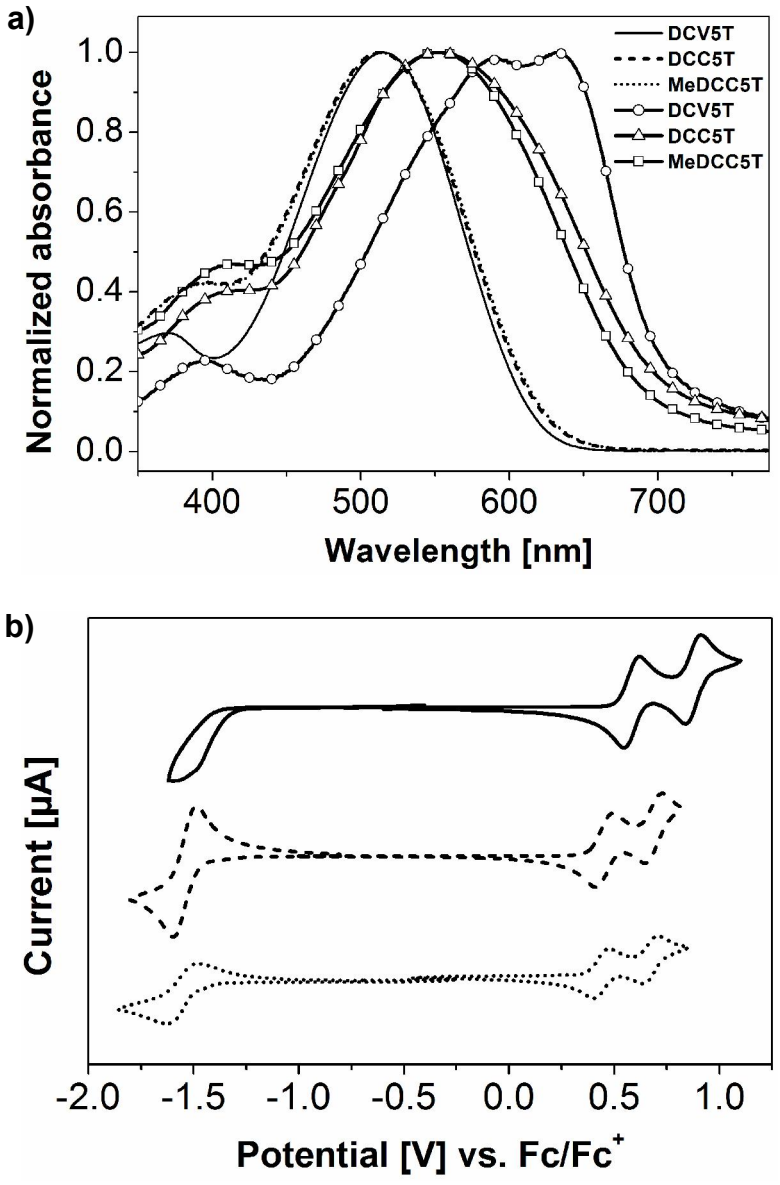

Figure 1. *(a) Absorption spectra of* ***5T*** *oligomers measured in chloroform (line without symbol) and of thin films spin-coated from chloroform (line with symbol). (b) Cyclic voltammograms of* ***5T*** *oligomers in dichloromethane, $TBAPF_6$ (0.1 M) measured versus the ferrocene/ferrocenyl (Fc/Fc^+) redox couple.* ***DCV5T-Bu*** *solid line,* ***DCC5T-Bu*** *dashed line and* ***MeDCC5T-Bu*** *dotted line.*

The incorporation of two additional double bonds in the molecule, as is the case for the DCC and MeDCC derivatives, led to observable changes in the oxidation and reduction. **DCC5T-Bu** oxidizes at lower potentials, 0.45 and 0.68 V, and the reduction wave becomes reversible

at -1.54 V. This is also the case for **MeDCC5T-Bu** which displayed two reversible oxidations at 0.44 V and 0.67 V and one reversible reduction wave at -1.55 V. HOMO and LUMO energy levels were found to be equal within error for **DCC5T-Bu** and **MeDCC5T-Bu** at -5.5 and -3.6 eV, respectively. The higher HOMO levels found for the DCC containing oligomers, is attributed to the elongation of the π-system due to incorporation of two additional double bonds, whereas the higher LUMO energy levels may be attributed the low electron-acceptor strength of the alkylated dicyanovinyl groups in **DCC5T-Bu** and **MeDCC5T-Bu**.

The maximum solubility of the oligomer series was determined using saturated chloroform solutions and measuring UV-vis absorption spectra. The calculated values are tabulated in the last column of Table 1. Maximum solubilities increase in the series **DCV5T-Bu**, **DCC5T-Bu** and **MeDCC5T-Bu** from 20 to 49 and 81 mg/mL, respectively. Thus, the introduction of the six-membered ring in **DCC5T-Bu** resulted in an increase in solubility by a factor of 2.4. The additional two methyl groups at the 5-position of the six-membered ring in **MeDCC5T-Bu** intensify the solubilizing effect, leading to an increase of a factor of 4 with respect to **DCV5T-Bu**.

Table 1. *Optical, electrochemical, and maximum solubility data for the **5T** oligomer series and fullerene $PC_{61}BM$. Absorption spectra measured in $CHCl_3$, thin films spin-coated from $CHCl_3$ and electrochemical measurements in $CH_2Cl_2/TBAPF_6$ solutions (HOMO/LUMO vs. Fc/Fc^+_{vac} = -5.1 eV).*

Compound	λ_{abs} (nm) soln	ε (L mol^{-1} cm^{-1}) soln	ΔE^{opt} (eV) soln	λ_{abs} (nm) film	ΔE^{opt} (eV) film	E^0_{ox1}, E^0_{ox2} (V)	E^0_{red} (V)	HOMO (eV)	LUMO (eV)	ΔE^{CV} (eV)	Solubility in $CHCl_3$ (mg/mL)
DCV5T-Bu	515	62 300	2.03	593, 633	1.76	0.58, 0.87	-1.50	-5.6	-3.7	1.87	20
DCB5T-Bu	513	62 700	1.99	551	1.77	0.45, 0.68	-1.54	-5.5	-3.6	1.85	49
MeDCB5T-Bu	514	63 100	1.99	553	1.81	0.44, 0.67	-1.55	-5.5	-3.6	1.86	81
$PC_{61}BM$	329	40 100	3.08	-	-	-	-	-6.3[23]	-4.0[23]	-	28

All solar cell devices presented herein have the same standard configuration: ITO | PEDOT:PSS | **5T**:$PC_{61}BM$ | LiF | Al. As previously mentioned, **DCV5T-Bu** was recently reported to show PCEs up to 3.0% when spin coated from hot chlorobenzene solutions at 80 °C (see Table 3). Due to the higher solubility of the compound in chloroform compared to chlorobenzene (20 vs. 3 mg/mL),[22] **DCV5T-Bu**:$PC_{61}BM$ based devices were also fabricated using $CHCl_3$ and the resulting *J-V* characteristics are summarized in Table 2. The absorption profiles for the active layer blends measured for **DCV5T-Bu**:$PC_{61}BM$ based devices spin-coated from various

solvents at various temperatures is depicted in Figure 2. The significant red-shift in the absorption maximum (~30 nm) when using chloroform as solvent, was initially interpreted to be an indication of improved blend morphology for the active layer, unfortunately this was not the case, and power conversion efficiencies decreased from 3.0% to 0.1% when the solvent was changed from CB/CN to $CHCl_3$. Moderate improvements in device characteristics were obtained by spin coating the active layers using warm chloroform solutions and substrates (60 °C), which increased the cell efficiency from 0.1 to 1.0%. We speculate that by depositing the active layer blend at 60 °C vs. room temperature, the solvent evaporates faster and results in smaller crystalline domains of **DCV5T-Bu**. AFM experiments will be described in a later section to allow correlations between solar cell results and the D:A blend morphology.

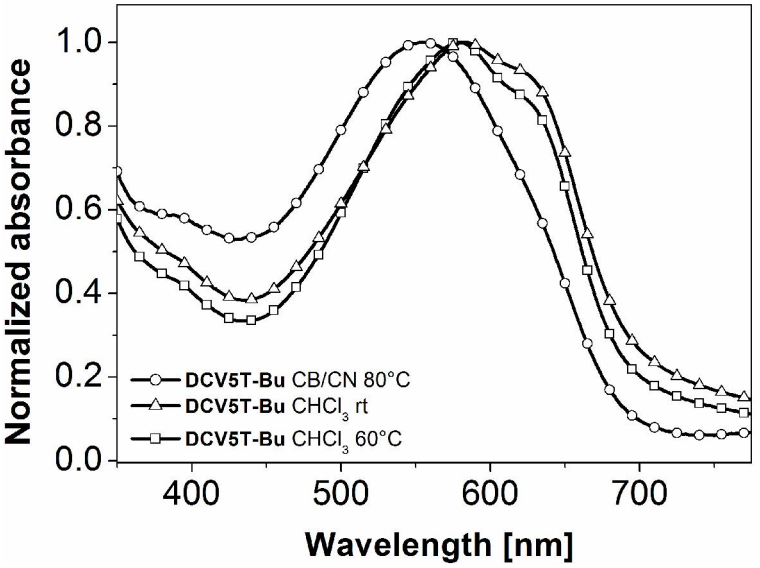

***Figure 2**. Absorption spectrum of **DCV5T-Bu**:$PC_{61}BM$ of thin films spin-coated from CB/CN at 80 °C, chloroform at room temperature and chloroform at 60 °C.*

For **DCC5T-Bu**:$PC_{61}BM$ blends deposited using $CHCl_3$ as solvent, a short-circuit current density (J_{SC}) of 4.5 mA/cm^2, an open-circuit voltage (V_{OC}) of 1.02 V, a fill factor (FF) of 0.30 were measured, resulting in an overall PCE of 1.4%. Further improvement of all photovoltaic parameters was found when 1,8-diiodooctane (DIO) was used as solvent additive. Figure 3 depicts the PCE dependence of the **DCC5T-Bu**:$PC_{61}BM$ devices on additive content in the solvent. By increasing the DIO content from 0 to 4 mg/mL, it was seen that the PCE improved to 2.1%. Addition of more DIO (5 mg/mL) was found to be the optimal amount of solvent additive and resulted in solar cells with a J_{SC} of 6.8 mA/cm^2, a V_{OC} of 1.06 V, a FF of 0.47 and a PCE of 3.4%. This significant enhancement in PCE from 1.4 to 3.4% will be discussed in more detail in the next section. Upon further increase of DIO content to 6 mg/mL, PCEs were found

to decrease to 3.2% and then to 1.5% using 7 mg/mL of the additive. **MeDCC5T-Bu** based devices were optimized with respect to donor:acceptor ratio. Upon increasing the amount of $PC_{61}BM$ in the blend from 1:1 to 1:2, the J_{SC} increased from 3.4 to 4.0 mA/cm^2, V_{OC}s remained similar at 1.03 and 1.02 V, FF increased slightly from 0.29 to 0.31, which led to an overall increase in the PCE from 1.0 to 1.3%, respectively. Further improvement of device performance was not observed when solvent additives or thermal treatment was applied. It seems likely that the two additional methyl groups on the terminal units hinder efficient packing of the molecules.

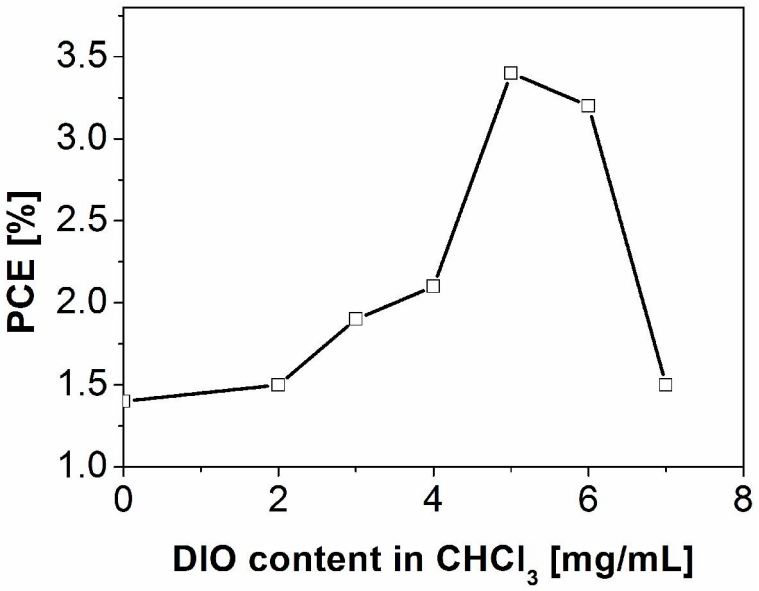

Figure 3. *Power conversion efficiency of* ***DCC5T-Bu****:$PC_{61}BM$ solution-processed solar cells as a function of DIO content in $CHCl_3$.*

Table 2. *Photovoltaic parameters of solar cells fabricated using* ***5T****:$PC_{61}BM$ from $CHCl_3$ and $CHCl_3$/DIO. Device structure: ITO | PEDOT:PSS |* ***5T****: $PC_{61}BM$ | LiF | Al.*

Donor:Acceptor	Solvent	Depostion temp. (°C)	D:A ratio	J_{SC} (mA/cm^2)	V_{OC} (V)	FF	PCE (%)
DCV5T-Bu:$PC_{61}BM$	$CHCl_3$	r.t.	1:1	0.5	1.21	0.14	0.1
DCV5T-Bu:$PC_{61}BM$	$CHCl_3$	60	1:1	4.4	1.11	0.20	1.0
DCC5T-Bu:$PC_{61}BM$	$CHCl_3$	r.t.	1:1	4.5	1.02	0.30	1.4
DCC5T-Bu:$PC_{61}BM$	$CHCl_3$:DIO	r.t.	1:1	6.8	1.06	0.47	3.4
MeDCC5T-Bu:$PC_{61}BM$	$CHCl_3$	r.t.	1:1	3.4	1.03	0.29	1.0
MeDCC5T-Bu:$PC_{61}BM$	$CHCl_3$	r.t.	1:2	4.0	1.02	0.31	1.3

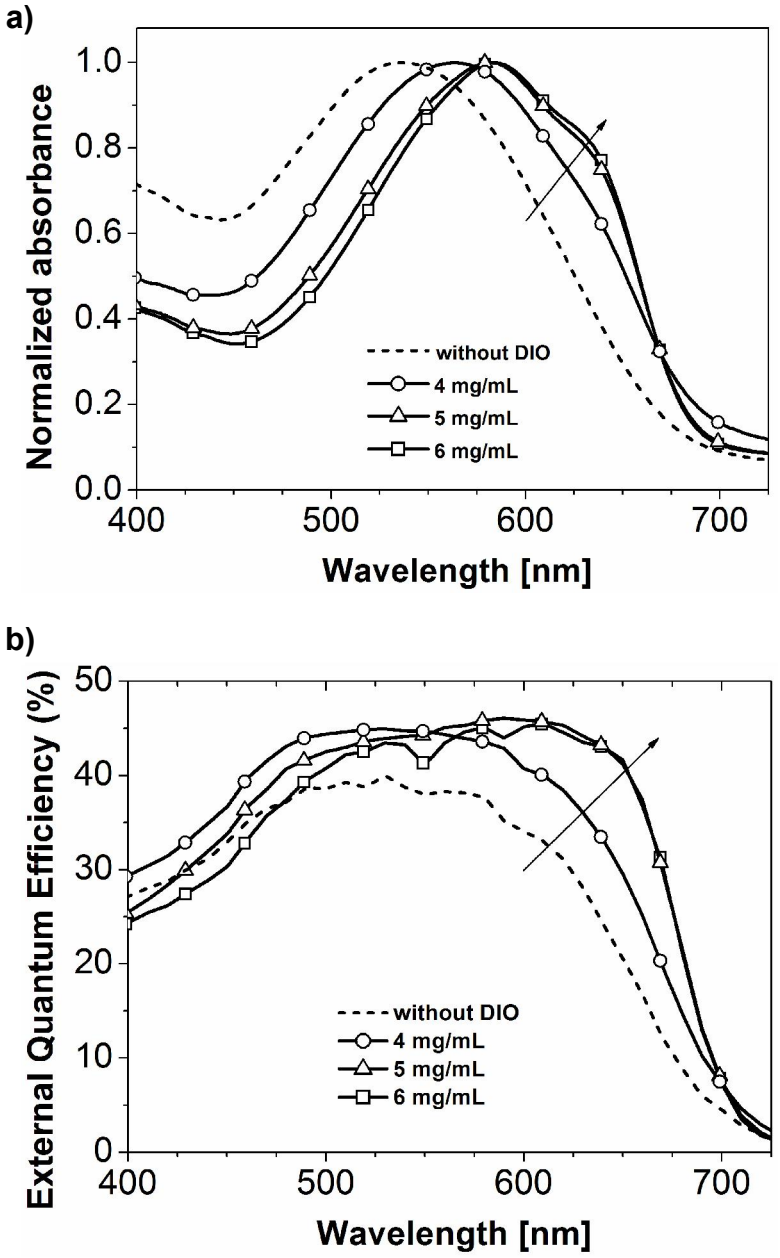

Figure 4. *(a) Normalized absorption spectra of* ***DCC5T-Bu****:$PC_{61}BM$ blends made with different amounts of DIO. All films were spin-coated on PEDOT:PSS, to accurately reproduce the active layer. (b) Spectral response plot of BHJ devices made using* ***DCC5T-Bu****:$PC_{61}BM$ blends made with different amounts of DIO. Device structure: ITO | PEDOT: PSS |* ***DCC5T-Bu****:$PC_{61}BM$ (1:1) | LiF | Al.*

The influence of DIO on the **DCC5T-Bu**:$PC_{61}BM$ active layer was also investigated by measuring UV-vis absorption of blend films and the resulting spectra are shown in Figure 4a. Films deposited from pure chloroform displayed broad and featureless absorption bands between 400 and 675 nm, with a maximum at 537 nm. Upon addition of 4 mg/mL of solvent additive, a red-shift of λ_{max} to 562 nm, as well as the appearance of a shoulder at 625 nm was observed. Further increase of diiodooctane content in chloroform to 5 or 6 mg/mL shifts λ_{max} to

581 nm, which corresponds to a difference of more than 45 nm compared to the blend film, processed from pure $CHCl_3$ solution. In addition, the shoulder seen at 625 nm becomes more pronounced, which is attributed to better packing and a higher degree of organization in the **DCC5T-Bu**:$PC_{61}BM$ blend. The trends seen in the absorption spectra are also observed in the corresponding spectral response plots of the analogous BHJ devices (Figure 4b). Upon increasing the DIO content in the blend, the external quantum efficiency (EQE) at wavelengths above 600 nm increases notably. The shoulder seen at 625 nm reaches a maximum EQE of 46% for the **DCC5T-Bu**:$PC_{61}BM$ blend containing 5 mg/mL DIO. The enhanced absorption of the active layer above 575 nm results in higher J_{SC} and FF values in photovoltaic devices, 4.5 vs. 6.8 mA/cm^2 and 0.30 vs. 0.47, respectively.

The surface morphology of the D:A blends was investigated using atomic force microscopy (AFM).[24] The samples were prepared in the same way as the photoactive layers for the solar cell devices; by spin-coating the **5T**:PCBM mixtures on ITO | PEDOT:PSS-coated substrates. Figure 5a-c depicts the phase images of **DCV5T-Bu**:$PC_{61}BM$ spin-coated from CB with CN (3.75 mg/mL) at 80°C, and $CHCl_3$ at room temperature and $CHCl_3$ at 60 °C, respectively. Figures 5d and 5e display the phase images of the **DCC5T-Bu**:$PC_{61}BM$ blends deposited from $CHCl_3$ and $CHCl_3$/DIO (5 mg/mL) solutions at room temperature. Figure 5f shows the surface of the active layer for the **MeDCC5T-Bu** blend with $PC_{61}BM$ spin-coated from pure $CHCl_3$. The blend film of **DCV5T-Bu**:$PC_{61}BM$ deposited from CB/CN shows a topography roughness (Rq) of 0.3 ± 0.1 nm. For blend films spin-coated from $CHCl_3$ solution, the film roughness is strongly reduced as a function of the solution temperature from a value of 9 ± 1 nm at room temperature to 0.5 ± 0.1 nm at 60 ºC. In the case of **DCC5T-Bu**, the addition of DIO to $CHCl_3$ increases film roughness from 0.3 ± 0.1 to 1.0 ± 0.1 nm; whereas **MeDCC5T-Bu** displays a R_q value of 0.4 ± 0.1 nm.

A relatively fine phase separation (domains between 10-30 nm) is visible for **DCV5T-Bu**:$PC_{61}BM$ spin-coated from CB/CN solution (Figure 5a). This blend, when deposited from $CHCl_3$ at room temperature (Figure 5b), presents coarse domains (up to ~500 nm in size) which correlate to the high roughness at 9 ± 1 nm. Performing the deposition from $CHCl_3$ at 60 ºC (Figure 5c), the domains are smaller than in the former case. For **DCC5T-Bu** and **MeDCC5T-Bu** depicted in Figure 5d-f, regions of bright and dark contrast are distinguishable. Lighter regions (higher phase shift) may be assigned to areas with mostly donor material (**5T**), whereas the darker regions (lower phase shift) contain mostly acceptor ($PC_{61}BM$).[25] Interestingly, **DCC5T-Bu** deposited from $CHCl_3$/DIO (Figure 5e) displays fibrilar features with finely interdigitated bright and dark regions. The fibrils have a width in the order of the exciton

diffusion length (~20 nm). Phase separation is coarser for **DCC5T-Bu** without DIO (Figure 5d), with dark regions up to 200 nm, and fine for **MeDCC5T-Bu** (domains of ~20 nm in size, see Figure 5f).

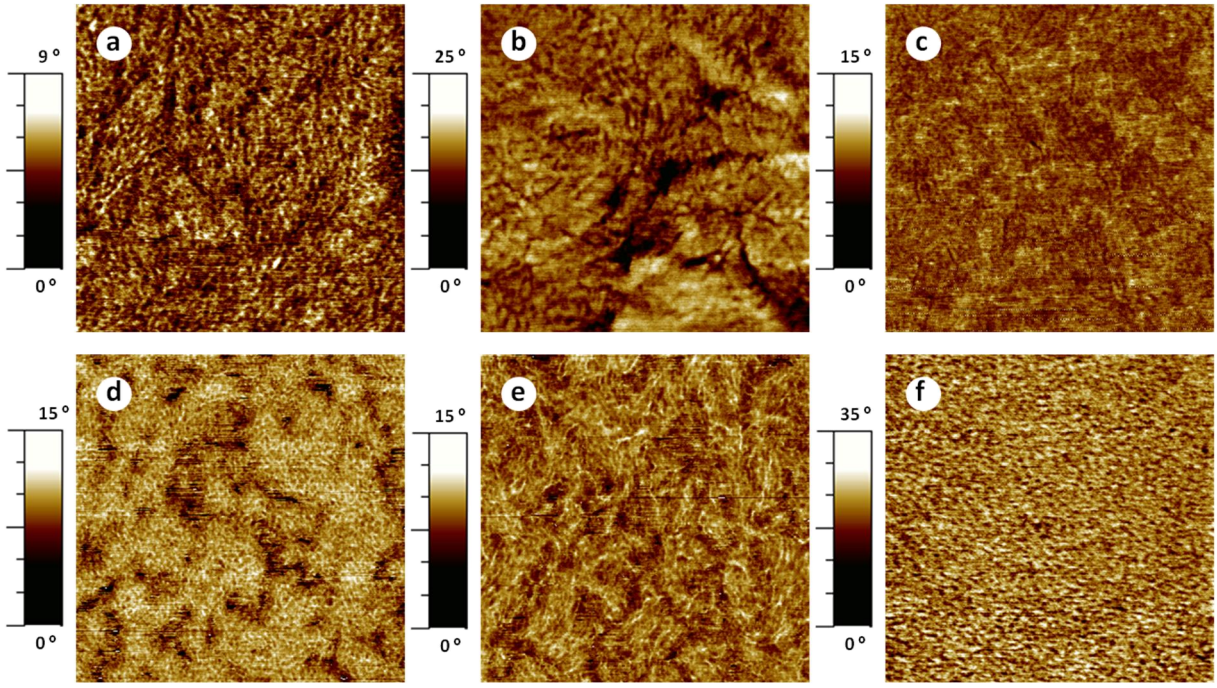

***Figure 5**. AFM phase images of samples spin-coated on ITO | PEDOT:PSS | (a) **DCV5T-Bu**:$PC_{61}BM$ from CB/CN (3.75 mg/mL) at 80 °C, (b) **DCV5T-Bu**:$PC_{61}BM$ from $CHCl_3$ at room temperature, (c) **DCV5T-Bu**:$PC_{61}BM$ from $CHCl_3$ at 60 °C, (d) **DCC5T-Bu**:$PC_{61}BM$ from $CHCl_3$ at room temperature, (e) **DCC5T-Bu**:$PC_{61}BM$ from $CHCl_3$/DIO (5 mg/mL) at room temperature, and (f) **MeDCC5T-Bu**:$PC_{61}BM$ from $CHCl_3$ at room temperature. Image size: 1 x 1 μm.*

In Table 3 and Figure 6 the data of the optimized solar cells of all three **5T** oligomers are compared. **MeDCC5T-Bu** displayed the lowest performances of the series and we speculate that this may be due to the presence of the methyl groups on the cyclohexene ring, which disrupt the packing of the donor molecules, leading to a intimately-mixed blend. **DCV5T-Bu** on the other hand showed encouraging improvements in all solar cell parameters, i.e. higher J_{SC} (6.5 mA/cm^2), higher V_{OC} (1.11 V), higher FF (0.41) and a moderate PCE of 3.0%. The disadvantage of this oligomer is the high temperature required to deposit the active layer. The modification of the terminal acceptor groups for **DCC5T-Bu** addressed this issue by increasing the solubility in common organic solvents to such an extent that processing at room temperature was possible. The performance of these cells was slightly better than those of **DCV5T-Bu**. The **DCC5T-Bu** based solar cells displayed a higher J_{SC} and FF (6.8 vs. 6.5 mA/cm^2 and 0.47 vs. 0.41) and lower V_{OC}s (1.06 vs. 1.11 V) resulting in a modest overall increase in PCE from 3.0 to 3.4% in

comparison to the **DCV5T-Bu** based devices. A further indication that the **DCC5T-Bu** devices are operating efficiently is its low saturation value. The saturation value is calculated by dividing the current density measured at -1 V with that at 0 V (J_{SC}). The resulting value describes the current density dependence on the electric field strength which means that the lower the saturation value, the lower the charge recombination. For **MeDCC5T-Bu**, $J_{-1\ V}$ / J_{SC} was calculated to be 1.46, this decreased to 1.28 for **DCV5T-Bu** and then further decreased to 1.18 for **DCC5T-Bu** based devices.

Table 3. *Comparing the optimized photovoltaic parameters of the solution-processed solar cells of the oligomer series. Device structure: ITO | PEDOT:PSS |* ***5T****:$PC_{61}BM$ | LiF | Al.*

Donor	Solvent	Depostion temp. (°C)	D:A ratio	J_{SC} (mA/cm^2)	V_{OC} (V)	FF	PCE (%)	$J_{-1\ V}$ / J_{SC}	EQE_{max} (%)
MeDCC5T-Bu	$CHCl_3$	r.t.	1:2	4.0	1.02	0.31	1.3	1.46	38
DCV5T-Bu	CB:CN	80	1:1	6.5	1.11	0.41	3.0	1.28	40
DCC5T-Bu	$CHCl_3$:DIO	r.t.	1:1	6.8	1.06	0.47	3.4	1.18	46

In Figure 6b one can also see how the external quantum efficiency increases within the series **MeDCC5T-Bu**, **DCV5T-Bu** and **DCC5T-Bu**, from 38 to 40 to 46%. We think that the presence of the shoulder 625 nm for **DCV5T-Bu** and **DCC5T-Bu** is a consequence of the formation of highly ordered D:A films, which is crucial for the reasonable functioning of the solar cells. In the literature there have been many publications about the influence of solvent additives on D:A blend morphology. It is generally understood that solvent additives can influence crystallization and orientation of the donor material. In some cases, this change in order and organization of the blend, can be followed by UV-vis spectroscopy, like in poly(3-hexylthiophene) (P3HT).[26,27] However this is not true in general for all polymeric or oligomeric materials, which have demonstrated significant enhancement of PCE with solvent additives, whereby only subtle changes can be observed in the absorption profiles.[16,28,29] In these cases, the solvent additive has a dramatic effect on the magnitude of the EQE spectrum but not its shape. The two quinquethiophene derivatives discussed herein, seem to be displaying analogous behavior to the extensively investigated regioregular P3HT. In this work, UV-vis absorption spectroscopy was used as a predictive tool to determine the optimal amount of DIO in $CHCl_3$ (see Figure 4a). For **DCC5T-Bu** blends with $PC_{61}BM$ we have observed both changes in blend morphology, i.e. the formation of fibrilar structures and a 46 nm red shift in the absorption maximum of the D:A blend upon incorporation of solvent additive.

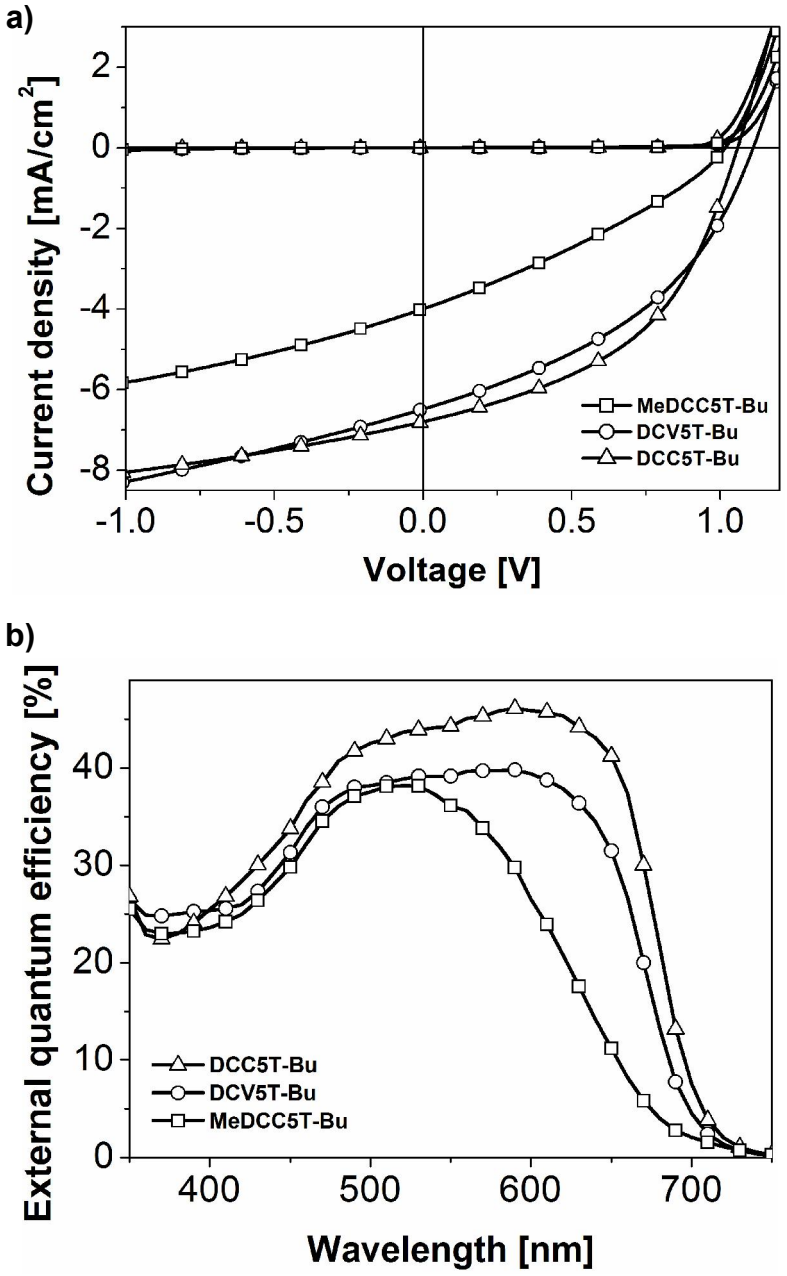

Figure 6. *(a) J-V curves of* ***5T****:$PC_{61}BM$ solution-processed solar cells made from blends spin-coated from best solvent system* ***DCV5T-Bu****:CB/CN,* ***DCC5T-Bu****:$CHCl_3$/DIO and* ***MeDCC5T-Bu****:$CHCl_3$. (b) Spectral response of the corresponding BHJ devices.*

3. CONCLUSION

Two new terminal groups were introduced with the aim of tuning the solubility and film forming properties compared to the well-established DCV-capped quinquethiophene **DCV5T-Bu**. Maximum solubilities of the donor materials in chloroform were increased to 80 mg/mL, allowing for processing of the solar cell active layers at room temperature. HOMO and LUMO

energy levels were found to be suitable for application in photovoltaic devices with $PC_{61}BM$ fullerene derivatives. In the case of **DCC5T-Bu**, the addition of diiodooctane to the solution strongly influenced both the absorption profile and phase separation of the D:A blend. The power conversion efficiency could be increased from 1.4 to 3.4% through use of a solvent additive.

4. Experimental Section

Materials and Methods

Dimethylformamide (DMF, Merck) was first refluxed over P_4O_{10} and distilled, then refluxed over BaO and distilled again. 1-Chloronaphthalene (CN, Aldrich) was distilled prior to use. 3-methoxy-5,5-dimethylcyclohex-2-enone **3** and (3,3",4,4"-tetrabutyl-[2,2':5',2"-terthiophene]-5,5"-diyl)bis(trimethylstannane) **8** were prepared according to published literature procedures.[21,31] 2,5-dibromothiophene **1** was purchased from Aldrich. Malononitrile and *β*-alanine were purchased from Merck. *n*-Butyl lithium (1.6 M solution in hexanes) was purchased from Acros. All synthetic steps were carried out under argon atmosphere. NMR spectra were recorded on a Bruker Avance 400 spectrometer (^{1}H NMR: 400 MHz, ^{13}C NMR: 100 MHz) or a Bruker AMX 500 (^{13}C NMR: 125 MHz) at 25 °C or 100 °C, respectively. Chemical shift values (δ) are expressed in parts per million using residual solvent protons (^{1}H NMR, δ_H = 7.26 for $CDCl_3$ and δ_H = 5.93 for tetrachloroethane-d_2; ^{13}C NMR, δ_C = 77.0 for $CDCl_3$ and δ_C = 74.20 tetrachloroethane-d_2) as internal standard. The splitting patterns are designated as follows: s (singlet), d (doublet) and m (multiplet). EI mass spectra (GC-MS) were recorded on a Varian Saturn 2000 and MALDI-TOF mass spectra on a Bruker Daltonic Reflex III using dithranol or DCTB (trans-2[3-4-tert.-butylphenyl]-2-methyl-2-propenylidene)-malononitrile) as matrices. Differential scanning calorimetric measurements (DSC) were performed on a Mettler Toledo DSC823e under argon atmosphere at a heating rate of 10 °C min-1. Melting points were determined using a Büchi B 545 apparatus and were not corrected. Elemental analyses were performed on an Elementar Vario EL. Preparative column chromatography was performed on glass columns packed with silica gel (Merck Silica 60, particle size 40-43 μm).

Optical solution measurements were carried out in 1 cm cuvettes with Merck Uvasol grade solvents; absorption spectra were recorded on a Perkin Elmer Lambda 19 spectrometer. Maximum solubility values were measured using UV-vis absorption spectroscopy. After determination of

the molar extinction coefficient, saturated solutions were made, stirred for 60 min at 60 °C then allowed to cool to room temperature. The saturated solutions were then filtered and diluted for absorption spectroscopy, and the corresponding concentrations could be determined. Cyclic voltammetry experiments were performed with a computer-controlled Metrohm Autolab PGSTAT30 potentiostat in a three-electrode single-compartment cell with a platinum working electrode, a platinum wire counter electrode, and an Ag/AgCl reference electrode. All potentials were internally referenced to the ferrocene/ferrocenium couple (-5.1 eV). High pressure liquid chromatography was performed on a Hitachi instrument equipped with a UV-vis detector L-7420, columns (Nucleosil 100-5 NO_2 with a pore size of 100 Å) from Machery-Nagel using a dichlormethane/n-hexane mixture (40:60) as eluent. Surface images were recorded with the help of a *Bruker* Nanoscope V AFM at ambient temperature in tapping mode.

Device Fabrication

Photovoltaic devices were made by spin-coating PEDOT:PSS (Clevios P, VP Al4083) onto pre-cleaned, patterned indium tin oxide (ITO) substrates (15 Ω per square) (Kintec). The photoactive layer (~ 80 nm) was deposited by spin-coating from of a mixed solution of 5T with $PC_{61}BM$ (total concentration of 17.5 mg/mL in chlorobenzene or 15 mg/mL in $CHCl_3$). $PC_{61}BM$ was purchased from Solenne BV, Netherlands. The counter electrode of LiF (1 nm) and aluminum (100 nm) was deposited by vacuum evaporation at $2 \cdot 10^{-6}$ Torr. The active areas of the cells were 0.2 cm^2. Film thicknesses were measured using a Dektak profilometer. *J-V* characteristics were measured under ~ 100 mW/cm^2 white light from a tungsten-halogen lamp filtered by a Schott GG385 UV filter and a Hoya LB120 daylight filter, using a Keithley 2400 source meter. Spectral response was measured under monochromatic light from a 300 W Xenon lamp in combination with monochromator (Oriel, Cornerstone 260), modulated with a mechanical chopper. The response was recorded as the voltage over a 220 Ω resistance, using a lock-in amplifier (Merlin 70104). A calibrated Si cell was used as reference. The devices were kept behind a quartz window in a nitrogen filled container.

Synthesis and Characterization

Synthesis of 3-[5-Bromothiophen-2-yl]cyclohex-2-enone ***4***: To a solution of 2,5-dibromothiophene **1** (6.05 g, 25.0 mmol) in diethyl ether (75 mL), stirred at -78 °C, *n*-butyllithium (1.6 M solution in hexanes, 15.6 mL, 25.0 mmol) was added dropwise over 15 minutes. After stirring at -78 °C for 10 minutes, a solution of 3-methoxy-2-cyclohex-2-enon **2** (3.16 g,

25.0 mmol) in diethylether (30 mL) was added and stirring was continued for 15 minutes. The solution was warmed to 0 °C, stirred for 3 hours and subsequently allowed to warm to room temperature and stirred for 16 hours. The reaction was quenched with brine (300 mL) and the product was extracted with diethyl ether (3 × 150 mL). The combined organic extracts were dried over $MgSO_4$, filtered and the solvents were removed *in vacuo*. Column chromatography (silica gel, DCM) and subsequent recrystallization from *n*-hexane yielded compound **4** (4.91 g, 19.1 mmol, 76%) as a colourless crystalline solid. M.p. 90.5-92 °C. ^{1}H NMR (chloroform-d_1, δ ppm) 7.12 (d, 1H, J = 4.0 Hz), 7.05 (d, 1H, J = 3.9 Hz), 6.29 (s, 1H), 2.70 (t, 2H, J = 6.0 Hz), 2.45 (t, 2H, J = 6.6 Hz), 2.16-2.09 (m, 2H). ^{13}C NMR (chloroform-d_1, δ ppm) 199.08, 151.19, 143.97, 131.20, 127.57, 122.80, 116.38, 37.18, 27.35, 22.29. EI mass 258 [M+H$^+$] (calcd. for $C_{10}H_9BrOS$ 257). Elemental analysis for $C_{10}H_9BrOS$: calcd. C, 46.71; H, 3.53; S, 12.47%; found: C, 46.97; H, 3.59; S, 12.48%.

Synthesis of 3-[5-Bromothiophen-2-yl]-5,5-dimethylcyclohex-2-enone ***5***: To a solution of 2,5-dibromothiophene **1** (6.05 g, 25.0 mmol) in diethyl ether (75 mL), stirred at -78 °C, *n*-butyl-lithium (1.6 M solution in hexanes, 15.6 mL, 25.0 mmol) was added dropwise over 15 minutes. After stirring at -78 °C for 15 minutes, a solution of 3-methoxy-5,5-dimethylcyclohex-2-enone **3** (3.86 g, 25.0 mmol) in diethylether (15 mL) was added and stirring was continued for 30 minutes. The solution was warmed to 0 °C, stirred for 3 hours and subsequently allowed to warm to room temperature and stirred for 16 hours. The reaction was quenched with brine (300 mL) and the product was extracted with diethyl ether (3 × 150 mL). The combined organic extracts were dried over $MgSO_4$, filtered and the solvents were removed *in vacuo*. Column chromatography (silica gel, DCM) yielded compound **5** (4.28 g, 15.0 mmol, 60%) as a pale yellow crystalline solid. M.p. 81.5-83 °C. ^{1}H NMR (chloroform-d_1, δ ppm) 7.12 (d, 1H, J = 4.0 Hz), 7.05 (d, 1H, J = 3.9 Hz), 6.30-6.29 (m, 1H), 2.57-2.56 (m, 2H), 2.32-2.31 (m, 2H), 1.11 (s, 6H). ^{13}C NMR (chloroform-d_1, δ ppm) 199.24, 149.05, 144.25, 131.18, 127.52, 121.73, 116.33, 50.90, 41.33, 33.53, 28.35. EI mass 286 [M+H$^+$] (calcd. for $C_{12}H_{13}BrOS$ 285). Elemental analysis for $C_{12}H_{13}BrOS$: calcd. C, 50.54; H, 4.59; S, 11.24%; found: C, 50.74; H, 4.62; S, 11.32%.

Synthesis of 2-[3-(5-Bromothiophen-2-yl)cyclohex-2-en-1-ylidene]malononitrile ***6***: A solution consisting of 3-[5-Bromothiophen-2-yl]cyclohex-2-enone **4** (4.00 g, 15.6 mmol), malononitrile (3.08 g, 46.7 mmol) and *β*-alanine (83 mg, 0.93 mmol) in a mixture of dichloroethane (100 mL) and ethanol (100 mL) was stirred under reflux for 6 days. The reaction mixture was allowed to cool to room temperature, the precipitate was filtered off and washed thoroughly with water.

After concentration of the filtrate *in vacuo* to about half the volume and cooling to room temperature, the resulting precipitate was collected by filtration and washed with water to afford a second crop of **6** (overall yield: 4.40 g, 14.4 mmol, 93%) as an orange crystalline solid. M.p. 195.5-197 °C. ^{1}H NMR (chloroform-d_1, δ ppm) 7.23 (d, 1H, J = 3.9 Hz), 7.10 (d, 1H, J = 3.9 Hz), 7.01 (s, 1H), 2.80 (t, 2H, J = 6.4 Hz), 2.74 (t, 1H, J = 5.9 Hz), 2.00 (p, 1H, J = 6.1 Hz). ^{13}C NMR (chloroform-d_1, δ ppm) 168.85, 149.24, 143.88, 131.71, 128.64, 118.57, 118.25, 113.28, 112.46, 78.34, 29.06, 27.73, 21.11. EI mass 306 [M+H$^+$] (calcd. for $C_{13}H_9BrN_2S$ 305). Elemental analysis for $C_{13}H_9BrN_2S$: calcd. C, 51.16; H, 2.97; N, 9.18; S, 10.51%; found: C, 51.38; H, 3.04; N, 9.15; S, 10.54%.

Synthesis of 2-[3-(5-Bromothiophen-2-yl)-5,5-dimethylcyclohex-2-en-1-ylidene]malononitrile 7: A solution consisting of 3-[5-Bromothiophen-2-yl]-5,5-dimethylcyclohex-2-enone **5** (2.60 g, 9.12 mmol), malononitrile (1.81 g, 27.3 mmol) and *β*-alanine (49 mg, 0.55 mmol) in a mixture of dichloroethane (30 mL) and ethanol (30 mL) was stirred under reflux. After 5 days additional portions of malononitrile (900 mg, 13.5 mmol) and *β*-alanine (20 mg, 0.22 mmol) were added to the solution and stirring under reflux was continued for one day. The reaction mixture was poured into water (250 mL), extracted with dichloromethane (3 × 150 mL), dried over $MgSO_4$ and the solvents were removed *in vacuo*. The crude product was purified by column chromatography (SiO_2, dichloromethane) to obtain **7** (2.36 g, 7.08 mmol, 78%) as a yellow crystalline solid. M.p. 135-136.5 °C. ^{1}H NMR (chloroform-d_1, δ ppm) 7.22 (d, 1H, J = 4.0 Hz), 7.10 (d, 1H, J = 4.1 Hz), 7.01 (m, 1H), 2.61-2.60 (m, 2H), 2.56-2.55 (m, 2H), 1.09 (s, 6H). ^{13}C NMR (chloroform-d_1, δ ppm) 168.45, 147.50, 144.06, 131.68, 128.62, 118.18, 117.52, 113.31, 112.48, 79.19, 42.57, 41.72, 32.09, 27.84. EI mass 334 [M+H$^+$] (calcd. for $C_{15}H_{13}BrN_2S$ 333). Elemental analysis for $C_{15}H_{13}BrN_2S$: calcd. C, 54.06; H, 3.93; N, 8.41; S, 9.62%; found: C, 54.22; H, 4.13; N, 8.48; S, 9.66%.

Synthesis of 2,2'-((3',3''',4',4'''-tetrabutyl-[2,2':5',2'':5'',2''':5''',2''''-quinquethiophene]-5,5''''-diyl)bis(cyclohex-2-en-3-yl-1-ylidene)) ***DCC5T-Bu***: A mixture of (3,3",4,4"-tetrabutyl-[2,2':5',2"-terthiophene]-5,5"-diyl)bis(trimethylstannane) **8** (650 mg, 814 µmol), 2-[3-(5-Bromo-thiophen-2-yl)-5,5-dimethylcyclohex-2-en-1-ylidene]malononitrile **6** (547 mg, 1.79 mmol) and tetrakis(triphenylphosphine)palladium(0) (47 mg, 41 µmol) was combined in degassed DMF (30 mL) and stirred at 80 °C for 20 hours. The reaction mixture was poured into water, extracted with dichloromethane, dried over $MgSO_4$ and the solvents were removed *in vacuo*. Column chromatography (silica gel, DCM) yielded compound ***DCC5T-Bu*** (472 mg, 511 µmol, 63%) as a dark purple solid. M.p. 198 (DSC) °C. ^{1}H NMR (tetrachloroethane-d_2, δ ppm) 7.42 (d, 2H, J =

4.0 Hz), 7.14 (d, 2H, *J* = 4.1 Hz), 7.10 (s, 2H), 7.02 (s, 2H), 2.76-2.68 (m, 16H), 1.97-1.91 (m, 4H), 1.55-1.48 (m, 8H), 1.46-1.39 (m, 8H), 0.96-0.90 (m, 12H). ^{13}C NMR (tetrachloroethane-d_2, δ ppm) 169.70, 150.98, 142.52, 142.15, 141.36, 141.04, 136.07, 131.70, 129.34, 126.96, 126.76, 120.51, 118.20, 114.34, 113.49, 76.64, 33.03, 32.67, 29.47, 28.37, 28.27, 23.35, 23.30, 21.59, 14.31, 14.25. MALDI-TOF mass 920 [M^+] (calcd. for $C_{54}H_{56}N_4S_5$ 920). Elemental analysis for $C_{54}H_{56}N_4S_5$: calcd. C, 70.39; H, 6.13; N, 6.08; S, 17.40%; found: C, 70.10; H, 6.02; N, 6.01; S, 17.39%.

Synthesis of 2,2'-((3',3''',4',4'''-tetrabutyl-[2,2':5',2'':5'',2''':5''',2''''-quinquethiophene]-5,5''''-diyl)bis(5,5-dimethylcyclohex-2-en-3-yl-1-ylidene)) ***MeDCC5T-Bu***: A mixture of (3,3",4,4"-tetrabutyl-[2,2':5',2"-terthiophene]-5,5"-diyl)bis(trimethylstannane) **8** (500 mg, 626 µmol), 2-[3-(5-Bromothiophen-2-yl)-5,5-dimethylcyclohex-2-en-1-ylidene]malononitrile **7** (438 mg, 1.32 mmol) and tetrakis(triphenylphosphine)palladium(0) (36 mg, 31 µmol) was combined in degassed DMF (20 mL) and stirred at 80 °C for 40 hours. The reaction mixture was poured into water, extracted with dichloromethane, dried over $MgSO_4$ and the solvents were removed *in vacuo*. Column chromatography (silica gel, DCM) yielded compound ***MeDCC5T-Bu*** (422 mg, 432 µmol, 69%) as a dark purple solid. M.p. 185 ^{o}C (DSC). ^{1}H NMR (tetrachloroethane-d_2, δ ppm) 7.41 (d, 2H, *J* = 4.0 Hz), 7.13 (d, 2H, *J* = 4.0 Hz), 7.10 (s, 2H), 7.02 (s, 2H), 2.72-2.70 (m, 8H), 2.57 (s, 4H), 2.54 (s, 4H), 1.55-1.49 (m, 8H), 1.46-1.38 (m, 8H), 1.04 (s, 12H), 0.96-0.90 (m, 12H). ^{13}C NMR (tetrachloroethane-d_2, 100 °C, δ ppm) 168.40, 148.73, 142.39, 142.09, 142.06, 141.19, 136.42, 131.82, 129.38, 127.12, 126.86, 120.62, 117.54, 113.80, 112.98, 78.42, 43.06, 42.60, 32.87, 32.67, 32.14, 28.31, 28.16, 28.08, 23.07, 13.93, 13.89. MALDI-TOF mass 976 [M^+] (calcd. for $C_{58}H_{64}N_4S_5$ 976). Elemental analysis for $C_{58}H_{64}N_4S_5$: calcd. C, 71.27; H, 6.60; N, 5.73; S, 16.40%; found: C, 71.19; H, 6.62; N, 5.86; S, 16.29%.

ACKNOWLEDGEMENTS

Thank you to Elena Mena-Osteritz for help with AFM experiments and interpretation, and to Jegadesan Subbiah for his assistance in making the first solar cells. We gratefully acknowledge the German Research Foundation (DFG) for financial support within the scope of the Priority Program "Elementary Processes of Organic Photovoltaics" (SPP 1355). We also thank the Spanish MINECO (MAT2010-21156-C03-03) and the University of the Basque Country (EHUA12/05) for supporting this work.

REFERENCES

[1] B. Walker, C. Kim, T.-Q. Nguyen, *Chem. Mater.* **2010**, *23*, 470.

[2] A. Sharenko, C. M. Proctor, T. S. van der Poll, Z. B. Henson, T.-Q. Nguyen, G. C. Bazan, *Adv. Mater*. **2013**, *25*, 4403.

[3] K. N. Winzenberg, P. Kemppinen, F. H. Scholes, G. E. Collis, Y. Shu, T. Birendra Singh, A. Bilic, C. M. Forsyth, S. E. Watkins, Chem. Comm. **2013**, *49*, 6307.

[4] T. V. Pho, F. M. Toma, B. J. Tremolet de Villers, S. Wang, N. D. Treat, N. D. Eisenmenger, G. M. Su, R. C. Coffin, J. D. Douglas, J. M. J. Fréchet, G. C. Bazan, F. Wudl, M. L. Chabinyc, *Adv. Energy Mater*. **2014**, *5*, n/a.

[5] A. Mishra, P. Bäuerle, *Angew. Chem., Int. Ed.* **2012**, *51*, 2020.

[6] Y. Liu, X. Wan, F. Wang, J. Zhou, G. Long, J. Tian, J. You, Y. Yang, Y. Chen, Adv. Energy Mater. **2011**, *1*, 771.

[7] B. Yin, L. Y. Yang, Y. S. Liu, Y. S. Chen, Q. J. Qi, F. L. Zhang, S. G. Yin, *Appl. Phys. Lett.* **2010**, *97*, 023303.

[8] G. Long, X. Wan, B. Kan, Y. Liu, G. He, Z. Li, Y. Zhang, Y. Zhang, Q. Zhang, M. Zhang, Y. Chen, *Adv. Energy Mater*. **2013**, *3*, 639.

[9] J. Zhou, X. Wan, Y. Liu, G. Long, F. Wang, Z. Li, Y. Zuo, C. Li, Y. Chen, *Chem. Mater.* **2011**, *23*, 4666.

[10] J. Zhou, X. Wan, Y. Liu, Y. Zuo, Z. Li, G. He, G. Long, W. Ni, C. Li, X. Su, Y. Chen, *J. Amer. Chem. Soc.* **2012**, *134*, 16345.

[11] Y. Liu, X. Wan, F. Wang, J. Zhou, G. Long, J. Tian, Y. Chen, *Adv. Mater*. **2011**, *23*, 5387.

[12] J. Zhou, Y. Zuo, X. Wan, G. Long, Q. Zhang, W. Ni, Y. Liu, Z. Li, G. He, C. Li, B. Kan, M. Li, Y. Chen, *J. Amer. Chem. Soc*. **2013**, *135*, 8484.

[13] G. He, Z. Li, X. Wan, Y. Liu, J. Zhou, G. Long, M. Zhang, Y. Chen*, J. Mater. Chem*. **2012**, *22*, 9173.

[14] Z. Li, G. He, X. Wan, Y. Liu, J. Zhou, G. Long, Y. Zuo, M. Zhang, Y. Chen, *Adv. Energy Mater.* **2012**, *2*, 74.

[15] Y. Liu, Y. Yang, C.-C. Chen, Q. Chen, L. Dou, Z. Hong, G. Li, *Adv. Mater.* **2013**, *25*, 4657.

[16] Y. Sun, G. C. Welch, W. L. Leong, C. J. Takacs, G. C. Bazan, A. J. Heeger, *Nat. Mater.* **2012**, *11*, 44.

[17] K. R. Graham, P. M. Wieruszewski, R. Stalder, M. J. Hartel, J. Mei, F. So, J. R. Reynolds, *Adv. Func. Mater.* **2012**, *22*, 4801.

[18] K. Schulze, C. Uhrich, R. Schüppel, K. Leo, M. Pfeiffer, E. Brier, E. Reinold, P. Bäuerle, *Adv. Mater.* **2006**, *18*, 2872.

[19] K. Schulze, M. Riede, E. Brier, E. Reinold, P. Bäuerle, K. Leo, *J. Appl. Phys*. **2008**, *104*, 074511.

[20] H. Ziehlke, L. Burtone, C. Koerner, R. Fitzner, E. Reinold, P. Bäuerle, K. Leo, M. Riede, *Org. Electron*. **2011**, *12*, 2258.

[21] S. Haid, A. Mishra, C. Uhrich, M. Pfeiffer, P. Bäuerle, *Chem. Mater.* **2011**, *23*, 4435.

[22] G. L. Schulz, M. Urdanpilleta, R. Fitzner, E. Brier, E. Mena-Osteritz, E. Reinold, P. Bäuerle, *Beilstein J. Nanotechnol*. **2013**, *4*, 680.

[23] K. Staub, G. A. Levina, S. Barlow, T. C. Kowalczyk, H. S. Lackritz, M. Barzoukas, A. Fort, S. R. Marder, *J. Mater. Chem*. **2003**, *13*, 825.

[24] M. Lenes, G.-J. A. H. Wetzelaer, F. B. Kooistra, S. C. Veenstra, J. C. Hummelen, P. W. M. Blom, *Adv. Mater*. **2008**, *20*, 2116.

[25] I. Horcas, R. Fernández, J. M. Gómez-Rodríguez, J. Colchero, J. Gómez-Herrero, A. M. Baro, *Rev. Sci. Instrum.* **2007**, *78*, 0137051.

[26] V. Shrotriya, Y. Yao, G. Li, Y. Yang, *Appl. Phys. Lett*. **2006**, *89*, 063505.

[27] H.-Y. Chen, H. Yang, G. Yang, S. Sista, R. Zadoyan, G. Li, Y. Yang, *J. Phys. Chem. C* **2009**, *113*, 7946.

[28] T. Salim, L. H. Wong, B. Brauer, R. Kukreja, Y. L. Foo, Z. Bao, Y. M. Lam, *J. Mater. Chem*. **2011**, *21*, 242.

[29] J. K. Lee, W. L. Ma, C. J. Brabec, J. Yuen, J. S. Moon, J. Y. Kim, K. Lee, G. C. Bazan, A. J. Heeger, *J. Amer. Chem. Soc*. **2008**, *130*, 3619.

[30] J. C. Bijleveld, A. P. Zoombelt, S. G. J. Mathijssen, M. M. Wienk, M. Turbiez, D. M. de Leeuw, R. A. J. Janssen, *J. Amer. Chem. Soc*. **2009**, *131*, 16616.

[31] C.-F. Shu, Y.-C. Shu, Z.-H. Gong, S.-M. Peng, G.-H. Lee, A. K. Y. Jen, *Chem. Mater*. **1998**, *10*, 3284.

SUMMARY

The steady increase in power conversion efficiencies (PCE) of donor/acceptor bulk heterojunction (BHJ) organic solar cells (OSC) over the recent years was made possible by systematic improvement of the donor materials with respect to optoelectronic and morphological properties. The main objective of this thesis was to synthesize and to characterize series of structurally related oligothiophene-based donor materials bearing electron-withdrawing terminal units (Chart 1). By correlation of thermal, optoelectronic, morphological and photovoltaic properties with the molecular structures, important structure-property-performance relationships were deduced.

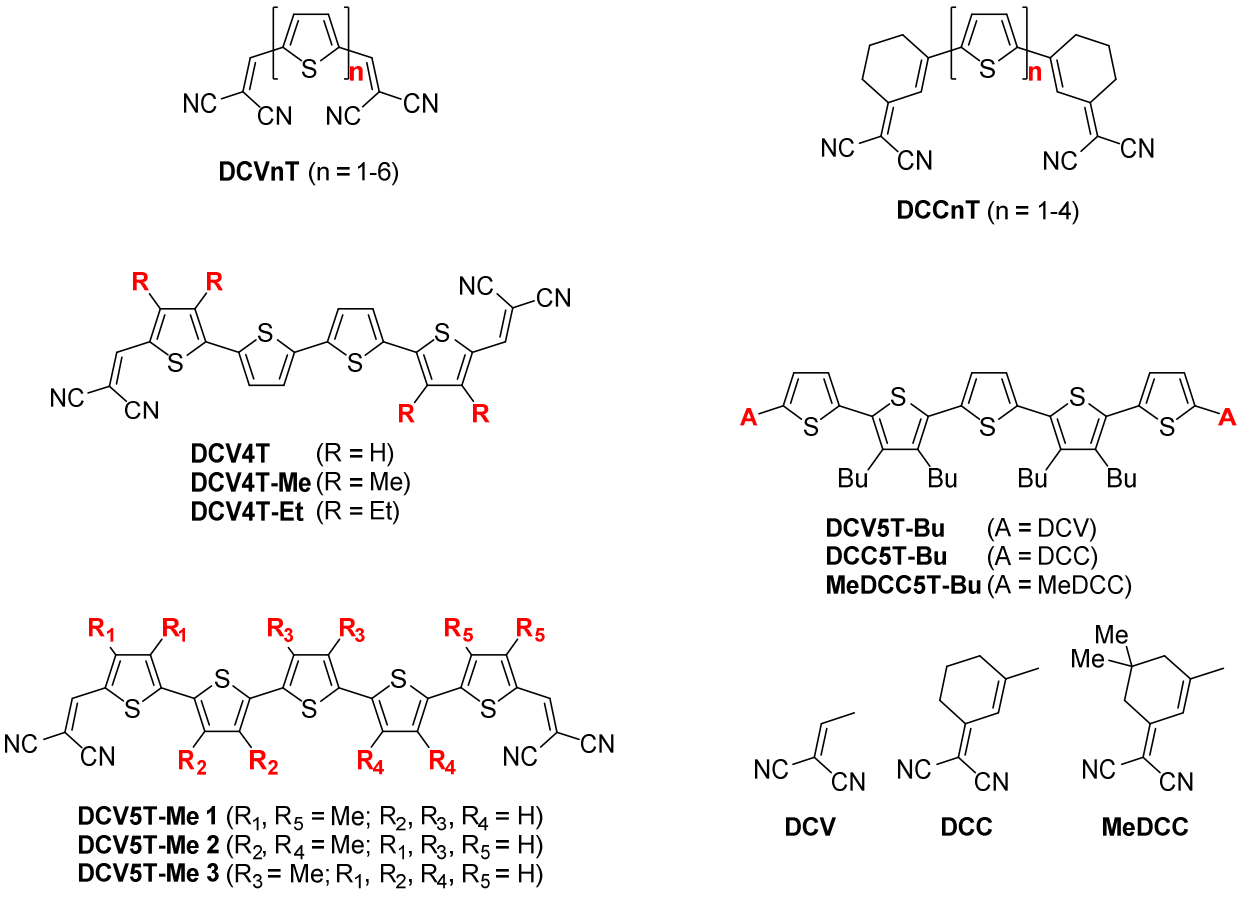

Chart 1. *Overview of the synthesized oligothiophene donor materials.*

Firstly, a homologous series of dicyanovinyl (DCV)-capped oligothiophenes (**nT**) from **DCV1T** to the hexamer **DCV6T** was investigated. Solubilizing alkyl side chains were omitted in the

molecular structures to improve thermal properties for vacuum-processing and to facilitate efficient molecular packing in the bulk. The longer poorly soluble oligothiophene target structures were prepared by palladium-catalyzed cross-coupling of halogenated terminal units with stannylated central building blocks. Final purification was accomplished by extractive recrystallization and thermal gradient sublimation. The extension of the conjugated π-system, going from **DCV1T** to **DCV6T** resulted in a reduction of the optical and electrochemical bandgaps, caused by increasing HOMO energy levels. Planar heterojunction (PHJ) solar cells fabricated for **DCV4T**, **DCV5T** and **DCV6T** showed PCE values of up to 2.8%. A record efficiency of 5.2% was achieved using **DCV5T** in an optimized device setup with a BHJ active layer.

In the second project, a correlation between single crystal X-ray structure analysis data and photovoltaic performance was established in a series of DCV-capped quaterthiophenes (**DCV4Ts**) with systematic variation of the substituents on the terminal thiophene units from hydrogen to methyl and ethyl. Best-performing methyl-substituted tetramer **DCV4T-Me** (PCE = 3.8%) exhibited the highest number of non-bonding short intermolecular contacts within the series, leading to a perfect coplanar layer structure with strong π–π interactions.

Next, a series of methylated quinquethiophene donor materials **DCV5T-Me 1-3** with different alkyl substitution patterns along the oligothiophene backbone was synthesized by Stille-type cross-coupling of methyl substituted building blocks. Centrally methylated **DCV5T-Me 3** yielded a superior efficiency of 6.1% in vacuum-processed BHJ solar cells compared to 4.8% for the other two oligomers. By optimization of the processing conditions and the device stack, a record PCE value of 6.9% was achieved for **DCV5T-Me 3**. X-ray diffraction measurements performed on co-evaporated blend layers of all three derivatives with the fullerene C_{60} acceptor material showed the highest crystallinity of donor and acceptor phases for the best-performing oligomer **DCV5T-Me 3**, thus rationalizing the improved photovoltaic performance.

The following chapter introduces the dicyanomethylenecyclohexene (DCC) terminal group as a structural variation of the DCV unit comprising an additional double bond conformationally locked in a cyclohexene ring. The comparison of a series of alkyl-free **DCCnTs** up to the tetramer to the previously investigated **DCVnTs** revealed very similar optical properties and frontier orbital energies for oligomers with equal numbers of double bonds, i.e. **DCCnTs** and **DCV(n+1)Ts**. In both oligothiophene series, derivatives with even numbers of thiophene units showed higher melting points and lower solubilities compared to odd-numbered oligomers which was assigned to the different molecular symmetries. The single crystal structure obtained for methylated **DCC3T-Me** displayed remarkable similarities to the molecular packing of

structurally related DCV-capped pentamer **DCV5T-Me**. In PHJ solar cells, **DCC3T-Me** showed a higher fill factor and an increased efficiency of 3.4% compared to 3.0% for alkyl-free **DCC3T**. Due to an improved short circuit current density (J_{SC}), a BHJ device incorporating a **DCC3T-Me**:C_{60} active layer displayed a PCE value of 4.4% surpassing the photovoltaic performance of the best DCV-capped quaterthiophene donor material **DCV4T-Me**, which showed similar frontier orbital energies.

Finally, a series of soluble butylated quinquethiophene compounds was investigated. Two novel oligomers bearing DCC and methylated MeDCC terminal units were synthesized and compared to the well-studied DCV-capped derivative **DCV5T-Bu**. In solution all three compounds showed very similar optical properties as the introduction of the additional cyclohexene double bonds caused an almost identical elevation of HOMO and LUMO levels. Absorption profiles of spin-cast thin films were less red-shifted relative to solution measurements for **DCC5T-Bu** and **MeDCC5T-Bu** compared to **DCV5T-Bu** which was ascribed to reduced molecular ordering in the bulk. The first solution-processed BHJ solar cells using [6,6]-phenyl C_{61} butyric acid methyl ester ($PC_{61}BM$) as the acceptor material displayed rather low PCE values of 1.4% and 1.3% for **DCC5T-Bu** and **MeDCC5T-Bu**, respectively. In the case of **DCC5T-Bu**, the use of diiodooctane (DIO) as solvent additive during processing significantly improved the device efficiency to 3.4%. This improvement was due to enhanced J_{SC} values caused by the appearance of a photoactive low-energy shoulder in the blend film absorption spectra. Atomic force microscopy experiments indicated a favorable phase separation for the **DCC5T-Bu** blend layer processed under optimized conditions, whereas the **MeDCC5T-Bu**:$PC_{61}BM$ film showed a much finer intermixing.

In summary, an efficient protocol for the synthesis of low soluble dicyanovinyl-capped oligothiophenes for application as donor materials in vacuum-processed organic solar cells has been elaborated. By correlation of thermal, optoelectronic and morphological behaviour with molecular structure and photovoltaic properties important structure-property-performance relationships were deduced for different series of oligomers with variation of conjugated chain legth and alkyl substitution pattern. The introduction of methylated thiophene units to the oligomer backbone was identified as an effective means to improve the solid state morphology of the photoactive layer in the solar cell device stack.

ZUSAMMENFASSUNG

Die stetige Steigerung des Wirkungsgrads der Energieumwandlung (PCE, *power conversion efficiency*) von organischen Solarzellen mit Donor/Akzeptor Mischheteroübergang (BHJ, *bulk heterojunction*) im Laufe der letzten Jahre wurde durch systematische Weiterentwicklung der Donormaterialien im Hinblick auf optoelektronische und morphologische Eigenschaften ermöglicht. Das zentrale Ziel der vorliegenden Arbeit war die Synthese und Charakterisierung von Serien strukturverwandter Oligothiophen-basierter Donormaterialien mit elektronenziehenden terminalen Einheiten (Schema 1). Durch Korrelation von thermischen, optoelektronischen, morphologischen und photovoltaischen Eigenschaften mit den Molekülstrukturen konnten wichtige Struktur-Eigenschafts-Leistungsfähigkeits-Beziehungen abgeleitet werden.

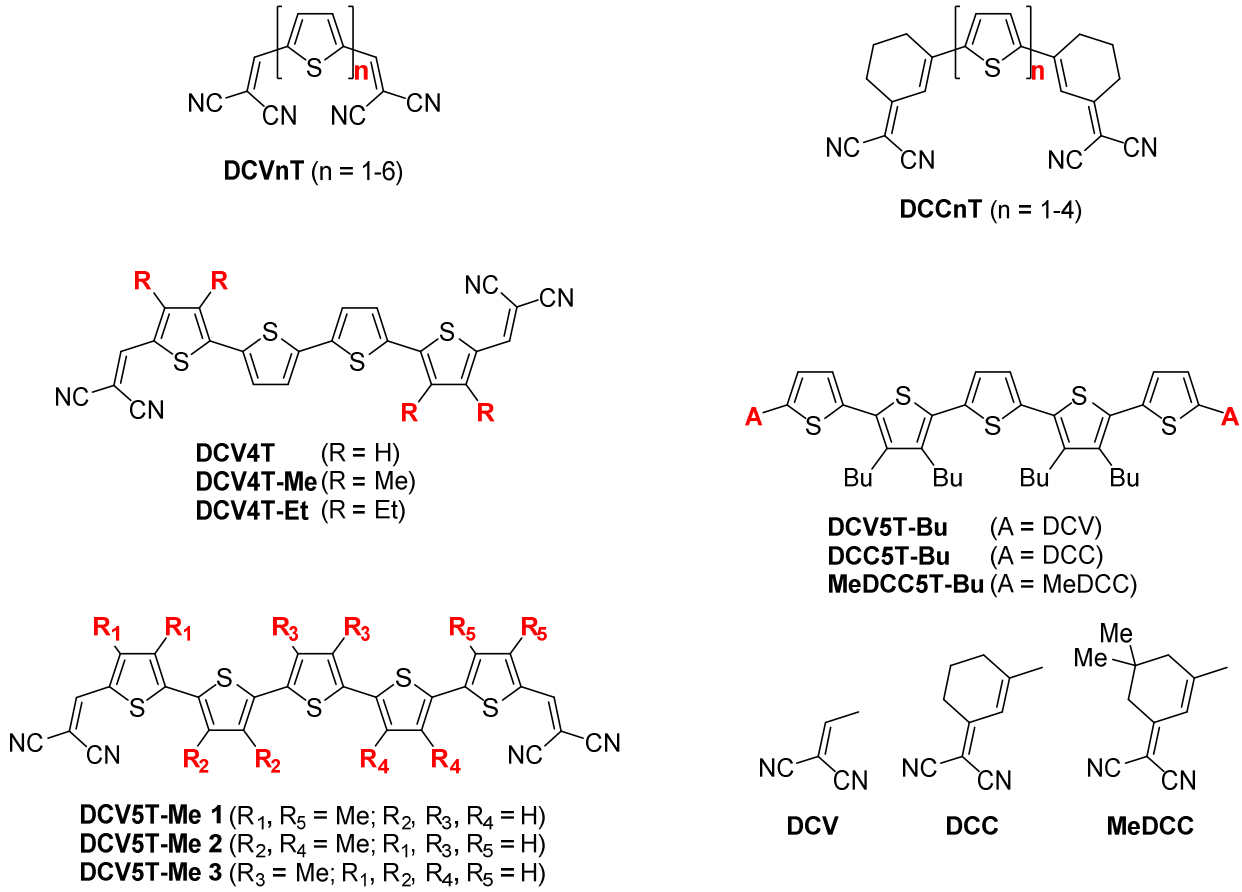

Schema 1. *Übersicht der synthetisierten Oligothiophen-Donormaterialien.*

Zunächst wurde eine homologe Serie Dicyanovinyl (DCV)-substituierter Oligothiophene (**nT**) von **DCV1T** bis zum Hexamer **DCV6T** untersucht. Dabei wurde auf löslichkeitsvermittelnde

Alkylseitenketten verzichtet, um die thermischen Eigenschaften für die Vakuumprozessierung zu verbessern und um eine effiziente Molekülpackung im Festkörper ermöglichen. Die längeren schwerlöslichen Oligothiophen-Zielverbindungen wurden durch Palladium-katalysierte Kreuzkupplung halogenierter Außen- mit stannylierten Mittelbausteinen hergestellt. Die finale Aufreinigung wurde durch extraktive Umkristallisation und thermische Gradientensublimation erreicht. Die Verlängerung des konjugierten π-Systems, ausgehend vom **DCV1T** zum **DCV6T** resultierte in einer Reduktion der optischen und elektrochemischen Bandlücken, bedingt durch ansteigende HOMO-Energieniveaus. Solarzellen mit flachem Heteroübergang (PHJ, *planar heterojunction*), die für **DCV4T**, **DCV5T** und **DCV6T** hergestellt wurden, wiesen Wirkungsgrade von bis zu 2.8% auf. Unter Verwendung eines optimierten Zellaufbaus mit BHJ-Aktivschicht wurde eine Rekordeffizienz von 5.2% erreicht.

Im zweiten Projekt wurde eine Serie DCV-substituierter Quaterthiophene (**DCV4Ts**), bei der die Substituenten an den terminalen Thiopheneinheiten systematisch von Wasserstoff über Methyl zu Ethyl variiert wurden, untersucht und ein Zusammenhang zwischen Einkristall-Röntgenstrukturanalysedaten und photovoltaischer Leistungsfähigkeit hergestellt. Das leistungsfähigste methylsubstituierte Tetramer **DCV4T-Me** (PCE = 3.8%) wies innerhalb der Serie die größte Anzahl nichtbindender intermolekularer Kontakte auf, was zu einer perfekten koplanaren Schichtstruktur mit starken π-π-Wechselwirkungen führte.

Als Nächstes wurde eine Serie methylierter Quinquethiophen-Donormaterialien **DCV5T-Me 1-3** mit verschiedenen Alkylsubstitutionsmustern entlang des Oligothiophenrückgrats durch Stille-Kreuzkupplung methylsubstituierter Bausteine synthetisiert. Das zentral methylierte **DCV5T-Me 3** zeigte in vakuumprozessierten BHJ Solarzellen eine überlegene Effizienz von 6.1%, verglichen mit 4.8% für die beiden anderen Oligomere. Durch Optimierung der Prozessierungsbedingungen und des Zellaufbaus wurde ein PCE-Rekordwert von 6.9% für **DCV5T-Me 3** erreicht. Röntgenbeugungsmessungen, die an koevaporierten Mischschichten aller drei Derivate mit dem Akzeptormaterial Fulleren C_{60} durchgeführt wurden, zeigten die höchste Kristallinität von Donor- und Akzeptor-Phasen für das leistungsfähigste Oligomer **DCV5T-Me 3** und lieferten somit eine Erklärung für die verbesserte photovoltaische Leistungsfähigkeit.

Im folgenden Kapitel wird die Dicyanomethylencyclohexen (DCC)-Endgruppe als strukturelle Variation der DCV-Einheit mit einer zusätzlichen Doppelbindung, die im Cyclohexenring konformativ fixiert ist, vorgestellt. Der Vergleich einer Serie alkylfreier **DCCnTs** bis zur Tetramerverbindung mit den vorher untersuchten **DCVnTs** zeigt sehr ähnliche optische Eigenschaften und Grenzorbitalenergien für Oligomere mit gleicher Anzahl an Doppelbindungen, also für **DCCnTs** und **DCV(n+1)Ts**. In beiden Oligomerserien weisen die

Derivate mit gerader Anzahl an Thiophen-Einheiten im Vergleich zu den ungeradzahligen Oligomeren höhere Schmelzpunkte und geringere Löslichkeiten auf, was auf die unterschiedlichen Molekülsymmetrien zurückgeführt wurde. Die Einkristallstruktur, die das methylierte **DCC3T-Me** erhalten wurde, zeigte bemerkenswerte Ähnlichkeiten zu der Molekülpackung des strukturverwandten DCV-substituierten Pentamers **DCV5T-Me**. In PHJ-Solarzellen wies **DCC3T-Me** einen höheren Füllfaktor und eine erhöhte Effizienz von 3.4% auf, verglichen mit 3.0% für das alkylfreie **DCC3T**. Aufgrund einer verbesserten Kurzschluss-stromdichte (J_{SC}) lieferte eine BHJ-Zelle mit **DCC3T-Me**:C_{60}-Aktivschicht einen PCE-Wert von 4.4%, was die photovoltaische Leistungsfähigkeit des besten DCV-substituierten Quater-thiophen-Donormaterials **DCV4T-Me** überstieg, für das ähnliche Grenzorbitalenergien bestimmt wurden.

Schließlich wurde eine Serie löslicher butylierter Quinquethiophene untersucht. Zwei neue Oligomere mit terminalen DCC- und methylierten MeDCC-Einheiten wurden synthetisiert und mit dem gut erforschten DCV-substituierten Derivat **DCV5T-Bu** verglichen. In Lösung zeigten alle drei Verbindungen sehr ähnliche optische Eigenschaften, da die Einführung der zusätzlichen Cyclohexen-Doppelbindungen zu fast gleichen Anhebungen von HOMO- und LUMO-Niveaus führten. Die Absorptionsprofile schleuderbeschichteter Dünnfilme von **DCC5T-Bu** und **MeDCC5T-Bu** waren verglichen zu **DCV5T-Bu** gegenüber den Lösungs-Messungen weniger rotverschoben, was einer geringeren Ordnung der molekularen Packung im Festkörper zugeschrieben wurde. Die ersten lösungsprozessierten BHJ-Solarzellen mit [6,6]-Phenyl-C_{61}-buttersäuremethylester ($PC_{61}BM$) als Akzeptormaterial zeigten eher geringe PCE-Werte von 1.4% und 1.3% für **DCC5T-Bu** bzw. **MeDCC5T-Bu**. Im Falle von **DCC5T-Bu** wurde die Zelleffizienz durch Verwendung von Diiodoktan (DIO) als Lösungsmitteladditiv während der Prozessierung wesentlich auf 3.4% erhöht. Diese Verbesserung war auf eine Erhöhung des J_{SC}-Wertes zurückzuführen, die durch das Auftreten einer photoaktiven niederenergetischen Schulter im Mischschicht-Absorptionsspektrum verursacht wurde. Rasterkraftmikroskop (AFM)-Experimente deuteten auf eine günstige Phasentrennung bei der unter optimierten Bedingungen prozessierten **DCC5T-Bu**-Mischschicht hin, während der **MeDCC5T-Bu**:$PC_{61}BM$-Film eine viel feinere Durchmischung aufwies.

Zusammenfassend wurde ein effizientes Syntheseprotokoll zur Darstellung von schwerlöslichen Dicyanovinyl-substituierten Oligothiophenen für die Anwendung als Donormaterialien in vakuumprozessierten organischen Solarzellen entwickelt. Durch die Korrelation von thermischem, optoelektronischem und morphologischem Verhalten mit der Molekülstruktur und den photovoltaischen Eigenschaften wurden für verschiedene Oligomer-Serien, bei denen die

konjugierte Kettenlänge und das Alkyl-Substitutionsmuster variiert wurde, wichtige Struktur-Eigenschafts-Leistungsfähigkeits-Beziehungen abgeleitet. Das Einführen von methylierten Thiopheneinheiten in das Oligomer-Rückgrat wurde als effektives Mittel zur Verbesserung der Festkörper-Morphologie der photoaktiven Schicht in der Solarzelle identifiziert.

PUBLICATIONS AND PRESENTATIONS

REFEREED PUBLICATIONS

R. Fitzner, E. Mena-Osteritz, K. Walzer, M. Pfeiffer, P. Bäuerle
"A-D-A-Type Oligothiophenes for Small Molecule Organic Solar Cells: Extending the π-System by Introduction of Ring-Locked Double Bonds"
Adv. Funct. Mater. **2015**, 25, 1845-1856.

Z. Yang, M. Corso, R. Robles, C. Lotze, R. Fitzner, E. Mena-Osteritz, P. Bäuerle, K. J. Franke, J. I. Pascual
"*Orbital Redistribution in Molecular Nanostructures Mediated by Metal-Organic Bonds*"
ACS Nano **2014**, *8*, 10715-10722.

C. Koerner, M. P. Hein, V. Kažukauskas, A. Sakavičius, V. Janonis, R. Fitzner, P. Bäuerle, K. Leo, M. Riede
"*Correlation between Temperature Activation of Charge-Carrier Generation Efficiency and Hole Mobility in Small-Molecule Donor Materials*"
ChemPhysChem **2014**, *15*, 1049-1055.

G. L. Schulz, M. Urdanpilleta, R. Fitzner, E. Brier, E. Mena-Osteritz, E. Reinold, P. Bäuerle
"*Optimization of solution-processed oligothiophene:fullerene based organic solar cells by using solvent additives*"
Beilstein J. Nanotechnol. **2013**, *4*, 680–689.

C. Elschner, M. Schrader, R. Fitzner, A. A. Levin, P. Bäuerle, D. Andrienko, K. Leo, M. Riede
"*Molecular Ordering and Charge Transport in a Dicyanovinyl-substituted Quaterthiophene Thin Film*"
RSC Adv. **2013**, *3*, 12117-12123.

C. Koerner, H. Ziehlke, R. Gresser, R. Fitzner, E. Reinold, P. Bäuerle, K. Leo, M. Riede
"*Temperature Activation of the Photoinduced Charge Carrier Generation Efficiency in Quaterthiophene:C_{60} Mixed Films*"
J. Phys. Chem. C **2012**, *116*, 25097-25105.

R. Fitzner, E. Mena-Osteritz, A. Mishra, G. Schulz, E. Reinold, M. Weil, C. Körner, H. Ziehlke, C. Elschner, K. Leo, M. Riede, M. Pfeiffer, C. Uhrich, P. Bäuerle
"*Correlation of π-Conjugated Oligomer Structure with Film Morphology and Organic Solar Cell Performance*"
J. Am. Chem. Soc. **2012**, *134*, 11064-11067.

M. Schrader, R. Fitzner, M. Hein, C. Elschner, B. Baumeier, K. Leo, M. Riede, P. Bäuerle, D. Andrienko
"*Comparative study of microscopic charge dynamics in crystalline acceptor-substituted oligothiophenes*"
J. Am. Chem. Soc. **2012**, *134*, 6052-6056.

R. Fitzner, C. Elschner, M. Weil, C. Uhrich, C. Körner, M. Riede, K. Leo, M. Pfeiffer, E. Reinold, E. Mena-Osteritz, P. Bäuerle
"*Interrelation between Crystal Packing and Small-Molecule Organic Solar Cell Performance*"
Adv. Mater. **2012**, *24*, 675-680.

C. Körner, C. Elschner, N. C. Miller, R. Fitzner, F. Selzer, E. Reinold, P. Bäuerle, M. F. Toney, M. D. McGehee, K. Leo, M. Riede
"*Probing the effect of substrate heating during deposition of DCV4T:C_{60} blend layers for organic solar cells*"
Org. Electron. **2012**, *13*, 623-631.

H. Ziehlke, L. Burtone, C. Körner, R. Fitzner, E. Reinold, P. Bäuerle, K. Leo, M. Riede
"*Increase of charge carrier lifetime in dicyanovinyl-quinquethiophene:fullerene blends upon deposition on heated substrates*"
Org. Electron. **2011**, *12*, 2258-2267.

H. Ziehlke, R. Fitzner, C. Körner, R. Gresser, E. Reinold, P. Bäuerle, K. Leo, M. K. Riede
"*Side Chain Variations on a Series of Dicyanovinyl-Terthiophenes: A Photoinduced Absorption Study*"
J. Phys. Chem. A **2011**, *115*, 8437-8446.

R. Fitzner, E. Reinold, A. Mishra, E. Mena-Osteritz, H. Ziehlke, C. Körner, K. Leo, M. K. Riede, M. Weil, O. Tsaryova, A. Weiß, C. Uhrich, M. Pfeiffer, P. Bäuerle
"*Dicyanovinyl-Substituted Oligothiophenes: Structure-Property Relationships and Application in Vacuum-Processed Small-Molecule Organic Solar Cells*"
Adv. Funct. Mater. **2011**, *21*, 897-910.

S. Götze, R. Fitzner, H. Kunz
"*Gold Catalysis in Glycosylation Reactions*"
Synlett **2009**, *20*, 3346-3348.

SELECTED PRESENTATIONS

BMBF-i Final Meeting, Ulm, Germany, June 3rd-4th **2013**.
Oral Presentation: "*Small Molecule Organic Solar Cells: Tailoring Materials for a Future Technology*"

Organic Chemistry Seminar Program at the Bio21 Institute, University of Melbourne, Australia, March 30th **2012**.
Oral Presentation: "*Dicyanovinyl-Capped Oligothiophene Donor Materials for Small Molecule Organic Solar cells*"

ISEOFM2012, Shanghai, China, March 11th-13th **2012**.
Poster presentation.

DFG SPP1355 Summer School, Veitshöchheim, Germany, June 20th-24th **2011**.
Poster presentation.

Fπ9, Atlanta, Georgia, USA, May 23rd-28th **2010**. Poster presentation.
DFG SPP1355 Spring School, Krippen, Germany, February 28th-March 3rd **2010**.
Poster presentation.

KOPO2009, Blaubeuren, Germany, September 13th-16th **2009**.
Poster presentation.

ISNA13, Luxembourg, July 19th-24th **2009**.
Poster presentation.

Parts of this dissertation are already published in:

R. Fitzner, E. Mena-Osteritz, K. Walzer, M. Pfeiffer, P. Bäuerle
"A-D-A-Type Oligothiophenes for Small Molecule Organic Solar Cells: Extending the π-System by Introduction of Ring-Locked Double Bonds"
Adv. Funct. Mater. **2015**, 25, 1845-1856.
DOI: 10.1002/adfm.201404210.
www.onlinelibrary.wiley.com/doi/10.1002/adfm.201404210/abstract
Copyright © 2015 WILEY-VCH Verlag GmbH & Co. KGaA, Weinheim.

R. Fitzner, E. Mena-Osteritz, A. Mishra, G. Schulz, E. Reinold, M. Weil, C. Körner, H. Ziehlke, C. Elschner, K. Leo, M. Riede, M. Pfeiffer, C. Uhrich, P. Bäuerle
"*Correlation of π-Conjugated Oligomer Structure with Film Morphology and Organic Solar Cell Performance*"
J. Am. Chem. Soc. **2012**, *134*, 11064-11067.
DOI: 10.1021/ja302320c.
www.pubs.acs.org/doi/abs/10.1021/ja302320c
Copyright © 2012 American Chemical Society.

R. Fitzner, C. Elschner, M. Weil, C. Uhrich, C. Körner, M. Riede, K. Leo, M. Pfeiffer, E. Reinold, E. Mena-Osteritz, P. Bäuerle
"*Interrelation between Crystal Packing and Small-Molecule Organic Solar Cell Performance*"
Adv. Mater. **2012**, *24*, 675-680.
DOI: 10.1002/adma.201104439.
www.onlinelibrary.wiley.com/doi/10.1002/adma.201104439/abstract
Copyright © 2012 WILEY-VCH Verlag GmbH & Co. KGaA, Weinheim.

R. Fitzner, E. Reinold, A. Mishra, E. Mena-Osteritz, H. Ziehlke, C. Körner, K. Leo, M. K. Riede, M. Weil, O. Tsaryova, A. Weiß, C. Uhrich, M. Pfeiffer, P. Bäuerle
"*Dicyanovinyl-Substituted Oligothiophenes: Structure-Property Relationships and Application in Vacuum-Processed Small-Molecule Organic Solar Cells*"
Adv. Funct. Mater. **2011**, *21*, 897-910.
DOI: 10.1002/adfm.201001639.
www. onlinelibrary.wiley.com/doi/10.1002/adfm.201001639/abstract
Copyright © 2011 WILEY-VCH Verlag GmbH & Co. KGaA, Weinheim.

CURRICULUM VITAE

Name	**Roland Fitzner**
Date of birth	6th November 1983
Place of birth	Ludwigshafen am Rhein, Germany
Citizenship	German
Email	ro.fitzner@gmail.com

since Oct 2013	Research scientist, Heliatek GmbH, Ulm, Germany.
Apr 2009 – Sep 2013	Postgraduate studies in the group of Prof. Peter Bäuerle, Institute of Organic Chemistry II and Advanced Materials, University of Ulm, Germany; Thesis topic: Functionalized Oligothiophenes for Application in Organic Solar Cells.
Mar 2012 – Apr 2012	Reaserch internship in the group of Prof. Andrew Holmes, Bio21 Institute, University of Melbourne, Australia.
Oct 2001 – Oct 2008	Studies of Chemistry, Johannes-Gutenberg-University, Mainz, Germany; Degree: Diploma (overall grade: 1.0).
Jan 2008 – Oct 2008	Diploma student in the group of Prof. Horst Kunz, Institute of Organic Chemistry, Johannes Gutenberg-University, Mainz, Germany; Thesis topic: Gold-catalyzed Glycosylations.
Oct 2005 – Mar 2006	Visiting student (ERASMUS program of the EU) in the group of Prof. Gérard Rousseau, Institute of Molecular Chemistry, University of Paris-Sud, France; Topic: Synthesis of Silapicenadol.
Sep 1992 – Jun 2001	Carl-Bosch-Gymnasium, Ludwigshafen am Rhein, Germany; Degree: Abitur (overall grade: 1.4).